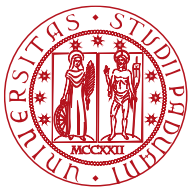

UNIVERSITÀ
DEGLI STUDI
DI PADOVA

DIPARTIMENTO DI INGEGNERIA INDUSTRIALE

CORSO DI LAUREA MAGISTRALE IN
INGEGNERIA ENERGETICA

TESI DI LAUREA MAGISTRALE IN
INGEGNERIA ENERGETICA

TECHNO-ECONOMIC ANALYSIS OF LNG PRODUCTION ALTERNATIVES

RELATORE: Prof. Andrea Lazzaretto
CORRELATORE: Prof. Brian Elmegaard (DTU)
CORRELATORE: Postdoc Tuong-Van Nguyen (DTU)

LAUREANDO: Matteo Nagy

ANNO ACCADEMICO 2015-16

Techno-economic analysis of LNG production alternatives

M.Sc. Thesis
submitted the 1st of July 2016
and defended the 6th of July 2016
at the
TECHNICAL UNIVERSITY OF DENMARK

for the Master of Science in Sustainable Energy

by
Matteo Nagy

under suggestion of:
Associate professor **Brian Elmegaard** (DTU), main supervisor
Associate professor **Andrea Lazzaretto** (UNIPD), main supervisor
Postdoc **Tuong-Van Nguyen** (DTU), main supervisor

Techno-economic analysis of LNG production alternatives

M.Sc. Thesis
Font: Utopia typeset with LaTeX 2_ε

DTU Mechanical Engineering
Section of Thermal Energy
Technical University of Denmark

Nils Koppels Allé, Bld. 403
DK-2800 Kongens Lyngby
Denmark
Phone: (+45) 4525 4131
Fax: (+45) 4588 4325
www.mek.dtu.dk

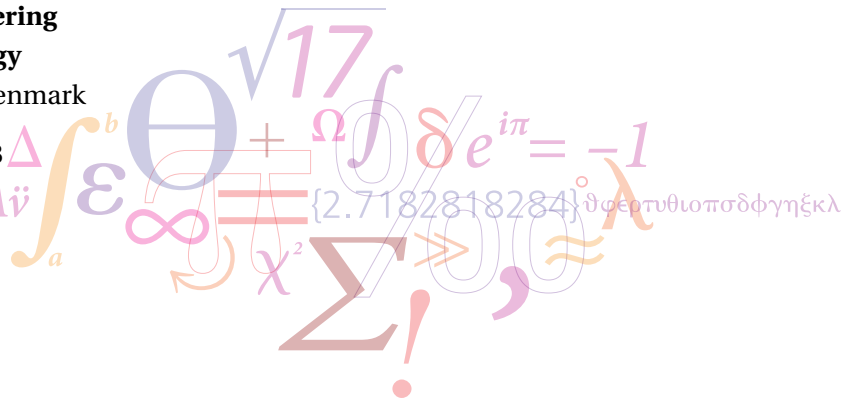

to my parents
for their constant support in all my choices

No man ever steps in the same river twice,
for it's not the same river
and he's not the same man.

— Heraclitus

Preface

The present thesis was prepared at the Section of Thermal Energy, Department of Mechanical Engineering, Technical University of Denmark (DTU). It is submitted as a partial fulfilment of the requirements for the Master's degree in Sustainable Energy - Thermal Energy at DTU and in Energy Engineering at University of Padua (UNIPD), Department of Industrial Engineering.

The work was carried out from 01/02/2016 to 01/07/2016 under supervision of Associate Professor Brian Elmegaard (DTU), Associate Professor Andrea Lazzaretto (UNIPD) and Postdoc Tuong-Van Nguyen (DTU).

The project is credited with 30 ECTS points.

København, 1st July 2016 Matteo Nagy

Acknowledgements

This thesis is the last page of an incredible book, which started more than two years ago when I decided to apply for the TIME Program, destination Copenhagen. I remember the huge amount of doubts that I had in mind at that time. Looking back now, that was the best choice I could ever make. I met many new friends and great people, I suffered for the distance from old ones. I hope these few, simple lines can express how grateful I feel to all who have made this experience unique.

First of all, I want to thank my supervisors, Brian Elmegaard and Andrea Lazzaretto, for the availability and the useful feedbacks they gave me along the road. My gratitude also goes to Allan Bruun from *Kosan Crisplant A/S* for exchanging with me some precious information.

Immense thanks to Tuong-Van, always prompt to provide me help and encouragement, even at more than 10000 km from here. Thanks for never making me feel lost during this journey. And many thanks for the inspiring discussions we had beside the thesis, you helped me grow up as a person.

This thesis period couldn't have been the same without Nicola. Thank you for the engaging discussions and for sharing with me your philosophical approach to work. I learnt a lot from you.

Many thanks to all the beautiful friends I met here in Denmark. Thanks to the Albertslund family, for helping me survive the life in DIK during the first year. Thanks to Edo, Fede and Vale for the amazing Rævehøj family, and to Righe, who is always welcome.
Thanks to the TIME guys, Albi, Fabio and Damiano, it was a pleasure to work with you.
Huge thanks to the 402 crew, to Toni and the German embassy in 426, thank you guys for making even the office life an unforgettable memory. You are great!

These are only a small part of the people I should mention, and only few among the reasons for which I should thank the people I mentioned. Thanks to all of you, guys, without you I wouldn't have been able to complete this adventure.

A special thought goes to Lucile, the most unexpected surprise of these two years. Thank you for bearing my stressed mood and for being always so patient and kind.

Acknowledgements

Infine queste ultime righe, ma non per questo meno importanti, le voglio dedicare alla mia famiglia e ai miei amici di Monselice.
Un grazie immenso ai miei genitori, senza il vostro aiuto probabilmente non sarei nemmeno partito due anni fa. Grazie perché quello che sono lo devo a voi. Un pensiero va ai miei fratelli, Andrea, Emma e al piccolo grande Ale. La distanza si è fatta e si fa sentire, ma voi tutti mi siete sempre stati vicino e questo per me è stato fondamentale.
Grazie a Enrico, Dimitri e Matteo per esserci ancora, nonostante tutto. Un pensiero a tutti gli amici di sempre, a Erica, Chiara e a tutti i tosi del Carmine, a Quei da Monseese e ai compagni di Università. Probabilmente non leggerete mai queste righe, ma sono comunque contento che ci siate su questa tesi per tutti i bei ricordi che ho delle esperienze passate insieme. Grazie!

Abstract

Interest in LNG as a marine fuel for the shipping sector is rapidly growing due to economic advantages over oil alternatives and stricter environmental regulations for shipboard NO_x and SO_x emissions.

LNG production is an energy intensive process, as high compression power is required to reach the cryogenic temperature levels needed for natural gas liquefaction. In light of this, the present thesis focuses on the thermodynamic modelling and optimisation of a specific liquefaction concept, the expander-based configuration. Models are realised using the simulation software Aspen Plus considering the Danish grid natural gas composition.
Thirteen alternatives are investigated, highlighting the drivers for efficiency improvements. Inter-cooled multi-stage compression should be implemented and the temperature difference between Hot and Cold Composite Curves at the cold box should be reduced. This can be achieved by (1) adding a pre-cooling stage, (2) realising a dual-expansion cycle or (3) designing a dual-refrigerant configuration.
Thermodynamic optimisation is performed by means of a genetic algorithm. The Figure of Merit for the expander-based concept is found to range between 17 % and 33 %. Unit energy consumption can be reduced from 2568 kJ per kg of produced LNG to 1336 kJ/kg.

The optimisation procedure emphasises the existing trade-off between power consumption and heat transfer area. This represents the rationale for further investigations of such systems. A simplified economic analysis and comparison of different liquefaction concepts is presented in the second part of this study. Cascade and Mixed-Refrigerant systems are included in the assessment and are compared with the most favourable expander-based configurations. Two plant sizes are considered, corresponding to a feed flow rate of 0.8 kg/s (small scale) and 5.5 kg/s (large scale). Results show that expander-based cycles are not competitive with the other liquefaction alternatives, regardless of the plant size.
Focus is put on the influence that cost correlations have on economic outcomes. The simultaneous minimisation of the investment associated to the compressor and heat exchange network pinpoints that the trade-off between operation and investment costs does not occur, as turbo-machinery is the most capital intensive equipment.

Sommario

L'interesse nel Gas Naturale Liquefatto (LNG) come combustibile per la propulsione marina è in rapida crescita. L'utilizzo del gas naturale presenta vantaggi economici ed ambientali rispetto ai combustibili derivati dal petrolio. In particolare la performance ambientale del gas naturale come combustibile risulta un fattore chiave alla luce dei diminuiti limiti di emissione per il trasporto navale come stabilito dall'Organizzazione Marittima Internazionale.

Il processo di liquefazione del gas naturale è energeticamente dispendioso a causa dell'elevata potenza di compressione necessaria per raggiungere le condizioni criogeniche (-162°C a pressione ambiente). Di conseguenza l'applicazione dei metodi termodinamici è di fondamentale importanza per la riduzione del consumo energetico degli impianti di liquefazione. Questa tesi si focalizza sull'analisi e ottimizzazione termodinamica di una specifica alternativa di impianto per la liquefazione del gas naturale, quella ad espansione del refrigerante per mezzo di un turbo-espansore. La modellazione è realizzata utilizzando il software Aspen Plus e considerando la composizione del gas naturale presente nella rete danese.
L'analisi termodinamica è basata sullo sviluppo di tredici modelli di ciclo e permette di identificare quali siano gli accorgimenti da adottare per incrementare l'efficienza del processo di liquefazione. Due sono le principali direzioni: l'implementazione di compressioni multistadio inter-refrigerate e la riduzione della differenza di temperature negli scambiatori di calore criogenici. Quest'ultima può essere ottenuta mediante (1) l'aggiunta di un ciclo di pre-cooling, (2) il design del processo di espansione a due stadi o (3) la realizzazione di un ciclo a doppio refrigerante.
Successivamente i tredici cicli sono ottimizzati utilizzando un algoritmo genetico. La Figura di Merito, ovvero il rendimento exergetico del ciclo di liquefazione, risulta variare tra 17 % e 33 %. Rispetto alla configurazione base il consumo unitario di energia può essere ridotto del 48 %, da 2568 kJ per kg di LNG prodotto a 1336 kJ/kg.

Il processo di ottimizzazione termodinamica permette di evidenziare il trade-off tra potenza di compressione e area di scambio termico. Questo rappresenta il fondamento per l'analisi economica dei sistemi di liquefazione. Tale analisi comprende i rimanenti concetti di impianto per la liquefazione del gas naturale, cioè i sistemi a cascata e i sistemi a miscela di refrigerante. Il confronto è condotto per due differenti scale d'impianto: piccola scala (portata di gas naturale in ingresso uguale a 0.8 kg/s) e larga scala (portata di gas naturale in ingresso uguale a 5.5 kg/s). I risultati dell'analisi mostrano come le configurazioni a turbo-espansore non riescano

ad essere competitive con le alternative a cascata e a miscela di refrigerante, a causa della minor efficienza.
Un'analisi di sensitività è proposta per investigare l'influenza che le correlazioni di costo impiegate hanno sulla performance economica. L'impiego delle correlazioni di costo proposte da Turton *et al.* fa sì che le turbo-macchine risultino i componenti più costosi, di conseguenza l'ottimo economico tende a coincidere con l'ottimo termodinamico. Tale risultato non è tuttavia confermato impiegando differenti correlazioni di costo. Di conseguenza un processo di validazione dei dati di costo è richiesto per rendere i risultati dell'analisi economica realistici.

Contents

Nomenclature

Abbreviations

APBT	Adjusted Pay-Back Time [years]
BWRS	Benedict-Webb-Rubin-Starling
CC	Composite Curve
CCC	Cold Composite Curve
CDCF	Cumulative Discounted Cash Flow [DKK]
CF	Cash Flow [DKK]
COP	Coefficient of Performance [-]
DCF	Discounted Cash Flow [DKK]
DMR	Dual Mixed-Refrigerant
ECA	Emission Control Area
EOS	Equation of State
FOM	Figure of Merit [-]
FPSO	Floating Production, Storage and Offloading
GA	Genetic Algorithm
GERG	Groupe Européen de Recherches Gazières
GHG	Greenhouse Gases
GWP	Global Warming Potential
HCC	Hot Composite Curve
HEX	Heat Exchanger
HFO	Heavy Fuel Oil
HHV	Higher Heating Value [J/kg]
HP	High-Pressure
IEA	International Energy Agency
IMO	International Marine Organization
LCA	Life Cycle Assessment
LHV	Lower Heating Value [J/kg]
LKP	Lee-Kesler-Plöcker
LMTD	Logarithmic Mean Temperature Difference [K]
LNG	Liquefied Natural Gas
LP	Low-Pressure
LT	Lifetime
MCT	Module Costing Technique
MDO	Marine Diesel Oil
MGO	Marine Gas Oil
MHEX	Multiple-Stream Heat Exchanger
MITA	Minimum Internal Temperature Approach [K]
MOO	Multi-Objective Optimisation
MR	Mixed-Refrigerant
MTPA	Million Tonnes Per Annum

Nomenclature

NG	Natural Gas
NPV	Net Present Value [DKK]
NTP	Normal Temperature and Pressure
O&M	Operation and Maintenance
PC-SAFT	Perturbated Chain with Statistical Association Fluid Theory
PM	Particulate Matter
PR	Peng-Robinson
PR	Pressure Ratio
Ro-Ro	Roll-on/Roll-off
SMR	Single Mixed-Refrigerant
SOO	Single-Objective Optimisation
SR	Sensitivity Ratio
SRK	Soave-Redlich-Kwong
STP	Standard Temperature and Pressure
TCI	Total Capital Investment [DKK]
UP	Unitary Profit [DKK/kg]

Greek letters

Δ	Difference
δ	Rational efficiency defect [-]
ϵ	Exergetic efficiency [-]
η_{C}	Carnot factor [-]
ρ	Pearson partial linear correlation coefficient [-]

Roman letters

$\dot{E}$	Exergy flow [W]
$\dot{m}$	Mass flow [kg/s]
$\dot{Q}$	Heat flow [W]
$\dot{S}_{\mathrm{gen}}$	Entropy generation rate [W/K]
$\dot{V}$	Volume flow rate [m^3/s]
$\dot{W}$	Mechanical power [W]
A	Capacity parameter for cost correlation
A	Dimensionless attractive parameter [-]
a	Natural gas constant in Peng-Robinson EOS
B	Dimensionless repulsive parameter [-]
b	Natural gas constant in Peng-Robinson EOS
C_{BM}	Bare Module Equipment Cost [DKK]
C_{P}^{0}	Basic purchased cost of equipment [DKK]
c_p	Isobaric specific heat capacity [J/kgK]
e	Specific exergy [J/kg]
F_{BM}	Bare Module Cost Factor [-]
F_{M}	Material Cost Factor [-]
F_{P}	Pressure Cost Factor [-]
h	Specific enthalpy [J/kg]
i	Discount rate [-]
n	Number of moles of gas [mol]
P	Pressure [bar]
R	Universal gas constant [J/molK]
s	Specific entropy [J/kgK]
T	Temperature [°C]

U	Heat exchanger overall heat transfer coefficient [W/m^{2}K]
UA	Heat exchanger UA-value [W/K]
V	Volume [m^3]
w	Unit energy consumption [J/kg]
x	Vapour quality [-]
Z	Gas compressibility factor [-]

Subscripts

0	Ambient condition
C	Cooling
comp	Compressor
D	Destruction
ev	Evaporator
exp	Expander
F	Fuel
G	Gas
int	Intermediate
L	Liquid
L	Loss
min	Minimum
P	Product
PC	Pre-cooling
ref	Refrigerant

Superscripts

in	Inlet
out	Outlet

1 Introduction

1.1 Framework

Presently one of society's major concerns deals with the anthropogenic emissions of Greenhouse Gases (GHG), which increase since the pre-industrial era is strictly correlated to the observed atmospheric warming [1]. Besides having a global impact, air pollution is also affecting the environment and human health on a regional and local scale. For instance pollutants like NO_x and SO_x are responsible for the acidification and eutrophication of natural ecosystems and freshwater and for the formation and transport of ground-level ozone [2].

Shipping contributes about 3 % of the global air pollution. Despite its marginal contribution, attention is growing as ship pollution is concentrated in relatively small areas, with the Baltic Sea being among the most critical ones [3]. Additionally, it is estimated that nearly 70 % of ship emissions are deposited within 400 km of land, significantly contributing to air quality degradation in coastal areas [4].
In 2012 annual shipboard NO_x emission was about 19 million tons, while SO_x emission was about 10.2 million tons, being 15 % and 13 % of the global NO_x and SO_x emissions, respectively [5]. Emission of Particulate Matter (PM) amounted to 1.4 million tons, representing 1-7 % of ambient PM_{10}, 1-14 % of $PM_{2.5}$ and 11 % of PM_1 [4]. Due to the increasing traffic volumes, NO_x and SO_x ship emissions are forecast to exceed European Union's land-based emissions [6].

The regulatory authority for the shipping sector is the International Marine Organization (IMO). The main goal of this institution is "*to ensure that ship operators cannot address their financial issues by simply cutting corners and compromising on safety, security and environmental performance*" [7].
The IMO defined ship pollution rules in the International Convention on the Prevention of Pollution from Ships, known as MARPOL 73/78. MARPOL entered into force in 1983 and as the 31st of December 2005 136 countries, representing 98 % of the world's shipping capacity, are parties to the Convention.

MARPOL's Annex VI [8] sets limits on NO_x and SO_x emissions from ship exhausts and prohibits intentional emissions of ozone-depleting substances. Additionally it acknowledges protected areas called Emission Control Areas (ECA's) in which limits are stricter. Annex VI implies subsequent steps for the reduction of NO_x emissions and for the restriction of fuel sulphur content. These stages are summarised in Tables 1.1 and 1.2. More specifically, after the 1st of January 2015 the allowed sulphur content in ECA zones is 0.1 % of the fuel mass. Furthermore the Convention aims at reducing stepwise NO_x emissions through a three-tier program to 80 % by 2016.

Table 1.1: Global and ECA limits for fuel sulphur content [8]

Date	**Global limit [% mass]**	**Date**	**ECA limit [% mass]**
Prior to 1/1/2010	4.5%	Prior to 1/7/2010	1.5%
After 1/1/2012	3.5%	After 1/7/2010	1.0%
After 1/1/2020	0.5%	After 1/1/2015	0.1%

Table 1.2: NO_x emission reduction program [8]

Tier	**Date**	**NO_x limit [g/kWh]**		
		$n < 130$	**$130 \leq n \leq 2000$**	**$n > 2000$**
Tier I	2000	17	$45 \times n^{-0.2}$	9.8
Tier II	2011	14.4	$44 \times n^{-0.2}$	7.7
Tier III	2016*	3.4	$9 \times n^{-0.2}$	1.96

*Only for NO_x ECA's (Tier II applies outside ECA's).
n = engine speed [rpm]

As depicted in Figure 1.1 the Baltic Sea and the North Sea including internal Danish waters are designated as ECA zones, together with the English Channel, Canadian and US coastal waters [9].

As a matter of fact the new regulation on fuel sulphur content and on shipboard emissions affects the overall competitiveness of short sea shipping as well as that of industries relying on cost-efficient transportation. Therefore ship owners must consider new fuels and/or technologies in order to obtain competitiveness in the short sea shipping sector.

Presently there are three compliance strategies: switch to Marine Gas Oil (MGO) or to Marine Diesel Oil (MDO), continue to use high sulphur-content fuel oil (Heavy Fuel Oil - HFO) but install scrubbers to wash the sulphur from the exhaust gas, or consider the use of Liquefied Natural Gas (LNG) as a marine fuel [10].

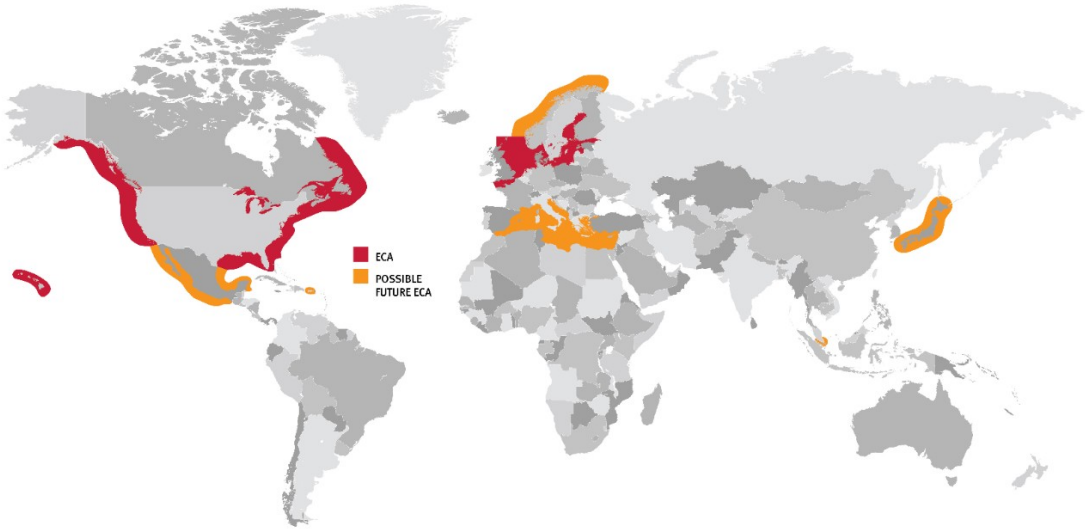

Figure 1.1: Emission Control Areas as defined by the IMO [9]

The use of LNG in the transportation sector falls within the European Union support strategy for alternative fuel markets in order to reduce the EU's dependency on oil imports, to improve the security of Europe's energy supply and to strengthen the competitiveness of European industry [11]. Besides there are additional drivers which can favour the introduction of LNG in the maritime transportation sector [12]. Natural Gas (NG) is cheaper than low-sulphur fuel oil and this situation is expected to last in the future given the difference in proved reserve availability for crude oil and natural gas [13]. Moreover LNG has been widely used as fuel in LNG carriers, leading to the development of market-ready reciprocating internal combustion marine engines capable of natural gas and/or dual-fuel operation. Finally, LNG is the cleanest among the marine fuels which are currently employed in the shipping sector. This outcome is emphasised in the comparative Life Cycle Assessment (LCA) study on marine fuels proposed by the Chalmers University of Technology [14] and summarized in Tables 1.3 and 1.4. The study considers the complete life cycle of each fuel. Fuels are utilised in a Roll-on/Roll-off (Ro-Ro) vessel and the functional unit of the study is one ton cargo transported for 1 km at normal cruise speed.

Table 1.3: Specific fuel consumption and GHG emission coefficient for marine propulsion using HFO, MGO and LNG [14]

	Unit	**HFO**	**MGO**	**LNG**
Specific fuel consumption	g/kWh*	4	3.7	3.3
GHG emissions	g CO_2-eq./ton km	203	213	183

*grams per kWh of engine work

Table 1.4: Emission coefficients for HFO, MGO and LNG [14]

	Unit	HFO	MGO	LNG
CO_2 emissions	g/MJ	188	179	118
NO_x emissions	g/MJ	3.9	3.7	0.4
PM_{10} emissions	g/MJ	0.25	0.08	0.02

Conversely the main challenge related to LNG introduction is the required effective infrastructure, which is on one side connected with the need for major investments and on the other side characterised by an initially poor utilization of the capacity due to limited demand. The lack of an existing bunkering infrastructure represents an important barrier, as highlighted by the European Commission [15].
Secondly, producing LNG is a very energy intensive process. Required liquefaction temperatures are around -160°C and this translates into large operating costs for liquefaction facilities, given the need for high compression power.

1.2 Problem statement

It is believed that an in-depth thermodynamic analysis is necessary in order to understand the main sources of irreversibilities in liquefaction systems and to enhance their performance, thus contributing to the reduction of power consumption. At the same time such analysis cannot overlook economic considerations, which are decisive for the viability of LNG projects.

1.2.1 Objectives

This M.Sc. project aims at contributing to the understanding of technical and economic aspects of natural gas liquefaction facilities. Focus is put on one particular alternative, that is the expander-based concept. Other liquefaction alternatives, namely cascade and Mixed-Refrigerant systems, are the main focus of the Master Thesis *Modelling and Optimisation of Cascade and Mixed-Refrigerant Cycles for Natural Gas Liquefaction* by Nicola Lonardi. This and the present work are developed independently. However they complement each other in the attempt to give a thorough overview about challenges and peculiarities of such systems. Moreover some of the results presented by Lonardi are used in this project for further analyses.

Expander-based systems are generally penalised by higher power consumption with respect to other liquefaction concepts. Therefore the first objective of this work is to identify the major sources of irreversibilities in expander-based configurations and to understand which design improvements can be adopted in order to reduce the power consumption. This is addressed by means of thermodynamic modelling with the simulation software Aspen Plus.

The second objective is to quantify the efficiency improvements that can be achieved. Thermodynamic optimisation by means of genetic algorithm is applied to answer this second research question.
Finally economic considerations are included. In general terms efficiency improvements come at the expense of heat transfer area and design simplicity, which in turns result into higher capital expenditures. The third objective of this project is therefore to further investigate the interplay between thermodynamic and economic performance for the three liquefaction concepts and to identify which one is the most favourable, both for small-scale and large-scale applications.

1.2.2 Approach

This thesis is exclusively a modelling work and no considerations on experimental aspects of LNG production facilities are included. Thermodynamic modelling of expander-based configurations is the point of departure, as the developed models are the basis for all the subsequent analyses, i.e. thermodynamic optimisation and economic performance determination. A literature review is conducted in order to highlight strengths and weaknesses of natural gas liquefaction concepts, particularly of expander-based systems. Moreover relevant inputs for the modelling stage are obtained.
Thermodynamic optimisation is performed using a genetic algorithm. Single-Objective Optimisations allow to address the objective of quantifying the performance improvements for different expander-based configurations. Moreover Multi-Objective Optimisations are performed to investigate the trade-off between power consumption and required heat transfer area.
Economic analysis is based on a Discounted Cash Flow approach and aims at identifying the most economically viable liquefaction alternatives for small-scale and large-scale applications. Some input data come from the companies *Kosan Crisplant A/S*, partner in the project, and *SWEP*. However most of the analysis is built on information and cost correlations found in the literature. For this reason a crucial aspect is the reliability of economic data, which is extensively discussed and which would require a careful stage of data validation for the results to be fully robust.

1.3 Thesis outline

The present thesis consists of 9 Chapters.

Chapter 1 introduces the project along with the framework, main objectives, adopted approach and overall outline of the report.

Chapter 2 sets the relevant background for the thesis, including information about natural gas and LNG properties, technical and thermodynamic features of liquefaction systems, and simulation of natural gas liquefaction cycles.

Chapter 3 outlines the general methodology applied throughout this project and introduces the used tools to the reader.

Chapter 4 presents the developed models for thirteen expander-based configurations. It describes the modelling assumptions and highlights how the expander-based configuration works and the design improvements that can be performed. Understanding the behaviour of expander-based cycles is the basis for setting sensible variation ranges for the decision variables in the optimisation problem.

Chapter 5 includes and discusses the results from the thermodynamic optimisation of the models described in Chapter 4. Exergy analysis is performed on thermodynamic optimal cycles to highlight the distribution of exergy losses and destructions among the different components. Multi-Objective Optimisations are presented with the aim of showing the trade-off between power consumption and heat transfer area. A statistical analysis is carried out on the optimal points constituting the Pareto frontiers, which outcome allows to understand some design implications.

Chapter 6 focuses on the economic analysis of the investigated expander-based configurations. Depending on the size the most convenient alternatives are identified. Sensitivity analyses on natural gas feed, LNG and electricity prices are presented.

Chapter 7 shows the economic comparison of the three different liquefaction concepts, both for small-scale and large-scale applications. Cascade and Mixed-Refrigerant systems modelled by Lonardi are included in the comparison. Influence of natural gas composition on the economic outcome is included in the assessment.

Chapter 8 summarises the main assumptions and limitations of this work.

Chapter 9 concludes the thesis, summarising the main findings and pinpointing possible future developments.

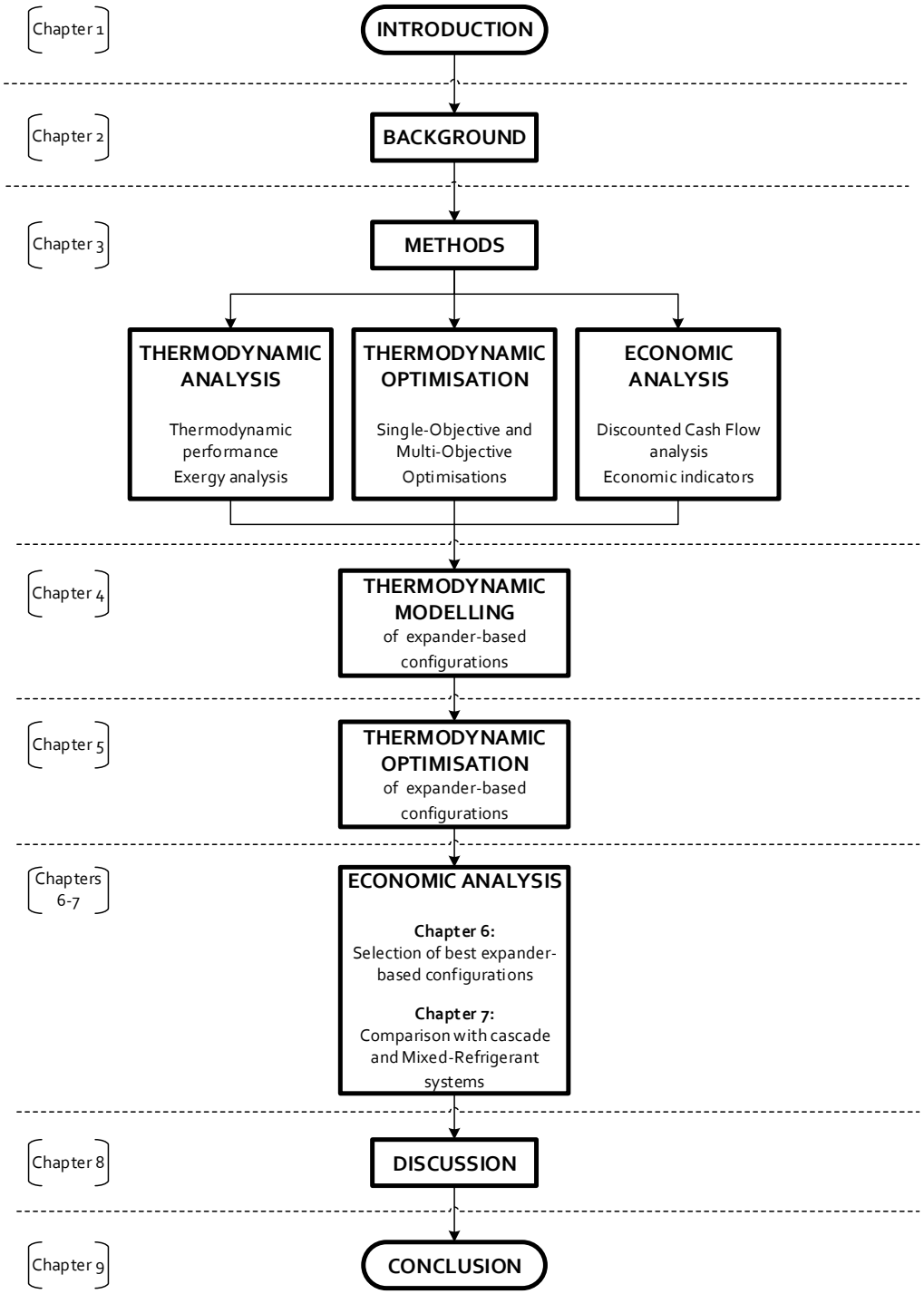
Chapter 1
INTRODUCTION
Chapter 2
BACKGROUND
Chapter 3
METHODS
THERMODYNAMIC ANALYSIS
Thermodynamic performance
Exergy analysis
THERMODYNAMIC OPTIMISATION
Single-Objective and Multi-Objective Optimisations
ECONOMIC ANALYSIS
Discounted Cash Flow analysis
Economic indicators
Chapter 4
THERMODYNAMIC MODELLING
of expander-based configurations
Chapter 5
THERMODYNAMIC OPTIMISATION
of expander-based configurations
Chapters 6-7
ECONOMIC ANALYSIS
Chapter 6:
Selection of best expander-based configurations
Chapter 7:
Comparison with cascade and Mixed-Refrigerant systems
Chapter 8
DISCUSSION
Chapter 9
CONCLUSION

2 Background

This Chapter introduces the background information related to fundamental natural gas properties, natural gas liquefaction process and developed LNG production configurations. It represents the point of departure for this thesis project, as it highlights the challenges and the opportunities for the development of efficient LNG production processes. In light of this it gives an overview of the context in which the present work is collocated.

2.1 Natural gas fundamentals

Among fossil fuels natural gas is the cleanest and the most efficient. Gas-fired electricity generation is characterised by lower capital investment, lower CO_2 emissions and higher thermal efficiency relatively to other fossil fuels, such as oil and coal. Gas-fired generation allows a greater flexibility in meeting peak demand, which can complement renewable energy sources and overcome the related intermittence problems, leading to a higher renewable share in the electricity mix [16].
Although the primary use of natural gas is as a fuel, it is also a source of hydrocarbons for the petrochemical industry and a major source of elemental sulphur [17].

2.1.1 Natural gas resources

Gas resources are classified in conventional and unconventional [18]. The range of conventional and unconventional hydrocarbons is depicted in Figure 2.1.
Conventional gas is typically "free" gas trapped in multiple porous zones in natural rock formations, i.e. carbonates, sandstones and siltstones. Conventional gas occurs in deep reservoirs and can be associated with crude oil. In this case natural gas is defined as associated gas. Conversely it is defined as non-associated gas if no crude oil is contained in the reservoir.

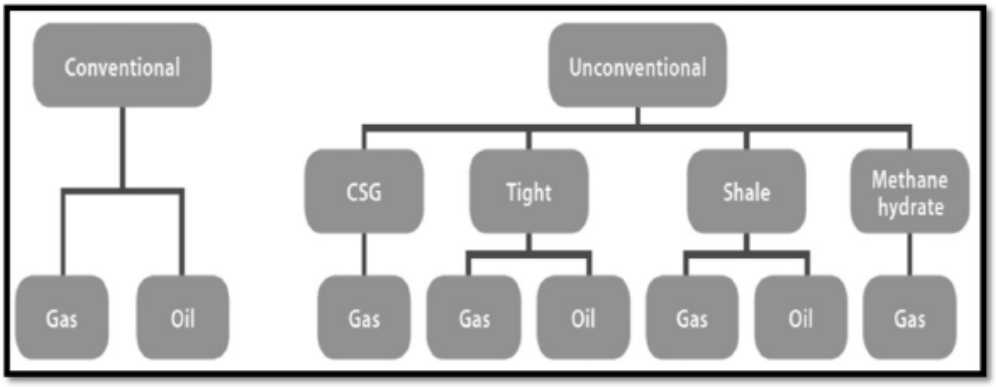

Figure 2.1: Hydrocarbon range [18]

According to the International Energy Agency (IEA) [19], global total resources of conventional natural gas could amount to 463 trillion cubic metres (tcm), representing more than a century of production at current levels. Proven reserves[1] amounted to 216 tcm at the end of 2014, guaranteeing more than 60 years of production at current levels. These are mainly concentrated in a small number of countries and regions such as North America, Russia, Iran and Qatar.
Unconventional gas reservoirs include tight gas, shale gas, coal bed methane and gas hydrates. Compared to conventional gas deposits they are generally lower in resource concentration and more dispersed over larger areas. Unconventional gas is usually found in impermeable rocks which cannot become a trap and form a conventional gas deposit, therefore hydraulic fracturing is commonly required for gas recovery. IEA estimates that the unconventional potentially recoverable gas resources could amount to 327 tcm, 20 % of which located in North America [19].
An overview of the regional and global status of conventional gas proven reserves and of potentially recoverable resources is given in Figure 2.2.

Natural gas represents the fastest increasing fossil energy resource demanded in the world. Global annual demand in 2014 was estimated at 3500 billion cubic metres (bcm) and the IEA Medium Term Gas Market Report predicts an average annual growth rate in natural gas demand of 2 % from 2014 to 2020, confirming the trend observed in the decade up to 2014 (annual average growth rate of 2.3 %) [20].

[1] Reserve refers to the amount of known or proven gas resources which recovery is economically viable using available technologies. On the contrary resource defines the amount of gas which is either proven but not economically viable or based on geological research but not yet proven. Reserves are not included in the resources, while total resources are the sum of the two [19].

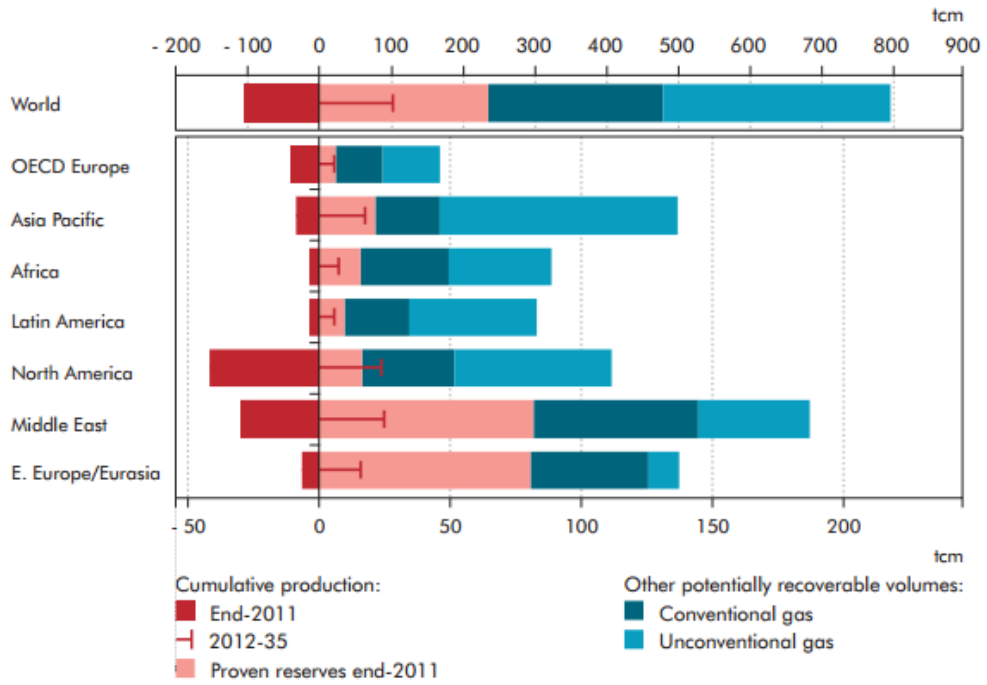

Figure 2.2: Cumulative production and proven reserves of conventional natural gas by region, together with potentially recoverable volumes [19]

2.1.2 Natural gas composition

Natural gas is a mixture of hydrocarbons and non-hydrocarbon components and exists in gaseous form under atmospheric conditions. It is mainly constituted by methane (CH_4), which accounts for 87 - 96 % by volume [21], but can also include significant quantities of ethane (C_2H_6), propane (C_3H_8), butane (C_4H_{10}), pentane (C_5H_{12}) as well as traces of hexane (C_6H_{14}) and heavier hydrocarbons. Many natural gases are also characterised by the presence of nitrogen (N_2), carbon dioxide (CO_2), hydrogen sulphide (H_2S) and other sulphur components as carbonyl sulphide (COS) and carbon disulphide (CS_2) [17].

Natural gases are commonly classified as either lean or rich according to their liquid content. The liquid content of a natural gas mixture is given by the presence of ethane and heavier hydrocarbons (C2+) and is usually measured in gallons of liquid recoverable per 1000 standard cubic feet, the so-called GPM. If ethane is not regarded as a valuable liquid, the GPM can be based on the presence of propane and heavier hydrocarbons (C3+). Lean natural gases have a liquid content lower than 2.5 GPM, while very rich natural gases have a liquid content higher than 5 GPM [22].

2.1.3 Natural gas phase behaviour

Natural gas phase behaviour is a plot of pressure versus temperature determining whether a natural gas stream at a given temperature and pressure consists of a single phase or two phases, gaseous and liquid [23].
For a mixture like natural gas there are two degrees of freedom in the two-phase region. Therefore in a pressure-temperature plot the bubble points and the dew points differ, leading to the definition of a phase envelope composed by the bubble point and the dew point curves, which meet at the critical point (Figure 2.3).
Two points of interest can be additionally identified: the cricondenbar and the cricondentherm. The cricondenbar is the pressure above which the two phases cannot exist together independently from the temperature. On the other hand the cricondentherm defines the temperature level above which the two phases cannot exist together irrespective of the pressure.
Natural gas phase behaviour is a function of the composition of the gas mixture. In particular it is strongly influenced by the presence of C6+ hydrocarbons, which leads to the increase of the phase envelope.

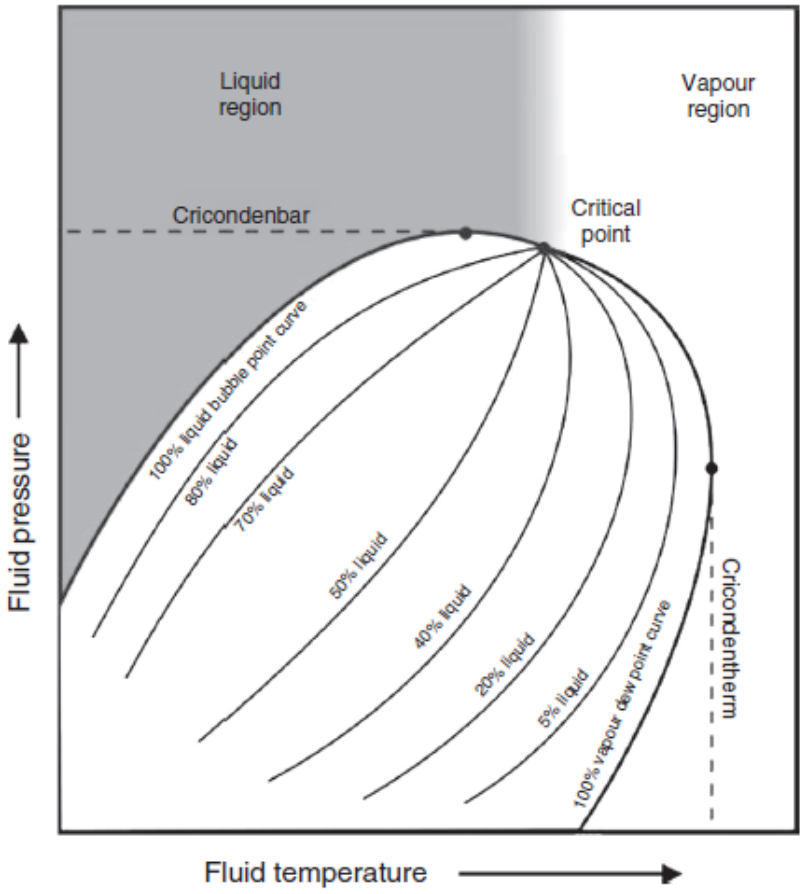

Figure 2.3: Pressure-temperature phase behaviour for a multi-component mixture [23]

2.1.4 Natural gas properties

Mokhatab *et al.* [17] and Bahadori [23] provide a comprehensive overview of natural gas properties. The most relevant ones will be introduced and described in this Section.

Natural gas is a colourless and odourless gas. The boiling point of natural gas at atmospheric pressure is -162°C. When mixed with air, natural gas burns when present in concentrations between 5 % and 15 % by volume. The stoichiometric air-fuel ratio is approximately 17.2[2] on a mass basis.
Natural gas is lighter than air. Its density at Standard Temperature and Pressure (STP)[3] ranges between 0.7 and 0.9 kg/m^3. Natural gas molecular weight varies between 17 and 20 kg/kmol depending on its composition.

Gas compressibility factor

Natural gas is a real gas, hence its behaviour generally differs from the one of an ideal gas. The ideal gas model is a satisfactory tool when dealing with gases at pressure that do not exceed 1 atm, with associated errors of 2 % - 3 %. For higher pressures the use of the ideal gas model becomes unacceptable.
The ratio of the real gas volume to the ideal gas volume is defined as gas compressibility factor Z. The gas compressibility factor is unitary for ideal gases and it represents a measure of the deviation of the real gas from perfect behaviour. Knowing Z, calculation of pressure-volume-temperature relationships can be performed employing the real gas Equation of State (EOS) written as:

$$PV = nZRT \tag{2.1}$$

where V is the volume, n is the number of moles of gas and R is the universal gas constant.

[2] As reported by Wei *et al.* [21] this value refers to the stoichiometric air-fuel ratio of methane. However, being methane the most abundant component in the natural gas mixture, physical and chemical properties of natural gas are very similar to those of methane.

[3] STP conditions refer to 0°C and 1 atm. On the contrary Normal Temperature and Pressure (NTP) conditions refer to 20°C and 1 atm.

Higher and Lower Heating Value

From the thermodynamic theory, the heat of reaction is the associated enthalpy change when both products and reactants are in specified conditions of 15°C and 1 atm [22].
The heating value of a fuel is the amount of heat released by its combustion. According to the reference status of the products two different heating values can be defined:

- Higher Heating Value (HHV) if the reaction products are returned to the reference temperature of 15°C, which implies that the latent heat of vaporization of water in the reaction products[4] is considered, as H_2O leaves in the liquid phase. The Higher Heating Value coincides with the heat of reaction for a combustion process changed in sign [24];
- Lower Heating Value (LHV) if the temperature of the combustion products is 150°C, which assumes that the latent heat of vaporization of water is not recovered, as H_2O leaves as vapour [25].

Therefore the difference between the two values is given by the latent heat of vaporization of the produced water and by the sensible heat which is released when the products are brought from 150°C to the reference temperature of 15°C.
LHV and HHV for natural gas are approximately 47 MJ/kg and 52 MJ/kg, respectively [25].

[4] When fuels containing hydrogen are burnt, water is produced.

2.2 Liquefied Natural Gas

With the increasing demand for natural gas, LNG is expected to play an important role. In 2035 LNG is expected to have a share of 15 % in global natural gas consumption, with an annual growth rate in LNG trade of 1.9 % [26].

LNG is an eco-friendly fuel [27]. The combustion of LNG for transportation and power generation allows to significantly reduce GHG emissions (70 % compared to coal and oil, mainly because of its lower carbon-to-hydrogen ratio [21]). The reduction of Particulate Matter, SO_x and NO_x is even more significant. PM and SO_x emissions can be almost eliminated, while nitrogen oxides emissions can be reduced by 80 % with respect to the combustion of other substitute fossil fuels.
Considering the entire life cycle of LNG a possible drawback is given by methane leakages that can occur during the phases of production, transportation and storage of natural gas [12]. These can negatively affect the environmental performance of gas systems, since methane has a Global Warming Potential (GWP) of 25 (100-year time horizon) [28]. Dealing with marine propulsion Bengtsson *et al.* [14] show that LNG presents a higher GWP than crude oil-based alternatives if more than 2.5 % of the LNG used leaks during the life cycle. Besides, LNG is assessed to perform better than HFO and MGO for all the considered impact categories, namely acidification potential, eutrophication potential, photo-oxidant formation potential and emission of particles.
The same authors show in [29] that the transition towards liquefied biogas as a marine fuel does not necessarily imply a decrease in the environmental impact. The use of liquefied biogas allows to significantly decrease the global warming impact from shipping, but at expense of greater environmental impact in terms of acidification, eutrophication and primary energy use.

LNG is produced by cooling natural gas down to temperatures between -159°C and -162°C through a process known as liquefaction [30]. LNG main component is methane, which is present in concentrations between 87 % and 99 % on a molar basis. Its composition includes C2+ hydrocarbons, nitrogen and traces of sulphur and CO_2 [31].
At -162°C and atmospheric pressure LNG is a clear, odourless, non-toxic and non-corrosive liquid, which density is approximately 0.4 - 0.5 kg/L. Therefore, if spilled on water, LNG floats on top and vaporises quickly, eliminating the need for clean-up in the case of spilling on water or land. In gaseous form, LNG burns mixed with air in concentrations between 5 % and 15 % by volume, know as flammability interval.
The major advantage of natural gas liquefaction is the reduction of volume by a factor of 600 at standard conditions [26] and the related increase of fuel energy density, with 1 ton of LNG carrying the energy equivalent of around 1500 cubic metres of natural gas [31]. Shipping LNG is therefore an economic way to transport large quantities of natural gas over long distances, overcoming the barriers which characterise natural gas transportation through pipelines and increasing energy security of supply through the exploitation of remote gas fields.

An example is the Norwegian LNG base-load plant located in Hammerfest called Snøhvit [32]. It is the first European LNG production facility, with a yearly train capacity of 4.3 million tonnes and with market outlets to the US and Spain [33].

2.2.1 Natural gas feed pretreatment

Before the liquefaction stage natural gas feed has to undergo a series of pretreatment processes in order to eliminate all the impurities, including carbon dioxide, sulphur compounds, mercury, heavier hydrocarbons and water ([30], [34]). The block flow diagram of the pretreatment section is represented in Figure 2.4.
Mercury has to be removed because its presence could lead to the failure of downstream plant equipment made in aluminium, such as brazed-aluminium heat exchangers.
As to the acid gas content, CO_2 has to be removed from the feed gas to less than 50 ppmv to prevent freezing and blockage in the downstream liquefaction unit. H_2S is a toxic compound and is extremely corrosive in presence of water. Typical specification for hydrogen sulphide removal is 4 ppmv.
The presence of water is undesired as it reduces the heating value of natural gas and causes freezing problems in the liquefaction facility.
Fractionation unit is needed when dealing with rich natural gas feeds. It allows to reduce the content of heavy hydrocarbons (C5+), which would otherwise freeze, sending dry (i.e. methane-rich) natural gas to the liquefaction facility.
If present in high concentrations in the natural gas, nitrogen has to be removed to meet LNG specifications, usually below 1 % on a molar basis [35]. As nitrogen condensates at even lower temperature than methane (-196°C), its rejection can take place at the end of the liquefaction process through flashing.

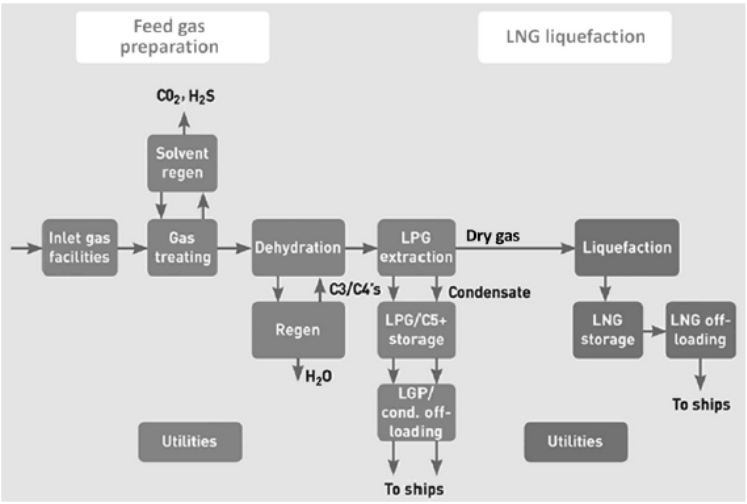

Figure 2.4: Gas to Liquefied Natural Gas block flow diagram [30]

2.2.2 Natural gas liquefaction

Natural gas liquefaction is an energy intensive process, as high compression power is required to reach the cryogenic temperatures needed to produce LNG. As an example, in the case of Snøhvit Project by *Statoil*, the specific compressor consumption is 230 kWh per tonne of LNG produced [36], corresponding to approximately 2 % of the gas energy content. It is therefore essential to optimise the employed refrigeration process in order to reduce the power consumption, thus the operating costs for the facility [37].
The cooling curve of natural gas is characterized by three zones, namely pre-cooling, liquefaction and sub-cooling zone. Being natural gas a zeotropic mixture, it condensates at gliding temperature, i.e. the liquefaction zone presents a slope in the temperature-heat plot. This is highlighted in Figure 2.7.
From the thermodynamic theory a heat transfer across a finite temperature difference causes irreversibilities that lead to the increase of power consumption. These irreversibilities grow with the magnitude of the temperature difference and with the decreasing temperature level below ambient conditions [38]. Therefore the most efficient liquefaction process is the one in which the refrigerant can duplicate the shape of the natural gas cooling curve.
The downside is that a smaller temperature difference between the process gas and the refrigerant leads to a larger requirement in terms of heat exchange area, impacting the investment costs for the liquefaction facility [37]. Finn *et al.* [39] show that the liquefaction process can account up to 50 % of the total capital cost of the LNG project.
Consequently LNG process design is a trade-off between efficiency optimisation, i.e. reduction of operating costs, and the decrease of capital costs through the reduction of the required heat exchange area. The optimal trade-off depends on the size and function of the liquefaction plant. Four categories can be identified, namely base-load, peak-shaving, small-scale and offshore plants ([30], [39]).

- **Base-load plants**: these are large plants directly linked to a specific gas field exploitation. The production capacity is typically larger than 3 Million Tonnes Per Annum (MTPA).

- **Peak-shaving plants**: these are small plants connected to a gas network. LNG is stored as a buffer in periods of low gas demand and is vaporised when demand is high. The liquefaction capacity is small (e.g. 200 tonnes per day), while the storage and vaporisation capacity is large (e.g. 6000 tonnes per day).

- **Small-scale plants**: unlike peak-shaving plants, small-scale plants are connected to a gas grid for the continuous production of LNG on a smaller scale. Liquefaction capacities are usually up to 0.5 MTPA.

- **Offshore plants**: these are floating facilities capable of processing, liquefying and storing natural gas. LNG Floating Production, Storage and Offloading (LNG FPSO) can be applied to liquefy associated gas instead of flaring it or to exploit several small offshore fields.

Liquefaction processes can be classified into three main groups: cascade, Mixed-Refrigerant (MR) and expander- or turbine-based processes [30].

Cascade process

The cascade solution aims at reducing the temperature difference between natural gas cooling curve and refrigerant warming curve by using a series of refrigerants, usually three, in separate loops. In each of the loops the refrigerant vaporises at constant temperature, being a pure substance [37]. This determines the typical ladder shape of the refrigerant warming curve (Figure 2.7).
An example of a cascade process is sketched in Figure 2.5. The pre-cooling cycle uses propane as refrigerant, while ethylene (or ethane) is used for the condensation phase and methane is employed for the sub-cooling zone. Each circuit normally has multi-stage expansion and compression in order to operate at three different evaporation temperature levels [39]. After the expansion each refrigerant is responsible for the cooling of both natural gas and all refrigerant streams.

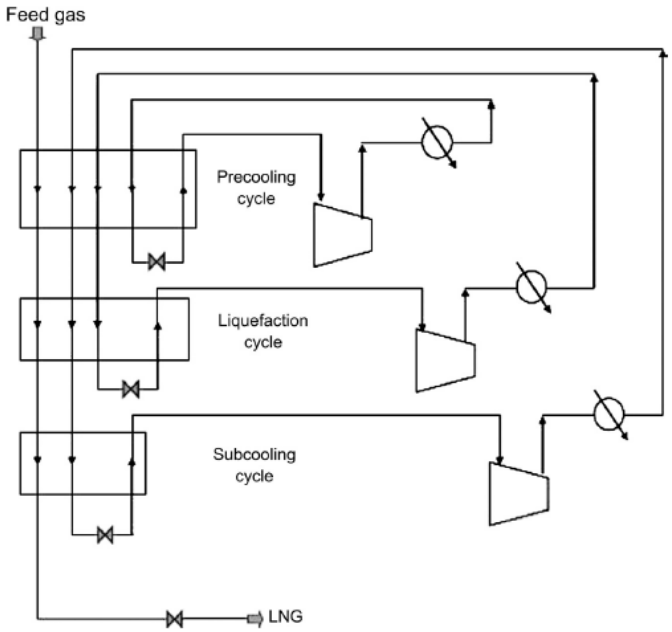

Figure 2.5: Example of a cascade process [37]

Cascade configurations require less power than any other liquefaction cycle. This is mainly due to the lower refrigerant mass flow rate which is employed compared to other cycles. Moreover it guarantees flexible operation as each refrigerant loop can be operated and controlled separately. Compared to MR processes the temperature difference between the Composite Curves is larger, therefore cascade cycle requires less heat exchange area.

The main disadvantage of cascade cycles is the relatively high investment cost due to the number of refrigeration circuits, each one requiring its own compressor and refrigerant storage. Therefore economies of scale impose that cascade solutions are particularly suitable for very high liquefaction capacities, for which the reduction in power consumption and heat exchange surface area can balance the high capital cost of having multiple equipments.

Mixed-Refrigerant process

Mixed-Refrigerant process achieves the cooling of natural gas through the use of a carefully selected mixture of nitrogen and hydrocarbons, which evaporates over a suitable temperature range reproducing natural gas cooling curve. As an example the simplest Mixed-Refrigerant process is sketched in Figure 2.6, known as *PRICO* cycle. *PRICO* cycle is a Single MR (SMR) process. Dual MR (DMR) process uses two independent MR loops, with the heavier hydrocarbon mixture being responsible for the pre-cooling phase [37].
Compared to cascade cycles the smaller temperature difference between the CC's leads to nearly irreversible operation, increased thermodynamic efficiency, reduced power consumption, thus the need for smaller machinery. However MR process usually has lower efficiency than the cascade cycle, mainly due to the higher refrigerant volume flow and its associated irreversibilities [39].

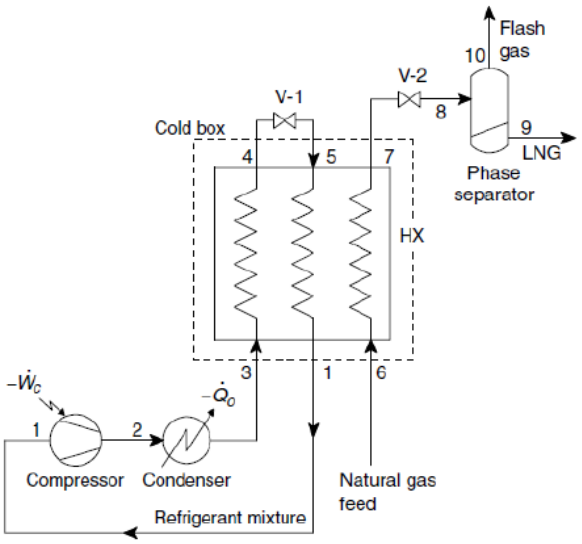

Figure 2.6: Process flowsheet of the Single Mixed-Refrigerant *PRICO* cycle [40]

The main advantages of MR cycles are the reduced number of equipments and their ability to adjust the composition of the refrigerant mixture if natural gas composition varies. Nevertheless this translates into longer start-up time, which can represent an important drawback for those applications requiring frequent start-up and shut-down [37].

Figure 2.7 reports the refrigerant warming profile for the case of propane pre-cooled Mixed-Refrigerant (*C3-MR*) process. As stated by Finn *et al.* [39] for larger MR plants it is cost-effective to implement a pre-cooling cycle using propane. As a consequence, the refrigerant mixture is composed solely of components lighter than propane, i.e. methane and ethane.
Due to its lower thermal efficiency, SMR process is normally suitable for small- and medium-scale applications in which simplicity and low investment cost are decisive factors for the economy of the liquefaction plant.

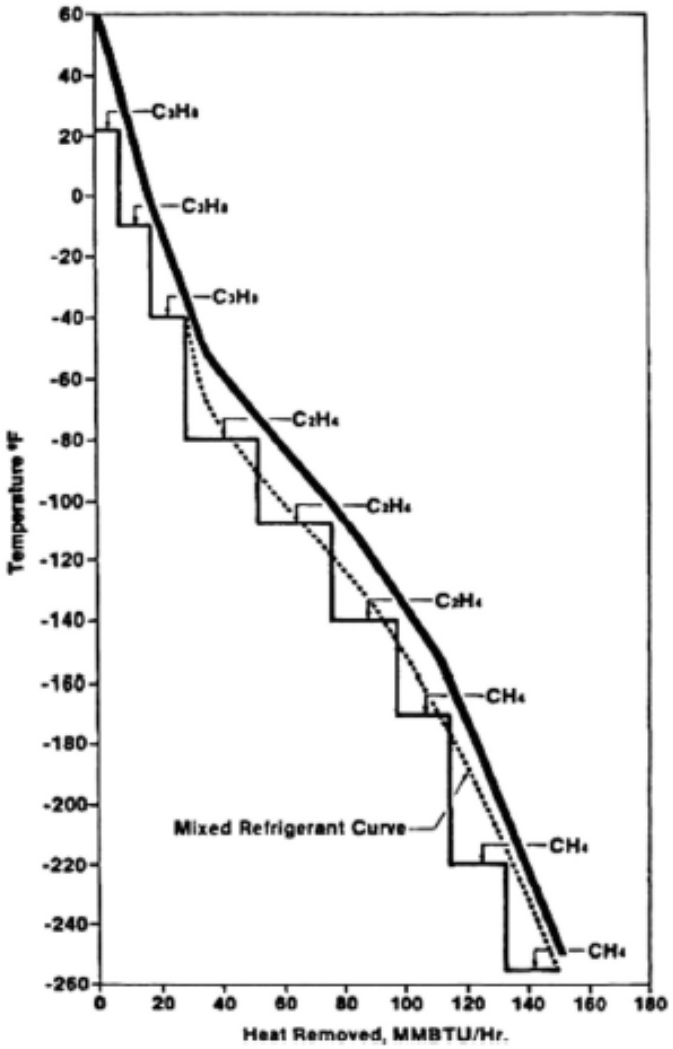

Figure 2.7: Cooling curve for natural gas (continuous thick line) and refrigerant warming curves in the case of cascade process (continuous line) and of propane pre-cooled Mixed-Refrigerant process (dotted line) [37]

Expander-based process

The expander-based process works by compressing and expanding a fluid to generate the required cooling effect. Figure 2.8 shows the sketch of the simplest expander-based cycle. Refrigerant is usually nitrogen or methane. The use of nitrogen allows the sub-cooling of natural gas to temperature levels which are low enough to eliminate the flashing. The CC's are usually characterised by a large temperature difference, typically at the warm end of the natural gas cooling curve [37].

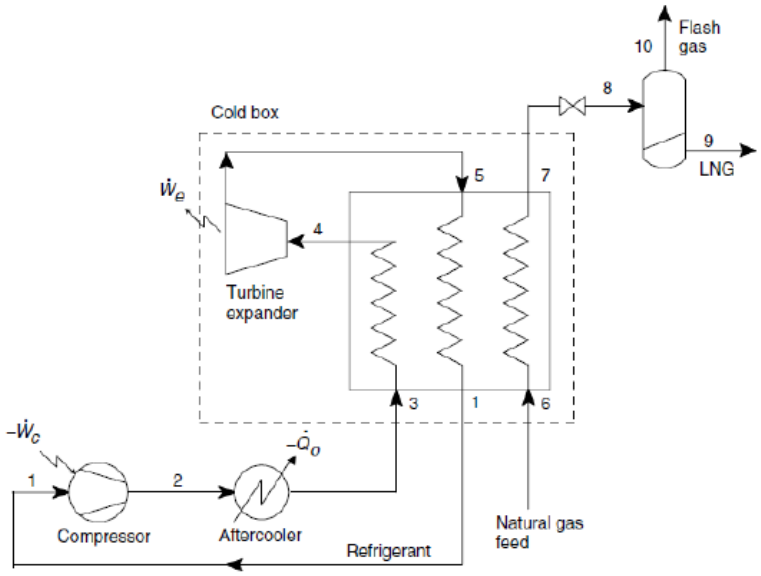

Figure 2.8: Flowsheet example for the expander-based process [40]

As reported by Finn *et al.* [39], the expansion-based cycle presents some advantages over cascade and MR processes. It has a simple design and enables quick start-up and shut-down, making it suitable for peak-shaving applications. The refrigerant is always in the gaseous phase throughout the expansion cycle, hence problems associated with vapour-liquid distribution in heat exchangers are avoided. Since two-phase distributors are not necessary, the cold box is more compact compared to MR processes. Moreover, given the relatively wide temperature difference with which heat exchangers operate, the process tolerates changes in natural gas composition without requiring major changes on the refrigerant side. Finally expander-based cycle is inherently safe as no hydrocarbon storage is required. Its features of simplicity, compactness and safety makes this liquefaction concept attractive also for offshore applications.
The major drawback of expander-based processes is the low efficiency which results in higher power consumption compared to cascade and MR cycles. This is the reason why expander-based liquefaction is not competitive for larger onshore applications, in which simplicity cannot compensate for the higher degree of operating costs.

As a consequence it is essential to decrease the power consumption associated with the expansion-based configuration in order to improve its competitiveness. Several studies can be found in the literature aiming at enhancing the efficiency of expander-based systems. According to He *et al.* [41] it is beneficial to add a natural gas pre-cooling cycle using R410A or propane. As a result, unit energy consumption can be reduced by 23 % and 20 %, respectively. Moreover the use of carbon dioxide for the pre-cooling loop is assessed in [42] and is considered valuable as it allows a reduction of the energy consumption while employing a safe, non-toxic, more environmentally friendly and non-combustible refrigerant. Besides the pre-cooling option, Khan *et al.* [43] show the thermodynamic superiority of a dual expander over a single expander process. Adding a second expansion stage on the refrigerant side improves the efficiency of the expansion-based cycle as it allows to reduce the gap between Hot and Cold Composite Curves.

To sum up, Tables 2.1 and 2.2 are proposed by Finn *et al.* [39] and give an overview of the features of the different liquefaction processes in terms of power consumption relative to the cascade cycle and of design criteria.

Table 2.1: Comparison of liquefaction cycle efficiency [39]

Cycle	**Approximate power consumption relative to cascade cycle**
Cascade	1.00
Single-stage MR	1.25
MR with propane pre-cooling	1.15
Multi-stage MR	1.05
Single expander	2.00
Single expander with propane pre-cooling	1.70
Double expander	1.70

Table 2.2: Liquefaction cycle evaluation [39]

Criteria	**Cascade**	**MR**	**Expander**
Efficiency	High	Moderate/High	Low
Complexity	High	Moderate	Low
Heat exchange area	Low	High	Low
Flexibility	High	Moderate	High

2.2.3 Simulation of natural gas liquefaction cycles

Liquefaction of natural gas is a complex and dynamic thermal process and accuracy in the simulation of LNG configurations is essential for the optimisation of such systems, in order to reach the expected thermodynamic and economic efficiency.
Compression, expansion, throttling and heat transfer processes determine a change in the thermal and physical properties of natural gas and refrigerants. The property method is a thermodynamic model which aim is to predict these changes as well as mixture phase equilibria. Equations of State are the most well-known thermodynamic models. They relate the absolute pressure to the temperature and the molar volume. They can also be formulated as a function of the compressibility factor Z.

Different types of EOS exist ([33],[44]). Cubic Equations of State are applicable over wide ranges of temperature and pressure and are computationally efficient. The term cubic refers to the fact that the volume term is of the first, second and third order. These Equations of State do not consider molecule associative effects, which makes them unsuitable when predicting phase equilibria of natural gas mixtures containing polar components. Examples are Peng-Robinson (PR) EOS and Soave-Redlich-Kwong (SRK) EOS.
A second category comprises the Equations of State of the virial family. They include Benedict-Webb-Rubin-Starling (BWRS) EOS and Lee-Kesler-Plöcker (LKP) EOS. These Equations of State are expressed as a power series of the molar volume in which the virial coefficients account for the interactions between molecules and are usually derived empirically.
Molecular-based Equations of State are derived from perturbation theories to predict molecular interactions in terms of repulsion and associative effects, such as hydrogen bonding. The most widely used EOS within this group is the Perturbated Chain with Statistical Association Fluid Theory (PC-SAFT).
The last category includes empirical multi-parameter Equations of State. The reference EOS for natural gas mixtures is the one developed by the Groupe Européen de Recherches Gazières (GERG) in its 2008 version [45].

Peng-Robinson cubic EOS is the most common property method used in the literature [38]. It can be expressed in terms of compressibility factor Z as shown in Equation 2.2 [42].

$$Z^3 - (1-B)Z^2 + (A - 3B^2 - 2B)Z - (AB - B^2 - B^3) = 0 \tag{2.2}$$

A and B are the dimensionless attractive and repulsive parameters and are determined according to Equations 2.3 and 2.4, in which a and b are constants related to the gas composition.

$$A = \frac{aP}{(RT)^2} \tag{2.3}$$

$$B = \frac{bP}{RT} \tag{2.4}$$

The equivalent formulation of Peng-Robinson EOS as a pressure-temperature-volume relation is given in Equation 2.5 [42].

$$P = \frac{RT}{V-b} - \frac{a}{V(V+b)-b(V-b)} \tag{2.5}$$

Yuan *et al.* [44] show the percentage deviations of experimental and calculated results comparing PR, SRK and LKP Equations of State. They conclude that PR equation is more accurate for the prediction of enthalpy, isobaric specific heat capacity and vapour-liquid equilibrium. On the contrary it performs poorly when evaluating gas density and dew point.

As highlighted in [33] and [44], GERG-2008 property package is the new reference EOS for natural gas mixtures consisting of up to 21 specific compounds. GERG-2008 is the most accurate property method when predicting all the thermodynamic properties and phase equilibria of natural gas mixtures over a wide interval of temperatures and pressures, as the predicted values fall within the range of experimental uncertainties. For instance densities are predicted with a deviation in the range of $\pm(0.06-0.4)$ %, while the uncertainty in the description of isobaric heat capacity at saturated liquid conditions falls within the range of ± 1 %.
Additionally Dauber *et al.* [33] compare the measured data of cooling load and power consumption for the liquefaction plant Snøhvit with Aspen simulation results. The use of GERG-2008 property method leads to deviations significantly lower than 1 % (-0.12 % and -0.65 %, respectively).
The downside of using GERG-2008 model is given by the greater computational requirements. Nevertheless this property method should be used in the field of gas liquefaction modelling and optimisation given its greater accuracy.

3 Methods

This Chapter presents the general methodology on which the thesis is built. It introduces to the reader the tools used in the study. Moreover, following the thesis outline, it describes how the steps of thermodynamic analysis, thermodynamic optimisation and economic analysis are performed.

3.1 Modelling tool

Aspen Plus [46] is the tool which is employed to model and analyse the LNG production configurations under investigation.
Aspen Plus is a commercial software specifically designed for the simulation of oil and gas processes as well as manufacturing facilities of petrochemical, biochemical and polymer industry. It presents a user-friendly interface in which the user can build the process flowsheet by simply dragging the built-in component models and properly linking them using material streams, which are displayed as arrows. Inputs to the model are the individual component specifications and stream composition and physical properties in terms of mass flow, temperature, pressure and vapour fraction. As to the stream composition, the main advantage of Aspen Plus is the possibility to access a library with a wide range of pre-defined chemical compounds.
The software works with a sequential approach, which means that a model is solved following the direction of the material streams and by using as input to a component the calculated output from the previous one.
In the modelling process two flowsheet options are extensively used, namely the transfer and the design specification.

- **Transfer**: this option allows to transfer input information across the flowsheet. Changes in transferred inputs are applied by the software to the streams or blocks where the information is sent to. The possibility of implementing transfers allows to break the cycle loop in the Aspen Plus flowsheet in order to have more computationally efficient simulations.

- **Design specification**: this option allows to obtain a desired value for a flowsheet variable by varying the value of a specific input. The range of allowable variation has to be specified together with a tolerance on the result. Design specifications are typically used for the achievement of Minimum Internal Temperature Approach (MITA) in heat exchangers.

Additionally Aspen Plus gives the possibility to run sensitivity analyses. This model analysis tool requires the definition of the flowsheet variables which have to be returned while varying a specified input within a given interval.

3.1.1 Property methods

Among the different property methods which are comprised in Aspen Plus simulation software, Peng-Robinson cubic EOS is selected, being computational efficient and the most common property method used in the literature [38]. Therefore a consistent benchmark on simulation results can be used.
As pointed out in Chapter 2 Peng-Robinson property method is not the most accurate, being e.g. inferior to GERG-2008. Despite its superiority, GERG-2008 is not chosen as property method for Aspen Plus simulations. The reason for this choice lies on the heavier computational burden and the instability encountered when using this property package. The influence of the chosen property method on the simulation results is assessed and is shown in Appendix A, where the simplest expander-based configuration for natural gas liquefaction is tested using different Equations of State.

3.2 Thermodynamic analysis

The process of natural gas liquefaction requires a refrigeration cycle that removes energy from the natural gas stream in terms of sensible and latent heat. The system works as a closed refrigeration cycle with a net power input and heat rejection to the ambient. The thermal load is distributed over the temperature range of NG flow from ambient to cryogenic LNG temperature.
For a liquefaction system like the one depicted in Figure 3.1 the first law of thermodynamics dictates the following balance:

$$\dot{m}_{\mathrm{NG}}(h_{\mathrm{G}} - h_{\mathrm{L}}) = \dot{Q}_0 - (\dot{W}_{\mathrm{comp}} - \dot{W}_{\mathrm{exp}}) \tag{3.1}$$

where $\dot{m}_{\mathrm{NG}}$ and h are natural gas mass flow rate and specific enthalpy, respectively. $\dot{Q}_0$ is the heat flow which is rejected to the ambient, while $\dot{W}_{\mathrm{comp}} - \dot{W}_{\mathrm{exp}}$ is the net power input to the cycle, i.e. the compressor power minus the expander recoverable power. The expander term $\dot{W}_{\mathrm{exp}}$ is applicable only to those configurations which present a device which can produce work, e.g. a turbo-expander. The term $\dot{W}_{\mathrm{comp}} - \dot{W}_{\mathrm{exp}}$ is considered the power input to the cycle regardless of the compressor-expander system design.

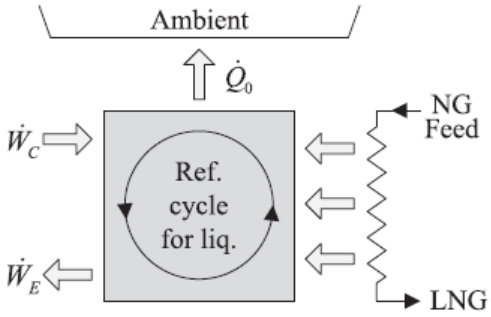

Figure 3.1: Energy and mass flows in a cryogenic refrigeration cycle for NG liquefaction [47]

Alternative to the work-producing expansion is the Joule-Thomson expansion [47]. The expansion process is in this case a throttling process through a flow resistance such as a valve. From the thermodynamic viewpoint this is modelled as isenthalpic, therefore the term $\dot{W}_{\text{exp}}$ in Equation 3.1 is zero.

3.2.1 Turbo-machinery modelling

Compression and work-producing expansion can be modelled through either the isentropic efficiency or the polytropic efficiency [48]. The use of polytropic efficiency is particularly indicated when dealing with compression and expansion processes with varying pressure ratios, for which the isentropic efficiency would not be constant.
In the present study it is chosen to model compression processes with the polytropic efficiency and expansion processes with the isentropic efficiency. The first choice originates from the need to fairly compare different LNG production configurations operating with different pressure ratios. As to the second choice, turbo-expanders can be modelled in Aspen Plus using the isentropic efficiency model only.
A value of 82 % is chosen for the compressor polytropic efficiency. This is in accordance with what was found in the literature. For example in [49] it is stated that current efficiency of centrifugal compressors for liquefaction systems exceeds 80 %, while Finn claims that compressor polytropic efficiency approaching 85 % can be expected [50]. As to the turbo-expander, a value of 85 % is selected for the isentropic efficiency. Again this value is within the current achievable range, with the highest isentropic efficiency approaching 87 - 90 % ([43],[50]).
No mechanical losses are considered, i.e. the mechanical efficiency of turbo-machinery is set equal to 1.

3.2.2 Liquefaction cycle performance evaluation

In order to evaluate the performance of a liquefaction cycle three different indicators can be introduced.
A first possibility is the specific or unit power consumption w, that is the amount of power consumed per unit of produced liquefied gas as in Equation 3.2:

$$w = \frac{\dot{W}_{\text{comp}} - \dot{W}_{\text{exp}}}{\dot{m}_{\text{LNG}}} \tag{3.2}$$

A second possibility is to define the Coefficient of Performance (COP) of the liquefaction cycle, being the ratio of natural gas cooling load to the net power input:

$$\text{COP} = \frac{\left|\dot{Q}_{\text{C}}\right|}{\dot{W}_{\text{comp}} - \dot{W}_{\text{exp}}} = \frac{\dot{m}_{\text{NG}}\,(h_{\text{G}} - h_{\text{L}})}{\dot{W}_{\text{comp}} - \dot{W}_{\text{exp}}} \tag{3.3}$$

From a thermodynamic viewpoint both specific power consumption and COP are unsatisfactory as they do not consider the second law of thermodynamics. The rigorous performance index is the Figure of Merit (FOM) of the liquefaction cycle, being a dimensionless parameter defined by the combined first and second laws of thermodynamics [47].
From the second law the entropy balance of the liquefaction system can be written as in Equation 3.4:

$$\dot{m}_{\text{NG}}(s_{\text{G}} - s_{\text{L}}) + \dot{S}_{\text{gen}} = \frac{\dot{Q}_0}{T_0} \tag{3.4}$$

where s is the specific entropy of the NG stream and T_0 is the reference temperature of the ambient where $\dot{Q}_0$ is rejected, expressed in Kelvin. $\dot{S}_{\text{gen}}$ is the entropy generation rate, which is zero in a reversible system, positive otherwise.
Isolating $\dot{Q}_0$ in Equation 3.1 and substituting in Equation 3.4 yields the following expression for the net power input:

$$\dot{W}_{\text{comp}} - \dot{W}_{\text{exp}} = \dot{m}_{\text{NG}}\left[(h_{\text{L}} - h_{\text{G}}) - T_0\,(s_{\text{L}} - s_{\text{G}})\right] + T_0\,\dot{S}_{\text{gen}} \tag{3.5}$$

From Equation 3.5 it can be inferred that the minimum amount of power input is the one that characterises an ideal reversible system, for which the entropy generation term is equal to zero. The FOM, also called exergetic efficiency ϵ, is therefore defined as the ratio of the minimum power input to the actual power input for the liquefaction system:

$$\epsilon = \frac{\dot{W}_{\text{min}}}{\dot{W}_{\text{comp}} - \dot{W}_{\text{exp}}} = \frac{(h_{\text{L}} - h_{\text{G}}) - T_0\,(s_{\text{L}} - s_{\text{G}})}{\left(\dot{W}_{\text{comp}} - \dot{W}_{\text{exp}}\right)/\dot{m}_{\text{NG}}} \tag{3.6}$$

3.2.3 Exergy analysis

Exergy can be defined as the the amount of useful energy that can be extracted from a process stream when brought to equilibrium with the surrounding ambient through a reversible process [51]. It is a thermodynamic state function which depends solely on the stream enthalpy and entropy. Unlike energy, exergy is not conserved because of system irreversibility.
In the case of flowsheet operations in steady state conditions kinetic and potential exergy can be ignored. Similarly chemical exergy can be disregarded when analysing processes in which no chemical reactions are involved, like in the present study where the stream chemical composition is constant[1]. Under these hypotheses the exergy of a stream at temperature T and pressure P is defined as shown in Equation 3.7, being the so-called physical exergy:

$$\dot{E} = \dot{m}e = \dot{m}\left[\left(h_{(T,P)} - h_0\right) - T_0\left(s_{(T,P)} - s_0\right)\right] \tag{3.7}$$

In the present work reference ambient temperature T_0 is set equal to 20°C (293.15 K), while reference ambient pressure is set equal to the atmospheric pressure.
When a stream is taken from one state to another through a reversible process, the reference terms in Equation 3.7 cancel out and the exergy difference is therefore given as following:

$$\Delta\dot{E}_{1-2} = \dot{m}\Delta e_{1-2} = \dot{m}\left[(h - T_0 s)_{\text{state 2}} - (h - T_0 s)_{\text{state 1}}\right] \tag{3.8}$$

In light of this the nominator in the definition of the exergetic efficiency ϵ in Equation 3.6 represents the specific exergy difference between the NG stream at inlet conditions and the LNG stream at cryogenic conditions. Moreover the term $T_0\dot{S}_{\text{gen}}$ in Equation 3.5 represents the exergy destruction rate, that is the amount of exergy which is lost because of process irreversibility. Equation 3.5 can therefore be reformulated as following:

$$\dot{E}_{\text{F}} = \dot{E}_{\text{P}} + \dot{E}_{\text{D}} \tag{3.9}$$

Equation 3.9 can be regarded as a general exergy balance stating that the difference between the exergy fuel or input and the exergy product is what is lost due to thermodynamic irreversibility.
In the present study the exergy destruction rate is calculated for all the process components by applying an entropy balance as the one presented in Equation 3.4 and subsequently multiplying the entropy generation term by the reference ambient temperature T_0 expressed in Kelvin.
In order to visualise how the different components contribute to the total exergy destruction, individual exergy destructions are divided by the exergy input to the cycle, that is the net power consumption, $\dot{W}_{\text{comp}} - \dot{W}_{\text{exp}}$[2].

[1] It must be underlined that in a liquefaction process a change in natural gas chemical composition could take place after the flashing and separation of the liquid and gaseous phases. Therefore chemical exergy should be considered. Nevertheless in the present study the boundaries for the exergy analysis are placed before the flashing. Under these conditions, the chemical composition of natural gas is constant.

[2] In this thesis report there is no distinction between mechanical power and mechanical work, as all the thermodynamic models are built for a unitary mass flow of feed natural gas.

Following the definition given by Kotas [52] the individual component rational efficiency defect δ is therefore defined as described in Equation 3.10.

$$\delta_{\mathrm{i}} = \frac{\dot{E}_{\mathrm{D,i}}}{\dot{E}_{\mathrm{F}}} = \frac{T_0 \dot{S}_{\mathrm{gen,i}}}{\dot{W}_{\mathrm{comp}} - \dot{W}_{\mathrm{exp}}} \tag{3.10}$$

The sum of individual efficiency defects δ_i and the cycle FOM is unitary:

$$\epsilon + \sum \delta_i = 1 \tag{3.11}$$

3.3 Thermodynamic optimisation

Optimisation is the mathematical process of finding the optimal value of an objective function (either the maximum or the minimum) by manipulating the decision variables within a feasible region defined through constraints.
Optimisation algorithms can be classified in deterministic and stochastic or non-deterministic [38]. Due to the high degree of non-linearity and non-continuity of thermodynamic systems, the use of stochastic algorithms is preferable as it decreases the possibility of finding a local optimum instead of the global one [53].
In the presents study a Genetic Algorithm (GA) is used for the optimisation process. Genetic Algorithms were developed by John Holland in the 1960s as means of importing the mechanisms of natural adaptation into numerical optimisation [54]. By analogy a solution represents an individual in a population and a new generation of individuals is used in the following iteration [55]. The new generation solution shares some of the features of the parent solutions and through the constraint definition only apt generations are conserved by the algorithm. The first set of the individual solution is generated randomly to cover the solution domain.

The optimiser which is employed in the present study is constituted by a set of Matlab [56] scripts and is provided by Postdoc Tuong-Van Nguyen. Matlab is used as interface between the optimiser and Aspen Plus and the optimisation procedure can be summarised as following:

1. all the relevant inputs are defined in Matlab and sent to Aspen Plus;
2. Aspen Plus model is run and the results are sent to Matlab;
3. the objective function is evaluated and a new generation of inputs is created accordingly.

The parameter which defines the magnitude of the randomly-generated initial solutions is the *initial population size* in the Matlab code. The number of iterations is defined by the *evaluation* parameter, that is the number of generations which are developed by the algorithm. The higher the number of points and mutations is, the more accurate the results can be expected. The drawback is the heavier computational effort. Therefore algorithm parameters were decided depending on the complexity of the investigated model seeking for a compromise between accuracy and computational burden.

The constraint definition is handled by transforming the problem into an unconstrained one but subjected to penalty functions. The role of the penalty functions is to deliberately assign a value to the objective function such that the algorithm disregards the solution whenever this implies the violation of thermodynamic limits (e.g. heat exchange feasibility) or technical limits (e.g. presence of liquid droplets at the compressor inlet).

In this thesis report two optimisation problems are addressed, namely Single-Objective Optimisation (SOO) and Multi-Objective Optimisation (MOO).
A SOO deals with the finding of the objective function's optimal value, therefore the solution is unique. The goal of the Single-Objective Optimisations which are performed within this project is the minimisation of net power input to the analysed liquefaction cycles. This is equivalent to the maximisation of the cycle COP and FOM, as it can be inferred from the relations presented in Section 3.2.2, once natural gas properties are kept constant.
A MOO consists of an optimisation problem in which several objective functions should be optimised simultaneously. With respect to the present study two objectives are considered, namely the minimisation of net power consumption and the minimisation of heat transfer area. The two objectives are conflicting as a lowered power consumption can be achieved when decreasing the temperature difference at the heat exchangers, thus resulting in an increase of the heat exchange area. Therefore there is no unique solution but there exists a potentially infinite set of Pareto-optimal solutions. A solution is called Pareto-optimal if "*any better-off for one objective results in a worse-off for the other one*" [55]. The set of solutions can be visualised in the form of a Pareto-optimal frontier (as in Figure 3.2).

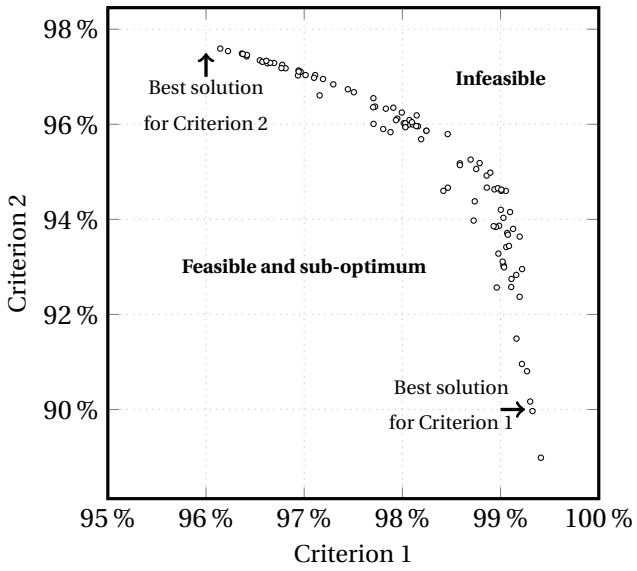

Figure 3.2: Example of Pareto-optimal frontier [55]

3.4 Economic analysis

Discounted Cash Flow (DCF) analysis is applied in order to evaluate the economy of LNG production configurations [57]. By using this method the time value of money is taken into account through the discounting of future cash flows which therefore have a lower value than present ones.
The adopted approach for the Discounted Cash Flow analysis falls within the private economic perspective. A discount rate of 8 % is assumed. It reflects the cost of capital and it includes inflation and industry-specific risks.
For a natural gas liquefaction facility the main economic elements are the following:

- **Total Capital Investment** (TCI), that is the initial investment comprising the cost of equipment and the ancillary cost for plant installation. It is assumed to occur at once before the plant can be operated (year 0);
- **Operation and Maintenance cost** (O&M) including electricity cost, feed natural gas cost, refrigerant cost and maintenance cost. It is considered as a negative cash flow occurring at the end of every year of operation;
- **Revenue** from LNG sales. It is handled as a positive cash flow occurring at the end of every year of operation.

For the sake of simplicity tax calculation and financial considerations are disregarded.

3.4.1 Economic performance indicators

The economic performance indicators used to compare different LNG production configurations are three, namely Unitary Profit (UP), Net Present Value (NPV) and the Adjusted Pay-Back Time (APBT).

1. **Unitary Profit** is defined as the profit per mass unit of produced LNG. It is calculated on an yearly basis as the ratio of the annual profit to the yearly LNG production.
   The analysis on a yearly basis is possible since all the annual cash flows are the same, i.e. no changes in plant operation are considered which could modify the power requirement and LNG production rate.
   The initial investment is annualised using the so-called PMT factor defined as following:

$$\mathrm{PMT} = \frac{i}{1-(1+i)^{-\mathrm{LT}}} \tag{3.12}$$

   The annualised investment cost is then calculated as the TCI times the PMT factor. This is summed to the yearly O&M cost to give the total annual cost. Yearly profit is finally computed as the yearly revenue minus the total annual cost.
   Discount rate i is 8 %, while a lifetime (LT) of 40 years is assumed for LNG production plants according to the Danish Maritime Authority [10].

2. **Net Present Value** is calculated as the sum of the Discounted Cash Flows over the LNG project lifetime minus the initial investment.

$$\mathrm{NPV} = -\mathrm{TCI} + \sum_{n=1}^{\mathrm{LT}} \frac{\mathrm{CF}_n}{(1+i)^n} \tag{3.13}$$

   A project yielding a negative NPV should be rejected as economically infeasible. When comparing different projects with positive NPV, the one with the highest NPV should be preferred.

3. **Adjusted Pay-Back Time** is calculated considering the Cumulative Discounted Cash Flow (CDCF), meaning that the Discounted Cash Flows should be summed from the beginning of the project until the respective year. As soon as this cumulative sum becomes zero, the investment is earned back.
   APBT is calculated as following:

$$\mathrm{APBT} = n_{\mathrm{CDCF}^-} - \frac{\mathrm{CDCF}^-}{\mathrm{CDCF}^+ - \mathrm{CDCF}^-} \tag{3.14}$$

   where n_{CDCF^-} is the last year characterised by a negative Cumulative Discounted Cash Flow, CDCF^- is the last negative Cumulative Discounted Cash Flow and CDCF^+ is the first positive.
   It should be noted that calculating the Adjusted Pay-Back Time as in Equation 3.14 introduces an approximation since the Cumulative Discounted Cash Flows are not linear. This is anyhow accepted as it allows to take into consideration the time value of money also when giving an estimation of the time required to return from the initial investment.

4 Thermodynamic modelling of expander-based LNG configurations

The first phase of this thesis project deals with the development of thermodynamic models for the investigated expander-based configurations. Thermodynamic modelling represents the basis for all the subsequent steps and analyses, e.g. thermodynamic optimisation and economic evaluation. This Chapter presents the developed models and gives an overview of their features with the aim to show how the system performance can be improved.

4.1 Introduction

In the attempt to make expander-based liquefaction cycles more efficient several configurations have been developed and extensively analysed in the literature. For the purpose of this thesis report they can be grouped into four main categories as following.

- **Single-expander configurations** ([26], [43], [58], [59]): nitrogen expansion process takes place in one single stage, whereas the compression process can be designed in one single stage or realising an inter-cooled multi-stage compression with the possibility of coupling a booster compressor with the expander. These configurations represent the simplest expander-based alternatives and are the least efficient given the wide range between the temperature profiles of natural gas and refrigerant.

- **Pre-cooling configurations** ([41], [42]): with respect to the single-expander cycle layout a pre-cooling step is added. Different refrigerants can be employed, e.g. R410A, propane (R290) and CO_2 (R744). Substantial reductions in unit energy consumption are achieved in the literature, reaching 20 % - 23 %. He *et al.* identify R410A as the most effective pre-cooling refrigerant.

- **Dual-expander configurations** ([43], [58], [60]): the expansion process takes place in two stages. Expanders can be arranged in several designs, e.g. being in parallel with a different or the same pressure ratio or being connected in series.

- **Dual-refrigerant configurations** ([58], [61], [62]): two single-expander cycles are implemented employing different refrigerants, i.e. nitrogen and methane, with the latter being claimed to be more efficient than the former for the pre-cooling and liquefaction phases. Furthermore natural gas itself can be used as refrigerant. The so-called *Niche* technology by *Statoil* [63] is based on this concept.

The developed models are presented and analysed according to this categorisation. The aim of the modelling stage is to thoroughly understand the behaviour of expander-based cycles, to quantify the main thermodynamic parameters and to investigate how the thermodynamic efficiency can be improved. In the perspective of the optimisation problem, this Chapter provides the bases for setting a sensible research space.

4.2 Methodology and relevant assumptions

The modelling process is performed using Aspen Plus simulation software. The adopted approach comprises the three following elements:

1. axial thermal equilibrium is assumed for all the heat exchange devices, i.e. hot streams are assumed to have the same temperature along the heat exchange process. As a consequence outlet hot streams have the same temperature;
2. the Minimum Internal Temperature Approach (MITA) is required to be 3 K for all the heat exchangers;
3. refrigerant always has to be in the gaseous phase, i.e. refrigerant vapour fraction always has to be unitary or "above" (super-heated vapour conditions).

All heat exchange processes are modelled as isobaric, i.e. pressure drops are neglected. Heat losses and gains are disregarded, as well as longitudinal heat conduction. Heat exchange process is simulated in Aspen through a discretisation of the heat exchangers into zones in which properties are assumed constant, according to a lumped approach per zone [64].
Natural gas enters the liquefaction cycle at 20°C and at 33 bar and is cooled down to -150°C. Its pressure is later reduced to 1.7 bar through a throttling valve. Subsequently an adiabatic flash allows to separate the LNG from off-gas. All the models are developed for a mass flow rate of 1 kg/s on natural gas side.
Natural gas feed composition is suggested by *Kosan Crisplant A/S* and is reported in Table 4.1 in terms of molar fractions. It corresponds to the Danish grid natural gas composition after CO_2 removal.

Table 4.1: Base case for natural gas molar composition as suggested by *Kosan Crisplant A/S*

CH_4	C_2H_6	C_3H_8	n-C_4H_{10}	i-C_4H_{10}	n-C_5H_{12}	i-C_5H_{12}	N_2
0.903	0.060	0.024	0.006	0.004	0.000	0.000	0.003

4.2.1 Model inputs and decision variables

In the design process a series of decision variables has to be set. For an expander-based liquefaction cycle the usual decision variables comprise the cycle pressure levels, the refrigerant's (or refrigerants') flow rate and the intermediate temperature levels.
Temperature approaches at the heat exchangers are achieved using Aspen Plus design specifications. In an iterative process the specified model variable is changed within a given interval until the 3 K-approach is obtained. This modelling procedure makes the involved variable a model output.
For each of the presented models, inputs will be stated as well as the decision variables governing the temperature approaches. Input values are generally set according to the relevant literature mentioned above.

4.2.2 UA-value calculation

The UA-values of two-stream and Multiple-Stream Heat Exchangers are directly given as output from Aspen Plus simulation. The same applies for the Logarithmic Mean Temperature Difference (LMTD), obtained as the ratio of exchanger heat duty to the UA-value. LMTD is an average based on the discretisation of the heat exchange device into zones, as mentioned above.
Conversely for coolers, i.e. for those heat exchange blocks with one single heat transfer stream, the UA-value has to be post-computed given specific assumptions on the secondary side fluid. In the present work it is assumed that cooling water is employed as secondary side fluid for all the coolers. Given the fact that the refrigerant temperature at cooler outlets is always set equal to 20°C, water is set to enter the coolers at 10°C. It is also assumed that water outlet temperature is 40°C. Therefore the Logarithmic Mean Temperature Difference is calculated as following:

$$\mathrm{LMTD} = \frac{\left(T_{\mathrm{ref}}^{\mathrm{in}} - 40\right) - \left(T_{\mathrm{ref}}^{\mathrm{out}} - 10\right)}{\ln\left(\frac{T_{\mathrm{ref}}^{\mathrm{in}} - 40}{T_{\mathrm{ref}}^{\mathrm{out}} - 10}\right)} \tag{4.1}$$

If the refrigerant temperature at the cooler inlet is lower or equal than 50°C, a LMTD of 10 K is applied.
The cooler UA-value is finally calculated as the ratio between heat load and LMTD.

$$UA = \frac{\left|\dot{Q}\right|}{\mathrm{LMTD}} \tag{4.2}$$

4.3 Natural gas liquefaction process

Figure 4.1 illustrates the Pressure-Temperature phase envelope for the considered natural gas feed composition together with the overall liquefaction process, divided in isobaric cooling and isenthalpic expansion through the throttling valve.

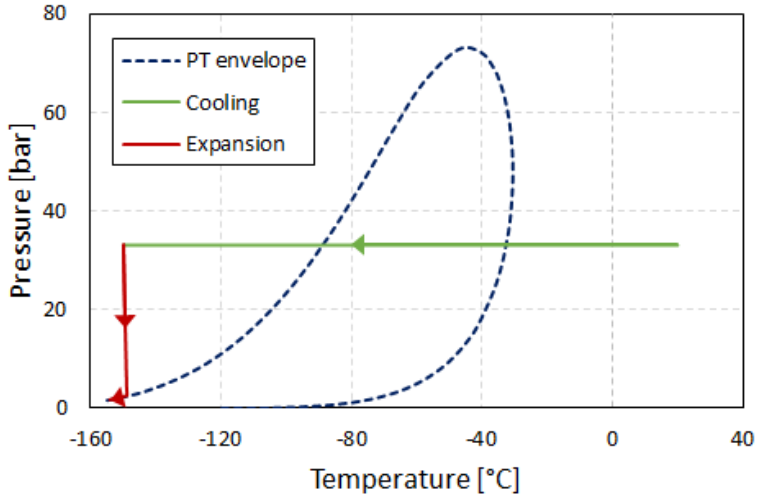

Figure 4.1: P-T diagram of the natural gas liquefaction process together with the natural gas phase envelope obtained from Aspen Plus using Peng-Robinson EOS

As aforementioned natural gas exits the cold box at -150°C and at 33 bar. After the flashing a two-phase mixture is generated characterised by a mass vapour fraction of 3.9 %. After the separation process LNG mass flow rate results 0.964 kg/s, hence the liquefaction rate is 96.4 %. LNG composition is reported in Table 4.2 in terms of molar fractions.
Natural gas total cooling load results equal to 793.3 kJ per kg of NG feed, of which the latent fraction amounts to 436.9 kJ/kg. Dew point is at -32.8°C, while bubble point is at -89.1°C.

Table 4.2: Molar composition of the output Liquefied Natural Gas

CH_4	C_2H_6	C_3H_8	n-C_4H_{10}	i-C_4H_{10}	n-C_5H_{12}	i-C_5H_{12}	N_2
0.900	0.063	0.025	0.006	0.004	0.000	0.000	0.002

4.4 Single-expander configurations

4.4.1 Single compression stage

The single-expander configuration with one compression stage is sketched in Figure 4.2. Refrigerant consists of pure nitrogen and enters the cold box at 20°C and 120 bar (state point 7). The cooling effect is generated through the expansion process of the refrigerant stream. Expander discharge pressure is fixed at 10 bar. Cold nitrogen (state point 9) cools down the natural gas feed at the two-stream Heat Exchanger (HEX 2) and the natural gas feed and the hot nitrogen stream in the Multiple-Stream Heat Exchanger (MHEX 1).

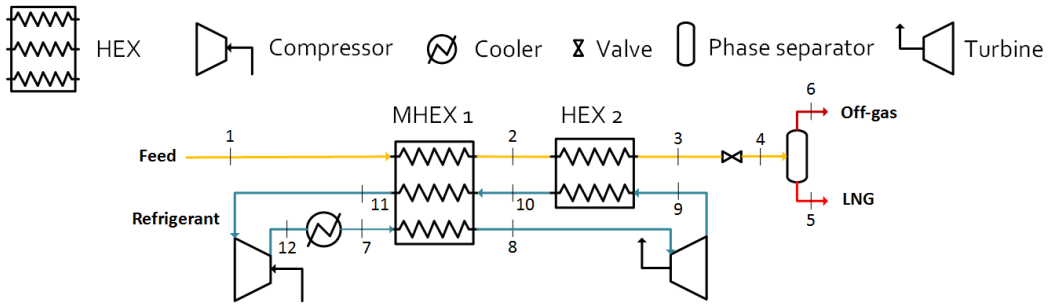

Figure 4.2: Process flowsheet of the single-expander configuration with one compression stage

The temperature approach at the Multiple-Stream Heat Exchanger is controlled by the refrigerant mass flow rate, whereas the approach at the two-stream Heat Exchanger is controlled by the expander inlet temperature.
Figure 4.3 shows refrigerant thermodynamic state points in a Temperature-Entropy diagram[1] together with the values of temperature, pressure and specific enthalpy listed on the right.
Results show that the necessary N_2 flow rate is equal to 7.48 kg/s. Correspondingly compression and expansion power are 3130 kW and 635 kW, respectively. Total heat duty results equal to 1402 kW (769 kW at the MHEX and 633 kW at the two-stream HEX). The UA-value is 59.9 kW/K for the MHEX and 29.2 kW/K for the HEX. The calculated UA-value for the cooler amounts to 3.3 kW/K giving an overall heat network conductance of 91.4 kW/K.
Table 4.3 summarises the simulation results and reports the performance indicators of the liquefaction cycle, namely COP, unit energy consumption and Figure of Merit. Moreover Figure 4.4 depicts the Composite Curves for the liquefaction cycle. Exchanged heat flow is reported on the x axis as a percentage of the total.

[1] The software EES [65] is used to draw refrigerants' cycles. For the sake of consistency and only for graphical representations the listed specific enthalpies are the ones given by EES. They differ from the values given by Aspen Plus due to differences in thermodynamic references. Values of heat, power and exergy flows are always calculated using Aspen Plus specific enthalpies and entropies. The reader should be aware that small deviations in Δh and Δs (lower than 1 %) are encountered when comparing the values provided by the two tools.

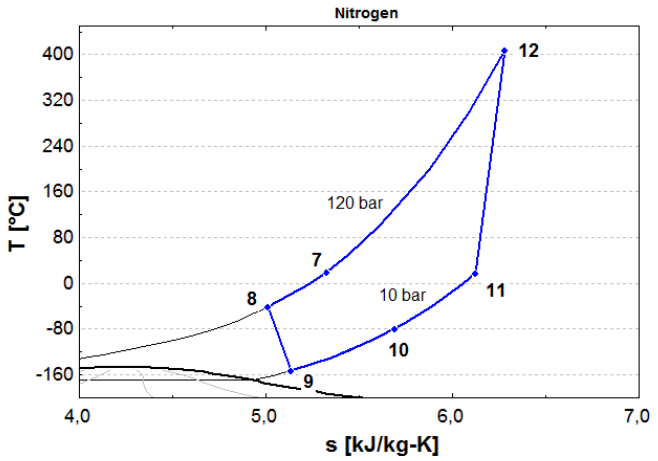

	T [°C]	P [bar]	h [kJ/kg]
7	20.0	120	280.4
8	-41.5	120	199.6
9	-153.0	10	111.1
10	-78.9	10	196.3
11	17.0	10	298.8
12	407.5	120	717.7

Figure 4.3: Representation of the T-s refrigerant cycle. Values of temperature, pressure and specific enthalpy are listed on the right

Table 4.3: Main results and performance indicators for the single-expander cycle with one compression stage

$\dot{W}_{net}$ [kW]	Total UA-value [kW/K]	COP [-]	w [kJ/kg$_{LNG}$]	FOM [%]
2495	91.4	0.318	2588	17.04

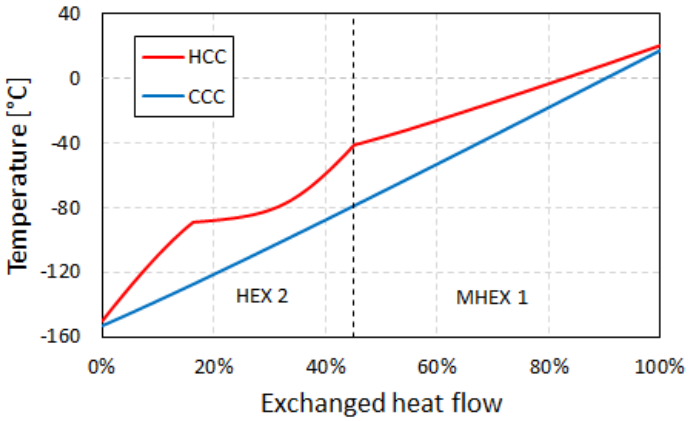

Figure 4.4: Hot and Cold Composite Curves for the single-expansion cycle with one compression stage

The temperature profiles show that the pinch point is activated at the cold box ends. More specifically the 3 K-approach is found at the cold end of the HEX and at the hot end of the MHEX. N_2 temperature at the expander inlet is -41.5°C. For the first heat exchange section (feed NG from 20°C to -41.5°C) LMTD is 13.1 K, while for the second section LMTD is 21.7 K.

4.4.2 Two compression stages

The single-expansion cycle design can be improved by adding a second compression stage in the refrigerant loop leading to an inter-cooled two-stage compression. Two possibilities are investigated. In the first, Low-Pressure (LP) compressor is not mechanically coupled with the expander, therefore its discharge pressure is a model variable. Conversely the second alternative considers the mechanical coupling between LP compressor and the expander, thus the intermediate pressure level is constrained. Mechanical coupling is advantageous as no driving equipment for the Low-Pressure compressor is needed.

The first two-stage compression cycle design is sketched in Figure 4.5. The same conditions are applied on the refrigerant side in terms of high and low pressure level and of cold box inlet temperature. Approaches at the MHEX and at the HEX are controlled by the same model variables as for the previous case.

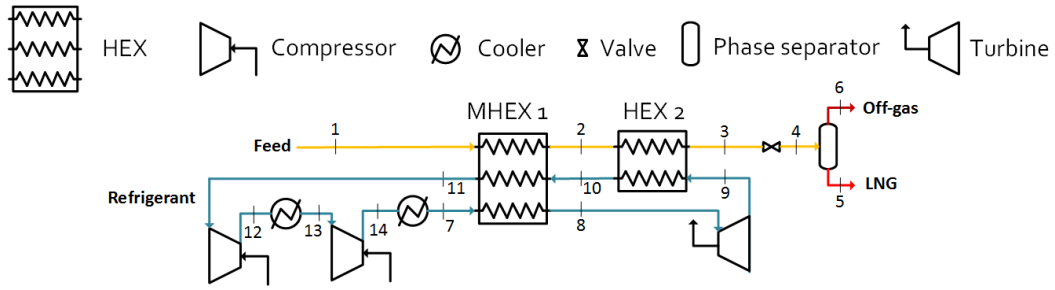

Figure 4.5: Process flowsheet of the single-expander configuration with two compression stages without mechanical coupling between LP compressor and expander

When no mechanical coupling is implemented, an optimal value for the intermediate pressure level can be found given the trade-off between Low-Pressure and High-Pressure (HP) compressor power consumption. This trade-off is highlighted in Figure 4.6. The optimal intermediate pressure level results equal to 35.7 bar and is therefore implemented in the model. This value is close to the geometric mean of high and low pressure levels, which is a frequently applied approximation for the optimum intermediate pressure in two-stage compression systems [66]. As a result Figure 4.7 shows the refrigerant thermodynamic state points in a Temperature-Entropy diagram together with the corresponding values of temperature, pressure and specific enthalpy.
Compression power consumption is 1260 kW for the LP compressor and 1210 kW for the HP compressor. Expander power production is 635 kW. With respect to the single-expansion cycle with one compression stage no differences are found in the heat exchange process. On the contrary heat rejected at the coolers is significantly lower than in the single-compression case (2628 kW against 3288 kW) due to the lower refrigerant temperature at compressor outlets. Calculated UA-values are 26.3 kW/K for the first cooler and 28.1 kW/K for the second. Total heat network conductance results equal to 142.5 kW/K.

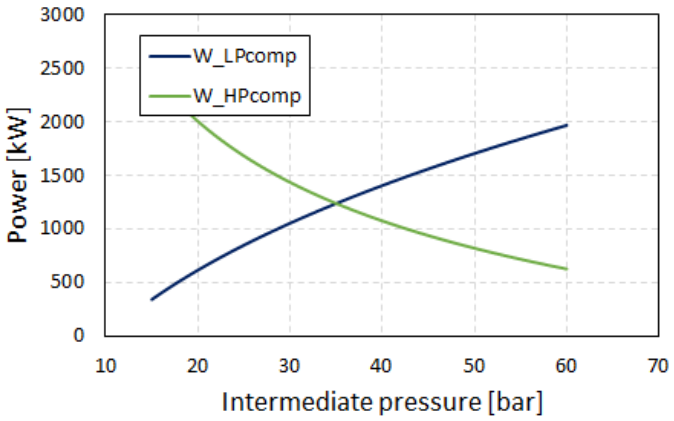

Figure 4.6: Trade-off between Low-Pressure and High-Pressure compressor power consumption

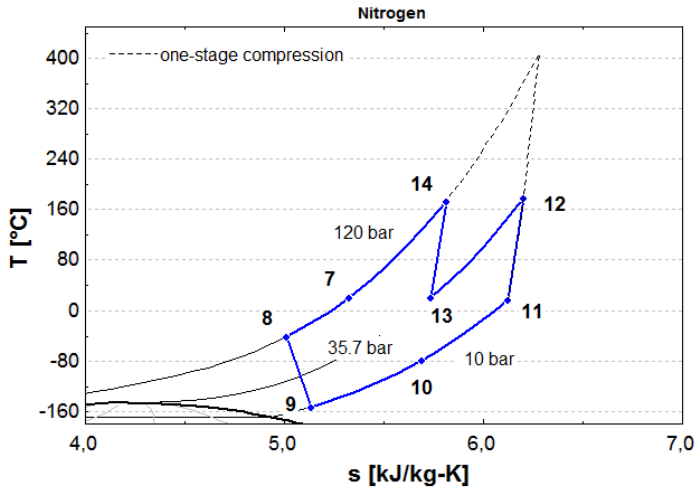

	T [°C]	P [bar]	*h* [kJ/kg]
7	20.0	120	280.4
8	-41.5	120	199.6
9	-153.0	10	111.1
10	-78.9	10	196.3
11	17.0	10	298.8
12	178.6	35.7	467.4
13	20.0	35.7	296.3
14	173.9	120	458.4

Figure 4.7: Representation of the T-s refrigerant cycle. Values of temperature, pressure and specific enthalpy are listed on the right. The dotted line in the T-s diagram refers to the refrigerant cycle in the single-compression case and shows how the net work input to the cycle is reduced by introducing an inter-cooled two-stage compression process

The two-stage compression cycle shows a better performance compared to the single-expander configuration with one compression stage. Net power consumption is 1835 kW. Correspondingly the cycle FOM is 23.17 %. This significant improvement is due to the inter-cooled two-stage compression which allows to reduce the new work input to the cycle, bringing the adiabatic compression closer to an isothermal one. This effect can be spotted in the T-s diagram of Figure 4.7 by comparing the present cycle with the single-compression one (black dotted line).

The second two-stage compression alternative is characterised by the mechanical coupling between the expander and LP compressor. This is depicted in Figure 4.8. The intermediate pressure level is no more a model variable but is instead calculated through a design specification imposing that the absolute values of expander and LP compressor power coincide.

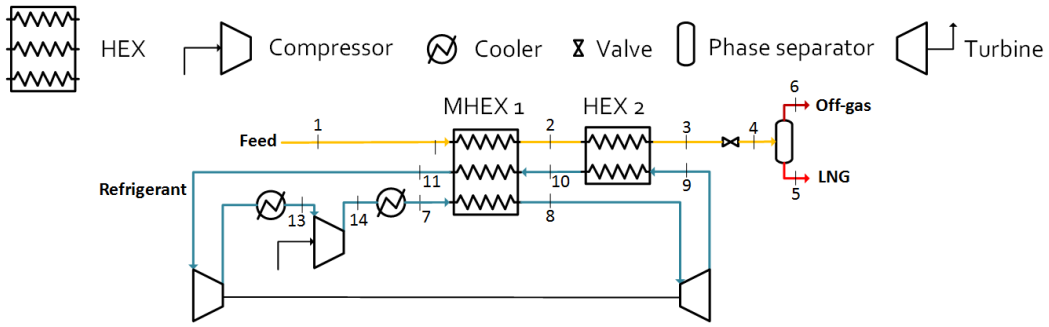

Figure 4.8: Process flowsheet of the single-expander configuration with two compression stages with mechanical coupling of LP compressor and expander

The intermediate pressure level results equal to 20.4 bar. Correspondingly the T-s transformations on nitrogen side are depicted in Figure 4.9.

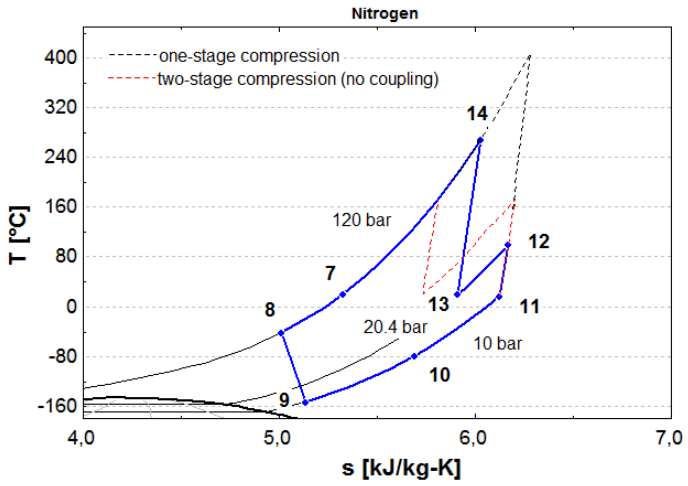

	T [°C]	P [bar]	*h* [kJ/kg]
7	20.0	120	280.4
8	-41.5	120	199.6
9	-153.0	10	111.1
10	-78.9	10	196.3
11	17.0	10	298.8
12	99.0	20.4	383.9
13	20.0	20.4	299.6
14	268.4	120	563.2

Figure 4.9: Representation of the T-s refrigerant cycle. Values of temperature, pressure and specific enthalpy are listed on the right. The dotted lines refer to the one-stage compression cycle (black) and two-stage compression cycle without mechanical coupling (red)

Given the lower intermediate pressure level compared to the previous case, heat rejected at the first cooler is lower (633 kW against 1286 kW), while heat rejected at the second cooler is higher (2131 kW compared to 1342 kW). The total heat rejection increases being 2764 kW. The first cooler UA-value results 22.9 kW/K while the UA-value for the second cooler is 30.5 kW/K.

Once again the design of the compression process does not affect the liquefaction part of the cycle. The temperature profiles are unaltered as well as the refrigerant mass flow rate, UA-values and LMTD's at the cold box.
Table 4.4 reports the comparison between the two-stage compression cycles. It can be seen that net power consumption for the case with mechanical coupling is slightly higher compared to the case with no mechanical coupling. This is expected as the constraint on Low-Pressure compressor power forces the intermediate pressure level to be sub-optimal.

Table 4.4: Main results and performance indicators for the single-expander cycle with two compression stages in the cases of no mechanical coupling and with mechanical coupling

	$\dot{W}_{net}$ [kW]	Total UA-value [kW/K]	COP [-]	w [kJ/kg$_{LNG}$]	FOM [%]
No mechanical coupling	1835	142.5	0.432	1904	23.17
With mechanical coupling	1970	141.5	0.403	2043	21.59

4.4.3 Sensitivity analyses

A series of sensitivity analyses is performed on the single-expander configuration with one compression stage to assess how input parameters affect the system performance. Investigated inputs are NG feed temperature, pressure and composition and turbo-machinery efficiency. The main outcomes are summarised in this Section. The interested reader can find the detailed results as well as the specific approaches in Appendix B.

- **Natural gas feed temperature**: net power consumption is found to be decreasing as the feed temperature decreases. Moreover results show that the temperature approach can be achieved at both ends of the cold box for feed temperatures below 24°C. Above this threshold there has to be a simultaneous change in nitrogen flow rate and cold box inlet temperature.
- **Natural gas feed pressure**: net power consumption decreases as the feed pressure increases. Conversely Figure of Merit and liquefaction rate are negatively affected, the former due to a larger mean temperature difference at the cold box.
- **Natural gas feed composition**: cooling load and net power consumption are found to increase as the methane fraction in the natural gas mixture increases. The minimum cooling load and power consumption are recorded for a mixture rich in nitrogen. Nevertheless unit energy consumption is large due to the considerably lower liquefaction rate, as most of the nitrogen content is flashed.
- **Turbo-machinery efficiency**: results show that it is more beneficial to improve the expander as the performance of the expansion process does not affect solely the amount of recoverable work, but also compressor power consumption through the influence on the required refrigerant flow rate.

4.5 Pre-cooling configurations

The single-expander cycle with pre-cooling is depicted in Figure 4.10. With respect to the single-expander case a pre-cooling cycle is added before the cold box. This additional cycle is a standard single-stage refrigerating cycle with the aim of pre-cooling nitrogen and the natural gas feed.

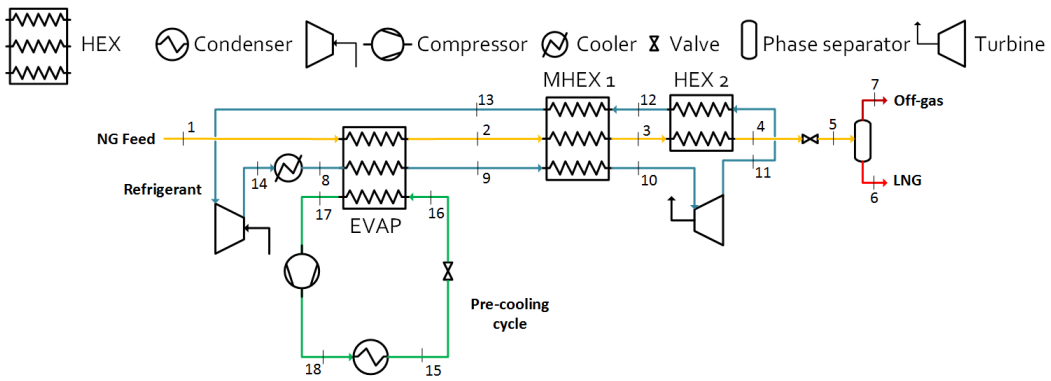

Figure 4.10: Process flowsheet of the single-expander configuration with pre-cooling cycle

For the pre-cooling cycle four different refrigerants are considered, namely R410A, propane and CO_2, the latter both in a sub-critical and in a super-critical cycle. R410A has to be defined in Aspen Plus as a mixture composed for half by CH_2F_2 and for the other half by CHF_2CF_3 on a molar basis.
In all these cases refrigerant stream enters the throttling valve at 20°C and the refrigerant high pressure level is set so that no sub-cooling is present, i.e. the vapour fraction at condenser outlet is 0. This design choice results in the following high pressure levels to be implemented in the Aspen models:

- **R410A**: 13.98 bar
- **Propane**: 8.37 bar
- **CO_2**: 57.35 bar

For the super-critical CO_2 case a high pressure level of 80 bar is assumed.
Pre-cooling temperature, i.e. the nitrogen and NG feed temperature at evaporator outlet, is set equal to -20°C. As to the nitrogen loop, high pressure level is 120 bar while expander discharge pressure is 10 bar.
Concerning the total UA-value calculation, the condenser (or gas cooler in the super-critical CO_2 case) is treated as a cooler having water as secondary-side heat exchange fluid.

The following design specifications are applied in order to achieve the 3 K-MITA in all the heat exchangers:

- **evaporator**: the cold-end approach is governed by the refrigerant low pressure, i.e. by the outlet pressure of the throttling valve, whereas the hot-end approach is governed by the refrigerant mass flow rate. This condition implicitly defines the super-heating temperature difference at the evaporator;
- **MHEX 1**: as for the previously presented models the approach is achieved by varying nitrogen mass flow rate;
- **HEX 2**: again the approach is imposed by varying nitrogen temperature at the expander inlet.

Once the pre-cooling temperature is fixed, no difference is recorded in the nitrogen cycle when varying the type of refrigerant used in the pre-cooling phase. In particular nitrogen mass flow rate results 6.05 kg/s and its temperature at the expander inlet is -41.5°C. Compression power is 2185 kW while expander power is 515 kW. The cold box heat duty amounts to 878 kW, of which 245 kW at the Multiple-Stream Heat Exchanger.
As a consequence the overall liquefaction cycle performance depends on the performance of the pre-cooling cycle. Table 4.5 reports the comparison between the different pre-cooling cycles in terms of refrigerant mass flow rate, low pressure level, power consumption and COP[2]. Furthermore Table 4.6 reports the value of net power consumption and heat network conductance for the four liquefaction cycles and the corresponding performance indicators.

Table 4.5: Comparison of pre-cooling cycles in terms of refrigerant mass flow rate, low pressure level, evaporator cooling load, power consumption and COP

	$\dot{m}_{ref}$ [kg/s]	P_{low} [bar]	$\dot{Q}_{ev}$ [kW]	$\dot{W}_{PC}$ [kW]	COP_{PC} [-]
R410A	2.3	3.5	409	112	3.65
Propane	1.1	1.1	409	104	3.91
Sub-critical CO_2	1.9	17.6	409	157	2.60
Super-critical CO_2	1.8	17.6	409	197	2.07

Table 4.6: Comparison of liquefaction cycles in terms of net power consumption, total heat network conductance, COP, unit energy consumption and Figure of Merit

	$\dot{W}_{net}$ [kW]	Total UA-value [kW/K]	COP [-]	w [kJ/kg$_{LNG}$]	FOM [%]
R410A	1783	153.2	0.445	1849	23.85
Propane	1775	156.1	0.447	1841	23.96
Sub-critical CO_2	1828	146.7	0.434	1896	23.26
Super-critical CO_2	1868	144.2	0.425	1938	22.76

[2] COP_{PC} is defined as the ratio of the evaporator cooling effect to the pre-cooling cycle power consumption.

Propane pre-cooling results to be the most effective alternative with a COP of 3.91. Correspondingly the Figure of Merit of the liquefaction cycle reaches almost 24 %. Detailed results in terms of refrigerants' thermodynamic state points (Figures 4.11 and 4.12) and Composite Curves (Figure 4.13) are presented below only for this case.

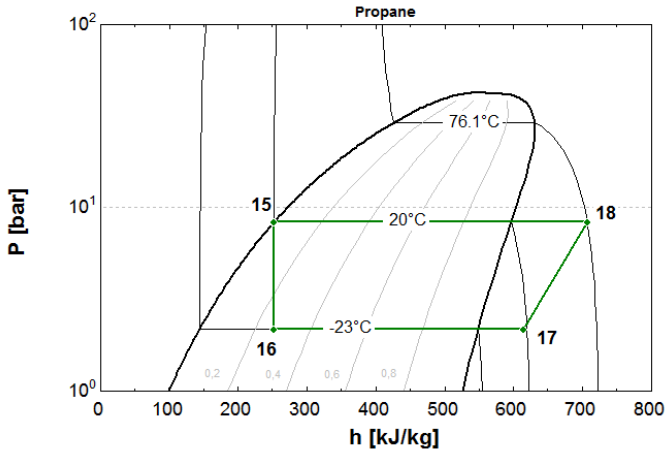

	T [°C]	P [bar]	*h* [kJ/kg]
15	20.0	8.37	252
16	-23.0	2.19	252
17	17.0	2.19	613.6
18	76.1	8.37	706.7

Figure 4.11: Representation of the propane pre-cooling cycle in the log P-h diagram. Values of temperature, pressure and specific enthalpy are listed on the right

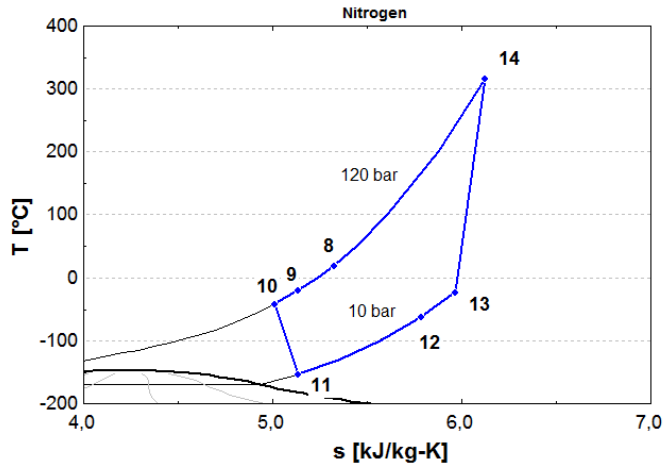

	T [°C]	P [bar]	*h* [kJ/kg]
8	20.0	120	280.4
9	-20.0	120	229.2
10	-41.5	120	199.6
11	-153.0	10	111.1
12	-60.6	10	216.1
13	-23.0	10	256.4
14	317.5	120	617.6

Figure 4.12: Representation of the nitrogen cycle in the T-s diagram. Values of temperature, pressure and specific enthalpy are listed on the right

Figure 4.13 depicts the effect of adding a pre-cooling stage on the shape of the Composite Curves. The type of refrigerant which is used in the pre-cooling cycle influences solely the Cold Composite Curve in the evaporator through the value of mass flow to achieve the pinch point at the evaporator hot end.

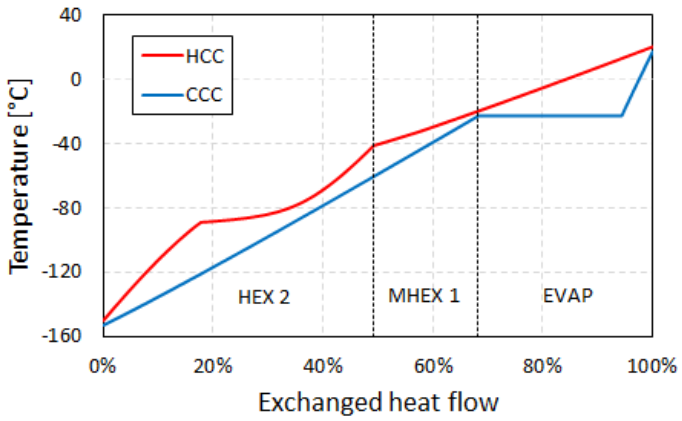

Figure 4.13: Hot and Cold Composite Curves for the single-expansion cycle with propane pre-cooling

In the propane case, the evaporator UA-value is 31.3 kW/K (average LMTD of 13 K) while the UA-values for the MHEX and the HEX are 29.1 kW/K and 45 kW/K, respectively (average LMTD's of 8.4 K and 14.1 K, respectively).

4.5.1 Sensitivity analyses

The influence of two model inputs are investigated, that are the pre-cooling temperature and the presence of sub-cooling in the condenser (this only for the sub-critical alternatives).

Sensitivity on pre-cooling temperature

The effect of pre-cooling temperature is assessed implementing the same design specifications at the heat exchangers as the ones previously presented. The base case for the pre-cooling temperature is -20°C and it is changed to 0°C and to -40°C. Results are presented only for the propane case. However, changes in the pre-cooling temperature affect the thermodynamic cycle in the same way regardless of the working fluid used for the pre-cooling phase.
When pre-cooling temperature is varied, the propane cycle changes in terms of refrigerant flow rate and low pressure to respect the approaches at the evaporator. The effect on the low pressure level of the pre-cooling cycle is visible in the log P-h diagram of Figure 4.14.
Table 4.7 reports the values of propane and nitrogen mass flow rate, together with the low pressure level in the pre-cooling cycle, pre-cooling compressor power consumption and net power consumption for the whole liquefaction cycle. Moreover Table 4.8 presents the values for the pre-cooling cycle COP and the nitrogen cycle COP[3], together with the overall COP and FOM.

[3] COP_{N_2} is calculated as the ratio of natural gas cooling load at the MHEX and at the HEX to the net power consumption of the nitrogen cycle.

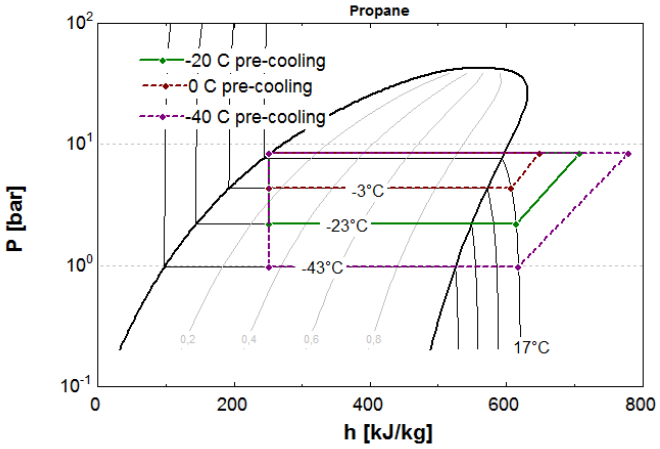

Figure 4.14: Log P-h diagram of the propane pre-cooling cycles when varying pre-cooling temperature

Table 4.7: Values of nitrogen and propane mass flow rate, low pressure level and power consumption for the pre-cooling cycle and net power consumption for the whole liquefaction cycle when varying pre-cooling temperature

T_{PC} [°C]	$\dot{m}_{N_2}$ [kg/s]	$\dot{m}_{ref}$ [kg/s]	P_{low} [bar]	$\dot{W}_{PC}$ [kW]	$\dot{W}_{net}$ [kW]
0	6.8	0.6	4.32	25.8	2090
-20	6.1	1.1	2.19	104.3	1775
-40	5.4	1.6	0.98	254.7	1596

Table 4.8: COP of pre-cooling and nitrogen cycles together with COP and FOM for the whole liquefaction cycle when varying pre-cooling temperature

T_{PC} [°C]	COP_{PC} [-]	COP_{N_2} [-]	COP [-]	FOM [%]
0	8.49	0.36	0.38	20.35
-20	3.91	0.42	0.45	23.96
-40	2.28	0.48	0.50	26.64

From Table 4.7 it can be observed that nitrogen mass flow rate increases as pre-cooling temperature increases, due to the higher cooling load which has to be provided by the nitrogen cycle. Correspondingly propane mass flow rate in the pre-cooling cycle decreases. This is the results of two contributions: on one side the decrease of the evaporator load, on the other the increase of evaporator inlet quality connected with the higher low pressure level.

Propane low pressure is found to be increasing as the pre-cooling temperature increases. It has to be remarked that this pressure is the propane saturation pressure at a temperature which is set to be 3 K lower than the pre-cooling temperature, i.e. -3°C, -23°C and -43°C.
As seen from Table 4.8 it is beneficial to decrease the pre-cooling temperature as much as -40°C, in other words it is beneficial that the pre-cooling cycle provides a larger share of the total cooling load. The reason for this can be spotted by comparing the Coefficients of Performance of propane and nitrogen cycles, with the former being more efficient than the latter. It could also be argued that a pre-cooling temperature as low as -40°C may not be desirable for a propane pre-cooled system as the saturation pressure of propane at -43°C is below atmospheric level (0.98 bar as in Table 4.7).
In conclusion Figure 4.15 depicts the Composite Curves for a pre-cooling temperature of 0°C (on the left) and -40°C (on the right). When the pre-cooling temperature is -40°C, the approach at the two-stream HEX is no more found at the cold end but is internal.

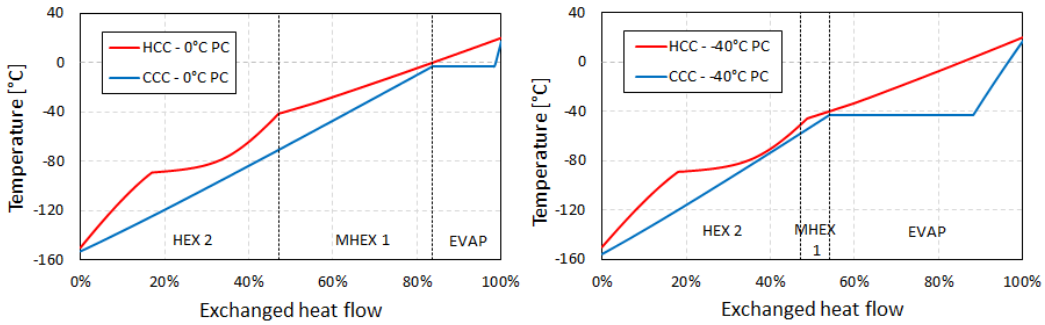

Figure 4.15: Composite Curves in the case of 0°C (on the left) and -40°C (on the right) pre-cooling temperature

Sensitivity on condenser sub-cooling

The effect of introducing sub-cooling in the condenser is investigated. Again the propane pre-cooling cycle is considered, however results are valid for the three sub-critical alternatives. A sub-cooling temperature difference of 5 K is applied. Pre-cooling temperature is kept fixed at -20°C.
The refrigerant is required to enter the throttling valve at 20°C, therefore the high pressure level has to increase in order to implement a 5 K-sub-cooling after the condenser compared to the situation with no sub-cooling. In the case of propane the high pressure has to be increased to 9.53 bar.
Due to the higher pressure ratio in the pre-cooling cycle, the compression power is expected to increase. On the other hand, the presence of sub-cooling causes the evaporator inlet quality to decrease, hence a reduction in refrigerant mass flow rate occurs, which could positively compensate the increase in power consumption.

Results show that propane mass flow rate does not decrease enough to compensate the increased power consumption. Mass flow rate results only 0.01 % lower than the one with no sub-cooling. This can be spotted in Figure 4.16 in which the only visible difference between the two cycles regards the high pressure level. This is due to the fact that isotherms in the sub-cooled liquid region are almost vertical.

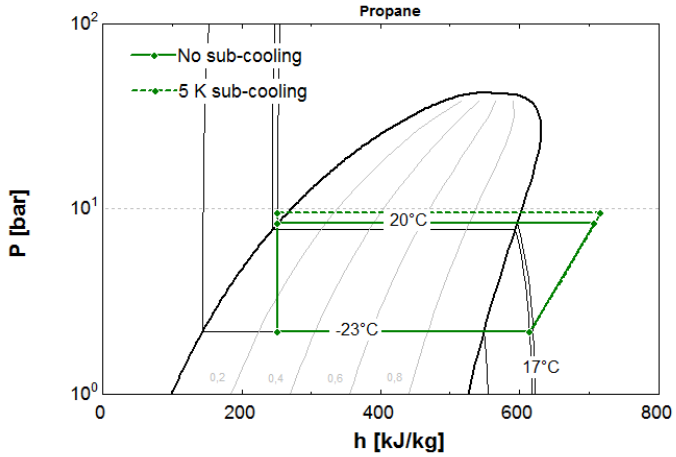

Figure 4.16: Log P-h diagram of the pre-cooling cycle with no sub-cooling (continuous line) and with a sub-cooling of 5 K (dotted line)

On the contrary power consumption in the pre-cooling cycle passes from 104 to 115 kW. Correspondingly the system FOM decreases passing from 23.96 % to 23.81 %. As expected, no changes are recorded in the nitrogen cycle.
In conclusion sub-cooling is found to negatively affect the performance of the liquefaction cycle, although the decrease in FOM is marginal. This originates from the design choice of fixing the refrigerant temperature at the throttling valve inlet.

4.6 Dual-expander configurations

Dual-expander configurations are presented adopting the nomenclature used by Chang *et al.* [60].

4.6.1 Dual-turbine cycle with different pressure ratio

The dual-turbine cycle with different pressure ratio is sketched in Figure 4.17. After the first Multi-Stream Heat Exchanger, the refrigerant stream is split into two separate circuits. A fraction of the refrigerant is sent to the High-Pressure (HP) expander, which is the one having the smaller pressure ratio. This first expansion is needed to provide the cooling effect for the first two MHEX's. The remaining refrigerant fraction is sent to the Low-Pressure (LP) expander which discharge pressure is lower and therefore provides the cooling effect needed for the completion of NG feed liquefaction and sub-cooling.
Before the two refrigerant fractions are mixed together the pressure is equalised through a Low-Pressure compressor which discharge pressure has to be equal to the HP expander discharge pressure.

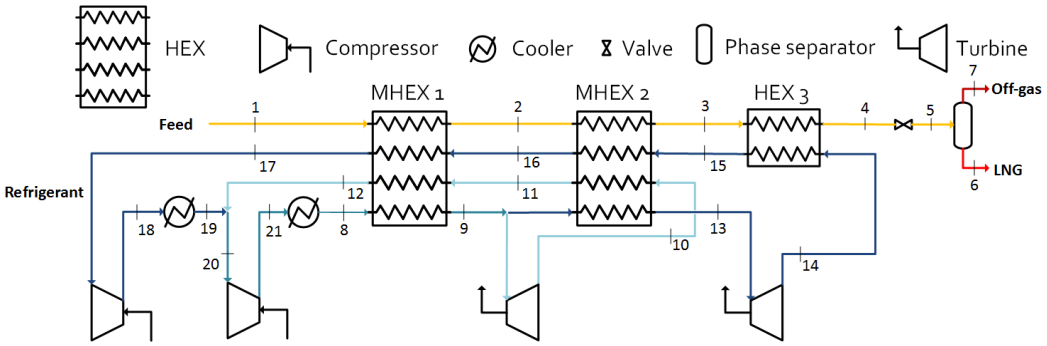

Figure 4.17: Process flowsheet of the dual-turbine configuration with different pressure ratio

Refrigerant is constituted by pure nitrogen and enters the cold box at 20°C and at 120 bar. Refrigerant mass flow rate is set equal to 12.5 kg/s. 40 % of it is sent in the low-pressure circuit. The other input to the model is the NG temperature after the second MHEX (point 3) which is set equal to -70°C following the assumption adopted by Chang *et al.* [60].
The remaining model inputs are computed in order to achieve the 3 K-MITA at the three heat exchangers:

- **first MHEX**: the approach is achieved by varying the cold-end outlet temperature, i.e. temperatures of points 2 and 9 (they are the same given the required thermal equilibrium along the horizontal axis for all the heat exchangers);
- **second MHEX**: the approach is governed by the HP expander discharge pressure;
- **two-stream HEX**: the approach is achieved acting on the LP expander discharge pressure.

As a result the outlet temperature at the cold end of the first MHEX is -20.7°C, HP and LP expander discharge pressures are 49.5 bar and 16.9 bar, respectively. Thermodynamic state points of the refrigerant cycle are reported in the T-s diagram of Figure 4.18.

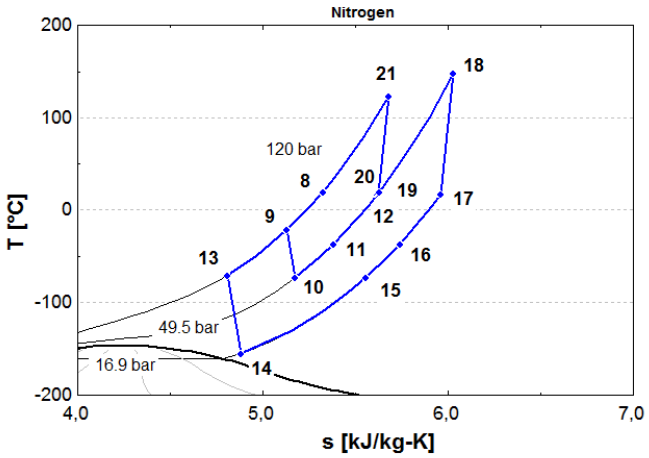

	T [°C]	P [bar]	*h* [kJ/kg]
8	20.0	120.0	280.4
9	-20.7	120.0	228.3
10	-73.0	49.5	182.8
11	-36.3	49.5	228.5
12	17.0	49.5	290
13	-70.0	120.0	155.6
14	-154.6	16.9	96.28
15	-73.0	16.9	199.3
16	-36.3	16.9	239.8
17	17.0	16.9	297.2
18	148.6	49.5	434.4
19	20.0	49.5	293.4
20	18.2	49.5	291.3
21	123.5	120.0	401.7

Figure 4.18: Representation of the T-s refrigerant cycle for the dual-turbine cycle with different pressure ratio. Values of temperature, pressure and specific enthalpy are listed on the right

Given the implemented design specifications the minimum refrigerant split fraction is 36 %. If nitrogen mass flow rate in the low-pressure circuit is too little, LP expander pressure ratio has to increase and this leads to the the formation of liquid nitrogen at the LP expander outlet. On the contrary, maximum split fraction is found to be 63 %. Higher split fractions lead to a crossover of the temperature profiles at the second MHEX due to the increased heat exchanger duty.
Total compression power is 2063 kW, while expansion power amounts to 616 kW. The total heat duty of the cold box is 1813 kW (755 kW at the first MHEX, 550 kW at the second MHEX and 508 kW at the two-stream HEX). Additionally 710 kW are rejected at the first cooler, while the duty of the second cooler results 1531 kW. The UA-value of the cold box amounts to 234.8 kW/K, while the total heat network conductance results equal to 303.1 kW/K.

Table 4.9 summarises the results from the simulation of the dual-expander cycle with different expander pressure ratio. Furthermore Figure 4.19 depicts the Composite Curves for the cold box highlighting the share of the total exchanged heat flow for each of the three heat exchangers. It can be noted that the approach at the first MHEX is at the hot end, while the 3 K-approach for the second MHEX is found at the cold end. This is also the pinch point for the final two-stream HEX. Average LMTD's are 7.6 K for the first MHEX, 6.3 K for the second MHEX and 10.5 K for the two-stream HEX.

Table 4.9: Main results and performance indicators for the dual-turbine cycle with different pressure ratio

$\dot{W}_{net}$ [kW]	Total UA-value [kW/K]	COP [-]	w [kJ/kg$_{LNG}$]	FOM [%]
1447	303.1	0.548	1501	29.38

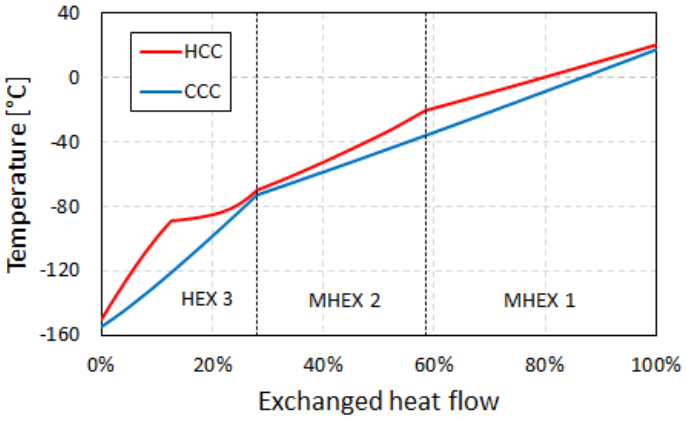

Figure 4.19: Hot and Cold Composite Curves for the dual-turbine cycle with different pressure ratio

4.6.2 Dual-turbine cycle with the same pressure ratio

Figure 4.20 sketches the design of the dual-turbine cycle with the same pressure ratio.

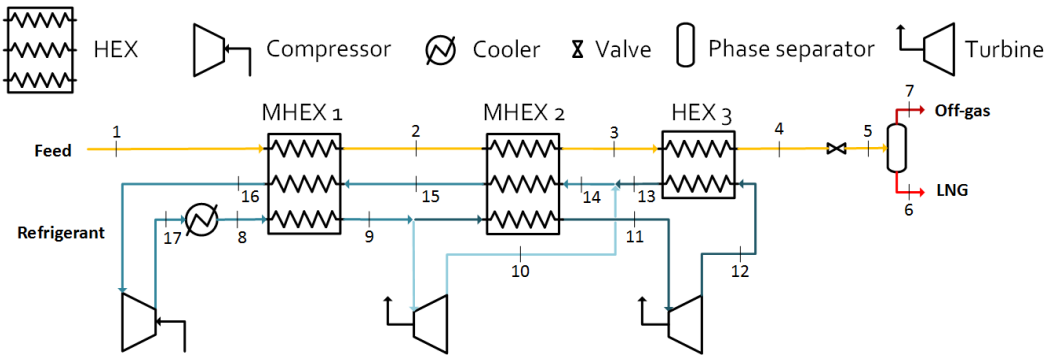

Figure 4.20: Process flowsheet of the dual-turbine configuration with the same expansion pressure ratio

Compared to the previous dual-turbine alternative the two expanders have the same pressure ratio. This is the reason why, after the expansion processes, the mixing of the two refrigerant streams occurs between the second MHEX and the two-stream HEX (i.e. between points 13

and 14). Consequently only one compression stage is needed.
Once again the employed refrigerant is pure nitrogen entering the cold box at 20°C and at 120 bar.

From a modelling viewpoint the constraint on the expander pressure ratio eliminates one degree of freedom in terms of variables which can be manipulated in order to find a solution giving 3 K-MITA's at all heat exchange devices. A design which fulfils the mentioned requirement is found imposing the following specifications:

- **first MHEX**: the approach is achieved by varying the total mass flow rate of the refrigerant;
- **second MHEX**: the approach is governed by the refrigerant split fraction;
- **two-stream HEX**: the approach is achieved acting on the discharge pressure of the two expanders.

Therefore the two intermediate temperature levels have to be fixed as inputs. The first intermediate temperature (temperature at points 2 and 9) is set equal to -20°C while the second intermediate temperature (temperature at points 3 and 11) is set equal to -90°C.

Results from Aspen Plus simulation indicates that the necessary nitrogen mass flow rate is 10 kg/s, of which 28.6 % is the fraction sent to the second expander to produce the cooling effect at the two-stream HEX. Finally low pressure level is 24.4 bar. Nitrogen cycle is reported in the Temperature-Entropy diagram of Figure 4.21[4].

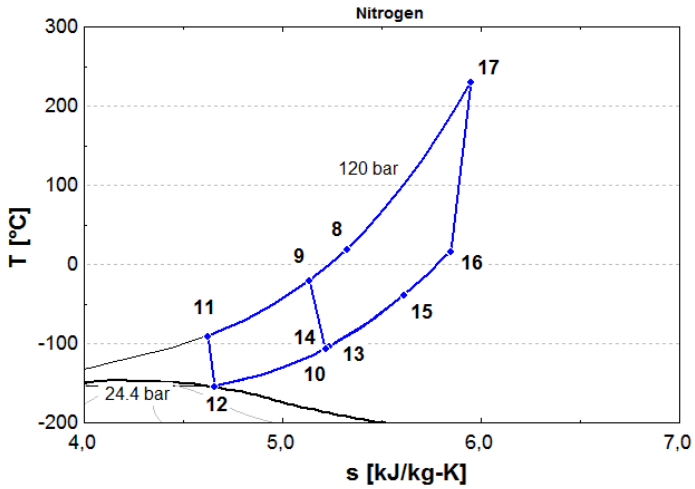

	T [°C]	P [bar]	*h* [kJ/kg]
8	20.0	120.0	280.4
9	-20.0	120.0	229.2
10	-106.2	24.4	155.7
11	-90.0	120.0	119.2
12	-153.0	24.4	78.27
13	-103.2	24.4	159.4
14	-105.4	24.4	156.7
15	-38.4	24.4	234.8
16	17.0	24.4	295.5
17	231.4	120.0	522.2

Figure 4.21: Representation of the T-s refrigerant cycle for the dual-turbine cycle with the same expansion pressure ratio. Values of temperature, pressure and specific enthalpy are listed on the right

[4]Nitrogen quality in 12 is 1.

Compression power results 2267 kW. Expansion power is 514 kW and 107 kW, respectively for the first and the second expander. The total heat duty of the cold box amounts to 1622 kW, with the second MHEX having the largest share (786 kW), followed by the first MHEX (612 kW) and the two-stream HEX (224 kW). Cooler heat duty is 2439 kW. The cold box UA-value results 224.2 kW/K, while the calculated UA-value for the cooler is 39.7 kW/K.
Table 4.10 reports the values of net power consumption and heat network conductance for the considered configuration together with the cycle performance indicators. Temperature profiles at the cold box are shown in Figure 4.22.

Table 4.10: Main results and performance indicators for the dual-turbine cycle with the same pressure ratio

$\dot{W}_{net}$ [kW]	Total UA-value [kW/K]	COP [-]	w [kJ/kg$_{LNG}$]	FOM [%]
1646	263.9	0.482	1707	25.84

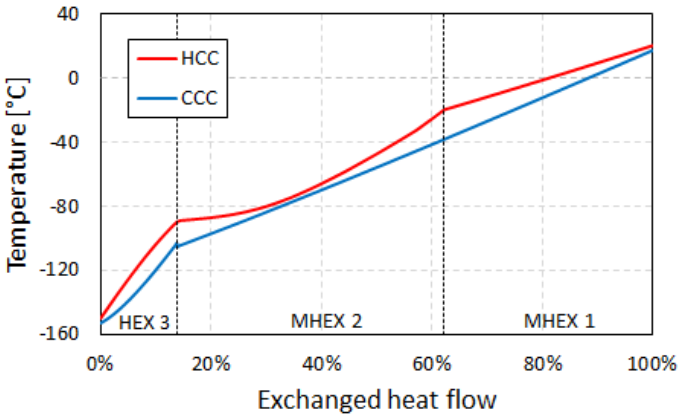

Figure 4.22: Hot and Cold Composite Curves for the dual-turbine cycle with the same pressure ratio

For the first MHEX and for the two-stream HEX approaches are external. Conversely the pinch point is internal for the second MHEX. Average LMTD's are 8.4 K for the first MHEX, 6 K for the second MHEX and 11.3 K for the two-stream HEX.
Two observations have to be made when looking at the Composite Curves of Figure 4.22. Firstly the Cold Composite Curve is not continuous when passing from the second MHEX to the two-stream HEX. This is caused by the mixing process between nitrogen streams in state 10 and 13. Secondly, the shape of the Cold Composite Curve in the two-stream HEX is not linear. Although nitrogen is always in gaseous form, a non-negligible variation of the isobaric specific heat capacity is recorded. At 24.4 bar the c_p of nitrogen passes from 3.7 kJ/kgK at -155°C to 2 kJ/kgK at -145°C. In a Temperature-Heat Flow diagram a decrease in c_p causes the slope of the temperature profile to increase and this explains the observed non-linearity.

4.6.3 Two-stage expansion cycle

The layout of the two-stage expansion cycle is reported in Figure 4.23.

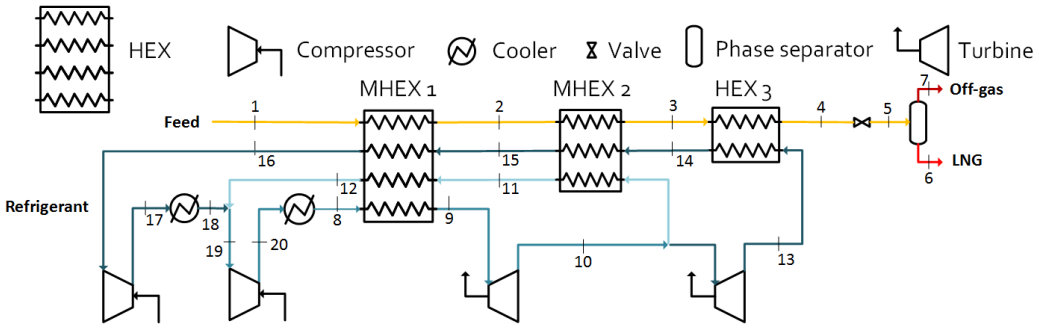

Figure 4.23: Process flowsheet of the two-stage expansion cycle

Compared to the other dual-turbine alternatives, the refrigerant split occurs after the first expansion in the High-Pressure expander (point 10). Only a fraction of the total mass flow rate of the refrigerant undergoes a second expansion in order to generate the cooling effect required to complete the liquefaction and sub-cooling of natural gas feed.
Due to the different pressure levels of the refrigerant streams in the two circuits (HP and LP circuit), a two-stage compression is needed such that the mixing process occurs when the refrigerant streams in point 12 and in point 18 have the same pressure.

Refrigerant is pure nitrogen which enters the cold box (point 8) at 20°C and at 120 bar. Nitrogen mass flow rate is 10 kg/s.
The design specifications which are implemented in order to achieve the 3 K-approach in all the heat exchange sections are listed below:

- **first MHEX**: the approach is achieved by varying the cold-side outlet temperature, that is the temperature of natural gas and nitrogen streams in points 2 and 11;
- **second MHEX**: the approach is governed by the intermediate pressure level, i.e. the discharge pressure of High-Pressure expander (point 10);
- **two-stream HEX**: the approach is achieved acting on the discharge pressure of the Low-Pressure expander (point 13).

As to the remaining model variables which have to be fixed as input, the second intermediate temperature level is -90°C (temperature of natural gas feed in point 3), while the splitter is set so that 47 % of the total nitrogen mass flow rate is sent to the low-pressure circuit.

As a result the calculated temperature at the cold-side outlet of the first MHEX is -40°C. The intermediate pressure level results 46.7 bar while Low-Pressure expander discharge pressure is 10.3 bar. Nitrogen cycle is shown in the T-s diagram of Figure 4.24 together with the corresponding values of temperature, pressure and specific enthalpy.

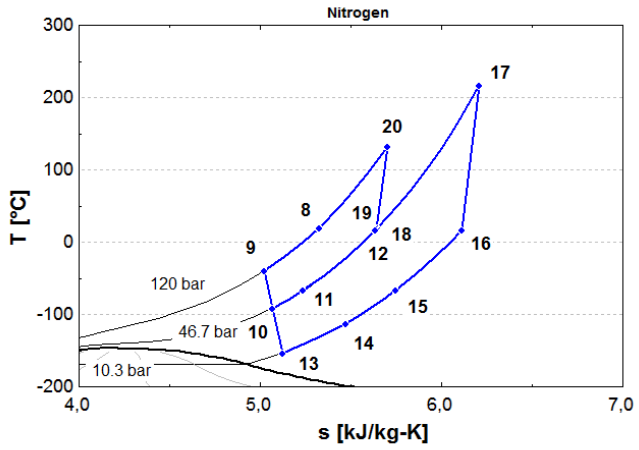

	T [°C]	P [bar]	*h* [kJ/kg]
8	20.0	120.0	280.4
9	-40.0	120.0	201.8
10	-91.5	46.7	159.4
11	-66.6	46.7	192.4
12	17.0	46.7	290.6
13	-153.0	10.3	110.7
14	-112.5	10.3	158.9
15	-66.6	10.3	209.5
16	17.0	10.3	298.8
17	217.2	46.7	508.4
18	20.0	46.7	294.0
19	18.4	46.7	292.2
20	131.9	120.0	411.2

Figure 4.24: Representation of the T-s refrigerant cycle for the two-stage expansion cycle. Values of temperature, pressure and specific enthalpy are listed on the right

It has to be noted that nitrogen streams in points 10 and 14, i.e. cold refrigerant stream entering the cold side of the second MHEX, are not characterised by the same temperature. Therefore the second Multiple-Stream Heat Exchanger which is presented in the model corresponds in reality to two separated heat exchange sections: a two-stream HEX in which the cold nitrogen stream in 14 warms up until it reaches the temperature in 10, and a MHEX in which the two refrigerant streams warm up passing from -91.5°C to -66.6°C.
It is also found that under these conditions the minimum nitrogen mass flow rate that can be sent to the low-pressure circuit is 23 % of the total. As the refrigerant flow rate in the low-pressure circuit is diminished the discharge pressure of the LP expander decreases and with that the refrigerant temperature at the LP expander outlet. However if the split fraction is below 23 % the expansion process ends in the two-phase region. On the contrary the maximum split fraction is 55 %, above which a crossover of the temperature profiles occurs at the second MHEX.
Total compression power is 2174 kW, of which 1189 kW in the High-Pressure compressor. HP expander power production is 419 kW while LP expander power is 215 kW.
The total heat duty at the cold box is 1585 kW. The first MHEX is the one providing the largest share of the total duty (946 kW), followed by the second MHEX (415 kW) and the two-stream HEX (224 kW). Cold box conductance is 171.9 kW/K. The heat rejected at the first cooler amounts to 1014 kW, while the heat duty of the second cooler is 1320 kW. Correspondingly the calculated UA-values for the coolers are 17.4 kW/K and 35.8 kW/K, respectively.
Results are summarised in Table 4.11 together with the performance indicators for the two-stage expansion cycle. Moreover Figure 4.25 reports the Composite Curves for the cold box of the liquefaction cycle.

Table 4.11: Main results and performance indicators for the two-stage expansion cycle

$\dot{W}_{net}$ [kW]	Total UA-value [kW/K]	COP [-]	w [kJ/kg$_{LNG}$]	FOM [%]
1540	225.1	0.515	1598	27.61

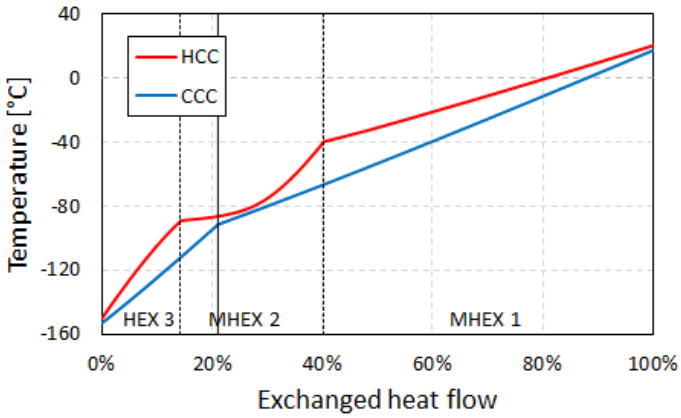

Figure 4.25: Hot and Cold Composite Curves for the two-stage expansion cycle. The continuous black vertical line indicates the two sections which are comprised within the second Multi-Stream Heat Exchanger

Considering the three heat exchangers as in Figure 4.25 it can be observed that pinch points are found at the hot end of the first MHEX, internally in the second MHEX and at the cold end of the two-stream HEX. Average LMTD's are 10.6 K for the first MHEX, 6.5 K for the second MHEX and 11.7 for the two-stream HEX.
As mentioned above, the second Multiple-Stream Heat Exchanger comprises in reality two separated heat exchange sections, which are made visible in Figure 4.23 through the continuous black vertical line. The change in slope of the Cold Composite Curve is the result of the temperature profile aggregation between the intermediate-pressure and low-pressure nitrogen stream which, from a heat network viewpoint, takes place when the low-pressure refrigerant temperature reaches -91.5°C.

4.6.4 Discussion

From a thermodynamic viewpoint it is beneficial to develop the single-expander configuration moving to a dual-turbine cycle. As shown in this Section the presence of a dual expansion process allows a significant reduction in the net power consumption and a closer match of the temperature profiles.
Among the analysed dual-expander configuration the one implementing a different pressure ratio is found to be the most efficient, followed by the two-stage cycle and the dual-expander cycle with a common pressure ratio for the expanders.
Having the expanders connected in parallel with different pressure ratio is more beneficial compared to the two-stage cycle, as this allows to decrease the overall cycle pressure ratio (low pressure level is 16.9 bar against 10.3 bar of the two-stage expansion alternative). Although nitrogen mass flow rate is higher, High-Pressure expander works with a lower flow rate, hence its thermodynamic performance is higher.
The dual-turbine cycle with the same expander pressure ratio achieves a close match of the temperature profiles through the splitting of the refrigerant. With respect to the other two alternatives it is however penalised by the compression process which takes place in one single stage, similarly to what is observed in Section 4.4.

4.7 Dual-refrigerant configurations

All the expander-based cycles which have been previously presented employ pure nitrogen as refrigerant medium. In this Section the possibility of having a two-refrigerant cycle is considered. Refrigerants are not mixed and they have separate circuits. Nitrogen is always one of the two refrigerants, while the second one can be methane or natural gas feed itself in an open cycle.

4.7.1 N_2 sub-cooling dual-refrigerant cycle

In the first dual-refrigerant configuration methane provides the cooling effect in the first part of the natural gas cooling curve, whereas nitrogen has to provide the cooling effect to complete the liquefaction and the sub-cooling of the natural gas feed. The cycle is sketched in Figure 4.26.

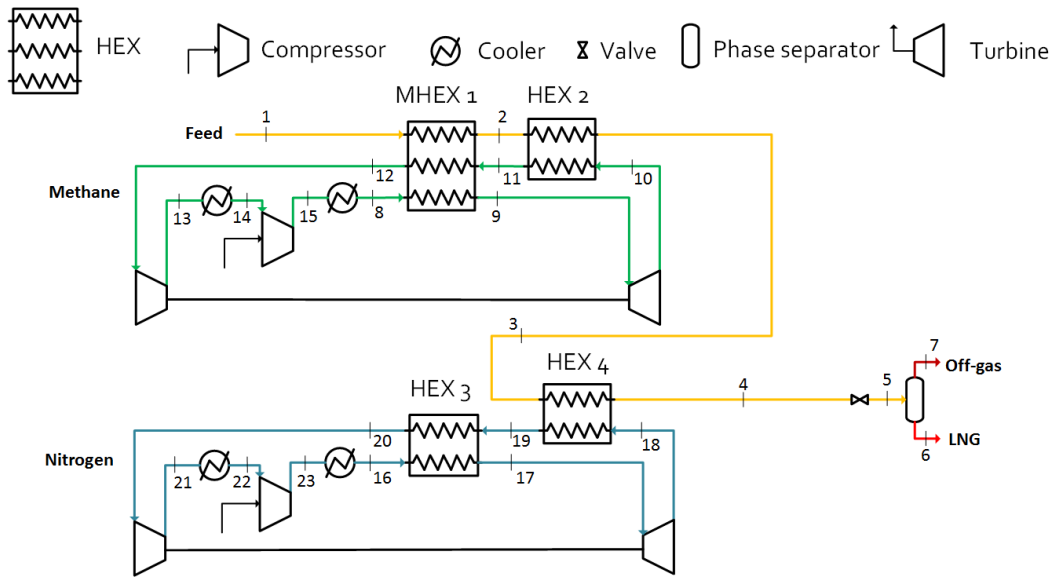

Figure 4.26: Process flowsheet of the dual-refrigerant cycle employing nitrogen for the last phase of the cooling process

Each of the refrigerant cycles is a single-expander cycle with a two-stage compression in which the Low-Pressure compressor is mechanically coupled to the expander.
Methane enters the first cold box at 20°C and 50 bar. Nitrogen enters the bottoming cold box at 20°C and 80 bar. In both cycles the expander discharge pressure is set equal to 15 bar.
Methane provides the cooling of the natural gas feed down to -80°C (point 3). At this temperature level NG feed is a two-phase mixture with a vapour fraction of 0.75 on mass basis. Therefore methane is mostly active in the sensible pre-cooling of the natural gas, while nitrogen provides the cooling effect for the completion of the liquefaction and for the sub-cooling

phase down to -150°C.
From a modelling viewpoint the intermediate pressure level for both cycles is constrained by the mechanical coupling of expander and LP compressor, therefore it is a model output. As to the temperature approaches at the heat exchangers, the following design specifications are applied:

- **methane cycle**: methane flow rate governs the approach at the first MHEX, while its temperature at the expander inlet is varied to achieve the MITA at the two-stream HEX;
- **nitrogen cycle**: the same modelling approach used for the methane cycle is applied, with nitrogen flow rate governing the approach at the nitrogen-nitrogen HEX.

Results indicate that the intermediate pressure levels are 24.7 bar in the methane cycle and 23 bar in the nitrogen cycle. Methane mass flow rate is 2.7 kg/s while nitrogen mass flow rate is 7.2 kg/s. Methane enters the expander at -19.2°C while nitrogen expander inlet temperature is -81.5°C. Methane and nitrogen cycles are shown in the T-s diagrams of Figures 4.27 and 4.28, respectively.
Power consumption at the High-Pressure compressors is 1206 kW and 375 kW for the nitrogen and methane cycle, respectively. Nitrogen expander produces 349 kW, while methane expander power production is 262 kW. As mentioned above, these are equal to the power consumption of the Low-Pressure compressors in the two cycles.
The total heat duty at the cold box is 2049 kW, of which 969 kW is the heat duty of the nitrogen-nitrogen HEX. Cold box heat conductance is 219.7 kW/K split as following among the different heat exchangers: as to the methane cycle, 38.1 kW/K at the MHEX and 46.2 kW/K at the two-stream HEX; as to the nitrogen cycle, 114.5 kW/K at the nitrogen-nitrogen HEX and 20.9 kW/K at the nitrogen-natural gas HEX.
The heat rejected at the coolers amounts to 2375 kW. The sum of the calculated UA-values for the coolers is 86.1 kW/K.

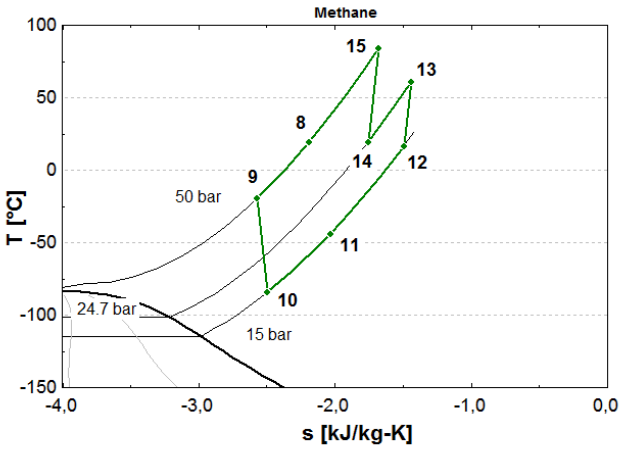

	T [°C]	P [bar]	*h* [kJ/kg]
8	20.0	50.0	-63.2
9	-19.2	50.0	-167.5
10	-84.1	15.0	-268.9
11	-43.5	15.0	-172.1
12	17.0	15.0	-33.3
13	61.4	24.7	63.1
14	20.0	24.7	-36.4
15	84.5	50.0	102.2

Figure 4.27: Representation of the T-s methane cycle for analysed dual-refrigerant configuration. Values of temperature, pressure and specific enthalpy are listed on the right

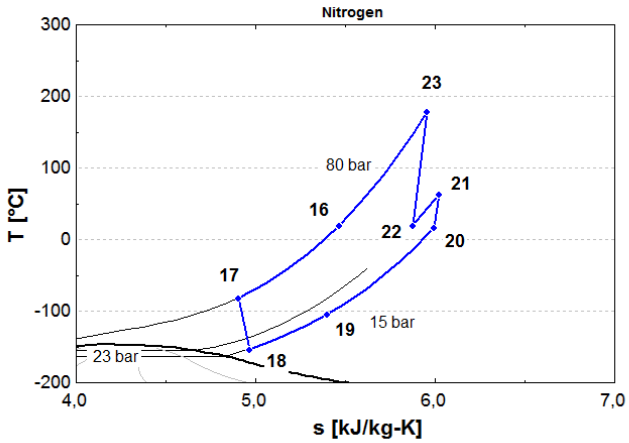

	T [°C]	P [bar]	h [kJ/kg]
16	20.0	80.0	287.3
17	-81.5	80.0	154.5
18	-153.0	15.0	102.8
19	-104.8	15.0	181.2
20	17.0	15.0	297.7
21	63.7	23.0	346.0
22	20.0	23.0	299.1
23	179.2	80.0	465.9

Figure 4.28: Representation of the T-s nitrogen cycle for the analysed dual-refrigerant configuration. Values of temperature, pressure and specific enthalpy are listed on the right

Table 4.12 reports the main results and the performance indicators for the presented dual-refrigerant cycle. Figure on the left 4.29 shows the aggregated temperature profiles for those heat exchangers having natural gas on the hot side. The temperature profiles for the nitrogen-nitrogen HEX are presented in Figure 4.29 on the right.

Table 4.12: Main results and performance indicators for the dual-refrigerant cycle employing nitrogen for the last phase of the cooling process

$\dot{W}_{net}$ [kW]	Total UA-value [kW/K]	COP [-]	w [kJ/kg$_{LNG}$]	FOM [%]
1581	305.8	0.502	1640	26.89

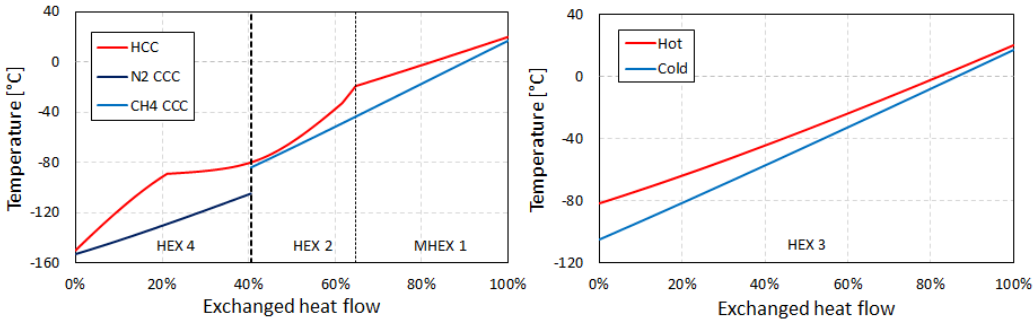

Figure 4.29: On the left: Hot and Cold Composite Curves for the part of cold box having natural gas on the hot side. The thick dotted line separates the methane-side cold box from the nitrogen-side cold box. On the right: hot and cold temperature profiles for the nitrogen-nitrogen HEX

On the methane side pinch points are activated at the hot end of the Multiple-Stream Heat Exchanger and internally in the two-stream HEX. Average LMTD's are 10 K and 5.7 K, respectively. On the nitrogen side the pinch point at the nitrogen-nitrogen HEX is found at the warm end (average LMTD of 8.5 K) while the nitrogen-natural gas HEX shows the approach at the cold end (average LMTD of 21 K).

Sensitivity analysis on natural gas intermediate temperature

Natural gas intermediate temperature is the temperature level at which the feed is brought by the methane cycle. As presented the base case is -80°C. The performance of the liquefaction cycle is assessed when this temperature is changed to -70°C and -90°C. From a modelling point of view the same approach is applied in terms of design specifications and inputs to the model.

Table 4.13 reports the results from the sensitivity analysis in terms of COP for the methane and nitrogen cycle together with COP and FOM for the whole liquefaction cycle.

Table 4.13: COP of methane and nitrogen cycles together with COP and FOM for the whole liquefaction cycle when varying natural gas intermediate temperature

T_{NG} [°C]	COP_{CH_4} [-]	COP_{N_2} [-]	COP [-]	FOM [%]
-70	1.075	0.363	0.476	25.53
-80	0.948	0.363	0.502	26.89
-90	0.768	0.363	0.584	31.30

Methane cycle proves to be more efficient than nitrogen cycle. As a consequence it can be concluded that it is beneficial to reduce the intermediate temperature, i.e. it is beneficial that methane cycle provides a larger share of the natural gas cooling load compared to nitrogen cycle.
The effect of decreasing the intermediate temperature level on the Composite Curves at the cold box is shown in Figure 4.30. It can be clearly seen how closer the profiles are. For the last heat exchange section, that is the nitrogen-natural gas HEX, average LMTD passes from 21 K to 10 K.

4.7.2 CH_4 sub-cooling dual-refrigerant cycle

In a specular way compared to the previous case methane can be employed to cover the last phases of the natural gas cooling process, while nitrogen can be used to cool natural gas in the warmer temperature range. The layout of this dual-refrigerant alternative is sketched in Figure 4.31.

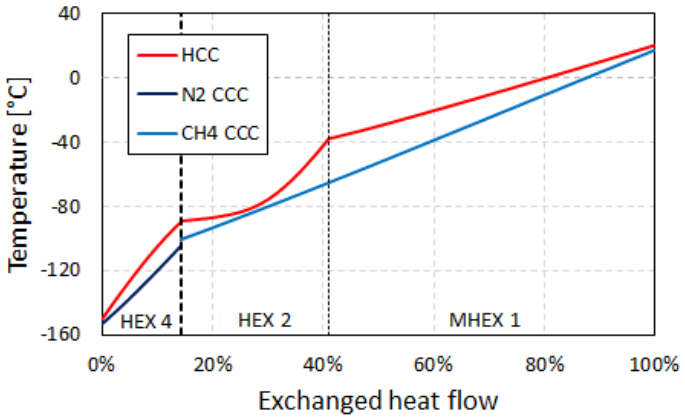

Figure 4.30: Hot and Cold Composite Curves for the heat exchange sections having natural gas on the hot side in the case of natural gas intermediate temperature level equal to -90°C

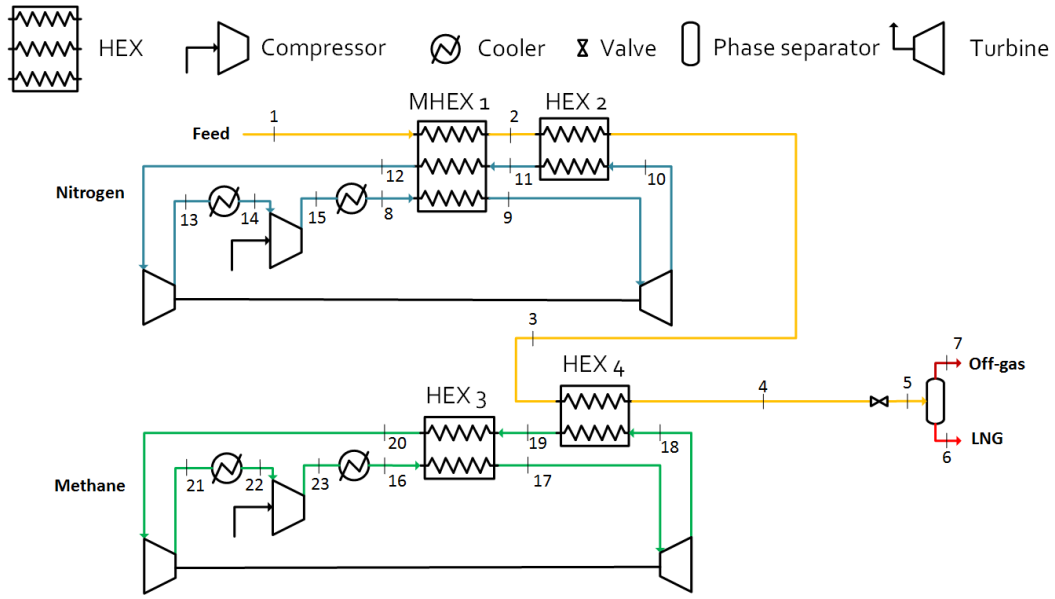

Figure 4.31: Process flowsheet of the dual-refrigerant cycle employing methane for the last phase of the cooling process

The main consequence of having methane acting in the last phase of natural gas cooling is that methane low pressure has to be significantly lower than the previous case (i.e. 15 bar) in order to provide the cooling effect down to -150°C. According to Aspen Plus simulation the maximum pressure level which can be implemented without having liquid formation at the expander outlet is 1.95 bar. In the present case low pressure level on methane side is set equal to 0.7 bar, while high pressure level is 3 bar. On nitrogen side the low pressure level is equal to 15 bar, while nitrogen enters the cold box at 80 bar.

Again natural gas intermediate temperature is set equal to -80°C. Temperature approaches are achieved manipulating the same variables as for the previous dual-refrigerant cycle.

Results from Aspen Plus simulation give an intermediate pressure level of of 30.9 bar on nitrogen side and of 1.1 bar on methane side. Nitrogen and methane flow rates are 3.6 kg/s and 5.4 kg/s, respectively. Nitrogen enters the expander at 1.5°C, while the expander inlet temperature on methane side is -109.4°C. Nitrogen and methane cycles are shown in the T-s diagrams of Figures 4.32 and 4.33.

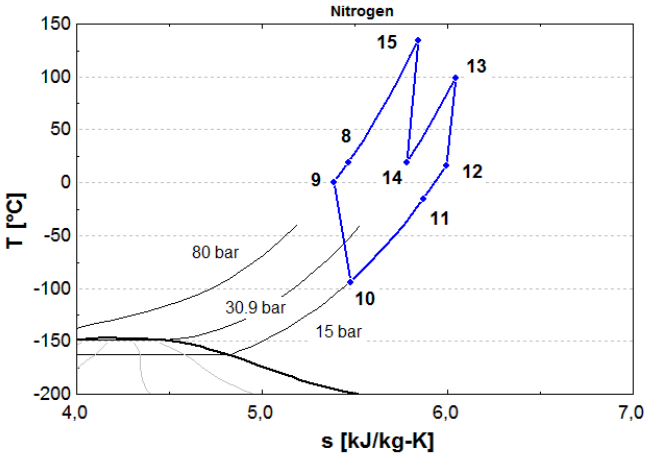

	T [°C]	P [bar]	h [kJ/kg]
8	20.0	80.0	287.3
9	1.5	80.0	265.3
10	-93.1	15.0	177.7
11	-15.0	15.0	263.4
12	17.0	15.0	297.7
13	100.0	30.9	383.8
14	20.0	30.9	297.3
15	135.5	80.0	417.8

Figure 4.32: Representation of the T-s nitrogen cycle for analysed dual-refrigerant configuration. Values of temperature, pressure and specific enthalpy are listed on the right

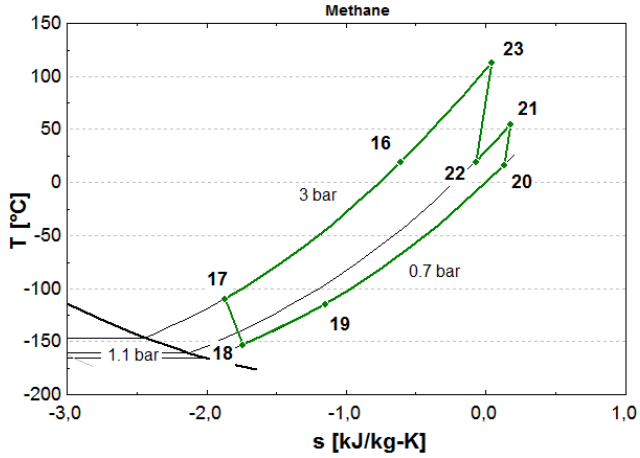

	T [°C]	P [bar]	h [kJ/kg]
16	20.0	3.0	-14.1
17	-109.4	3.0	-294.3
18	-153.0	0.7	-379.8
19	-114.4	0.7	-298.1
20	17.0	0.7	-18.5
21	54.9	1.1	66.7
22	20.0	1.1	-12.2
23	113.2	3.0	205.2

Figure 4.33: Representation of the T-s methane cycle for the analysed dual-refrigerant configuration. Values of temperature, pressure and specific enthalpy are listed on the right

Compression power on nitrogen side is 436 kW while it is 1172 kW for the methane High-Pressure compressor. Nitrogen expander produces 311 kW, while methane expander power production is 460 kW. The heat duty of the cold box is in total 2381 kW, of which 1507 kW represent the heat duty at the methane-methane heat exchanger. The cold-box heat conductance results equal to 502.7 kW/K, remarkably larger than the case of having N_2 providing the sub-cooling of natural gas. This is mainly due to the methane-methane heat exchanger, which heat conductance is given by Aspen Plus equal to 404.7 kW/K.
The heat rejected at the coolers is 2401 kW, of which 791 kW in the nitrogen cycle. Calculated UA-values for the coolers are: 11.3 kW/K and 12.6 kW/K for the first and second cooler on the nitrogen side, 34.7 kW/K and 37.3 kW/K for the first and second cooler on the methane side.
Table 4.14 summarises the simulation results and introduces the performance indicators for the analysed dual-refrigerant alternative. Moreover Figure 4.34 on the left shows the aggregated temperature profiles for those heat exchangers contributing to the natural gas cooling. On the right in Figure 4.34 the temperature profiles at the methane-methane heat exchanger are presented.

Table 4.14: Main results and performance indicators for the dual-refrigerant cycle employing methane for the last phase of the cooling process

$\dot{W}_{net}$ [kW]	Total UA-value [kW/K]	COP [-]	w [kJ/kg$_{LNG}$]	FOM [%]
1608	598.6	0.494	1667	26.45

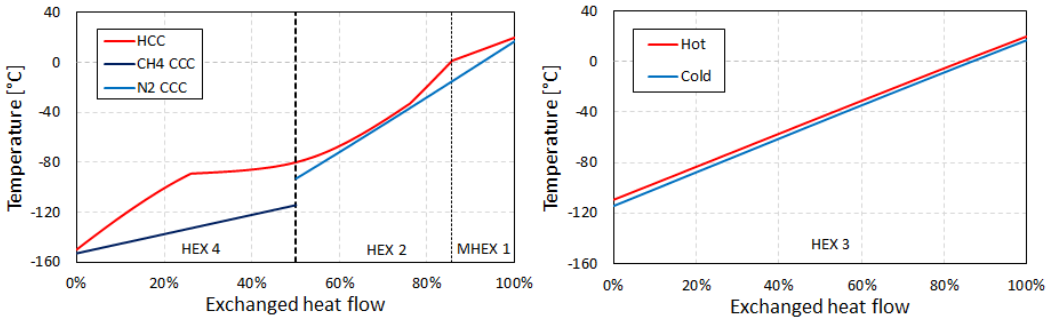

Figure 4.34: On the left: Hot and Cold Composite Curves for the part of cold box having natural gas on the hot side. The thick dotted line separates the nitrogen-side cold box from the methane-side cold box. On the right: hot and cold temperature profiles for the methane-methane HEX

The situation is analogous to the previous dual-refrigerant case as to the location of pinch points. Average LMTD's are 7.9 K and 4.9 K for the MHEX and the two-stream HEX on nitrogen side, while on methane side methane-natural gas HEX has an average LMTD of 22.9 K and methane-methane HEX's average LMTD is 3.7 K.

The temperature profiles at the methane-methane HEX give the reason for the very high UA-value at this two-stream heat exchanger. They are almost parallel given the small difference in pressure between the cold methane stream (0.7 bar) and the warm methane stream (3 bar).

Similarly to what observed for N_2 sub-cooling dual-refrigerant cycle, the large temperature difference at the last heat exchanger (in this case, methane-natural gas HEX) can be significantly reduced by decreasing the natural gas intermediate temperature. In the -90°C-case the average LMTD for this heat exchanger becomes 11.9 K. Once again it is beneficial to decrease natural gas intermediate temperature as shown in Table 4.15.

Table 4.15: COP of nitrogen and methane cycles together with COP and FOM for the whole liquefaction cycle when varying natural gas intermediate temperature

T_{NG} [°C]	COP_{N_2} [-]	COP_{CH_4} [-]	COP [-]	FOM [%]
-70	0.877	0.373	0.471	25.22
-80	0.817	0.373	0.494	26.45
-90	0.656	0.373	0.541	29.00

4.7.3 *Niche* cycle

The last dual-refrigerant configuration which is modelled and analysed is the so-called *Niche* cycle. The layout of this dual-refrigerant cycle is sketched in Figure 4.35.

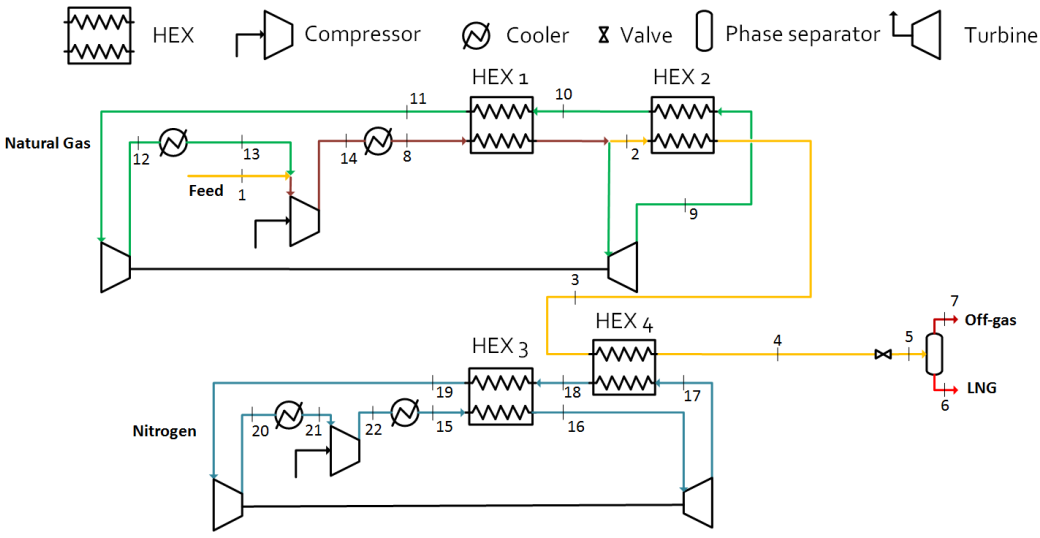

Figure 4.35: Process flowsheet of the *Niche* cycle

The main feature of this configuration is the use of a part of natural gas feed as a refrigerant to cool down natural gas feed itself. This leads to the realisation of an open configuration on natural gas side.
The feed is mixed with the recirculated natural gas (state point 15) which is at 20°C and at 33 bar as the feed itself in order to avoid mixing losses. From a modelling point of view this means that the intermediate pressure level on the natural gas side is now an input (33 bar), hence the expander discharge pressure is a model variable given the constraint on the mechanical coupling between Low-Pressure compressor and expander. The opposite occurs on the nitrogen side, with the intermediate pressure level being a model variable and depending on the chosen expander discharge pressure.
High pressure level on natural gas side is set equal to 40 bar. After the first two-stream HEX, the natural gas stream is split so that 1 kg/s is the flow rate that is sent to the nitrogen cycle, whereas the remaining mass flow rate is the one being recirculated and undergoing the expansion process. Expander inlet temperature on natural gas side is set equal to -10°C.
On the nitrogen side high pressure level is 80 bar, while expander discharge pressure is set equal to 15 bar.

Temperature approaches are achieved implementing the following design specifications:

- **natural gas cycle**: total natural gas flow rate (NG feed plus recirculated flow rates) governs the approach at the first two-stream HEX, while natural gas intermediate temperature (i.e. temperature in point 3) is varied to achieve the MITA at the second HEX;
- **nitrogen cycle**: nitrogen mass flow rate governs the approach at the nitrogen-nitrogen HEX, while expander inlet temperature is varied in order to achieve the pinch point at the natural gas-nitrogen HEX.

Results from Aspen simulation show that the recirculated natural gas flow rate has to be 2.9 kg/s. Low pressure level on natural gas side is 26.5 bar. Natural gas intermediate temperature is -31°C. As to the nitrogen cycle, the calculated mass flow rate is 10.8 kg/s while the expander inlet temperature is -81.5°C. The intermediate pressure level results 23 bar.
The thermodynamic state points for both cycles are listed in Table 4.16[5]. Temperature-Entropy diagrams are omitted being analogous to the ones presented for the N_2 sub-cooling dual-refrigerant cycle.
Compression power on natural gas and nitrogen side is 115 kW and 1802 kW, respectively. Natural gas expander produces 98 kW, while nitrogen expander power production is 522 kW. The total heat load at the cold box is 2446 kW, 1448 kW being the heat duty of the nitrogen-nitrogen heat exchanger. The cold box heat conductance is 236.1 kW/K. Again the biggest contribution to it comes from the nitrogen-nitrogen HEX (171 kW/K).

[5]Only for the present case the listed values of specific enthalpy for the natural gas mixture are the ones given by Aspen Plus using Peng-Robinson EOS as property method.

As to the coolers, the total heat rejected results 2710 kW. The majority of it is rejected on nitrogen side (2456 kW). The sum of the calculated UA-values for the coolers amounts to 97.1 kW/K. It has to be remarked that on natural gas side the refrigerant enters the cooler at a temperature lower than 50°C. As previously stated, in these cases a LMTD of 10 K is applied. Table 4.17 summarises the results and reports the values of the performance indicators for the *Niche* cycle.

Table 4.16: Thermodynamic state points on nitrogen (left) and natural gas (right) side for the *Niche* cycle. Values of natural gas specific enthalpy are given by Aspen Plus

	T [°C]	P [bar]	h [kJ/kg]
15	20.0	80.0	287.3
16	-81.5	80.0	154.5
17	-153.0	15.0	102.8
18	-104.8	15.0	181.2
19	17.0	15.0	297.7
20	63.7	23.0	346.0
21	20.0	23.0	299.1
22	179.2	80.0	465.9

	T [°C]	P [bar]	h [kJ/kg]
8	20.0	40.0	-4290
2	-10.0	40.0	-4364
9	-34.0	26.5	-4398
10	-26.0	26.5	-4379
11	17.0	26.5	-4279
12	34.9	33.0	-4245
13	20.0	33.0	-4280
14	35.9	40.0	-4251

Table 4.17: Main results and performance indicators for the *Niche* cycle

$\dot{W}_{net}$ [kW]	Total UA-value [kW/K]	COP [-]	w [kJ/kg$_{LNG}$]	FOM [%]
1917	333.2	0.414	1992	22.18

In order to fairly compare all the liquefaction alternatives the same boundaries have to be applied for the calculation of COP and FOM. In the case of the *Niche* cycle, the liquefied natural gas exits the cold box at -150°C and 40 bar, whereas in all the previous configurations the outlet pressure is 33 bar. Therefore COP and FOM are calculated using the values of specific enthalpy and entropy for the natural gas mixture at -150°C and 33 bar.
Figure 4.36 on the left shows the aggregated temperature profiles for those heat exchangers contributing to natural gas cooling. On the right in Figure 4.36 the temperature profiles at the nitrogen-nitrogen heat exchanger are presented.
Pinch points are activated at the extremities of both natural gas-side and nitrogen-side cold boxes. The average LMTD's are 7.8 and 7.7 K for the first and the second two-stream HEX on natural gas side, while on nitrogen side they are 8.5 K for the nitrogen-nitrogen HEX and 32 K for the natural gas-nitrogen HEX.

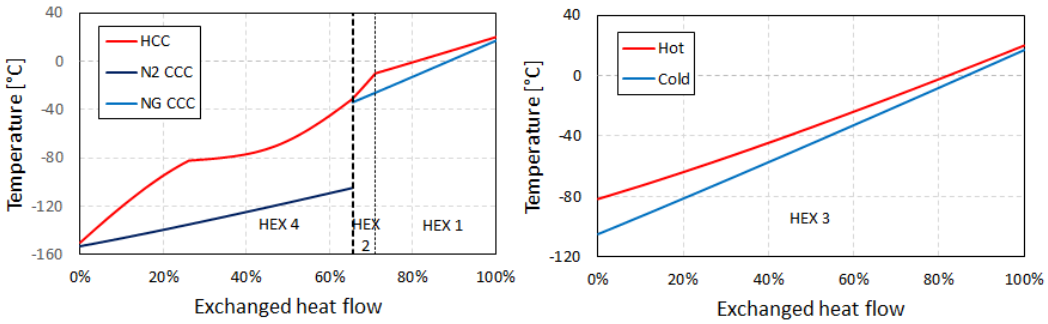

Figure 4.36: On the left: Hot and Cold Composite Curves for the part of cold box having natural gas on the hot side. The thick dotted line separates the natural gas-side cold box from the nitrogen-side cold box. On the right: hot and cold temperature profiles for the nitrogen-nitrogen HEX

As shown for the previous dual-refrigerant configurations, a way to reduce the large temperature difference for the last two-stream HEX is to reduce the natural gas intermediate temperature. However this is not possible for the *Niche* cycle. If natural gas intermediate temperature decreases, the same has to occur for the natural gas temperature at the expander outlet. There are two limitations for this: firstly, natural gas at the expander outlet has to remain in the gaseous form; secondly, discharge pressure cannot be too low as the expander power is forced to be equal to the one of Low-Pressure compressor, which discharge pressure is fixed at 33 bar.

4.8 Conclusive remarks

Thirteen expander-based configurations are modelled using Aspen Plus simulation software and they are presented and analysed in this Chapter focusing on their thermodynamic performance. Simulation results are summarised in Table 4.18. Figure of Merit for the liquefaction process can be improved from 17 % to 30 %. This increase corresponds to a reduction in net power consumption from 2500 kW to 1450 kW.
The least efficient alternative is the single-expander cycle with one-stage compression. The reason is twofold. On one side a large temperature difference at the cold box is recorded. On the other side a single-stage compression process is inefficient and can be significantly improved by adding a second compression stage and an inter-cooler between the two compressors. Results show that implementing an inter-cooled two-stage compression allows a reduction in net power consumption of 26.5 %. As discussed, the design of the compression process does not affect the heat exchange section of the cycle, the so-called cold box, where natural gas is cooled and liquefied.

Table 4.18: Summary of the simulation results for the developed models

	$\dot{W}_{net}$ [kW]	Total UA-value [kW/K]	COP [-]	w [kJ/kg$_{LNG}$]	FOM [%]
Single-expader - one comp. stage	2495	91.4	0.318	2588	17.04
Two-stage comp. (no coupling)	1835	142.5	0.432	1904	21.17
Two-stage comp. (with coupling)	1970	141.5	0.403	2043	21.59
R410A pre-cooling	1783	153.2	0.445	1849	23.85
Propane pre-cooling	1775	156.1	0.447	1841	23.96
Sub-critical CO_2 pre-cooling	1828	146.7	0.434	1896	23.26
Super-critical CO_2 pre-cooling	1868	144.2	0.425	1938	22.76
Dual-turbine - different PR	1447	303.1	0.548	1501	29.38
Dual-turbine - same PR	1646	263.9	0.482	1707	25.84
Two-stage expansion	1540	225.1	0.515	1598	27.61
N_2 sub-cooling	1581	305.8	0.502	1640	26.89
CH_4 sub-cooling	1608	598.6	0.494	1667	26.45
Niche	1917	333.2	0.414	1992	22.18

A first possibility of reducing the gap between the temperature profiles at the cold box is to add a pre-cooling phase. Among the considered refrigerants propane results the most effective, allowing an increase in FOM of almost 7 %. Correspondingly net power consumption is reduced by almost 30 %. It is also shown that the pre-cooling cycle should cover a larger share of the natural gas cooling demand.
Pre-cooling alternatives are compared given the same pre-cooling temperature, i.e. given the same contribution from the pre-cooling cycle to the fulfilment of the natural gas cooling demand. Therefore the low-pressure levels in the pre-cooling cycle vary depending on the employed refrigerant and could go below atmospheric level (0.98 bar for the propane-case with -40°C as pre-cooling temperature).

Another category of expander-based cycles comprises the dual-expander configurations in which expansion process takes place in two different expanders. Three expansion designs are presented. The highest benefit in terms of reduction of net power consumption is recorded when having different expander pressure ratios (-42 % compared to the single-expansion cycle with one compression stage).

Finally dual-refrigerant configurations are presented. Refrigerants (nitrogen and methane or nitrogen and natural gas itself) contribute to the natural gas cooling in separate loops. If nitrogen and methane are used, nitrogen is found to be more effective than methane to cool natural gas in the lower temperature range, i.e. for feed liquefaction and sub-cooling. N_2 sub-cooling dual-refrigerant cycle allows a reduction of net power consumption of almost 37 % with respect to the least efficient alternative, which can go up to 44 % if the natural gas intermediate temperature is reduced. A lower intermediate temperature level leads to a significant reduction of the average LMTD at the last two-stream heat exchanger of the cold

box (from 21 K to 10 K), thus decreasing the exergy loss during the heat exchange process. In fact from the thermodynamic theory the influence of the heat-transfer driving force increases with decreasing temperature level at which the heat transfer takes place [67].
Niche cycle uses natural gas itself as refrigerant medium in an open configuration. This expander-based alternative is not as interesting as the other dual-refrigerant cycles given the smaller reduction in power consumption (-23 % compared to the single-expansion cycle with one compression stage), linked to the impossibility of reducing natural gas intermediate temperature as much as in the other dual-refrigerant configurations.

As extensively presented through the use of the Composite Curve representation, all the further developments of the single-expander cycle, namely pre-cooling cycles, dual-expander cycles and dual-refrigerant cycles, allow a substantial reduction in power consumption thanks to a closer match of the temperature profiles. The average cold box LMTD can be used as an indicator for the spread between the Hot and Cold Composite Curves. It is calculated as the ratio of cold box heat duty to its total UA-value. Values are listed below for the best cycles of each category.

- single-expander cycle: 16 K
- propane pre-cooled single-expander cycle: 12 K
- dual-expander cycle with different pressure ratio: 8 K
- N_2 sub-cooling dual-refrigerant cycle: 9 K

This result was expected as the area between the Composite Curves is related to the exergy destruction in the heat exchange process. As presented by Linnhoff and Dhole [68] a Composite Curve can be redrawn by replacing the temperature with the Carnot factor η_C resulting in the so-called "exergy Composite Curve". The area between the exergy Composite Curves is directly proportional to the lost work during the heat exchange process, thus to the net work input to the cycle [51].
In light of this concept the choice of modelling and presenting liquefaction cycle designs in which all the heat exchange devices present a temperature approach of 3 K goes in the direction of optimising the configurations. However a number of model inputs had to be arbitrarily set and these values might be sub-optimal. A rigorous thermodynamic optimisation is therefore required and is the main focus of the next Chapter.
The optimisation target is not only the minimisation of net power input to the cycle but also the minimisation of the overall heat network conductance, or UA-value, which is an indicator of the required heat exchange area. The reason for this choice originates from the conflicting relation between net power consumption and total UA-value which is observed throughout the thermodynamic modelling phase. As the net power consumption is reduced, the total UA-value increases, passing from 91 kW/K for the least efficient cycle to 303 kW/k for the most efficient alternative.

5 Thermodynamic optimisation of expander-based LNG configurations

This Chapter presents the results from the thermodynamic optimisation of the developed models. The optimisation process gives a robust answer to the research aim of quantifying the performance improvement that can be achieved for an expander-based liquefaction cycle. Moreover it provides the optimal design for each of the thirteen cycles which will be used for the subsequent steps of economic evaluation and comparison with other liquefaction alternatives.

5.1 Introduction

Thermodynamic optimisation is performed using the tool *OSMOSE* [69] developed at the École Polytechnique Fédérale de Lausanne (EPFL). This tool is suitable for process integration and optimisation and is run using Matlab platform as control interface of Aspen Plus. The optimisation algorithm is genetic.
The thermodynamic optimisation is performed in two subsequent steps and its aim is twofold. The objective of the first step is the minimisation of the net power consumption. Successively a series of Multi-Objective Optimisations is performed with the aim of simultaneously minimising the net power consumption and the required heat transfer area, the latter through the total UA-value for the liquefaction cycle.
The presentation of the results follows the categorisation introduced in Chapter 4. For each expander-based configuration the set of decision variables is presented with the corresponding variation ranges and optimal values. Successively the optimised cycle performance is discussed by means of an exergy analysis. Finally the Pareto fronts which are obtained from the Multi-Objective Optimisations are illustrated per group of expander-based configurations. For the sake of readability and conciseness the cold box Composite Curves for the optimal cycles are not shown in this Chapter but are presented in Appendix C.

5.2 Methodology

Before running an optimisation the relevant decision variables have to be identified and for each of them a sensible variation interval has to be provided. A large interval theoretically improves the probability of finding the global optimum. Nonetheless it increases computational burden and the possibility of non-convergence. The optimisation of a thermodynamic system is not a trivial problem due to the high degree of non-linearity, non-continuity and to the large research space. In the literature this is addressed by limiting the degrees of freedom for complex systems, thus decreasing the computational burden. The drawback is that potentially good solutions may be left outside the research space [38].
In the present work the variation ranges for the decision variables are set based on the literature and the sensitivity analyses presented in Chapter 4. Decision variables will be presented for each model together with the corresponding boundaries. They normally coincide with the design variables presented in Chapter 4 during the modelling process.

5.2.1 Penalty function formulation

The optimisation problem is constrained by the introduction of penalty functions. Their aim is to ensure that the following conditions are fulfilled:

- the temperature approach at every heat exchanger cannot be lower than 3 K. For computational reasons this boundary is set equal to 2.995 K.
- the vapour fraction at both compressor and expander inlets and outlets cannot be lower than 1. Again for computational reasons this boundary is set equal to 0.995.

The two penalty conditions are addressed differently.
In the case of refrigerant vapour fraction at the suction and discharge of turbo-machinery, the algorithm is required to discard any solution which brings the vapour fraction below the threshold of 1.
Conversely for the temperature approach two situations can be identified: a negative temperature approach, corresponding to thermodynamic infeasibility, and a positive temperature approach but below the 3 K-threshold, corresponding to technical infeasibility.
Solutions that are thermodynamically feasible but impracticable are penalised following a "functional" approach, according to which the objective function's value is set to linearly decrease from a 0-K to a 3-K temperature difference[1]. This way a solution bringing a temperature approach of e.g. 2 K is further investigated by the optimiser.
Solutions that are impossible from a thermodynamic viewpoint are directly discarded as in the case of the vapour fraction constraint.

[1] The interested reader can find additional explanation in Appendix D together with an assessment of the influence that penalty function formulations have on the optimisation outcome.

5.2.2 Exergy analysis

Exergy analysis is performed on the optimal cycle design. The main goal of the exergy analysis is to visualise the distribution of exergy destructions and losses in the liquefaction cycle. For this purpose components' rational efficiency defects are calculated.
The reader should refer to the work of Kotas [52] for the definitions of exergy fuel and product of compressors, expanders, heat exchangers, valves and mixers.
A remark has to be made regarding the coolers and more generally all the heat exchange blocks with only one stream. The purpose of these components is to reject heat to the ambient. For the sake of the exergy analysis this rejection is regarded as an exergy loss[2]. Therefore the cooler rational efficiency defect is calculated as the ratio of the exergy loss to the net power input to the cycle.
The boundaries for the exergy analysis are placed before the expansion and flashing of the liquefied natural gas. Given this assumption chemical exergy can be disregarded as no change in chemical composition occurs.

5.2.3 Statistical analysis

The tool *OSMOSE* allows to run a statistical analysis as post-computational phase of a Multi-Objective Optimisation (MOO). It allows to understand the distribution of the decision variables' values along the Pareto front and the dependencies between decision variables and objective functions.
In the present work Pearson partial linear correlation coefficients ρ are post-computed and discussed in this Chapter after the MOO's regarding the simultaneous minimisation of net power consumption and total UA-value. These coefficients describe the relation between the variables x and y when the influence of all the other variables z is eliminated.

$$\rho_{x,y\cdot z} = \frac{\rho_{x,y} - \rho_{x,z}\rho_{y,z}}{\sqrt{(1-\rho_{x,z}^2)(1-\rho_{y,z}^2)}} \tag{5.1}$$

The Pearson partial linear coefficient are used to discuss the dependency of objective functions on a specific decision variable in datasets containing n values, when the influence of all the other decision variables is eliminated. Values of ± 1 indicate a perfect linear correlation, while a value of 0 indicates absence of linear correlation [55].

[2] In rigorous terms this exergy loss accounts for (1) the exergy destruction due to the temperature difference between the heat exchange fluids at the cooler, and (2) the actual exergy lost to the ambient. The absence of the secondary-side fluid makes these two terms indistinguishable, therefore the cooler is characterised by a pure exergy loss.

5.3 Single-expander configurations

5.3.1 Single compression stage

Table 5.1 shows the decision variables and their corresponding optimal values. The performance of the optimised single-expander cycle is summarised in Table 5.2.

Table 5.1: Decision variables, corresponding variation ranges and optimal values for the single-expander cycle with one compression stage

Decision variable	Unit	Range	Optimal value
P_{high}	bar	[60 130]	116.8
P_{low}	bar	[1 20]	12.6
T^{in}_{exp}	°C	[-100 0]	-54.1
$\dot{m}_{N_2}$	kg/s	[5 20]	8.7

Table 5.2: Main results and performance indicators for the optimised single-expander cycle with one compression stage

$\dot{W}_{net}$ [kW]	Total UA-value [kW/K]	COP [-]	w [kJ/kg$_{LNG}$]	FOM [%]
2475	137.4	0.320	2568	17.18

It is observed that all the solutions around the optimum present similar values for the decision variables. Figure 5.1 shows the distribution of exergy destructions and losses in the cycle.

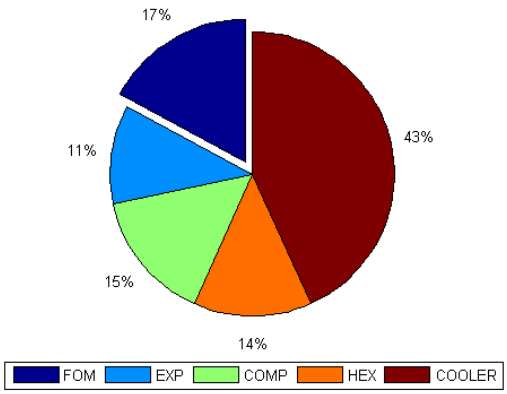

Component	$\dot{E}_D$ [kW]	$\dot{E}_L$ [kW]	δ [%]
Comp	369	-	14.89
Exp	278	-	11.24
MHEX 1	134	-	5.40
HEX 2	201	-	8.12
Cooler	-	1069	43.17

Figure 5.1: Figure of Merit and distribution of exergy destructions and losses for the optimised single-expander cycle with one compression stage

With respect to the model presented in Section 4.4.1 the optimisation provides a slightly better design, achieving a reduction of 0.8 % in net power consumption. This is obtained through a reduction of the cycle pressure ratio, which in turns causes the required refrigerant flow rate to be higher. Figure 5.1 shows that the cooler is the component dissipating the highest fraction of the exergy input to the cycle. The highest exergy destruction takes place in the compressor given the high pressure ratio (above 9).

5.3.2 Two compression stages

Table 5.3 lists the decision variables for the optimisation of the two-stage compression cycles. As presented in Section 4.4.2 the mechanical coupling makes the intermediate pressure level a model variable. In the optimal configuration the intermediate pressure level is equal to 15.6 bar. Table 5.4 shows the optimised performance of the two-stage compression cycles.

Table 5.3: Decision variables, corresponding variation ranges and optimal values for the single-expander cycles with two compression stages (without and with mechanical coupling)

Decision variable	**Unit**	**Range**	**Optimal value**	
			no mech. coupling	**with mech. coupling**
$\mathbf{P_{high}}$	bar	[60 130]	129.6	114.3
$\mathbf{P_{low}}$	bar	[1 10]	7.8	6.6
$\mathbf{P_{int}}$	bar	[11 59]	33.6	(constrained)
$\mathbf{T^{in}_{exp}}$	°C	[-100 0]	-25.2	-24.6
$\dot{m}_{N_2}$	kg/s	[5 20]	6.3	6.3

Table 5.4: Main results and performance indicators for the optimised single-expander cycle with two compression stages in the cases of no mechanical coupling and with mechanical coupling

	$\dot{W}_{net}$ **[kW]**	**Total UA-value [kW/K]**	**COP [-]**	w **[kJ/kg$_{LNG}$]**	**FOM [%]**
No mech. coupling	1796	133.8	0.441	1863	23.67
With mech. coupling	1945	135.3	0.408	2018	21.86

No variability in terms of decision variables is recorded close to the optimum for both cases. In both cases the optimiser provides a better design compared to the ones presented in Section 4.4.2. For the two-stage compression cycle with no mechanical coupling between LP compressor and expander a decrease of 3.6 % in net power consumption is achieved. The improvement is smaller when mechanical coupling is implemented (-1.3 % in net power consumption).

With respect to the single-expander cycle with one compression stage the reduction in net power consumption is 27 % in the case of no mechanical coupling, 21 % in the case of mechanical coupling. The compression process design is therefore confirmed to be highly influencing for the performance of an expander-based liquefaction cycle.
Figures 5.2 and 5.3 illustrate the distribution of exergy destructions and losses for the optimal design.

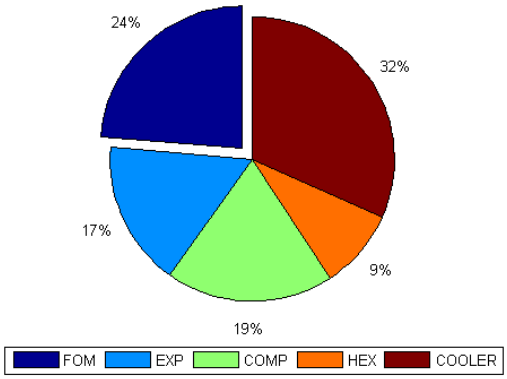

Component	$\dot{E}_D$ [kW]	$\dot{E}_L$ [kW]	δ [%]
LP Comp	175	-	9.77
HP Comp	165		9.21
Expander	297	-	16.54
MHEX 1	36	-	2.01
HEX 2	127	-	7.05
Cooler 1	-	290	16.12
Cooler 2	-	281	15.63

Figure 5.2: Figure of Merit and distribution of exergy destructions and losses for the optimised single-expander cycle with two compression stages and no mechanical coupling

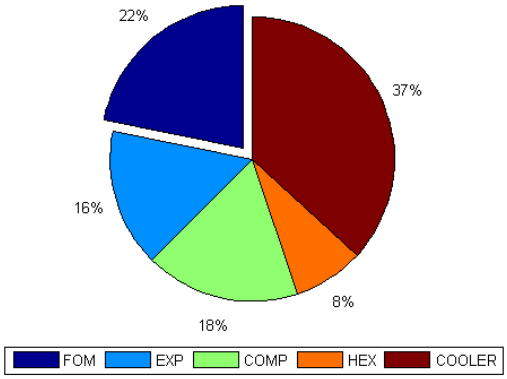

Component	$\dot{E}_D$ [kW]	$\dot{E}_L$ [kW]	δ [%]
LP Comp	103	-	5.28
HP Comp	240		12.35
Exp	305	-	15.67
MHEX 1	34	-	1.73
HEX 2	122	-	6.25
Cooler 1	-	90	4.62
Cooler 2	-	627	32.24

Figure 5.3: Figure of Merit and distribution of exergy destructions and losses for the optimised single-expander cycle with two compression stages and mechanical coupling

The exergy loss at the coolers represents the largest dissipation in both cycles. Nevertheless the two-stage compression allows to significantly reduce this exergy loss when compared with the single-stage alternative. This is expected as the inter-cooled two-stage compression process leads to lower compressor outlet temperatures, thus a lower heat rejection to the ambient.

Moreover having a more efficient compression process allows to enlarge the cycle pressure ratio, hence allowing a reduction in the required nitrogen flow rate (6.3 kg/s against 8.7 kg/s). Finally, a significant reduction in exergy destruction at the cold box is observed when comparing the single-stage and the two-stage compression alternatives.
Comparing the two-stage compression alternatives it can be noted that implementing the mechanical coupling leads to a lower exergetic performance for the overall compression process given the sub-optimality of the intermediate pressure level. As a consequence, exergy dissipation at the coolers is slightly higher (717 kW against 571 kW).
From a thermodynamic viewpoint, given the high pressure ratio (above 16 in both cases) it is meaningful to design the compression process with more than two stages, as this results to be beneficial in terms of power consumption reduction.

5.3.3 Multi-Objective Optimisation

Figure 5.4 illustrates the Pareto fronts obtained from the Multi-Objective Optimisation of the single-expander configurations. The total UA-value is reported on the y axis.

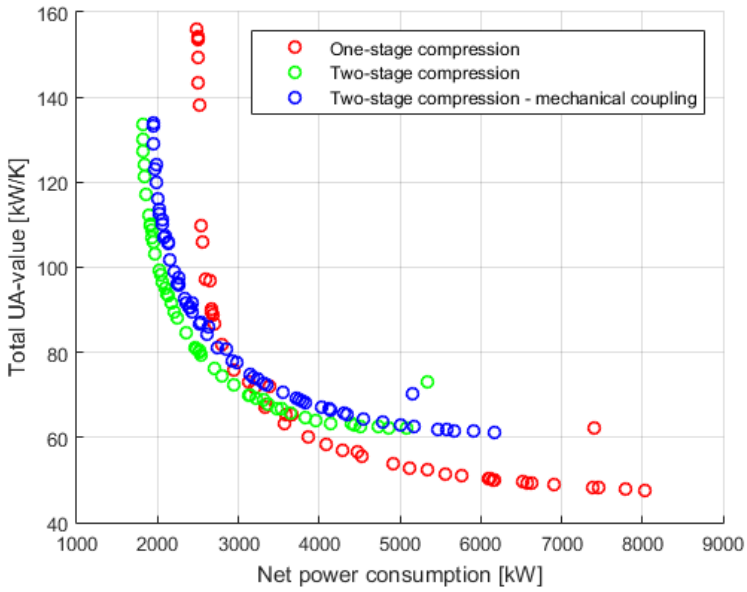

Figure 5.4: Pareto fronts for the single-expander configurations

The ranking of the three alternatives in terms of minimum net power consumption (thus maximum Figure of Merit) is clearly visible. It can also be noted that in the best possible design the required heat transfer area is much higher for the one-stage compression case. This is also the configuration which achieves the lowest total UA-value at higher power consumptions.

The distribution analysis of the decision variables indicates that the optimal value of nitrogen high pressure is always close to the upper bound of 130 bar. Conversely nitrogen mass flow rate is always close to the lower bound of 5 kg/s. The lowest values of nitrogen flow rate characterise the solutions minimising the heat network conductance.
The expander inlet temperature shows the lowest values in those solutions minimising the net power consumption. If the minimisation of the total UA-value is the objective, a value close to 0°C has to be chosen.
Refrigerant low pressure level is the decision variable showing the highest variability among the optimal points constituting the Pareto frontiers. Low pressure level has to be kept as high as possible if the objective is to minimise the power consumption, as low as possible if instead heat transfer area has to be minimised. The same consideration holds for the intermediate pressure level, when applicable.

Considering the Pearson partial linear coefficients, for the one-stage compression cycle low pressure level is the decision variable showing the highest correlation with net power consumption. Pearson partial coefficient is -0.7. Therefore an increase in refrigerant low pressure level is connected to a decrease in net power consumption, given the smaller pressure ratio. As to the correlation of the total heat transfer area with the decision variables, an increase in nitrogen low pressure level leads to a higher heat network conductance (ρ of +0.3).
When considering the two-stage compression cycle with no mechanical coupling, nitrogen temperature at the expander inlet and intermediate pressure level present a positive correlation coefficient with respect to net power consumption (ρ of +0.5 in both cases). Once again nitrogen low pressure level is the most correlated decision variable with respect to the total UA-value, with a Pearson partial coefficient of +0.4.
For the two-stage compression cycle with mechanical coupling the decision variable which is mostly correlated with both objectives is the low pressure level of the refrigerant. Pearson coefficient is -0.6 when considering the net power consumption, +0.6 regarding the total UA-value. If the low pressure level increases, the temperature at the expander outlet gets higher, thus reducing the average temperature difference available for natural gas sub-cooling.

Overall it is interesting to notice how the partial coefficient analysis confirms the trade-off between the two conflicting objectives. Especially regarding the refrigerant low pressure level, a change in this decision variable leads to opposite effects on net power consumption and total UA-value.

5.4 Pre-cooling configurations

Four pre-cooling alternatives are optimised, each one employing a different refrigerant in the pre-cooling cycle, namely R410A, propane, sub-critical and super-critical CO_2.
Tables 5.5 and 5.6 list the decision variables, the corresponding variation ranges and optimal values for the four alternatives. They differ only in terms of variation ranges for the decision variables of the pre-cooling cycle, which are tailored on the specific refrigerant.
As to the sub-critical pre-cooling cycles, the high pressure level ranges from the saturation pressure at 20°C to the critical pressure for each of the considered refrigerants. In the case of the super-critical CO_2 the lower bound is the critical pressure, while the upper is set equal to 100 bar. The refrigerant temperature at the throttling valve inlet is kept fixed at 20°C during the optimisation process.
Low pressure level range is defined in such a way that the refrigerant can achieve evaporation temperatures as low as -43°C and as high as -3°C, these values being connected to the variation range of the pre-cooling temperature.
Refrigerant mass flow rate in the pre-cooling cycle is not a decision variable but is calculated in order to achieve the desired super-heating at the evaporator, thus the temperature approach at the evaporator warm side.

Table 5.5: Decision variables, corresponding variation ranges and optimal values for the R410A pre-cooled (on the left) and propane pre-cooled (on the right) single-expander cycle

Decision variable	**Unit**	**Range**	**Optimal value**
$\mathbf{P_{high,N_2}}$	bar	[60 130]	82.8
$\mathbf{P_{low,N_2}}$	bar	[1 10]	8.7
$\mathbf{T^{in}_{exp}}$	°C	[-100 -45]	-55.1
$\dot{\boldsymbol{m}}_{\mathbf{N_2}}$	kg/s	[1 15]	6.3
$\mathbf{P_{high,PC}}$	bar	[13.98 49]	13.98
$\mathbf{P_{low,PC}}$	bar	[1 8]	1.5
$\mathbf{T_{PC}}$	°C	[-40 0]	-39.4

Decision variable	**Unit**	**Range**	**Optimal value**
$\mathbf{P_{high,N_2}}$	bar	[60 130]	108
$\mathbf{P_{low,N_2}}$	bar	[1 10]	9.9
$\mathbf{T^{in}_{exp}}$	°C	[-100 -45]	-46.6
$\dot{\boldsymbol{m}}_{\mathbf{N_2}}$	kg/s	[1 15]	5.6
$\mathbf{P_{high,PC}}$	bar	[8.37 42.5]	8.37
$\mathbf{P_{low,PC}}$	bar	[0.5 5]	0.98
$\mathbf{T_{PC}}$	°C	[-40 0]	-39.9

Table 5.6: Decision variables, corresponding variation ranges and optimal values for the sub-critical (on the left) and super-critical (on the right) CO_2 pre-cooled single-expander cycle

Decision variable	Unit	Range	Optimal value
$\mathbf{P_{high,N_2}}$	bar	[60 130]	103.4
$\mathbf{P_{low,N_2}}$	bar	[1 10]	9.4
$\mathbf{T^{in}_{exp}}$	°C	[-100 -45]	-46.5
$\dot{m}_{N_2}$	kg/s	[1 15]	5.6
$\mathbf{P_{high,PC}}$	bar	[57.35 73.8]	57.35
$\mathbf{P_{low,PC}}$	bar	[5 35]	8.8
$\mathbf{T_{PC}}$	°C	[-40 0]	-40

Decision variable	Unit	Range	Optimal value
$\mathbf{P_{high,N_2}}$	bar	[60 130]	105.6
$\mathbf{P_{low,N_2}}$	bar	[1 10]	9.3
$\mathbf{T^{in}_{exp}}$	°C	[-100 -45]	-45.1
$\dot{m}_{N_2}$	kg/s	[1 15]	5.7
$\mathbf{P_{high,PC}}$	bar	[73.9 100]	73.9
$\mathbf{P_{low,PC}}$	bar	[5 35]	10.4
$\mathbf{T_{PC}}$	°C	[-40 0]	-35.4

Once again small variability in decision variable values is observed around the optimum for all the four pre-cooling alternatives.
Looking at the optimum values for the decision variable two main features can be spotted. Firstly all the optimal solutions present a high pressure level which tends to hit the lower bound of the feasible variation range. This is expected as compression power in the pre-cooling cycle is reduced if the pressure ratio is smaller. Secondly all the sub-critical alternatives show an optimal pre-cooling temperature towards the lower bound of -40°C, given the higher COP of the pre-cooling cycle. This confirms the trends observed and discussed in Section 4.5.1.
Table 5.7 reports the comparison of the optimised pre-cooling configurations.

Table 5.7: Comparison of optimal pre-cooling cycles in terms of refrigerant mass and volume flow rates, net power consumption, total heat network conductance, COP, unit energy consumption and FOM

	$\dot{m}_{ref}$ [kg/s]	$\dot{V}_{ref}$ [m^3/s]	$\dot{W}_{net}$ [kW]	Total UA-value [kW/K]	COP [-]	w [kJ/kg_{LNG}]	FOM [%]
R410A	3.4	0.19	1626	153.9	0.488	1687	26.14
Propane	1.6	0.25	1559	176.2	0.509	1617	27.27
Sub-critical CO_2	2.6	0.06	1711	169.1	0.464	1774	24.85
Super-critical CO_2	2.3	0.04	1772	154.6	0.448	1838	24.00

Propane is the most effective refrigerant among the ones simulated, closely followed by R410A and sub-critical CO_2. R410A-case is instead more convenient than propane when considering the high-pressure level on the nitrogen side and the volume flow rate at the evaporator, which is connected to the required heat transfer area in the pre-cooling cycle. As expected, the super-critical CO_2 alternative is not advantageous in terms of net power consumption.

With respect to the best solution which is described in Section 4.5 (propane pre-cooling at -40°C) the optimiser provides a slightly better solution, with a decrease in net power consumption of 2.3 % (from 1596 kW to 1559 kW). With respect to the optimised single-expander cycle with one compression stage, a 37 % reduction in net power consumption is achieved.
The distribution of exergy destructions and losses is shown below only for the propane case.

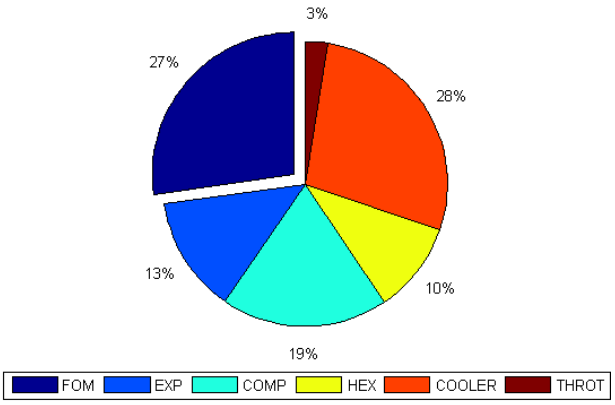

Component	$\dot{E}_D$ [kW]	$\dot{E}_L$ [kW]	δ [%]
N_2 Comp	254	-	16.30
Exp	205	-	13.16
MHEX 1	3	-	0.18
HEX 2	92	-	5.93
Cooler	-	394	25.25
PC Comp	41	-	2.60
Condenser	-	38	2.41
Valve	40	-	2.59
Evaporator	67	-	4.31

Figure 5.5: Distribution of exergy destructions and losses for the optimised propane pre-cooled single-expander cycle

The exergy lost to cool the refrigerants is again the largest dissipation in the cycle, followed by the exergy destruction during the compression process. The presence of a pre-cooling cycle reduces the exergy destruction caused by the heat exchange process in the nitrogen cycle. This is due to the reduction of the average LMTD's at the MHEX and HEX when pre-cooling temperature is -40°C (as shown in Figure 4.15 in Section 4.4.2).
Pre-cooling cycle is responsible for 21 % of the total exergy destruction and for 9 % of the total exergy loss.

5.4.1 Multi-Objective Optimisation

Figure 5.6 illustrates the Pareto fronts obtained from the Multi-Objective Optimisation of the pre-cooling configurations.
The four alternatives are quite close to each other, both in terms of minimum net power consumption and minimum total UA-value. Propane is the most effective refrigerant for the pre-cooling phase. Nevertheless this is achieved with the highest heat network conductance among the considered pre-cooling cycles.

Considering the decision variable distribution along the Pareto fronts similar conclusions for the four pre-cooling alternatives can be drawn. Nitrogen mass flow rate, expander inlet temperature and low pressure level in the pre-cooling cycle do not vary and they are all close to their respective optimal points shown in Tables 5.5 and 5.6.

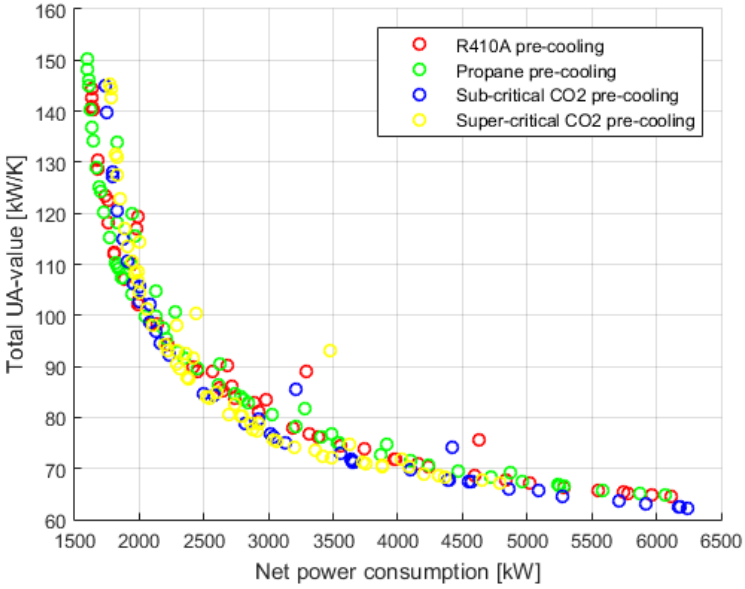

Figure 5.6: Pareto fronts for the pre-cooling configurations

Conversely the other decision variables show a large variability. In particular a pre-cooling temperature as low as -40°C is beneficial for the minimisation of net power consumption, while it hits the upper bound of 0°C for those solutions presenting the minimum total UA-value. The same trend is observed for the high pressure level in the pre-cooling cycle, which has to be kept as low as possible if net power consumption has to be minimised. A higher value for this pressure level goes in the direction of heat transfer area minimisation, as it is connected to an increase of refrigerant quality at the evaporator inlet, thus to a decrease in flow rate.
Quite surprisingly the optimal solutions for the minimisation of net power consumption show a high pressure level on nitrogen side which tends to be closer to the upper bound of 130 bar. Only the R410A-case achieves the optimum at a nitrogen high pressure lower than 100 bar, as shown in Table 5.5. Solutions giving a low heat network conductance are instead characterised by high pressure levels closer to 60 bar.

The analysis of the Pearson partial coefficients indicates that net power consumption is particularly correlated with the high pressure level on nitrogen side. Values of ρ for N_2 high pressure range from -0.5 in the R410A case to -0.9 in the propane case. Pre-cooling temperature level shows in general a lower degree of linear correlation (ρ ranging from +0.3 to +0.5).
As to the relation between decision variables and the total heat transfer area, low pressure levels both on nitrogen side and in the pre-cooling cycles result to be the most correlated decision variables with values for the Pearson partial coefficient between +0.6 and +0.8.

5.5 Dual-expander configurations

The three dual-expander cycles which are presented in Section 4.6, namely dual-turbine cycle with different pressure ratio, dual-turbine cycle with the same pressure ratio and two-stage cycle, are optimised and the optimisation outcome is reported in this Section.
In general terms the relevant decision variables are the pressure levels and flow rate of the refrigerant, natural gas intermediate temperatures and the split fraction, that is the fraction of the refrigerant flow rate which is sent to the low-pressure circuit.
Intermediate pressure level is applicable only for those configurations having different pressure ratios for the expanders. For this reason the decision variables for the dual-turbine cycle with different pressure ratio and the two-stage expansion cycle are presented together in Table 5.8. Table 5.9 shows the same for the dual-turbine cycle with the same expander pressure ratio.

Table 5.8: Decision variables, variation ranges and optimal values for the dual-turbine cycle with different pressure ratio (on the left) and for the two-stage expansion cycle (on the right)

Decision variable	**Unit**	**Range**	**Optimal value**
$\mathbf{P_{high}}$	bar	[80 130]	116.5
$\mathbf{P_{low}}$	bar	[1 25]	18.5
$\mathbf{P_{int}}$	bar	[30 75]	50.8
$\mathbf{T^{NG}_{int,1}}$	°C	[-45 0]	-29
$\mathbf{T^{NG}_{int,2}}$	°C	[-100 -50]	-73.9
$\dot{\boldsymbol{m}}_{\mathbf{N_2}}$	kg/s	[5 20]	13.8
Split frac.	-	[0.05 0.5]	0.36

Decision variable	**Unit**	**Range**	**Optimal value**
$\mathbf{P_{high}}$	bar	[80 130]	109.2
$\mathbf{P_{low}}$	bar	[1 25]	10.1
$\mathbf{P_{int}}$	bar	[30 75]	38.9
$\mathbf{T^{NG}_{int,1}}$	°C	[-45 0]	-44.4
$\mathbf{T^{NG}_{int,2}}$	°C	[-100 -50]	-89
$\dot{\boldsymbol{m}}_{\mathbf{N_2}}$	kg/s	[5 20]	11.4
Split frac.	-	[0.05 0.5]	0.29

Table 5.9: Decision variables, corresponding variation ranges and optimal values for the dual-turbine cycle with the same pressure ratio

Decision variable	**Unit**	**Range**	**Optimal value**
$\mathbf{P_{high}}$	bar	[80 130]	94.9
$\mathbf{P_{low}}$	bar	[1 50]	22.6
$\mathbf{T^{NG}_{int,1}}$	°C	[-45 0]	-26.8
$\mathbf{T^{NG}_{int,2}}$	°C	[-100 -50]	-94.7
$\dot{\boldsymbol{m}}_{\mathbf{N_2}}$	kg/s	[5 20]	11.4
Split frac	-	[0.05 0.5]	0.29

As previously mentioned the presence of a two-stage compression (as in the case of the dual-expansion cycles with different expander pressure ratio) leads to a larger cycle pressure ratio. The optimal values for nitrogen flow rate are higher compared to the required flow rates for single-expander cycles and pre-cooling cycles.

All the solutions close to the thermodynamic optimum are characterised by similar values for the decision variables in the three dual-expander configurations.
Table 5.10 shows the comparison between the optimised cycles in terms of net power consumption, heat network conductance and performance indicators.
The dual-turbine cycle with different pressure ratio results to be the best performing among the dual-expander cycles, closely followed by the two-stage expansion cycle. As discussed in Section 4.6, the dual-turbine cycle with the same pressure ratio is penalised compared to the other two alternatives by the single-stage compression process.
The optimisation procedures allows to improve all the considered cycle with respect to the modelled ones. The largest improvement in terms of net power consumption is achieved with the two-stage expansion cycle (-4.4 %).
The introduction of a dual-expansion process is found to largely improve the single-expansion cycle with one compression stage. The best alternative gives a reduction in net power consumption of 42 %, higher than the reduction which can be achieved with the best pre-cooling alternative.

Table 5.10: Main results and performance indicators for the optimised dual-expander cycles

	$\dot{W}_{net}$ [kW]	Total UA-value [kW/K]	COP [-]	w [kJ/kg$_{LNG}$]	FOM [%]
Dual-turbine - different PR	1431	280.0	0.554	1484	29.71
Dual-turbine - same PR	1614	288.1	0.492	1674	26.35
Two-stage expansion	1472	240.0	0.539	1527	28.88

The three optimal dual-expansion cycles are compared in terms of exergy destructions and losses. Results are presented in Figures 5.7 to 5.9.

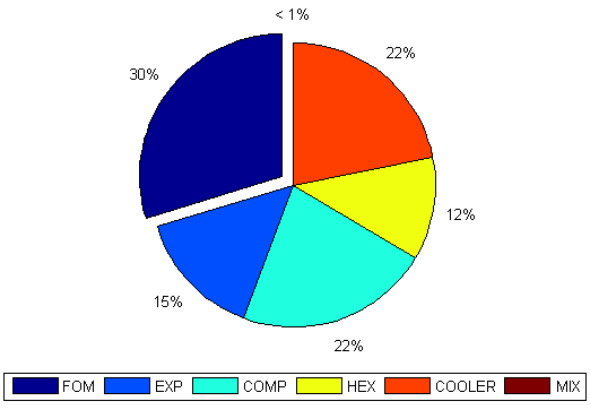

Component	$\dot{E}_D$ [kW]	$\dot{E}_L$ [kW]	δ [%]
LP Comp	96	-	6.72
HP Comp	220	-	15.37
LP Exp	113	-	7.90
HP Exp	96	-	6.68
MHEX 1	44	-	3.10
MHEX 2	28	-	1.95
HEX 3	96	-	6.69
Cooler 1	-	105	7.36
Cooler 2	-	208	14.53
Mixer	< 0.1	-	< 0.01

Figure 5.7: Figure of Merit and distribution of exergy destructions and losses for the optimised dual-turbine cycle with different pressure ratio

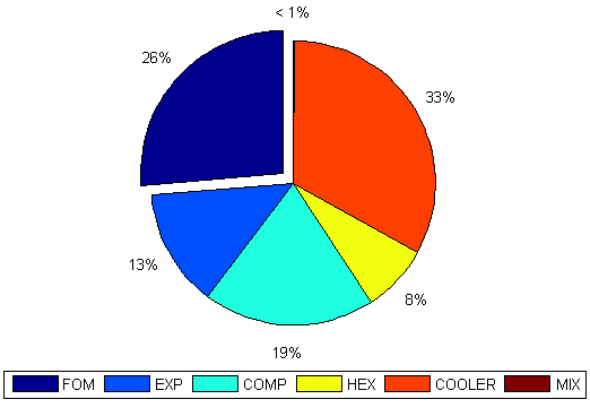

Component	$\dot{E}_D$ [kW]	$\dot{E}_L$ [kW]	δ [%]
Comp	315	-	19.50
Exp 1	166	-	10.31
Exp 2	49	-	3.03
MHEX 1	37	-	2.31
MHEX 2	49	-	3.02
HEX 3	38	-	2.33
Cooler	-	533	33.06
Mixer	1	-	0.08

Figure 5.8: Figure of Merit and distribution of exergy destructions and losses for the optimised dual-turbine cycle with the same pressure ratio

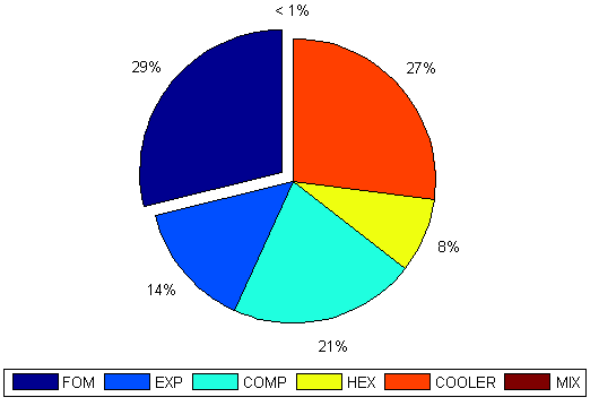

Component	$\dot{E}_D$ [kW]	$\dot{E}_L$ [kW]	δ [%]
LP Comp	86	-	5.83
HP Comp	226		15.34
LP Exp	59	-	4.02
HP Exp	152	-	10.31
MHEX 1	81	-	5.47
MHEX 2	25	-	1.70
HEX 3	19	-	1.31
Cooler 1	-	130	8.84
Cooler 2	-	269	18.3
Mixer	< 0.1	-	< 0.01

Figure 5.9: Figure of Merit and distribution of exergy destructions and losses for the optimised two-stage expansion cycle

The dual-turbine cycle with the same pressure ratio is the alternative presenting the most efficient heat exchange process at the cold box. Exergy destruction at the cold box amounts to 124 kW (it is 168 kW for the dual-expander cycle with different pressure ratio). In spite of this it shows the lowest Figure of Merit, mainly due to the high exergy dissipation at the cooler.
For the dual-turbine cycle with different pressure ratio and the two-stage expansion cycle the exergy destruction at the compressors becomes as impacting as the exergy loss due to the refrigerant cooling process. Expansion process is ranked third and is found to be slightly more efficient in the dual-turbine cycle with different pressure ratio, mostly because in this alternative both HP and LP expanders work with a fraction of the total nitrogen flow rate, whereas in the two-stage expansion cycle the splitting of refrigerant flow rate takes place after the first expansion.

5.5.1 Multi-Objective Optimisation

The Pareto fronts for the three considered dual-expansion configurations are illustrated in Figure 5.10.

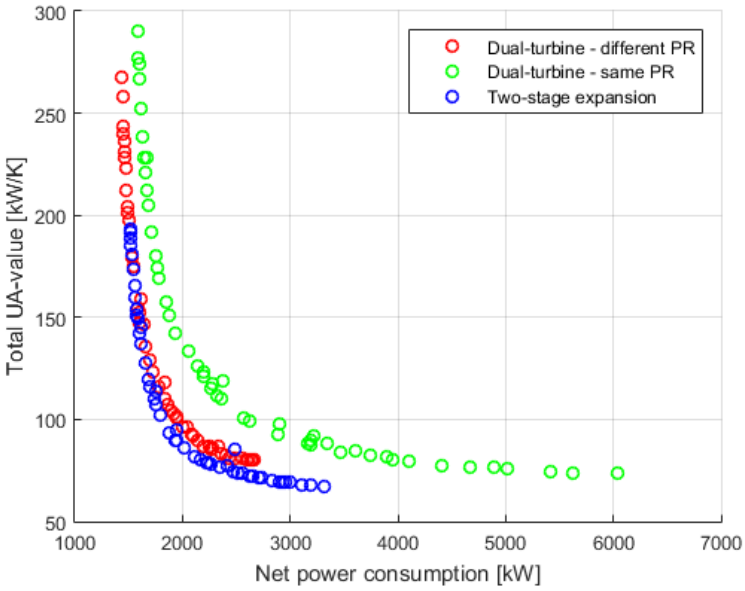

Figure 5.10: Pareto fronts for the dual-expander configurations

The two-stage expansion cycle is the one achieving the optimum in terms of net power consumption with the lowest heat network conductance. The dual-turbine cycle with the same expander pressure ratio shows not to be convenient as it is the alternative requiring a highest total heat transfer area without achieving net power consumption levels as low as for the other two configurations.

The distribution analysis of the decision variables gives some common indications for the dual-expander configurations. Specifically it is found that the low pressure level of the refrigerant and natural gas intermediate temperatures largely vary along the Pareto fronts. If net power consumption has to be minimised, refrigerant low pressure level has to be kept as high as possible, while natural gas intermediate temperatures have to be moved towards the corresponding lower bounds. This way the temperature difference between the refrigerant and the natural gas in the sub-cooling phase can be reduced and with that net power consumption.

As to the Pearson partial linear coefficients, it is found that net power consumption is highly correlated with the refrigerant low pressure level, with a coefficient ρ of -0.9 in the case of dual-turbine cycle with different pressure ratio and of -0.4 in the case of dual-turbine cycle with the same pressure ratio. As the low pressure level increases, the cycle pressure ratio decreases and with that the required power consumption. Net power consumption is also found to increase whether nitrogen flow rate increases (ρ of +0.8 for the dual-turbine cycle with different pressure ratio) or natural gas first intermediate temperature increases (ρ of +0.6 in the two-stage expansion cycle).
The total heat transfer area is found particularly correlated with the intermediate pressure level (ρ of +0.4 for the first dual-turbine alternative and of +0.6 for the third) and with natural gas first intermediate temperature level (ρ of -0.5 for the second dual-turbine configuration).

5.6 Dual-refrigerant configurations

Dual-refrigerant configurations are presented in Section 4.7. They are characterised by the use of two refrigerants in separate loop, namely nitrogen and methane or nitrogen and natural gas itself, the latter being known as *Niche* cycle.
For the sake of thermodynamic optimisation dual-refrigerant configurations are generally two separate single-expander cycles, each of them implementing an inter-cooled two-stage compression with the mechanical coupling between Low-Pressure compressor and the expander. Therefore the decision variables for each of the refrigerant loops are analogous to the ones presented in Section 5.3.2 with the addition of the natural gas intermediate temperature, which is the natural gas temperature after the first refrigerant loop.
Niche cycle differs from this approach for the absence of the low pressure level on natural gas side. As explained in Section 4.7.3 the intermediate pressure level has to coincide with natural gas feed pressure (33 bar), hence the low pressure level is constrained such that the expander power production coincides in absolute terms with LP compressor consumption.

Tables 5.11 and 5.12 list the decision variables for the three analysed dual-refrigerant configurations with the corresponding variation ranges and optimal values.
For the first dual-refrigerant alternative, namely N_2 sub-cooling dual-refrigerant cycle, intermediate pressure levels are 21.5 bar on nitrogen side and 30.9 bar on methane side.
Intermediate pressure levels are 37.3 bar on nitrogen side and 3.3 bar on methane side in the CH_4 sub-cooling dual-refrigerant case.
For the *Niche* cycle intermediate pressure level on nitrogen side is 16.4 bar, while low pressure level on natural gas side is 24.5 bar.

Table 5.11: Decision variables, corresponding variation ranges and optimal values for N_2 sub-cooling (on the left) and CH_4 sub-cooling (on the right) dual-refrigerant configurations

Decision variable	Unit	Range	Optimal value
$\mathbf{P_{high,N_2}}$	bar	[60 90]	74.8
$\mathbf{P_{high,CH_4}}$	bar	[60 90]	85.8
$\mathbf{P_{low,N_2}}$	bar	[5 30]	13.8
$\mathbf{P_{low,CH_4}}$	bar	[5 30]	19.1
$\mathbf{T^{in}_{exp,N_2}}$	°C	[-100 -50]	-81.1
$\mathbf{T^{in}_{exp,CH_4}}$	°C	[-50 0]	-24.8
$\mathbf{T^{NG}_{int}}$	°C	[-120 -20]	-98.3
$\dot{\boldsymbol{m}}_{\mathbf{N_2}}$	kg/s	[1 5]	3.0
$\dot{\boldsymbol{m}}_{\mathbf{CH_4}}$	kg/s	[1 5]	3.8

Decision variable	Unit	Range	Optimal value
$\mathbf{P_{high,N_2}}$	bar	[60 130]	77.4
$\mathbf{P_{high,CH_4}}$	bar	[2.5 20]	13.2
$\mathbf{P_{low,N_2}}$	bar	[1 30]	22.7
$\mathbf{P_{low,CH_4}}$	bar	[0.1 2]	1.9
$\mathbf{T^{in}_{exp,N_2}}$	°C	[-100 0]	-32.4
$\mathbf{T^{in}_{exp,CH_4}}$	°C	[-130 -80]	-86.4
$\mathbf{T^{NG}_{int}}$	°C	[-120 -20]	-87.4
$\dot{\boldsymbol{m}}_{\mathbf{N_2}}$	kg/s	[1 8]	7.4
$\dot{\boldsymbol{m}}_{\mathbf{CH_4}}$	kg/s	[1 8]	2.5

Table 5.12: Decision variables, corresponding variation ranges and optimal values for *Niche* cycle

Decision variable	Unit	Range	Optimal value
P_{high,N_2}	bar	[60 90]	85.5
$P_{high,NG}$	bar	[30 80]	42.9
P_{low,N_2}	bar	[1 30]	8.4
T^{in}_{exp,N_2}	°C	[-100 0]	-51.8
$T^{in}_{exp,NG}$	°C	[-15 0]	-2.3
T^{NG}_{int}	°C	[-50 -20]	-31.9
$\dot{m}_{N_2}$	kg/s	[5 12]	6.8
$\dot{m}_{NG}$[3]	kg/s	[1.1 5]	3.1

As for all the previous expander-based configurations, solutions close to the thermodynamic optimum are characterised by similar values of decision variables.
Looking at the optimal values for the decision variables it can be observed that for closed-loop configurations the optimisation algorithm tends to push natural gas intermediate temperature towards the lower bound of its variation range, confirming what was discussed in Section 4.7. Moreover it is interesting to notice that for the CH_4 sub-cooling alternative the optimiser gives a solution in which low pressure on methane side is above atmospheric level.

Table 5.13 reports the comparison of the optimised dual-refrigerant configurations in terms of net power consumption, total UA-value and performance indicators.
N_2 sub-cooling results the most efficient among the considered dual-refrigerant configurations and among all the expander-based cycles. With respect to the optimised single-expander cycle with one compression stage it allows a reduction in net power consumption of almost 48 %. Furthermore it is confirmed that *Niche* cycle is not an interesting alternative as it performs worse than the optimised dual-refrigerant, dual-expander and sub-critical pre-cooling configurations.

Table 5.13: Main results and performance indicators for the optimised dual-refrigerant cycles

	$\dot{W}_{net}$ [kW]	Total UA-value [kW/K]	COP [-]	w [kJ/kg$_{LNG}$]	FOM [%]
N_2 sub-cooling	1288	285.9	0.616	1336	33.02
CH_4 sub-cooling	1429	342.2	0.555	1482	29.76
Niche	1758	277.1	0.450	1828	24.18

[3] Total natural gas mass flow rate, i.e feed flow rate (1 kg/s) plus recirculated flow rate.

Comparing the optimised results with those obtained during the modelling stage substantial improvements are brought by the thermodynamic optimisation for all the three dual-refrigerant alternatives. The highest reduction in net power consumption occurs for N_2 sub-cooling cycle (-18.5 %, -5.2 % when considering the modelled alternative with lowered natural gas intermediate temperature).
Figures from 5.11 to 5.13 illustrate the distribution of exergy destructions and losses in the three optimised dual-refrigerant configurations.

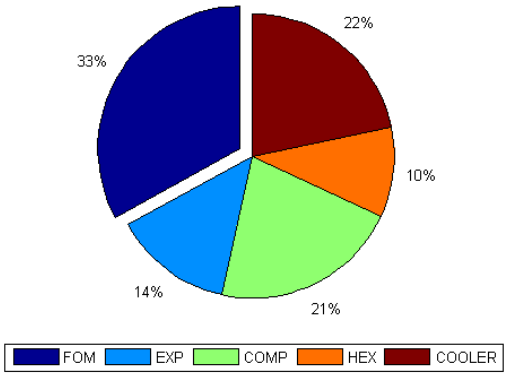

Component	$\dot{E}_D$ [kW]	$\dot{E}_L$ [kW]	δ [%]
N_2 LP Comp	25	-	1.97
N_2 HP Comp	73	-	5.64
N_2 Exp	67	-	5.17
CH_4 LP Comp	58	-	4.49
CH_4 HP Comp	120	-	9.35
CH_4 Exp	107	-	8.33
MHEX 1	51	-	3.95
HEX 2	39	-	2.99
HEX 3	28	-	2.20
HEX 4	15	-	1.18
N_2 Cooler 1	-	10	0.79
N_2 Cooler 2	-	109	8.46
CH_4 Cooler 1	-	23	1.78
CH_4 Cooler 2	-	138	10.68

Figure 5.11: Figure of Merit and distribution of exergy destructions and losses for the optimised N_2 sub-cooling dual-refrigerant cycle

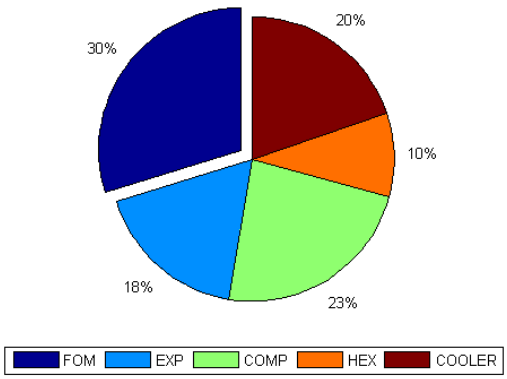

Component	$\dot{E}_D$ [kW]	$\dot{E}_L$ [kW]	δ [%]
N_2 LP Comp	70	-	4.88
N_2 HP Comp	104	-	7.25
N_2 Exp	127	-	8.88
CH_4 LP Comp	48	-	3.36
CH_4 HP Comp	114	-	7.96
CH_4 Exp	124	-	8.69
MHEX 1	38	-	2.69
HEX 2	23	-	1.59
HEX 3	22	-	1.53
HEX 4	53	-	3.69
N_2 Cooler 1	-	33	2.31
N_2 Cooler 2	-	88	6.14
CH_4 Cooler 1	-	20	1.42
CH_4 Cooler 2	-	141	9.85

Figure 5.12: Figure of Merit and distribution of exergy destructions and losses for the optimised CH_4 sub-cooling dual-refrigerant cycle

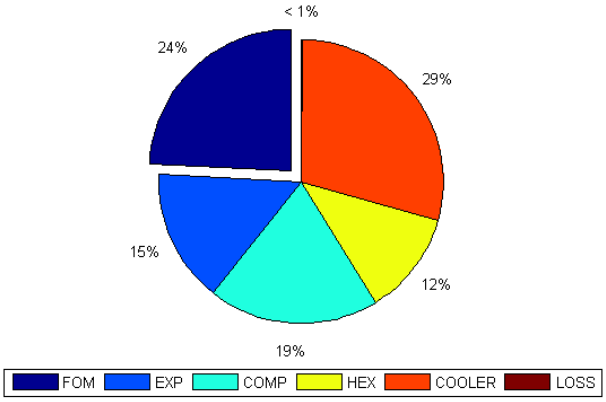

Component	$\dot{E}_D$ [kW]	$\dot{E}_L$ [kW]	δ [%]
N_2 LP Comp	88	-	4.95
N_2 HP Comp	219	-	12.29
N_2 Exp	248	-	13.88
NG LP Comp	17	-	0.98
NG HP Comp	22	-	1.25
NG Exp	22	-	1.23
MHEX 1	7	-	0.38
HEX 2	3	-	0.19
HEX 3	30	-	1.67
HEX 4	171	-	9.6
N_2 Cooler 1	-	58	3.25
N_2 Cooler 2	-	454	25.42
NG Cooler 1	-	4	0.22
NG Cooler 2	-	6	0.34
Loss	-	3	0.17

Figure 5.13: Figure of Merit and distribution of exergy destructions and losses for the optimised *Niche* cycle

For the close-loop dual-refrigerant alternatives the exergy destruction connected to the compression process is as impacting as the exergy dissipated for refrigerant cooling. The expansion process is generally ranked third and it is observed that the largest irreversibility takes place in the pre-cooling cycle expander. The exergy lost at the coolers is considerably smaller compared to the previous expander-based configurations, mainly due to the comparatively lower refrigerant temperature at compressor outlets.
As already pointed out, *Niche* cycle is penalised compared to the other dual-refrigerant alternatives by the large temperature difference occurring at the last heat exchanger (nitrogen-natural gas heat exchanger). Moreover in Figure 5.13 an additional exergy loss is introduced. As discussed in Section 4.7.3 the liquefied natural gas exits the cold box at a higher pressure compared to all other expander-based cycles (42.9 bar against 33 bar). In order to fairly compare the different configurations the physical exergy difference linked to this pressure difference is regarded as an exergy loss.

5.6.1 Multi-Objective Optimisation

Figure 5.14 illustrates the Pareto fronts for the analysed dual-refrigerant configurations.

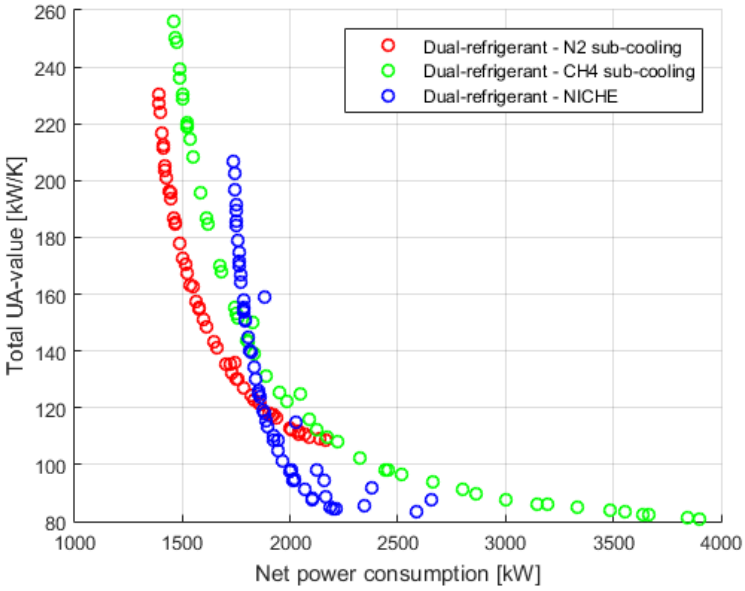

Figure 5.14: Pareto fronts for the dual-refrigerant configurations

Having methane active in the lower temperature range is less beneficial than having nitrogen. In fact a smaller net power consumption can be achieved with the N_2 sub-cooling case. Moreover the optimal point in terms of net power consumption is achieved with a lower requirement in terms of heat transfer area. This is due to the lower UA-value at the nitrogen-nitrogen heat exchanger compared to the methane-methane case.

Analysing the distribution of the decision variables along the Pareto fronts, it can be observed that for all the three dual-refrigerant alternatives refrigerants' low pressure and expander inlet temperature show a remarkable variability. Similarly to what already discussed for other expander-based configurations, the low pressure level for both refrigerants is found to be higher at the left end of the Pareto fronts (minimum net power consumption) while it hits the lower bound of its variation range on the right end (minimum heat transfer area). The opposite happens with refrigerants' expander inlet temperature.
Some differences can also be highlighted. For instance in the N_2 sub-cooling case all the solutions show a similar value of natural gas intermediate temperature and of refrigerants' flow rates. This is not the case for the CH_4 sub-cooling configuration, in which natural gas intermediate temperature is found to move towards the lower bound of its variation range as the Pareto front is followed from the left to the right, i.e. as net power consumption increases. The same happens with refrigerants' flow rates.

Conversely in the *Niche* cycle the variation of natural gas intermediate temperature along the Pareto front is opposite, that is a natural gas intermediate temperature as high as -20°C characterises those solutions minimising the required heat transfer area.

The analysis in terms of Pearson partial coefficients confirms what observed about the decision variable distribution.
For N_2 sub-cooling dual-refrigerant cycle the net power consumption is negatively correlated with nitrogen low pressure level (ρ of -0.9) and nitrogen temperature at the expander inlet (ρ of -0.7). An increase in both these decision variables leads to a closer match of the temperature profiles, thus to a lower net power consumption.
Respecting the trade-off between net power consumption and heat transfer area, the total UA-value is positively correlated with low pressure level and temperature at the expander inlet on methane side (ρ of +0.6 for both decision variables). Moreover methane high pressure level shows a Pearson partial coefficient of -0.4 with respect to the total UA-value.
When considering the CH_4 sub-cooling alternative the net power consumption is found highly correlated with methane high pressure level (Pearson partial coefficient of +0.6). The total UA-value is confirmed to be positively correlated with methane and nitrogen low pressure levels (ρ of +0.8 and +0.9, respectively) and is found negatively correlated with refrigerants' flow rates (ρ of -0.8).
In the case of *Niche* cycle the net power consumption is perfectly linearly correlated with nitrogen low pressure level. A high negative correlation is recorded with nitrogen temperature at the expander inlet (ρ of -0.8). Pearson partial linear coefficients are generally lower when considering the total heat transfer area. The total UA-value presents a positive linear correlation with nitrogen low pressure level (ρ of +0.5).

5.7 Discussion

This Chapter presents the results from the thermodynamic optimisation of thirteen different expander-based configurations for natural gas liquefaction.
The aim is to understand which design improvements can be adopted and to quantify their influence in terms of net power consumption and, at a later stage, of required heat transfer area. The need for a rigorous optimisation procedure through a genetic algorithm is justified by the relatively high number of decision variables that expander-based cycles present, usually pressure, temperature levels and refrigerant flow rates. As a remark, when comparing the optimisation outcome with the modelling results (presented in Chapter 4) it can be seen that all the optimised models perform better than the modelled ones. Moreover close-loop dual-refrigerant configurations overcome the dual-expander cycles in terms of thermodynamic performance.
The base case is the single-expander cycle with one compression stage, which achieves a net power consumption of 2475 kW. With respect to this, the design improvements that can be pursued are listed in Table 5.14 and discussed below.

Table 5.14: Summary of the Single-Objective Optimisation results for the developed models

	$\dot{W}_{net}$ [kW]	Total UA-value [kW/K]	COP [-]	w [kJ/kg$_{LNG}$]	FOM [%]
Single-expader - one comp. stage	2475	137.4	0.320	2568	17.18
Two-stage comp. (no coupling)	1796	133.8	0.441	1863	23.67
Two-stage comp. (with coupling)	1945	135.3	0.408	2018	21.86
R410A pre-cooling	1626	153.9	0.488	1687	26.14
Propane pre-cooling	1559	176.2	0.509	1617	27.27
Sub-critical CO_2 pre-cooling	1711	169.1	0.464	1774	24.85
Super-critical CO_2 pre-cooling	1772	154.6	0.448	1838	24.00
Dual-turbine - different PR	1431	280.0	0.554	1484	29.71
Dual-turbine - same PR	1614	288.1	0.492	1674	26.35
Two-stage expansion	1472	240.0	0.539	1527	28.88
N_2 sub-cooling	1288	285.9	0.616	1336	33.02
CH_4 sub-cooling	1429	342.2	0.555	1482	29.76
Niche	1758	277.1	0.450	1828	24.18

- Adopting an inter-cooled two-stage compression reduces the power consumption by 27 %. If Low-Pressure compressor is driven by the expander this reduction is lower, but fewer equipment is required. From a thermodynamic viewpoint it can be concluded that inter-cooled multi-stage compression design should be implemented.
- Pre-cooling of natural gas is beneficial and leads to a 37 %-saving in net power consumption. Pre-cooling cycle should cover a larger share of natural gas cooling load. Limitation to that is given by the pre-cooling refrigerant's saturation pressure and volume flow rate.
- Adopting a dual expansion process reduces net power consumption by 42 % for the best dual-turbine cycle.

- The highest benefit is recorded when choosing a dual-refrigerant cycle in which both refrigerants are used in closed loops. Nitrogen is confirmed to be more suitable than methane for natural gas cooling at lower temperature range. Net power consumption is reduced by 48 % with respect to the base case.

First and foremost it has to be said that further reductions in power consumption could have been achieved by coupling two design improvement steps, i.e. dual expansion with a pre-cooling cycle or pre-cooling single-expander cycle with inter-cooled two-stage compression. As an example He *et al.* [70] investigate and optimise a dual-turbine cycle with different pressure ratio adding R410A pre-cooling and inter-cooled three-stage compression, achieving a Figure of Merit of 56 %. This is not covered in the present work and could represent a future development of it. However this goes in the direction of a more complex cycle design, which is usually avoided for small-scale liquefaction plants.
It could also be argued that the dual-refrigerant alternatives perform the best as they combine the dual-refrigerant concept with the inter-cooled two-stage compression process. This modelling choice is adopted as these cycles are designed in such a way in "real-life" applications. Moreover the inter-cooled two-stage compression is also implemented in some of the considered dual-expander configurations, therefore the provided ranking is considered robust.

Comparing the obtained results with the ones presented in the literature some differences can be highlighted.
For instance He *et al.* [41] claim that R410A is the most effective pre-cooling refrigerant, whereas in this work it is found that propane achieves the best performance. This difference originates from the variation range which is set for the pre-cooling temperature, as the authors set a lower bound of -44°C for R410A and of -37°C for propane. On one side this penalises the propane alternative, on the other hand it avoids having sub-atmospheric refrigerant in the pre-cooling cycle, a condition which is not required and fulfilled in the present work.
As to dual-expander cycles, Khan *et al.* [43] achieve a unit energy consumption of 2700 kJ/kg for the base-case single-expander cycle and of 1800 kJ/kg for the dual-turbine cycle with different pressure ratio (relative difference of -33 %). Values are slightly higher than the ones achieved in this work, mainly because authors select lower isentropic efficiency for the turbo-machinery (0.75 for both compressors and expanders) and a lower natural gas outlet temperature (-158.5°C). This difference is however mitigated by the presence of an inter-cooled four-stage compression process.
Dual-turbine cycle with different pressure ratio is the best dual-expander alternative also in the work of Chang *et al.* [60]. However the same authors show that dual-expander alternatives achieve improvements in Figure of Merit of 15 % compared to the single-expander cycle, slightly higher than what found in the present work. They select a lower expander isentropic efficiency (0.8) but they consider a richer natural gas feed, which liquefaction is shown to be less energy intensive. Moreover the same authors find that the two-stage expansion cycle performs slightly worse than the dual-turbine cycle with the same pressure ratio. Therefore further investigation could be performed about these aspects.

An exergy analysis in terms of components' rational efficiency defects is performed on the optimal cycle designs. The exergy dissipated to the ambient due to the cooling process of the refrigerant is the largest loss. Waste heat could be utilised e.g. for district heat purposes as the refrigerant temperature at compressor outlets is usually higher than 100°C. Compression process shows the largest fraction of exergy destruction, followed by the refrigerant expansion. Exergy destruction at the cold box is linked to the spread of the temperature profiles, hence it tends to become less and less impacting as the single-expander cycle with one compression stage is improved. An overview of the exergy destructions (at compressors, expanders and cold box heat exchangers) and losses (at refrigerant coolers) is given in Figure 5.15.

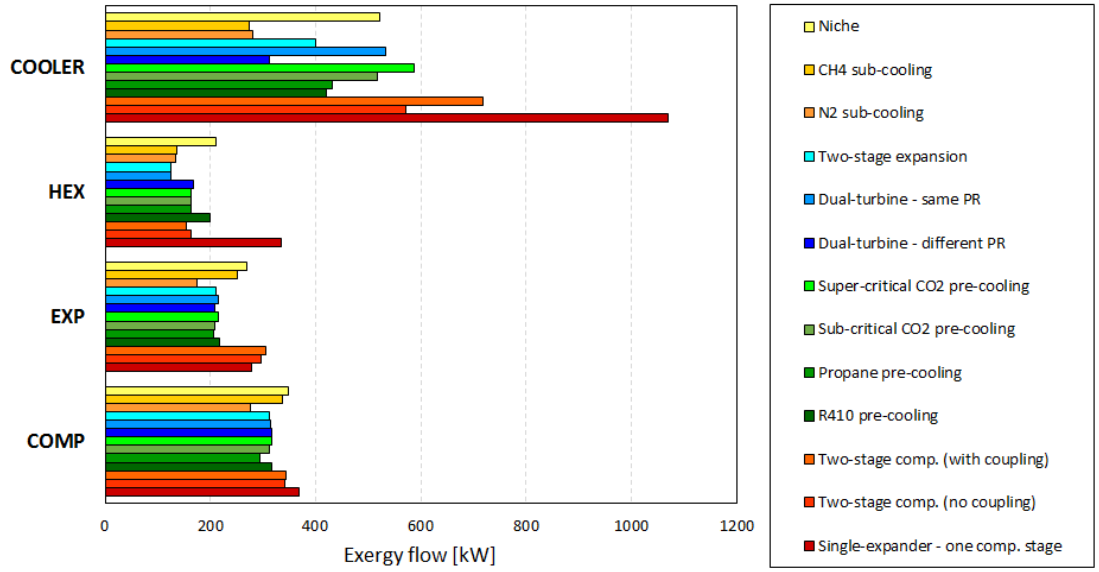

Figure 5.15: Exergy destructions and losses grouped per component category for the optimised expander-based configurations

Overall compression is the process responsible for the largest exergy destruction, followed by expansion and cold box heat exchange. This ranking is confirmed in the literature ([42], [70]). The exergy loss at the cooler is significantly influenced by the assumed refrigerant outlet temperature and is generally more impacting in less efficient cycles, whereas in the best alternatives it impacts less than the thermodynamic efficiency of compressors.

The trade-off between net power consumption and required heat transfer area is illustrated by means of Pareto fronts. In the Chapter they are presented per category of expander-based configurations. Additionally Figure 5.16 shows all the Pareto fronts in one single graph in order to remark how reductions in net power consumption are achieved at the expense of total UA-value.

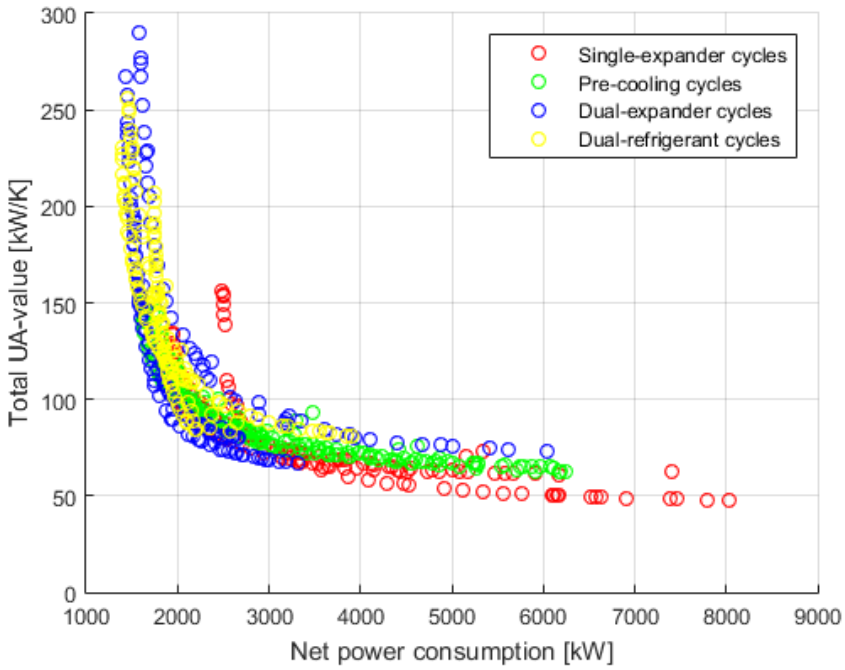

Figure 5.16: Pareto fronts for the thirteen analysed expander-based configurations grouped according to the followed categorisation

The trade-off is also highlighted by the statistical analysis in terms of decision variable distribution and Pearson partial linear coefficients. The most recurring result is the negative correlation between refrigerant's (or refrigerants') low pressure level with net power consumption, whereas the required heat transfer area is positively correlated with the same decision variable.

5.8 Conclusion

Thermodynamic optimisation is performed on the modelled expander-based configuration with the aim of minimising net power consumption and to find the thermodynamic optimal design for each of them. Results show that the N_2 sub-cooling dual-refrigerant cycle is the most efficient cycle, achieving a Figure of Merit of 33 %. Correspondingly net power consumption is reduced by 48 % with respect to the single-expander cycle with one compression stage.
Multi-Objective Optimisations are included in order to highlight the trade-off between power consumption and required heat transfer area, the latter through the total UA-value for the liquefaction cycle. As a result, for the expander-based concept net power consumption is found to range between 1300 and 8000 kW, while heat network conductance can range between 50 and 300 kW/K.

6 Economic analysis of expander-based LNG configurations

This Chapter presents the economic analysis performed on the developed and optimised expander-based models. Its aim is to identify the most promising alternatives from an economic point of view which will be used for the comparison with other liquefaction concepts hereafter.
The main economic figures are calculated for each configuration in the thermodynamic optimal design. Two sizes for the liquefaction facility are considered and the economic ranking is obtained accordingly. The most influencing parameters are identified through a series of sensitivity analyses.

6.1 Introduction

The tool *OSMOSE* allows to retrieve output data from Aspen simulations and use them as input for further analyses. The performed economic evaluation is based on this concept through the use of cost functions which translate a thermodynamic value into a monetary figure for the liquefaction cycle.
The starting point is the set of optimal designs which are obtained through the rigorous thermodynamic optimisation presented in Chapter 5. As extensively discussed in the literature, the economic optimum may not coincide with the thermodynamic optimum given the trade-off between power consumption and heat transfer area. In light of this, the choice of comparing the expander-based configurations in their optimal design is discussed further in this Chapter.
Following the present introduction, the applied methodology is presented as well as the main data and cost assumptions. Successively the thirteen expander-based configurations are ranked according to the three economic performance indicators introduced in Section 3.4.1, namely Unitary Profit (UP), Net Present Value (NPV) and Adjusted Pay-Back Time (APBT). Finally a series of sensitivity analyses is presented to highlight the most influencing parameters on the economic analysis outcome.

6.2 Methodology and data assumptions

The economic analysis is set up for two different plant sizes, a small-scale plant size and a large-scale plant size.
The Danish Maritime Authority considers in [10] a throughput of 52000 m^3/yr for a small-scale liquefaction facility, and of 343000 m^3/yr for a large-scale one (volume flow rates are given at LNG storage conditions). Given the assumptions on natural gas side (discussed in Section 4.3) this translates into a natural gas feed flow rate of 0.8 kg/s for the small-scale case and of 5.5 kg/s for the large-scale case.
Again according to the Danish Maritime Authority report, a lifetime of 40 years is considered for both plant sizes. Availability factor of 95 % is assumed considering that LNG facilities are intended for ship bunkering.

6.2.1 Determination of the main economic figures

The economic analysis of natural gas liquefaction configurations is performed according to the Module Costing Technique (MCT) which is extensively used for preliminary cost estimations of chemical plants [71]. According to this approach all direct and indirect costs are related to the purchased cost of equipment evaluated at some base conditions, C_P^0, as a function of the capacity parameter A.

$$\log_{10} C_P^0 = k_1 + k_2 \log_{10} A + k_3 \left(\log_{10} A\right)^2 \tag{6.1}$$

This is then adjusted for the actual operating conditions of the equipment, in terms of e.g. working pressure, and for the construction material, obtaining the actual purchased cost of equipment.
All the expenses directly and indirectly related to the equipment, such as transportation costs, civil works, labour and materials for installation, piping, insulation and electrical equipment, are accounted in the so-called Bare Module Cost Factor, F_{BM}. If the Bare Module Cost Factor contains the multiplying factors accounting for construction material (F_M) and working pressure (F_P), the Bare Module Equipment Cost C_{BM} is calculated as in Equation 6.2.

$$C_{BM} = C_P^0 \cdot F_{BM} \tag{6.2}$$

In this work the Bare Module Equipment Cost for centrifugal compressors, radial expanders, compressor electric drives, refrigerant coolers and phase separators is calculated applying the correlations given by Turton *et al.* [71], rescaling the obtained value using the CEPCI index for 2014 (equal to 576.1) in order to estimate the current price from the 1998 one (CEPCI index equal to 382) [72]. Details of applied correlations can be found in Appendix E together with the Matlab scripts used for their implementation.
cost data for Multiple-Stream and two-stream Heat Exchangers are provided by *SWEP* for flat-plate heat exchangers. The same data are assumed valid for plate-fin heat exchangers. The Bare Module Cost Factor given by Turton *et al.* for flat-plate heat exchangers is applied.

The Total Capital Investment (TCI) is calculated as in Toffolo *et al.* [73].

$$\mathrm{TCI} = 1.18 \sum_{i}^{n} C_{\mathrm{BM},i} \tag{6.3}$$

where 1.18 is assumed to be the Bare Module Cost Factor for contingencies and fees.

As to the Operation and Maintenance cost the following inputs are applied:

- plant maintenance is set to be 2 % of the Total Capital Investment [10];
- natural gas feed price is set equal to 14.85 €/MWh as suggested by *Kosan Crisplant A/S*;
- electricity price is 8.79 c€/kWh as in the third EU Quarterly Report on 2015 European Electricity Markets for Danish industrial consumers [74]. Electricity consumption is given by the total compressor power requirement, thus expander power production is disregarded;
- LNG price is assumed to be 28 €/MWh as suggested by *Kosan Crisplant A/S*;
- cost data for working fluids are reported in Table 6.1.

Table 6.1: Cost data for working fluids

Fluid	**Cost [$/kg]**	**Reference**
Nitrogen	3.5	[75]
R410A	227.9	[76]
Propane	103.6	[76]
CO_2	51.8	[76]
Methane	103.6	assumption

As stated by *Kosan Crisplant A/S*, natural gas feed and LNG prices are based on Higher Heating Value. Given the considered feed composition and the assumption on flashing end pressure, HHV is 54.45 MJ/kg for the natural gas feed and 54.54 MJ/kg for the produced LNG. These values are calculated by Aspen Plus. Natural gas feed price does not include PSO taxes as the liquefaction facility is not the gas end-user.
For the working fluids a Bare Module Factor of 1.25 is assumed to take into consideration installation costs [73].
The economic figures are calculated in Danish Krone (DKK). Conversion factors for Euro and Dollar are 7.45 and 6.6, respectively [77].

6.2.2 Estimation of heat exchanger area and U-values

A separate Section of the methodology has to deal with the estimations of heat exchanger area and the overall heat transfer coefficient, U.

Aspen Plus calculates the UA-values for Multiple-Stream and two-stream Heat Exchangers by discretisation of the heat exchanger into finite control volumes. Therefore the U-value has to be estimated in order to obtain a sensible value for the heat transfer area to be used in cost correlations. This estimation is performed using *SWEP* software [78] by implementing temperature and pressure conditions for the heat exchange fluids as in the optimised models. Average values are considered. Pressure drops are requested by the software as input data and are set equal to 1 % of the gas pressure, as this is the usual range in process specifications [79]. Table 6.2 reports the U-values in W/m^{2}K for the different heat exchange possibilities. Methane is analysed both in medium- and low-pressure conditions (15 bar and 3 bar, respectively) given the differences in its low pressure level between the N_2 sub-cooling and CH_4 sub-cooling dual-refrigerant cases.

Table 6.2: U-values in W/m^{2}K for the different heat exchange possibilities

Cold-side fluid	**Hot-side fluid**				
	Nitrogen	**Methane**	**Gaseous hydrocarbon**	**Condensing hydrocarbon**	**Liquid hydrocarbon**
Nitrogen - medium pressure	250	-	225	400	550
Methane - medium pressure	-	375	375	750	750
Methane - low pressure	-	80	80	100	150

For Multiple-Stream Heat Exchangers the lowest U-value among the applicable fluid pairs is selected. For those two-stream Heat Exchangers having natural gas on the hot side, the U-value is computed taking into consideration natural gas inlet and outlet quality.

The approach is necessarily different for refrigerant coolers (and condensers, when applicable) given the fact that they are modelled as heat exchange devices with only one stream, therefore the UA-value is not calculated by Aspen Plus. For the sake of economic analysis, the heat transfer area for refrigerant coolers is directly computed using *SWEP* software assuming a flat-plate heat exchanger design. Details are provided in Appendix E.[1]

[1] Alternatively the coolers could have been replaced by two-stream HEX's with water as cold-side fluid entering at 10°C and exiting at 40°C. Expected film coefficients are in the range of 2200 W/m^{2}K for water and 400 W/m^{2}K for high-pressure nitrogen and methane.

6.3 Results

Table 6.3 presents the main economic figures and performance indicators for the small-scale expander-based configurations. The same is shown in Table 6.4 for the large-scale case. Yearly revenues are 73 Million DKK (MDKK) for the small-scale configurations and 502 MDKK for the large-scale ones. They do not vary with the configuration as revenues only depend on LNG price, liquefaction rate and availability factor.

Table 6.3: Total Capital Investment, O&M cost and economic performance indicators for small-scale expander-based configurations

	TCI [MDKK]	**O&M [MDKK/year]**	**UP [DKK/kg_{LNG}]**	**NPV [MDKK]**	**APBT [years]**
Single-expander - one comp. stage	115	56	0.321	89	10.1
Two-stage comp. (no coupling)	99	53	0.520	143	6.4
Two-stage comp. (with coupling)	104	51	0.591	163	6.0
R410A pre-cooling	84	51	0.651	179	4.7
Propane pre-cooling	**80**	**50**	**0.683**	**188**	**4.4**
Sub-critical CO_2 pre-cooling	85	51	0.633	174	4.9
Super-critical CO_2 pre-cooling	88	52	0.606	167	5.2
Dual-turbine - diff. PR	87	51	0.646	178	4.9
Dual-turbine - same PR	92	52	0.587	162	5.5
Two-stage expansion	89	51	0.626	173	5.1
N_2 sub-cooling	**80**	**47**	**0.822**	**227**	**3.7**
CH_4 sub-cooling	**105**	**48**	**0.684**	**188**	**4.4**
Niche	102	50	0.630	173	5.7

Table 6.4: Total Capital Investment, O&M cost and economic performance indicators for large-scale expander-based configurations

	TCI [MDKK]	**O&M [MDKK/year]**	**UP [DKK/kgLNG]**	**NPV [MDKK]**	**APBT [years]**
Single-expander - one comp. stage	732	383	0.362	685	8.8
Two-stage comp. (no coupling)	599	361	0.572	1084	5.4
Two-stage comp. (with coupling)	636	347	0.642	1216	5.2
R410A pre-cooling	519	349	0.688	1303	4.1
Propane pre-cooling	**495**	**346**	**0.721**	**1366**	**3.8**
Sub-critical CO_2 pre-cooling	530	351	0.669	1267	4.3
Super-critical CO_2 pre-cooling	551	354	0.640	1213	4.6
Dual-turbine - diff. PR	530	348	0.692	1311	4.2
Dual-turbine - same PR	585	355	0.616	1168	5.0
Two-stage expansion	551	350	0.666	1262	4.5
N_2 sub-cooling	**470**	**324**	**0.874**	**1656**	**3.1**
CH_4 sub-cooling	**611**	**331**	**0.755**	**1431**	**4.4**
Niche	618	341	0.683	1291	4.8

It can be noticed that Unitary Profits increase passing from small scale to large scale. Consequently the Adjusted Pay-Back Time decreases. This is expected as the liquefaction facilities benefit from economies of scale.
For both sizes the three most promising configurations are, in order, N_2 sub-cooling dual-refrigerant cycle, CH_4 sub-cooling dual-refrigerant cycle and propane pre-cooled single-expander cycle. The least favourable alternative is the single-expander cycle with one compression stage.
The threshold LNG price is calculated as the minimum sale price to get a zero-NPV. It is maximum for the least convenient alternative, being around 185 DKK per kg of produced LNG (i.e. 24.8 €), and minimum for the N_2 sub-cooling dual-refrigerant cycle (approximately 150 DKK per kg of LNG, corresponding to 20 €). This translates into a LNG-to-NG price threshold ratio between 1.4 and 1.7, depending on configuration and size.
Overall it can be inferred that those configurations achieving the lowest net power consumption are the ones yielding the best economic results. Nevertheless some cases deviate from this general trend. Propane pre-cooling cycle results to be more favourable than dual-expander configurations given the fewer equipment. Moreover the two-stage compression cycle with mechanical coupling between LP compressor and expander is more advantageous than the one without coupling due to the electricity saving at the Low-Pressure compressor.

6.3.1 Sensitivity analyses

A series of sensitivity analyses is performed. The influence of natural gas, electricity and LNG prices is assessed here and the applied parameter variation is reported in Table 6.5. One parameter is changed at the time. The influence of maintenance cost, U-values and cost of working fluids is also assessed but is not reported as these parameters are found not to be as influencing[2].

Table 6.5: Parameter variation for the conducted sensitivity analyses

Parameter	Unit	Base case	High case: +10%	Low case: -10%
NG price	[€/MWh]	14.85	16.335	13.365
Electricity price	[c€/kWh]	8.79	9.67	7.91
LNG price	[€/MWh]	28	30.8	25.2

Results are displayed in Figures 6.1 to 6.3 reporting the Unitary Profit percentage variation corresponding to a ±10 % variation of the input parameter. Given the high number of configurations which have to be evaluated, spider plots illustrate only the maximum and minimum output percentage variation. All the intermediate cases fall within the shaded area.

[2] If maintenance passes from 2 % to 3 % of the Total Capital Investment (relative increase of +50 %), a decrease in Unitary Profit occurs ranging between -15 % and -4 %. Moreover a 10 %-variation in U-values and cost of working fluids has an almost negligible effect on Unitary Profits (percentage variations smaller than 1 % for all cases).

Results show that the boundary cases are always the single-expander cycle with one compression stage and the N_2 sub-cooling dual-refrigerant cycle, the former being more influenced than the latter by the variations in natural gas, electricity and LNG prices. Though similar, the variations are slightly smaller for the large-scale cases. This is due to the economy of scale effect which favours large-scale configurations and makes less impacting a change in the investigated input parameters.

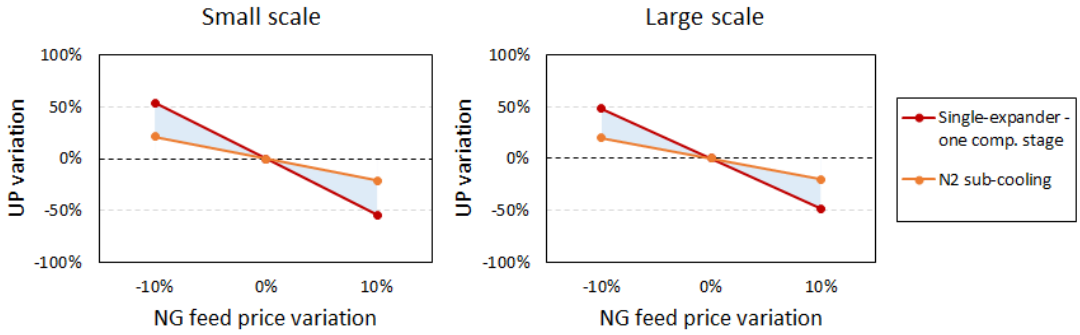

Figure 6.1: Results from natural gas price sensitivity

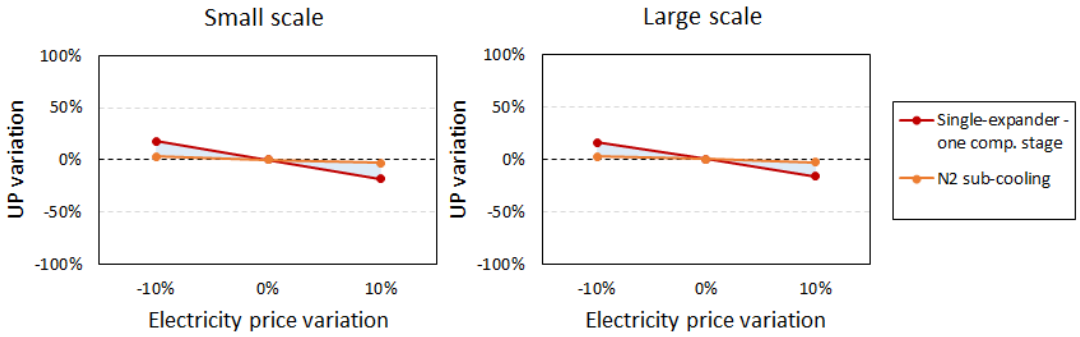

Figure 6.2: Results from electricity price sensitivity

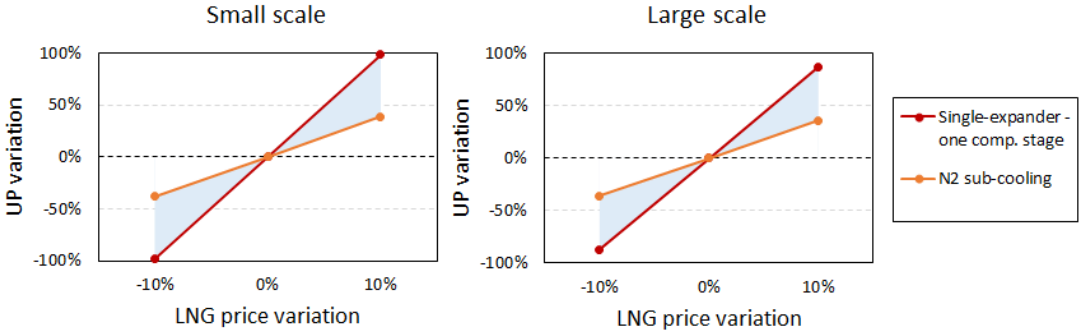

Figure 6.3: Results from LNG price sensitivity

LNG sale price is the most influencing parameter. Considering the small-scale case, a 10% increase in LNG price results in a Unitary Profit increase of 38.5 % for the most promising configuration, of 98.4 % for the worst performing one. Values for the large-scale case are 36 % and 87 %, respectively. Natural gas feed price is ranked second (Unitary Profit variations between ±20 % and ±50 %), while electricity price is the least influencing parameter (Unitary Profit variations between ±3 % and ±18 %). They affect Unitary Profit in an opposite way compared to LNG price, as they contribute to the O&M cost for the liquefaction facility.

6.4 Discussion

This Chapter presents the economic analysis of the developed expander-based models for LNG production and ranks them according to the three considered economic performance indicators. Unitary Profits varying from 0.32 DKK/kg_{LNG} to 0.87 DKK/kg_{LNG} are obtained, depending on the configuration and on the size.
Very little is found in the literature about economic analysis and in most cases this aspect is addressed by investigating the trade-off between power consumption and heat transfer area, which partly reflects the trade-off between investment and operation cost, as the capital expenditure may be dominated by the turbo-machinery cost.
Economic figures are determined combining thermodynamic results with cost functions, which reliability is therefore crucial to obtain sensible results. The correlations given by Turton *et al.* are widely applied for preliminary cost estimation of chemical plants. Nevertheless they may be unsuitable given the peculiarities of a cryogenic application like natural gas liquefaction. Moreover an important simplification is introduced when applying flat-plate heat exchanger cost correlation to Multiple-Stream plate-fin heat exchangers, which correlations are not well developed and not found in the literature.

In the present study many simplifications are adopted in the Discounted Cash Flow analysis. For instance, no tax and financial considerations are included. The choice of a 8 %-discount rate may be argued as well, since the industry-related risk for a small-scale LNG facility can contribute to a considerable increase in the cost of capital. In light of these simplifications the aim of this analysis is not to give a realistic indication about the economic profitability of a LNG production facility in the Danish context, but rather to couple thermodynamic results with economic data to further understand the interplay between them.
As an example it is found that coupling a booster compressor with the expander is not thermodynamically convenient, but is economically favourable, as the booster compressor does not need an electric motor and its power consumption is fully provided by the expander. Moreover the simpler design of pre-cooling configurations determines the economic superiority of small-scale R410A and propane pre-cooled cycles over the dual-expander configurations.

Sensitivity analyses are performed applying the same percentage variation on the three main economic inputs, namely natural gas feed, electricity and LNG prices. This is done with the

aim of providing the mathematical sensitivity of economic results given the identical percentage variation on the inputs. This way the reader is made aware that LNG price is the most influencing parameter on the economic outcome. However this approach disregards the real variations that can be experienced by a liquefaction facility.
For instance LNG price is claimed to be highly variable. *Kosan Crisplant A/S* suggests a possible variation range between 28 and 40 €/MWh, while the Danish Maritime Authority in [10] builds three LNG price scenarios in which the lower bound is 32 €/MWh and the upper one is 48 €/MWh. The choice of 28 €/MWh is therefore conservative.
Conversely it is expected that electricity price is the least variable input given the fact that liquefaction facilities are large power consumers and they are likely to have special supply contracts.
Natural gas price for the liquefaction facilities is the spot market price. A variation range of ±10 % with respect to the base case of 14.85 €/MWh covers the fluctuations of the spot market price observed from December 2015 to June 2016, as in Figure 6.4.

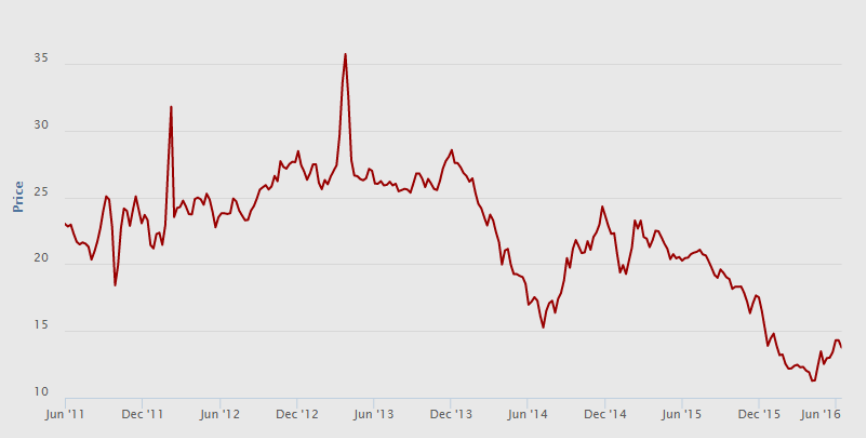

Figure 6.4: Evolution of natural gas spot market price in €/MWh [80]

As aforementioned, performing the economic comparison on thermodynamic optimum cycles is a key assumption. This might be unfair as the economic optimum is likely not to coincide with the thermodynamic one. To understand that, a series of Multi-Objective Optimisations is performed on the least and the most economically favourable alternatives with the aim of simultaneously minimising compressor and heat exchange network investment costs. Results are displayed in Figure 6.5 for the single-expander cycle with one compression stage and in Figure 6.6 for the N_2 sub-cooling dual-refrigerant cycle.
As expected compressor investment cost increases together with power consumption, while the investment cost relative to the heat exchange network decreases. However it can be seen that compressor cost is much higher than the investment in heat exchangers for all cases. Given the same increase in net power consumption, the increase in investment associated to the compressors is one order of magnitude greater than the decrease in investment relative to heat exchangers.

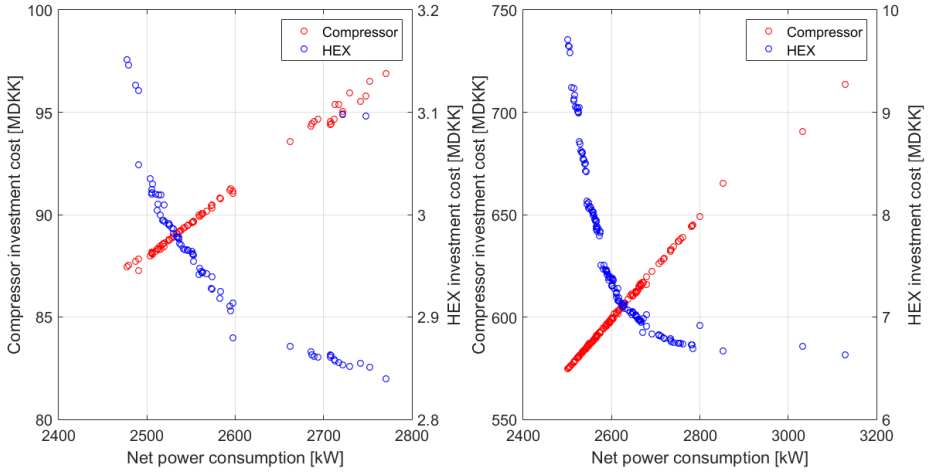

Figure 6.5: Results from the Multi-Objective Optimisations on the single-expander cycle with one compression stage for the small-scale (left) and large-scale (right) case. HEX investment cost is reported on the secondary vertical axis

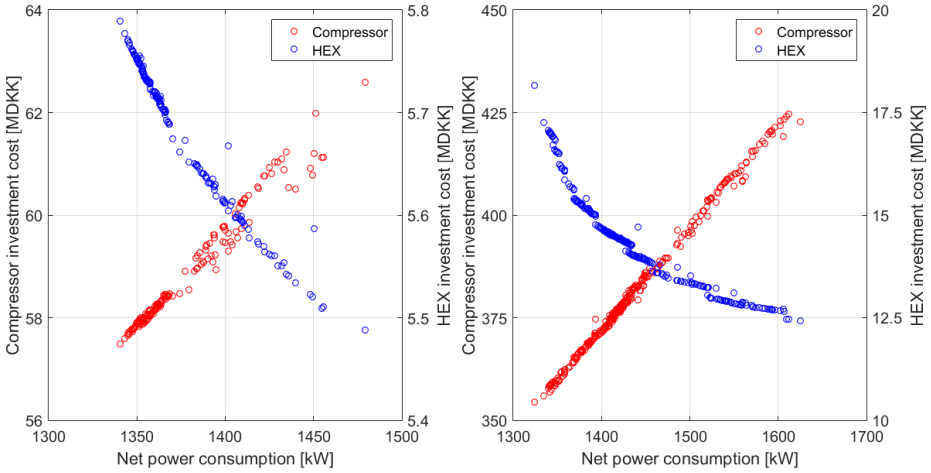

Figure 6.6: Results from the Multi-Objective Optimisations on the N_2 sub-cooling dual-refrigerant cycle for the small-scale (left) and large-scale (right) case. HEX investment cost is reported on the secondary vertical axis

As a remark, Figure 6.7 illustrates that with the employed cost correlations the investment cost associated to compressors represents the largest share of the Total Capital Investment. The small-scale N_2 sub-cooling dual-refrigerant case is taken as an example, however similar results are obtained for the large-scale case and for the other configurations. As a consequence, no trade-off between compressor and heat exchanger cost occurs, therefore the thermodynamic optimum coincides with the economic one.

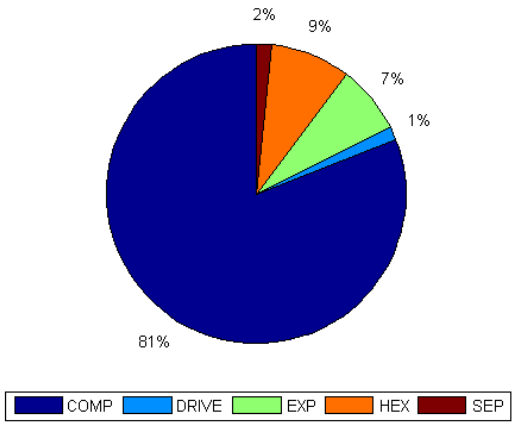

Figure 6.7: Breakdown of Total Capital Investment for the small-scale N_2 sub-cooling dual-refrigerant cycle (thermodynamic optimal design)

The negligible influence that U-value uncertainty plays on the economic performance of the investigated configurations is connected to this outcome.

In order to further investigate the cost correlation influence, an additional set of cost correlations for compressors and heat exchangers is applied to the small-scale N_2 sub-cooling dual refrigerant case. The formulation is reported in Section E.7 of Appendix E.
Figure 6.8 on the left depicts the Pareto fronts obtained from the simultaneous minimisations of compressor and heat exchange network investment costs. Moreover Figure 6.9 illustrates the breakdown of Total Capital Investment for the thermodynamic optimum design.
It can be clearly understood that when using the second set of cost correlations a trade-off between compressor and heat exchanger investment costs occurs, therefore the minimum value for the investment cost associated to these two components is not located in the thermodynamic optimum (as shown in Figure 6.8 on the right).
It is also found that the capital cost for the heat exchange network is similarly estimated in both cases (as noticeable in Figures 6.6 and 6.8 on the left). Conversely Turton's correlation largely overestimates compressor investment cost compared to the second applied correlation. This outcome is not affected by the construction material, as the same Bare Module Cost Factor is applied in both cases (equal to 6.3, corresponding to stainless steel). Moreover the selected type of compressor is not influencing either, given that according to Turton *et al.* centrifugal, axial and reciprocating compressors present the same Bare Module Cost.
Finally the system costs and the economic performance indicators for the three most favourable alternatives are re-calculated using the additional set of cost correlations for compressors and flat-plate heat exchangers. Once again thermodynamic optimal cycles are considered. Results are listed in Table 6.6 for the small-scale case and in Table 6.7 for the large scale-one.

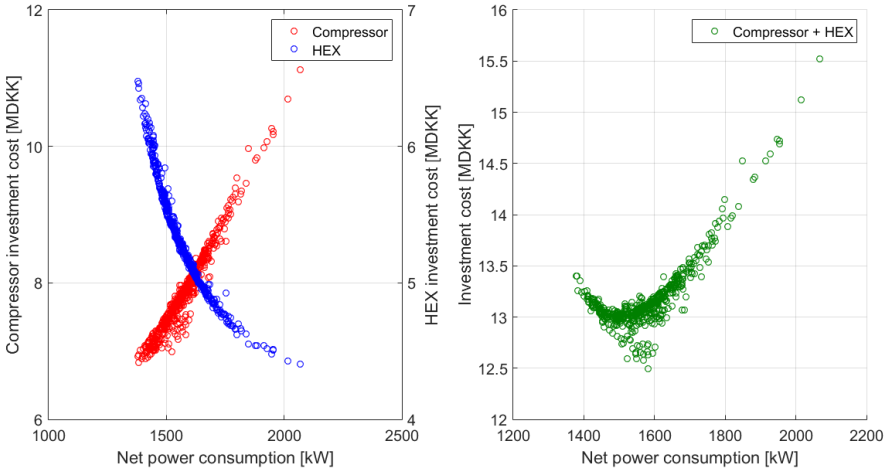

Figure 6.8: On the left: Pareto fronts from the simultaneous minimisation of compressor and heat exchange network investment costs. On the right: sum of compressor and heat exchange network investment costs highlighting the existing trade-off

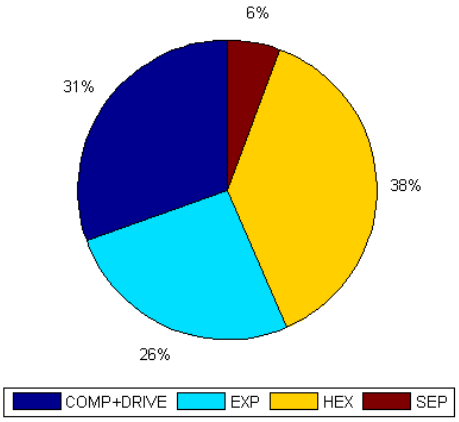

Figure 6.9: Breakdown of Total Capital Investment for the small-scale N_2 sub-cooling dual-refrigerant cycle (thermodynamic optimal design)

It can be noted that Total Capital Investments are lower than the ones presented in Tables 6.3 and 6.4 given the lower influence of compressor investment cost. This is confirmed by the fact that TCI increases as the cycle design becomes more complex and the heat network conductance increases, while previously it was found to follow the trend in power consumption.
A change of ranking occurs in the small-scale case, in which propane pre-cooling cycle is more convenient than the CH_4 sub-cooling dual-refrigerant alternative, the latter being penalised by the higher heat network conductance (342.2 kW/K against 176.2 kW/K).

Table 6.6: System costs and economic performance indicators for the three most favourable small-scale expander-based configurations when using the additional set of cost correlations

	TCI [MDKK]	O&M [MDKK/year]	UP [DKK/kg_{LNG}]	NPV [MDKK]	APBT [years]
Propane pre-cooling	18	49	0.96	266	0.8
N_2 sub-cooling	22	46	1.08	298	0.9
CH_4 sub-cooling	50	47	0.93	256	2.2

Table 6.7: System costs and economic performance indicators for the three most favourable large-scale expander-based configurations when using the additional set of cost correlations

	TCI [MDKK]	O&M [MDKK/year]	UP [DKK/kg_{LNG}]	NPV [MDKK]	APBT [years]
Propane pre-cooling	66	337	1.00	1898	0.4
N_2 sub-cooling	77	316	1.13	2142	0.4
CH_4 sub-cooling	158	322	1.05	1992	0.9

As to the large-scale comparison, the ranking obtained using Turton's correlations is confirmed.
The second set of cost correlations was made available only at the end of the thesis period, therefore the economic comparison of different LNG production alternatives is performed applying Turton's correlation for compressors and considering LNG production configurations in their thermodynamic optimum design. Nevertheless this Chapter highlights the implications of this choice and sets the basis for future developments in terms of cost data validation and, if applicable, research of the economic optimum for the different expander-based configurations. This could be done by choosing as objective function the total annual cost for the facility as sum of the annualised investment and the O&M cost.

6.5 Conclusions

The thirteen expander-based configurations are analysed in this Chapter from an economic point of view. Two plant sizes are considered in the assessment, corresponding to natural gas feed flow rates of 0.8 kg/s (small scale) and 5.5 kg/s (large scale). The comparison is performed on the optimal cycle design for each configuration.
Results show that in both small and large scale N_2 sub-cooling dual refrigerant cycle is the most favourable alternative, followed by CH_4 sub-cooling dual-refrigerant cycle and propane pre-cooled single-expander cycle. These three configurations are therefore selected for the comparison with cascade and Mixed-Refrigerant systems, which is the content of next Chapter.
A discussion is presented about the cost correlation influence on the economic results. In the present case compressor investment cost covers the largest share of the Total Capital Investment, therefore the economic optimum coincides with the thermodynamic one.

7 Economic comparison of LNG production alternatives

Natural gas liquefaction cycles can be classified according to three main concepts, namely cascade, Mixed-Refrigerant and expander-based systems. This Chapter presents the economic comparison of these three different alternatives. The most favourable expander-based configurations identified in Chapter 6 are compared with the cascade and Mixed-Refrigerant configurations modelled and optimised in the Master Thesis *Modelling and Optimisation of Cascade and Mixed-Refrigerant Cycles for Natural Gas Liquefaction*. Depending on the configuration size, modifications to the cycles are applied in order to compare realistic designs.

7.1 Introduction

Cascade and Mixed-Refrigerant (MR) systems are included in the economic analysis, and the comparison between the three LNG production concepts is the content of this Chapter. Aspen Plus models for the investigated cascade and Mixed-Refrigerant cycles are developed by Nicola Lonardi and their features are extensively described in the Master Thesis *Modelling and Optimisation of Cascade and Mixed-Refrigerant Cycles for Natural Gas Liquefaction* [81]. The reader should therefore refer to this work for the details of these LNG production alternatives. In this Chapter only the relevant pieces of information are provided.
Single-stage and two-stage cascade cycles are taken as examples of cascade systems, the latter characterised by a two-stage compression process for each of the three refrigerant loops, namely propane pre-cooling, ethylene liquefaction and methane sub-cooling. The conventional design of *Conoco Phillips* [49] is considered, in which each of these loops employs a pure fluid as refrigerant, hence the need for several cooling stages in order to reduce the gap between natural gas and refrigerant temperature profiles. The cooling effect is generated through a Joule-Thomson expansion. Given the increased design complexity, the two-stage cascade system is considered only for large-scale applications.

The Mixed-Refrigerant category comprises a Single Mixed-Refrigerant process, that is the *PRICO* cycle, and the propane pre-cooled Mixed-Refrigerant cycle, which is referred to as *C3-MR* cycle, adopting the same nomenclature as in Lonardi [81]. These cycles are characterised by the use of a mixture as refrigerant, which composition is optimised in order to reproduce the shape of the natural gas cooling curve. The refrigerating effect is again obtained through a Joule-Thomson expansion. *PRICO* cycle is suitable for small-scale applications, as its design presents fewer equipment, whereas *C3-MR* cycle is considered for large-scale applications, given the increased design complexity and the higher efficiency.
The process flowsheet of the selected LNG configurations is sketched in Appendix F.
Following the present introduction, the applied methodology is described and the relevant assumptions are detailed. Successively results are presented distinguishing between small-scale and large-scale cases. The sensitivity of economic results to natural gas, electricity and LNG prices is quantified. The influence of natural gas composition on economic performance is included in a separate section.

7.2 Methodology

In the attempt of comparing the different LNG production configurations in realistic conditions, modifications are applied to the reference models.
For small-scale applications only two-stream heat exchangers are required. This goes in the direction of employing simpler and cheaper equipment in the liquefaction facility design. Therefore Aspen Plus models are modified accordingly through the introduction of refrigerant stream splitting on the cold side of Multiple-Stream Heat Exchangers, as in Figure 7.1.

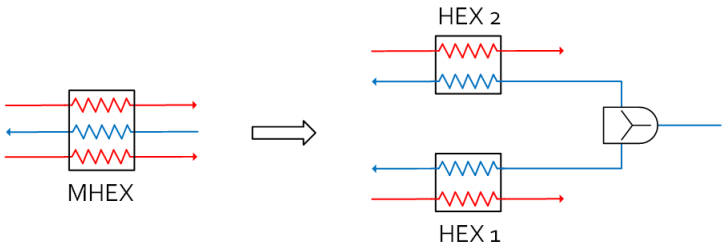

Figure 7.1: Graphical representation of the splitting procedure

Flow rate splitting introduces a degree of freedom in the model which is normally used to control the temperature approach at the new heat exchangers. A new series of thermodynamic optimisations is performed to determine the new optimal design. The optimisation of one-stage cascade and *PRICO* cycles with only two-stream heat exchangers is performed and discussed in the work *Modelling and Optimisation of Cascade and Mixed-Refrigerant Cycles for Natural Gas Liquefaction.*

For large-scale application Multiple-Stream Heat Exchangers are instead considered. The difference with the reference models is the turbo-machinery efficiency, which is increased to the maximum limit as found in the literature. Compressor polytropic efficiency is increased from 0.82 to 0.85, while expander isentropic efficiency is improved passing from 0.85 to 0.9.
This has a non-negligible impact on the cycle design of expander-based configurations. In fact a change in the expansion efficiency makes the set of optimal designs as in Chapter 5 no longer applicable, since changes in the refrigerant temperature before the cryogenic heat exchanger are recorded[1]. As a consequence thermodynamic optimisation is required to determine the optimum for the expander-based configurations when expander isentropic efficiency is increased. The new set of optimal decision variables for the three expander-based configurations is reported in Appendix F.
This does not apply for cascade and Mixed-Refrigerant systems, as a change in compressor polytropic efficiency only influences the refrigerant temperature at cooler inlets, thus cooler heat duty[2]. As a consequence, optimal values for the decision variables are not affected and the results from the thermodynamic optimisation presented in the work *Modelling and Optimisation of Cascade and Mixed-Refrigerant Cycles for Natural Gas Liquefaction* are used as such.

The methodology and assumptions for the economic analysis are analogous to those presented in the previous Chapter. The price of pure hydrocarbons and hydrocarbon mixtures which are used as refrigerants in cascade and Mixed-Refrigerant systems is assumed to be equal to the price of propane, i.e. 103.6 $/kg.

[1] This outcome is emphasised in Appendix B through the sensitivity analysis on the expander isentropic efficiency.

[2] Once again this is discussed in Appendix B through the sensitivity analysis on the compressor polytropic efficiency.

7.2.1 U-value estimation

The U-values for the heat exchange processes in cascade and Mixed-Refrigerant cycles differ from the ones presented in Chapter 6 given the fact that refrigerants (mainly pure hydrocarbons or hydrocarbon mixtures) are not always in the gaseous phase, as it was instead required for nitrogen (and methane, when applicable) in the expander-based configurations.
These U-values are estimated using the AspenTech tool *Exchanger Design and Rating* implementing the actual refrigerant conditions (e.g. including the super-heating phase at the cold side of all the heat exchangers of cascade systems).
The applied U-values are listed in Table 7.1 for cascade systems. Tables 7.2 and 7.3 present the U-value estimations for Mixed-Refrigerant systems.

Table 7.1: U-values in W/m^{2}K for the different heat exchange possibilities in cascade systems

Cold-side fluid	**Hot-side fluid**		
	Gaseous hydrocarbon	**Condensing hydrocarbon**	**Liquid hydrocarbon**
Pure hydrocarbon[3]	120	400	2000

Table 7.2: U-values in W/m^{2}K for the different heat exchange possibilities in the *PRICO* cycle

Cold-side fluid	**Hot-side fluid**	
	Condensing MR	**Natural Gas**
Mixed Refrigerant	300	660

Table 7.3: U-values in W/m^{2}K for the different heat exchange possibilities in the *C3-MR* cycle

Cold-side fluid	**Hot-side fluid**			
	Gaseous hydrocarbon	**Condensing hydrocarbon**	**Condensing MR**	**Liquid hydrocarbon**
Mixed Refrigerant	120	400	300	2000

[3] As a remark, the cold-side refrigerant in cascade systems undergoes the evaporation process, followed by the super-heating stage in order to achieve the temperature approach at the warm end of all heat exchangers. The U-value estimation takes that into account.

7.3 Results

The considered LNG production alternatives are ranked according to Unitary Profit (UP), Net Present Value (NPV) and Adjusted Pay-Back Time (APBT). As discussed in the previous Chapter, the comparison is performed on thermodynamic optimal cycles.

7.3.1 Results from small-scale comparison

Table 7.4 reports the thermodynamic performance of the small-scale LNG production alternatives. Moreover Table 7.5 ranks them according to the three economic performance indicators. The annual revenues for small-scale configurations are equal to 73 MDKK.

Table 7.4: Comparison of optimal small-scale liquefaction cycles in terms of net power consumption, total heat network conductance, COP, unit energy consumption and Figure of Merit

	$\dot{W}_{net}$ [kW]	Total UA-value [kW/K]	COP [-]	w [kJ/kg$_{LNG}$]	FOM [%]
Propane pre-cooling	1559	176.2	0.509	1617	27.27
N_2 sub-cooling	1288	285.9	0.616	1336	33.02
CH_4 sub-cooling	1429	342.2	0.555	1482	29.76
PRICO	1489	1231	0.533	1544	28.57
Cascade - one stage	1152	445.8	0.689	1195	36.86

Table 7.5: Total Capital Investment, O&M cost and economic performance indicators for small-scale LNG production alternatives

	TCI [MDKK]	O&M [MDKK/year]	UP [DKK/kg$_{LNG}$]	NPV [MDKK]	APBT [years]
Propane pre-cooling	80.7	50.5	0.682	187.9	4.4
N_2 sub-cooling	79.8	47.3	0.823	226.7	3.7
CH_4 sub-cooling	104.7	48.4	0.684	188.5	4.4
PRICO	71.1	48.0	0.824	227.0	3.4
Cascade - one stage	**52.9**	**47.3**	**0.919**	**253.2**	**2.4**

It has first to be highlighted that the small-scale expander-based optimal cycles are identical to the ones presented in Chapter 5, i.e. the splitting of Multiple-Stream Heat Exchangers into two-stream HEX's does not affect the cycle design in terms of pressure levels, temperatures and refrigerant mass flow rates. The same occurs for the one-stage cascade cycle, whereas *PRICO* cycle is largely affected, mainly due to the increase of the required refrigerant flow rate. This is detailed in the Master Thesis *Modelling and Optimisation of Cascade and Mixed-Refrigerant Cycles for Natural Gas Liquefaction*.

One-stage cascade cycle is together the most efficient and the most economically convenient alternative. This outcome is expected after what discussed in Chapter 6. Despite its simpler design, *PRICO* cycle is slightly less convenient than N_2 sub-cooling dual-refrigerant cycle, mainly due to the larger power consumption.
For the one-stage cascade cycle the threshold of LNG sale price, i.e. the LNG sale price yielding a zero-NPV, is 148 DKK per kg of produced LNG (corresponding to 19.9 €). For *PRICO* cycle this threshold is at 154 DKK per kg of LNG.

7.3.2 Results from large-scale comparison

Table 7.6 reports the thermodynamic performance of the large-scale LNG production alternatives. The economic ranking is provided in Table 7.7. The annual revenues for large-scale configurations are equal to 502 MDKK.

Table 7.6: Comparison of large-scale liquefaction cycles in terms of net power consumption, total heat network conductance, COP, unit energy consumption and Figure of Merit

	$\dot{W}_{net}$ [kW]	Total UA-value [kW/K]	COP [-]	w [kJ/kg$_{LNG}$]	FOM [%]
Propane pre-cooling	1371	152.5	0.578	1423	31.00
N_2 sub-cooling	1127	273.7	0.704	1169	37.72
CH_4 sub-cooling	1319	515.1	0.601	1368	32.24
C3-MR	880	541.5	0.901	913	46.51
Cascade - two stages	872	488.5	0.909	905	48.75

Table 7.7: Total Capital Investment, O&M cost and economic performance indicators for large-scale LNG production alternatives

	TCI [MDKK]	O&M [MDKK/year]	UP [DKK/kg$_{LNG}$]	NPV [MDKK]	APBT [years]
Propane pre-cooling	473.3	340.4	0.767	1454	3.5
N_2 sub-cooling	460.6	318.7	0.911	1725	2.9
CH_4 sub-cooling	690.7	329.1	0.724	1372	5.0
C3-MR	**279.5**	**307.7**	**1.076**	**2038**	**1.6**
Cascade - two stages	305.6	308.0	1.060	2008	1.8

Comparing the thermodynamic performance of large-scale and small-scale expander-based configurations it can be noted that the improvements in turbo-machinery equipment lead to a significant reduction in net power consumption (maximum reduction of 12.5 % in the N_2 sub-cooling dual-refrigerant case). Once again the best performing cycle is the two-stage cascade cycle, closely followed by the propane pre-cooled Mixed-Refrigerant alternative.

The most advantageous alternative from an economic viewpoint is the *C3-MR* cycle. Despite its lower power consumption, the two-stage cascade cycle is penalised by the more complex design and by the higher number of heat exchangers and compressors. As to the expander-based configurations, large-scale propane pre-cooling cycle overcomes the CH_4 sub-cooling dual-refrigerant alternative. These two cycles are characterised by almost the same net power consumption, but the dual-refrigerant alternative is penalised by the more complex design and by the larger heat network conductance (more than three times higher than in the pre-cooling cycle case).
For *C3-MR* and the two-stage cascade cycles the threshold for LNG sale price is approximately 138 DKK per kg of produced LNG, corresponding to 18.5 €.

7.3.3 Sensitivity analyses

Similarly to what presented in Chapter 6, the sensitivity of the economic results to natural gas feed, electricity and LNG sale price is assessed. One parameter is changed at the time. A ±10 %-variation is applied on the input parameters as in Table 6.5 and the percentage variation on Unitary Profit is calculated and graphically reported in Figures 7.2, 7.3 and 7.4.

The least affected cycles are the cascade and Mixed-Refrigerant alternatives. Among the dual-expander configurations, N_2 sub-cooling dual-refrigerant cycle is the one presenting the smallest percentage variations in Unitary Profit. This is due to the fact that more efficient cycles are generally characterised by smaller O&M cost, therefore a variation in the O&M cost fraction connected to natural gas feed and electricity consumption is less impacting on the economic outcome. As to LNG sale price, a change in the yearly revenue for the liquefaction facility affects less its economy if the variable costs are less decisive.
Due to economies of scale, the output percentage variations are smaller in the large-scale cases for all the investigated input parameters.

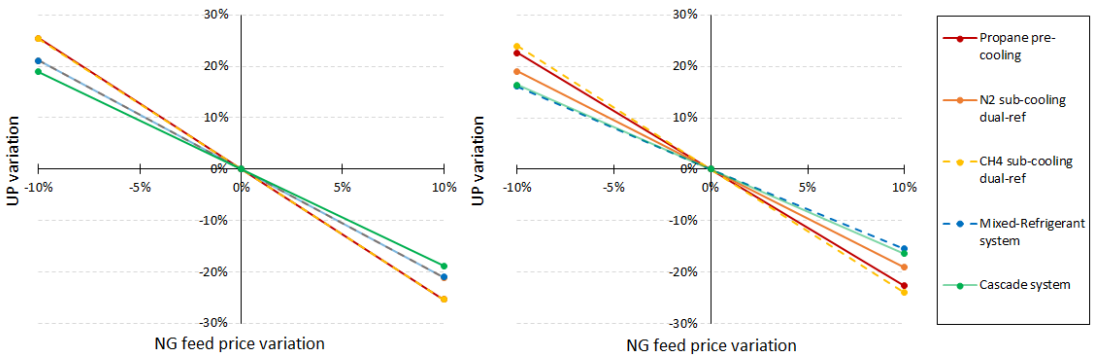

Figure 7.2: Results from natural gas price sensitivity for small-scale (on the left) and large-scale (on the right) cases

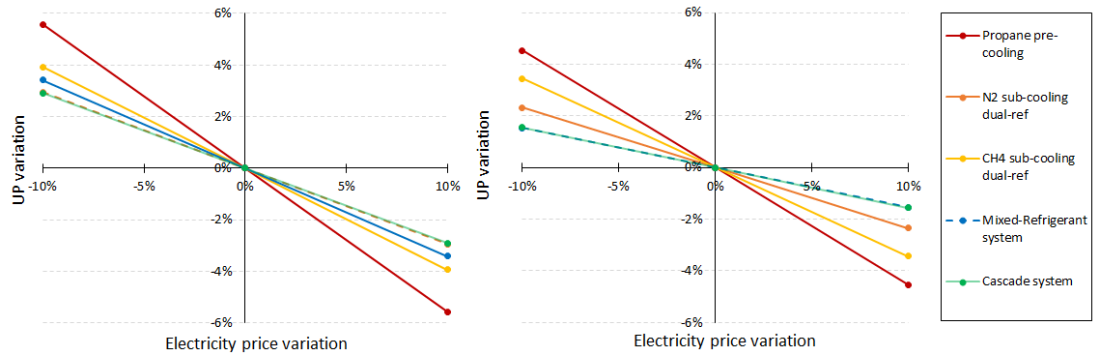

Figure 7.3: Results from electricity price sensitivity for small-scale (on the left) and large-scale (on the right) cases

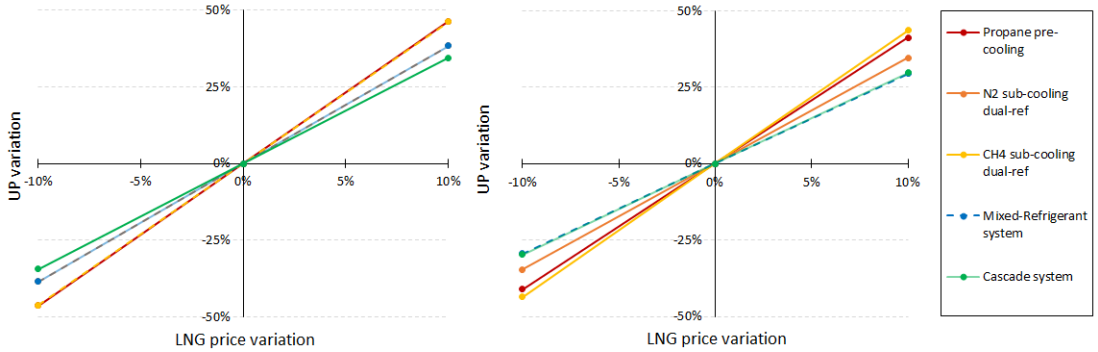

Figure 7.4: Results from LNG sale price sensitivity for small-scale (on the left) and large-scale (on the right) cases

In absolute terms LNG sale price proves to be the most influencing parameter. A +10 %-increase in LNG sale price causes the Unitary Profit to increase by 46 % for small-scale propane pre-cooling. The percentage increase is 41 % for the large-scale case. Natural gas feed price is ranked second, while electricity price is the least influencing input.
The U-value estimation and other inputs (e.g. the cost of working fluids and maintenance cost) are assessed as well. Results are not presented here as these parameters are not as influencing. For instance, a ±10 %-variation in the U-value estimation has almost a negligible effect on Unitary Profit, with percentage variations smaller than 1 % for all cases.

7.3.4 Influence of natural gas composition on economic performance

Among the considered natural gas feed compositions presented in Section B.3 of Appendix B, three cases are selected, namely Italian, German and Spanish grid natural gases. The corresponding compositions are presented in Table 7.8 together with the Danish reference case.

Table 7.8: Natural gas grid composition for Denmark (suggestion of *Kosan Crisplant A/S*) and for three different European countries as given in [82] in terms of molar fractions

	CH_4	C_2H_6	C_3H_8	n-C_4H_{10}	i-C_4H_{10}	n-C_5H_{12}	i-C_5H_{12}	N_2
Denmark	0.903	0.060	0.024	0.006	0.004	0.000	0.000	0.003
Italy	0.980	0.007	0.002	0.001	0.000	0.000	0.000	0.009
Germany	0.839	0.038	0.008	0.004	0.002	0.003	0.002	0.104
Spain	0.816	0.134	0.037	0.004	0.003	0.000	0.000	0.007

This selection is made to highlight three different deviations from the Danish natural gas grid composition:

- increase of methane fraction at the expense of C2+ hydrocarbon content (Italian case);
- increase of nitrogen fraction at the expense of methane fraction (German case);
- increase of C2+ hydrocarbon content at the expense of methane fraction (Spanish case).

The composition of the natural gas feed affects the economic performance of the liquefaction facility through several parameters. The natural gas feed price is based on feed Higher Heating Value. Revenues depend on LNG Higher Heating Value and liquefaction rate. Finally, the natural gas feed composition affects the required net power consumption. With respect to that, Table 7.9 summarises the main properties of the considered natural gas feed compositions. The minimum ideal liquefaction work per kg of natural gas feed is provided as an indicator for the different power consumption in the four cases.

Table 7.9: Natural gas and LNG HHV's, minimum ideal liquefaction work and liquefaction rate for the considered natural gas compositions

	HHV_{NG} [MJ/kg]	HHV_{LNG} [MJ/kg]	w_{min} [kJ/kg_{NG}]	Liquefaction rate [%]
Denmark	54.45	54.54	425.2	96.40
Italy	54.57	54.98	470.2	94.53
Germany	46.27	51.70	416.5	83.53
Spain	53.70	53.93	392.8	96.58

The interested reader can find additional details about the influence of natural gas feed composition on the liquefaction cycle from a thermodynamic viewpoint in Appendix B. In general terms, the heating values increase together with the methane fraction in the natural gas mixture. The same does power consumption, given the higher cooling load. As to the liquefaction rate, methane and nitrogen are the components mostly present in the off-gas after the flashing, hence the lower liquefaction rates for Italian and German cases.

It has to be added that LNG in the German case is characterised by a nitrogen molar fraction of 3.7 %, which is above the usual specification on nitrogen content (normally below 1 %). Therefore the German grid natural gas should undergo a pretreatment stage upstream in order to reduce its nitrogen content.

The optimal designs cannot be applied as such when changing the natural gas feed composition. For instance, a change in cooling load requires a different refrigerant flow rate given the same temperature approach. Moreover, the feed composition affects the shape of the natural gas cooling curve, leading to potential crossovers at the cold box.
In order to evaluate the economic figures when varying the natural gas feed composition, the following methodology is applied:

- no changes in the cycle pressure levels are performed;
- for all the systems the refrigerant mass flow rates are adjusted in order to achieve the 3 K-approach at the heat exchangers;
- only for expander-based configurations the expander inlet temperature has to be changed as well, in order to avoid crossovers of the temperature profiles in those heat exchangers active in the liquefaction part of the natural gas cooling curve.

Results are reported in Table 7.10 for the small-scale comparison and in Table 7.11 for the large-scale case in terms of percentage deviations of Unitary Profit with respect to the Danish reference case (as in Tables 7.5 and 7.7).

Table 7.10: Unitary Profits for the different natural gas feed composition as percentage deviation from the Danish reference case (small-scale case)

	Unitary Profit [% variation]		
	Italy	**Germany**	**Spain**
Propane pre-cooling	-14.2	-29.0	+3.2
N_2 sub-cooling	-10.2	-27.5	+3.6
CH_4 sub-cooling	-19.7	-36.1	+8.8
PRICO	-22.1	-29.3	+6.3
Cascade - one stage	-5.2	-24.2	+1.4

The Italian and German grid compositions determine a worsening of economic performance. The Italian grid natural gas requires a higher compression power than the Danish one, hence both compressor investment cost and O&M cost increase. The higher LNG HHV is compensated by the lower liquefaction rate, therefore the yearly revenues are lower (72.2 MDKK in small scale, 496 MDKK in large scale).

Table 7.11: Unitary Profits for the different natural gas feed composition as percentage deviation from the Danish reference case (large-scale case)

	Unitary Profit [% variation]		
	Italy	**Germany**	**Spain**
Propane pre-cooling	-8.3	-21.5	+1.4
N_2 sub-cooling	-10.7	-24.1	+2.7
CH_4 sub-cooling	-10.0	-27.7	+6.9
C3-MR	-16.8	-25.3	+0.5
Cascade - two stages	-4.5	-20.1	+1.2

Conversely, compression power is lower for the German grid natural gas composition, which leads to a decrease of both Total Capital Investment and O&M cost. However this is offset by the significantly lower liquefaction rate and by the lower LNG HHV. The yearly revenues are 60 MDKK for small-scale cycles and 412 MDKK for large-scale configurations.
The Spanish grid natural gas composition allows an improvement in the economic performance thanks to the lower net power consumption and to the higher liquefaction rate, which positively offset the decrease in LNG Higher Heating Value, hence the lower yearly revenues (72.3 MDKK in small scale, 497 MDKK in large scale).
Among the different alternatives, expander-based and Mixed-Refrigerant configurations are highly influenced by the natural gas feed composition. Conversely, cascade systems overall present the smallest percentage variations in Unitary Profit. This outcome derives from the smaller changes in refrigerant flow rates for cascade systems compared to the other liquefaction concepts.

7.4 Discussion

The economic analysis performed in this Chapter bases itself on the same assumptions which are discussed in Chapter 6, therefore results have the same limitations. In particular, the use of Turton's cost correlation for compressors makes the economic optimum coincide with the thermodynamic one. This is anyhow verified given the fact that cascade and Mixed-Refrigerant systems generally require larger heat transfer area than expander-based configurations. The small-scale *PRICO* cycle is considered, as it presents a heat network conductance more than three times higher than expander-based cycles.
Figure 7.5 on the left depicts how compressor and heat exchanger investment costs vary along with net power consumption. On the right the breakdown of Total Capital Investment is provided for the thermodynamic optimal design.

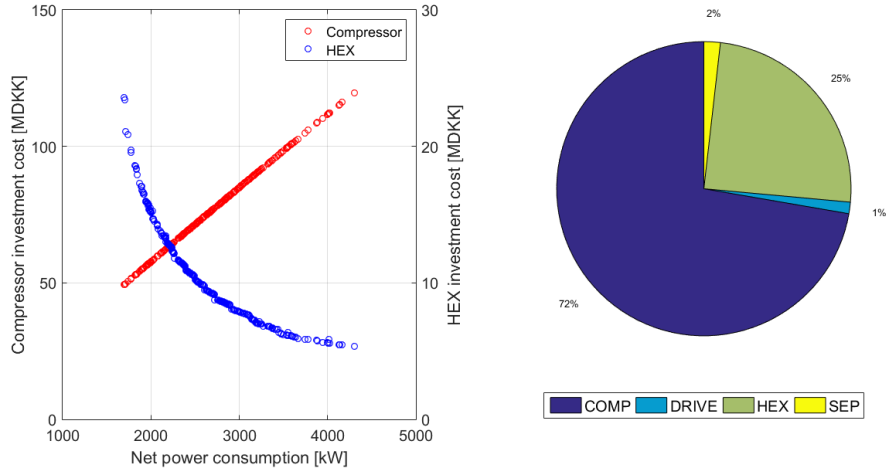

Figure 7.5: On the left: Pareto frontiers for the simultaneous minimisation of compressor and heat exchange network investment costs. On the right: breakdown of Total Capital Investment for small-scale optimal *PRICO* cycle

No trade-off between compressor and heat exchange network investments occurs. This would be observed when applying the second set of cost correlations used in Chapter 6, which could result in a different economic optimum for the small-scale *PRICO* cycle.

Small-scale comparison is performed after changing the design of the considered cycles so that only two-stream heat exchangers are implemented. Refrigerant splitting on the cold side is therefore required to change a Multiple-Stream Heat Exchanger into two two-stream HEX's. It is found that this procedure does not alter the optimal cycle for expander-based configurations. A similar result is highlighted by Lonardi for cascade systems. The same author shows that for Mixed-Refrigerant systems this is no longer valid, i.e. refrigerant splitting highly influences the liquefaction cycle, particularly in terms of required refrigerant flow rate.
As a general outcome it can be inferred that when the refrigerant is a pure fluid and when the temperature approaches are external, the splitting does not alter the required flow rates. Observing the temperature profiles for the optimal expander-based configurations reported in Appendix C, it can be claimed that for some systems (e.g. dual-refrigerant cycles) the temperature approaches are located internally in some heat exchangers. However these are already two-stream HEX's and are not affected by the splitting procedure.

Additional remarks have to be made about the way the influence of natural gas feed composition on the economic outcome is assessed.
The thermodynamic optimum depends on the feed composition, therefore the liquefaction facility should be optimised accordingly. This is computationally intensive and is not performed due to time constraints.

The results cannot be read either as indicators of the configuration flexibility when the feed composition changes. An off-design analysis would be required to give such outcome. Overall a change in the natural gas composition translates into a different cooling load. Once the refrigerant flow rate is kept fixed, a change in the temperature approaches at the heat exchangers occurs, which may lead to technical and thermodynamic violations.
The basic idea was to apply the least number of modifications to the optimal cycles, mainly to respect the 3 K-approach requirements at the heat exchangers, and to assess which economic figures are affected by the feed composition and why. The main modification regards the refrigerant flow rates, which have to be adjusted according to the natural gas cooling load. Expander-based configurations also require the control of the expander inlet temperature, being a key model variable to avoid crossovers in that part of the cold box active in the liquefaction phase.
Finally, the economic figures are calculated changing the feed composition but keeping the same inputs as for the Danish context. This is done to highlight the influence that natural gas composition has on the economic outcome when all the other inputs are kept constant. Nevertheless a thorough analysis would require to update natural gas, electricity and LNG prices according to the different European countries where the liquefaction facility is located. Looking at the data given by the European Commission about electricity markets for 2015 [74], it can be spotted that Denmark has the lowest electricity price for industrial consumers (the highest case being Italy, with 16.93 c€/kWh). Therefore the economic outcome for Italian, German and Spanish cases would be worse compared to what presented. The better profitability of the Spanish case should be checked, as the reduction in power consumption could be offset by the higher electricity price (35 % higher than the Danish case).
Further data analyses are required for natural gas and LNG prices in the different European countries. As an example, the Italian Energy Market Manager gives a natural gas spot price of approximately 15.1 €/MWh [83], slightly higher than the one used for the Danish case.

7.5 Conclusion

This Chapter outlines the economic ranking for small-scale and large-scale natural gas liquefaction alternatives. In the attempt to make the comparison more realistic, only two-stream heat exchangers are implemented in small-scale applications, whereas large-scale cycles present the highest efficiency for turbo-machinery equipment.
Results show that one-stage cascade cycle is the most attractive alternative in small scale, yielding a Unitary Profit of 0.92 DKK per kg of produced LNG. Among large-scale configurations *C3-MR* cycle is the most favourable with a Unitary Profit of 1.08 DKK per kg of produced LNG.
The influence of feed composition on economic performance is assessed showing that very high methane or nitrogen content in the natural gas mixture is not beneficial, the former due to the increased power consumption, the latter due to the decreased liquefaction rate and Higher Heating Value of the output LNG.

8 Discussion

This thesis bases itself on many assumptions and the presented results are subjected to various limitations. The aim of this Chapter is to summarise the discussions which are performed throughout the report and to highlight how assumptions and limitations affect the outcomes. Possible improvements to the study are mentioned.

Thermodynamic modelling

The modelling stage is fundamental for this thesis work and represents the basis for thermodynamic optimisation first, and subsequently for economic considerations. Therefore all the assumptions which are adopted in this phase affect the results.
Thermodynamic simulation is based on Peng-Robinson model. On one side this choice enables to have computational effectiveness and to get a consistent literature benchmark with which to compare the results. On the other side it introduces inaccuracies in the estimation of key thermodynamic variables. As shown in Appendix A, the Figure of Merit is slightly overestimated, while a larger underestimation of the heat transfer area can be expected. Result validation should be performed using GERG-2008 property method to provide more accurate indications. The barrier is given by heavier computational burdens and non-convergence issues.

Overestimation of the thermodynamic performance is also caused by the assumption on turbo-machinery mechanical efficiency (which is set unitary) and on pressure losses (disregarded in heat exchange processes). Mechanical efficiency is anyhow high in real equipment. Conversely, disregarding pressure losses may lead to significant underestimation of real energy consumption, given the high working pressure levels and especially for large-scale systems.

Heat transfer plays a central role in the liquefaction process. Nevertheless this is not the focus of this thesis work and heat exchange processes are simulated relying on the approach and assumptions comprised in Aspen Plus. The software adopts a Distributed Parameter

Model (DPM), which means that the heat exchange device is divided into zones of variable size and is simulated applying a lumped parameter model in each of them [64]. The number of zones has to be set, and in the present work 50 zones are always considered for all heat exchangers, requiring the addition of extra zones in those parts presenting non-linear temperature profiles. Variables like UA-value and Logarithmic Mean Temperature Difference are averaged based on the discretisation of heat exchangers into zones.
Moreover the software works by assuming the same temperature for the hot-side streams at the outlet of each discretisation zone. This is a simplification and justifies the absence of pinch point violations when reporting the Composite Curves for Multiple-Stream Heat Exchangers. Other assumptions are the absence of axial thermal conduction and heat gains/losses.

Thermodynamic optimisation

Thermodynamic optimisation by means of genetic algorithm requires a compromise between research space, iterations and number of evaluations on one side, and the computational burden on the other one. For this work the optimisation routine was deliberately computational- and time-intensive. As a consequence, optimisation outcomes are claimed to be robust. This is overall confirmed when comparing the obtained results with the literature, as discussed in Chapter 5. Moreover the thermodynamic superiority of Mixed-Refrigerant and cascade cycles is verified through the comparison with the work of Lonardi [81], which main results are included in Chapter 7.
From a designer point of view the optimisation effort may be not as worthy. Although the optimisation procedure always allows to reduce the net power consumption with respect to the modelled cycles, the achieved reductions are overall quite small (smaller than 5 % for most expander-based cases). What is found to be decisive is instead to seek for cycle designs yielding a small temperature difference in heat exchangers, mainly acting on the refrigerant flow rates, pressure and temperature levels. This is also a general finding of the Master Thesis *Modelling and Optimisation of Cascade and Mixed-Refrigerant Cycles for Natural Gas Liquefaction* when dealing with cascade systems. Conversely, the optimisation routine is fundamental when considering Mixed-Refrigerant systems given the key role played by the refrigerant composition.

Economic considerations

The main uncertainty associated to the economic results is identified in the cost correlations which are used to translate thermodynamic outputs into economic figures for the liquefaction facility.
Given the fact that natural gas liquefaction is highly energy intensive, compression power represents a decisive voice for the O&M cost. Reducing power consumption comes at the expense of heat transfer area, as extensively shown in this report. Therefore a trade-off between operation and investment costs could occur. This is mainly dependent on the share of turbomachinery investment cost, which could be dominant in the Total Capital Investment.

In the present work, the use of Turton's cost correlations makes the compressor the most capital-intensive component, therefore the economic optimum coincides with the thermodynamic one. Consequently, only if different configurations have a similar power consumption, the effect of factors like design complexity and heat transfer area is spotted in the economic results. In light of this, the superiority of one-stage cascade cycle for small-scale applications is regarded to be a biased result, as the other small-scale alternatives are characterised by larger power consumption. The inferiority of expander-based cycles for small-scale applications is another consequence.
An additional set of cost correlations for compressors and heat exchangers is assessed leading to a different result. This uncertainty highlights the need for cost data validation, which is outside the scope of this thesis and is left as necessary future work to make such analyses reliable.

Beside the influence of cost correlations, many simplifications are adopted in the economic analysis. Among them, the Discounted Cash Flow model does not take into account any bankability consideration, therefore results cannot be fully taken as realistic indication of LNG project profitability in a Danish context. Cost data provided by *SWEP* are valid for flat-plate heat exchangers and are applied as such to Multiple-Stream plate-fin heat exchangers. Moreover many of the analysed cases present working pressure above 100 bar on the refrigerant side, which is beyond the operating conditions for *SWEP* heat exchangers (normally up to 60 bar).

9 Conclusion

This thesis focuses on the thermodynamic and economic analysis of different LNG production configurations. Interest in LNG is growing in the shipping sector due to economic advantages over oil alternatives and stricter environmental regulations for shipboard NO_x and SO_x emissions.
LNG production is highly energy intensive, therefore a thorough thermodynamic analysis and optimisation is required to reduce the compression power consumption. Focus is put on the expander-based configuration and thirteen models are developed using the software Aspen Plus. The modelling stage highlights two main drivers for efficiency improvements: the compression process design and the reduction of the mean temperature difference at the cold box.
Inter-cooled multi-stage compression should be preferred to the single-stage one. Secondly, the temperature difference at the cold box is a decisive factor for the exergy destruction during the liquefaction process and can be reduced by:

- adding a pre-cooling stage;
- introducing a dual-expansion process;
- implementing a dual-refrigerant cycle.

Thermodynamic optimisation by means of genetic algorithm is performed to quantify the efficiency improvements.
Among the pre-cooling alternatives, the one employing propane is the best performing achieving a Figure of Merit of 27.3 % and a unit energy consumption of 1617 kJ per kg of produced LNG.
If a dual-turbine cycle is designed, the two expanders should have different pressure ratios, as this is the solution yielding the highest Figure of Merit (29.7 %).
As to the dual-refrigerant alternatives, the use of nitrogen is found beneficial for the liquefaction and sub-cooling phases, while methane should be employed for the sensible pre-cooling of the natural gas feed. The N_2 sub-cooling alternative is the most efficient among the thirteen cycles under investigation, providing a Figure of Merit of 33 % and requiring 1336 kJ/kg as unit energy consumption.

Exergy analysis is performed on the thermodynamic optimal cycles. Components' rational efficiency defects are computed to highlight the distribution of exergy destructions and losses. Exergy loss at refrigerant coolers generally represents the largest dissipation of useful work. The waste heat should be utilised given the high temperature level of the refrigerant streams at cooler inlets. Compression processes are responsible for the greatest share of exergy destruction, followed by expansions.

The reduction in power consumption comes at the expense of heat transfer area. This is pinpointed through a series of Multi-Objective Optimisations aiming at simultaneously minimising the net power consumption and the overall heat network conductance. The latter is found to range between 50 kW/K and 300 kW/K for the expander-based concept.

The existence of a trade-off between power consumption and heat transfer area justifies an economic analysis for the LNG production configurations. A simplified Discounted Cash Flow model is set up and the different alternatives are compared based on Unitary Profit, NPV and Adjusted Pay-Back Time. Two plant sizes are considered, which differ for the natural gas feed flow rate, being 0.8 kg/s in the small-scale case and 5.5 kg/s for large-scale applications. Liquefaction cycles are assessed and compared in their thermodynamic optimal design.
Both for small-scale and large-scale applications N_2 sub-cooling dual-refrigerant configuration results the most favourable. Unitary Profits are 0.82 (small scale) and 0.87 (large scale) DKK per kg of produced LNG. Correspondingly NPV is 227 MDKK in small scale (Pay-Back Time of 4 years) and 1656 MDKK in large scale (Pay-Back Time of 3 years).
The most economically viable expander-based alternatives are selected and compared with cascade and Mixed-Refrigerant configurations. Aspen Plus models for these two liquefaction concepts are developed and optimised in the Master Thesis *Modelling and Optimisation of Cascade and Mixed-Refrigerant Cycles for Natural Gas Liquefaction*. Results show that the expander-based concept is not economically competitive with cascade and Mixed-Refrigerant systems. The most convenient small-scale configuration is the one-stage cascade (Unitary Profit of 0.92 DKK per kg of LNG), while among large-scale cycles propane pre-cooled Mixed-Refrigerant configuration is the most favourable (Unitary Profit of 1.08 DKK per kg of produced LNG).

The main influencing parameters for the economic performance are, in order, LNG sale price, natural gas feed price and electricity price. The reliability of economic outcomes is largely discussed, as it mostly depends on the employed cost correlations. The ones used for this work make compressors the most capital-intensive components, leading to the coincidence of thermodynamic and economic optimum. The assessment of alternative cost correlations highlights the need for cost data validation as a necessary future development of the present thesis. This goes in the direction of bringing a modelling- and simulation-based work closer to the reality of natural gas liquefaction facilities, including more realistic modelling and off-design considerations.

Bibliography

[1] IPCC. Climate Change 2014. Synthesis Report. Summary Chapter for Policymakers. Technical report, 2014. URL https://www.ipcc.ch/pdf/assessment-report/ar5/syr/AR5_SYR_FINAL_SPM.pdf.

[2] Veronika Eyring, James J. Corbett, David S. Lee, and James J. Winebrake. Brief summary of the impact of ship emissions on atmospheric composition, climate, and human health. *Document submitted to the Health and Environment sub-group of the International Maritime Organization*, 2007. URL http://www.pa.op.dlr.de/~VeronikaEyring/Eyringetal_IMOBriefSummary_FINAL.pdf.

[3] Fabio Burel, Rodolfo Taccani, and Nicola Zuliani. Improving sustainability of maritime transport through utilization of Liquefied Natural Gas (LNG) for propulsion. *Energy*, 57: 412–420, 2013. ISSN 03605442. URL http://dx.doi.org/10.1016/j.energy.2013.05.002.

[4] Mar Viana, Pieter Hammingh, Augustin Colette, Xavier Querol, Bart Degraeuwe, Ina de Vlieger, and John van Aardenne. Impact of maritime transport emissions on coastal air quality in Europe. *Atmospheric Environment*, 90:96–105, 2014. ISSN 18732844. URL http://dx.doi.org/10.1016/j.atmosenv.2014.03.046.

[5] Cengiz Deniz and Burak Zincir. Environmental and economical assessment of alternative marine fuels. *Journal of Cleaner Production*, 113(X):438–449, 2016. ISSN 09596526. URL http://linkinghub.elsevier.com/retrieve/pii/S0959652615018119.

[6] Janusz Cofala, Markus Amann, Chris Heyes, Fabian Wagner, Zbigniew Klimont, Max Posch, Wolfgang Schöpp, Leonor Tarasson, Jan Eiof Jonson, Chris Whall, and Andrianna Stavrakaki. Analysis of Policy Measures to Reduce Ship Emissions in the Context of the Revision of the National Emissions Ceilings Directive. Final Report. 2007. URL http://webarchive.iiasa.ac.at/rains/reports/IR06-107_Ships.pdf.

[7] United Nations. International Marine Organization. URL http://www.imo.org/en/About/Pages/Default.aspx. Accessed February 2016.

[8] International Marine Organization. Revised MARPOL Annex VI: Regulations for the Prevention of Air Pollution from Ships and NOx. Technical report, October 2009.

[9] Environmental Protection Agency. Ministry of Environment and Food of Denmark. Reducing shipping emissions. URL http://eng.mst.dk/topics/air/reducing-shipping-emissions/. Accessed January 2016.

[10] Danish Maritime Authority. North European LNG Infrastructure Project. Technical report. URL http://www.dma.dk/themes/LNGinfrastructureproject/Documents/FinalReport/LNG_Summary_Report_20120522_optimerad.pdf.

[11] European Commission. COMMUNICATION FROM THE COMMISSION TO THE EUROPEAN PARLIAMENT, THE COUNCIL, THE EUROPEAN ECONOMIC AND SOCIAL COMMITTEE AND THE COMMITTEE OF THE REGIONS. Clean Power for Transport: A European alternative fuels strategy. COM/2013/017, . URL http://eur-lex.europa.eu/legal-content/EN/ALL/?uri=CELEX%3A52013PC0017. Accessed February 2016.

[12] Heather Thomson, James J. Corbett, and James J. Winebrake. Natural gas as a marine fuel. *Energy Policy*, 87:153–167, 2015. ISSN 03014215. URL http://dx.doi.org/10.1016/j.enpol.2015.08.027.

[13] eia. U.S. Energy Information Administration. International Energy Statistics. URL https://www.eia.gov/cfapps/ipdbproject/IEDIndex3.cfm?tid=5&pid=57&aid=6. Accessed February 2016.

[14] Selma Bengtsson, Karin Andersson, and Erik Fridell. Life cycle assessment of marine fuels - A comparative study of four fossil fuels for marine propulsion. Technical Report 11:125, Chalmers University of Technology, Gothenburg, Sweden, 2011. URL http://www.dma.dk/themes/LNGinfrastructureproject/Documents/Fuelsandenvironment/LCAoffourpossiblemarinefuels.pdf.

[15] European Commission. European Commissions' study on LNG as a shipping fuel shows industry's support, . URL http://ec.europa.eu/transport/modes/maritime/news/2015-03-03-lng_en.htm. Accessed February 2016.

[16] Peter D. Lund, Juuso Lindgren, Jani Mikkola, and Jyri Salpakari. Review of energy system flexibility measures to enable high levels of variable renewable electricity. *Renewable and Sustainable Energy Reviews*, 45:785–807, 2015. ISSN 13640321. URL http://dx.doi.org/10.1016/j.rser.2015.01.057.

[17] Saeid Mokhatab, William A. Poe, and John Y. Mak. Natural Gas Fundamentals. In *Handbook of Natural Gas Transmission and Processing*, chapter 1. 2015. ISBN 9780128014998.

[18] Alireza Bahadori. Overview of Natural Gas Resources. In *Natural Gas Processing. Technology and Engineering Design*, chapter 1, pages 1–22. 2014. ISBN 9780080999715. URL http://linkinghub.elsevier.com/retrieve/pii/B9780080999715000015.

[19] IEA. International Energy Agency. *Resources to Reserves 2013 - Oil, Gas and Coal Technologies for the Energy Markets of the Future*. 2013. ISBN 9789264083547. URL http://www.iea.org/publications/freepublications/publication/resources-to-reserves-2013.html.

[20] IEA. International Energy Agency. Natural Gas. URL https://www.iea.org/aboutus/faqs/naturalgas/. Accessed February 2016.

[21] Lijiang Wei and Peng Geng. A review on natural gas/diesel dual fuel combustion, emissions and performance. *Fuel Processing Technology*, 142:264–278, 2016. ISSN 03783820. URL http://dx.doi.org/10.1016/j.fuproc.2015.09.018.

[22] Francis S. Manning and Richard E. Thomson. Characterization of Natural Gas and Its Products. In *Oilfield Processing of Petroleum: Natural Gas, volume 1*, chapter 2, page 7. PennWell Books, 1991. URL https://books.google.dk/books?id=FnDp8V9TX9oC&printsec=frontcover&hl=it&source=gbs_ge_summary_r&cad=0#v=onepage&q&f=false.

[23] Alireza Bahadori. Natural Gas Properties. In *Natural Gas Processing. Technology and Engineering Design*, chapter 2, pages 23–58. 2014. ISBN 9780080999715.

[24] Stephen R. Turns. *An Introduction to Combustion - Concepts and Applications*. Third edition, 2012.

[25] U.S. Department of Energy. Appendix A. Lower and Higher Heating Values of Gas, Liquid and Solid Fuels. Biomass Energy Data Book. URL http://cta.ornl.gov/bedb/appendix_a.shtml. Accessed March 2016.

[26] Bjørn Austbø and Truls Gundersen. Optimization of a single expander LNG process. *Energy Procedia*, 64(C):63–72, 2015. ISSN 18766102. URL http://dx.doi.org/10.1016/j.egypro.2015.01.009.

[27] Satish Kumar, Hyouk Tae Kwon, Kwang Ho Choi, Wonsub Lim, Jae Hyun Cho, Kyungjae Tak, and Il Moon. LNG: An eco-friendly cryogenic fuel for sustainable development. *Applied Energy*, 88(12):4264–4273, 2011. ISSN 03062619. URL http://dx.doi.org/10.1016/j.apenergy.2011.06.035.

[28] IPCC. Changing in Atmospheric Costituents and in Radiative Forcing. In *IPCC Fourth Assessment Report (AR4)*, chapter 2. 2007. URL https://www.ipcc.ch/pdf/assessment-report/ar4/wg1/ar4-wg1-chapter2.pdf.

[29] Selma Bengtsson, Erik Fridell, and Karin Andersson. Environmental assessment of two pathways towards the use of biofuels in shipping. *Energy Policy*, 44:451–463, 2012. ISSN 03014215. URL http://dx.doi.org/10.1016/j.enpol.2012.02.030.

[30] Alireza Bahadori. Liquefied Natural Gas. In *Natural Gas Processing. Technology and Engineering Design*, chapter 13. 2014. ISBN 9780124202047.

[31] Saeid Mokhatab, William A. Poe, and John Y. Mak. LNG Fundamentals. In *Handbook of Liquefied Natural Gas*, chapter 1, pages 1–106. Elsevier, 2014. ISBN 9780124045859. URL http://www.sciencedirect.com/science/article/pii/B9780124045859000015.

[32] Statoil. Snøhvit. URL http://www.statoil.com/en/OurOperations/ExplorationProd/ncs/snoehvit/Pages/default.aspx. Accessed March 2016.

[33] Florian Dauber and Roland Span. Modelling liquefied-natural-gas processes using highly accurate property models. *Applied Energy*, 97:822–827, 2012. ISSN 03062619. URL http://dx.doi.org/10.1016/j.apenergy.2011.11.045.

[34] Chonghun Han and Youngsub Lim. *LNG Processing. From Liquefaction to Storage*, volume 31. Elsevier B.V., 2012. ISBN 1570-7946. URL http://dx.doi.org/10.1016/B978-0-444-59507-2.50013-5.

[35] Saeid Mokhatab and William A. Poe. Basic Concepts of Natural Gas Processing. In *Handbook of Natural Gas Transmission and Processing (Second Edition)*, chapter 3, pages 181–193. 2012. ISBN 978-0-12-386914-2. URL http://www.sciencedirect.com/science/article/pii/B9780123869142000042.

[36] Roy Scott Heiersted. Snøhvit LNG Project: Europe's First Base-Load LNG Production, 2005. URL http://www.venezuelagas.net/documents/Liquid-2005-05.pdf.

[37] Saeid Mokhatab, William A. Poe, and John Y. Mak. Natural Gas Liquefaction. In *Handbook of Liquefied Natural Gas*, chapter 3, pages 147–183. Elsevier, 2014. ISBN 9780124045859. URL http://www.sciencedirect.com/science/article/pii/B9780124045859000039.

[38] Bjørn Austbø, Sigurd Weidemann Løvseth, and Truls Gundersen. Annotated bibliography-Use of optimization in LNG process design and operation. *Computers and Chemical Engineering*, 71:391–414, 2014. ISSN 00981354. URL http://dx.doi.org/10.1016/j.compchemeng.2014.09.010.

[39] Adrian J. Finn, Grant L. Johnson, and Terry R. Tomlinson. LNG technology for offshore and mid-scale plants. *GPA Annual Convention Proceedings*, 2000. ISSN 00968870.

[40] Aida Kheradmand, Seid Ehsan Marashi, and Masoud Ghorbanian. Offshore LNG Production. Technical report, NTNU, Trondheim, 2010.

[41] T.B. He and Y.L. Ju. Performance improvement of nitrogen expansion liquefaction process for small-scale LNG plant. *Cryogenics*, 61:111–119, 2014. ISSN 00112275. URL http://linkinghub.elsevier.com/retrieve/pii/S0011227513000866.

[42] Zongming Yuan, Mengmeng Cui, Ying Xie, and Chunlin Li. Design and analysis of a small-scale natural gas liquefaction process adopting single nitrogen expansion with carbon dioxide pre-cooling. *Applied Thermal Engineering*, 64(1-2):139–146, 2014. ISSN 13594311. URL http://dx.doi.org/10.1016/j.applthermaleng.2013.12.011.

[43] Mohd Shariq Khan, Sanggyu Lee, Mesfin Getu, and Moonyong Lee. Knowledge inspired investigation of selected parameters on energy consumption in nitrogen single and dual expander processes of natural gas liquefaction. *Journal of Natural Gas Science and Engineering*, 23:324–337, 2015. ISSN 18755100. doi: 10.1016/j.jngse.2015.02.008.

[44] Zongming Yuan, Mengmeng Cui, Rui Song, and Ying Xie. Evaluation of prediction models for the physical parameters in natural gas liquefaction processes. *Journal of Natural Gas*

Science and Engineering, 2015. ISSN 18755100. URL http://dx.doi.org/10.1016/j.jngse.2015.09.042.

[45] O. Kunz and W. Wagner. The GERG-2008 wide-range equation of state for natural gases and other mixtures: An expansion of GERG-2004. *Journal of Chemical and Engineering Data*, 57(11):3032–3091, 2012. ISSN 00219568. URL http://pubs.acs.org/doi/pdf/10.1021/je300655b.

[46] Aspen Technology. Aspen Plus. URL http://www.aspentech.com/products/engineering/aspen-plus/. Accessed March 2016.

[47] Ho Myung Chang. A thermodynamic review of cryogenic refrigeration cycles for liquefaction of natural gas. *Cryogenics*, 72:127–147, 2015. ISSN 00112275. URL http://dx.doi.org/10.1016/j.cryogenics.2015.10.003.

[48] Damian Vogt. Efficiencies. In *KTH. Turbomachinery Lecture Notes.*, pages 1–8. 2007. URL http://www.energy.kth.se/compedu/webcompedu/WebHelp/media%5CLecture_notes%5CS2%5Cefficiencies.pdf.

[49] Weldon Ransbarger. A fresh look at LNG process efficiency. *Hydrocarbon Engineering*, 12, 2007. ISSN 14689340. URL http://lnglicensing.conocophillips.com/Documents/SMID_016_WeldonsPaperLNGIndustry.pdf.

[50] Adrian J. Finn. Are floating LNG facilities viable options? *Hydrocarbon Processing*, 88(7):31–39, 2009. URL https://issuu.com/androsov.info/docs/hp_2009_07.

[51] C.W. Remeljej and A.F.A. Hoadley. An exergy analysis of small-scale liquefied natural gas (LNG) liquefaction processes. *Energy*, 31(12):1669–1683, 2006. ISSN 03605442. doi: 10.1016/j.energy.2005.09.005.

[52] T.J. Kotas. *The Exergy Method of Thermal Plant Analysis*. Elsevier Science, 2013. ISBN 9781483100364. URL https://books.google.dk/books?id=-QLLBAAAQBAJ.

[53] Hoseyn Sayyaadi and M. Babaelahi. Exergetic Optimization of a Refrigeration Cycle for Re-Liquefaction of LNG Boil-Off Gas. *International Journal of Thermodynamics*, 13(4):127–133, 2010. ISSN 13019724.

[54] Hoseyn Sayyaadi and M. Babaelahi. Multi-objective optimization of a joule cycle for re-liquefaction of the Liquefied Natural Gas. *Applied Energy*, 88(9):3012–3021, 2011. ISSN 03062619. doi: 10.1016/j.apenergy.2011.03.041.

[55] T-V. Nguyen, B. Elmegaard, P. Breuhaus, and F. Haglind. *Modelling, analysis and optimisation of energy systems on offshore platforms*. PhD thesis, Technical University of Denmark, 2014.

[56] MathWorks. MATLAB. URL http://se.mathworks.com/products/matlab/. Accessed March 2016.

[57] Lena Kitzing, Marie Münster, and Jonas Katz. Evaluating projects - Basic economic principles and methods. Technical report, DTU Management Engineering, Energy Economics and Regulation & Energy System Analysis, 2015.

[58] M. Roberts, F. Chen, and Ö. Saygi-Arslan. Brayton refrigeration cycles for small-scale LNG. *Gas Processing*, pages 27–32. July-August 2015.

[59] Maya Kusmaya and Jostein Pettersen. Liquefaction Process Evaluation for Floating LNG, 2014. URL http://www.gas.uni-miskolc.hu/publics/Projekt-feladat_liquefaction-process-evaluation-for-flng_rev2.pptx.pdf.

[60] H.M. Chang, J.H. Park, K.S. Cha, S. Lee, and K.H. Choe. Modified Reverse-Brayton Cycles for Efficient Liquefaction of Natural Gas. *Cryocoolers 17*, pages 435–442, 2012.

[61] Sultan Seif Pwaga. *Sensitivity Analysis of Proposed LNG liquefaction Processes for LNG FPSO*. Master thesis, NTNU, 2011.

[62] J.H. Foglietta. LNG production using dual independent expander refrigeration cycles, 2002. URL http://www.google.com/patents/US6412302. US Patent 6412302.

[63] Lummus Technology. NicheLNG Liquefaction Technology. Technical report, 2011. URL http://www.digitalrefining.com/data/literature/file/1300330005.pdf.

[64] Julio César Pacio. *Multiscale thermo-hydraulic modeling of cryogenic heat exchangers*. PhD thesis, Norwegian University of Science and Technology, 2012.

[65] EES - Engineering Equation Solver. URL http://www.fchart.com/ees/. Accessed May 2016.

[66] Todd B. Jekel and Douglas T. Reindl. Single- or Two-Stage Compression. *ASHRAE Journal*. August 2008.

[67] Bjørn Austbø and Truls Gundersen. *Using thermodynamic insight in the optimization of LNG processes*, volume 33. Elsevier, 2014. URL http://dx.doi.org/10.1016/B978-0-444-63455-9.50047-7.

[68] B. Linnhoff and V. R. Dhole. Shaftwork targets for low-temperature process design. *Chemical Engineering Science*, 47(8):2081–2091, 1992. ISSN 00092509. doi: 10.1016/0009-2509(92)80324-6.

[69] Industrial Energy Systems Laboratory LENI. OSMOSE Platform. URL http://leni.epfl.ch/osmose. Accessed June 2016.

[70] Tianbiao He and Yonglin Ju. Optimal synthesis of expansion liquefaction cycle for distributed-scale LNG (liquefied natural gas) plant. *Energy*, 88:268–280, 2015. ISSN 03605442. URL http://dx.doi.org/10.1016/j.energy.2015.05.046.

[71] Richard Turton, Richard C. Bailie, Wallace B. Whiting, Joseph A. Shaeiwitz, and Debangsu Bhattacharyya. *Analysis, Synthesis and Design of Chemical Processes*. Prentice Hall, fourth edition, 2012.

[72] CEPCI index. URL http://www.chemengonline.com/pci-home. Accessed May 2016.

[73] Andrea Toffolo, Andrea Lazzaretto, Giovanni Manente, and Marco Paci. A multi-criteria approach for the optimal selection of working fluid and design parameters in Organic Rankine Cycle systems. *Applied Energy*, 121:219–232, 2014. ISSN 03062619. URL http://dx.doi.org/10.1016/j.apenergy.2014.01.089.

[74] European Commission. Quarterly Report on European Electricity Markets. Technical report, 2015. URL https://ec.europa.eu/energy/sites/ener/files/documents/quarterly_report_on_european_electricity_markets_q3_2015.pdf.

[75] J. Walker and E.R. Bingham. *Low-Capacity Cryogenic Refrigeration*. Clarendon Press, The University of Calgary, 1994.

[76] EmersonTechnologies Climate. Refrigerant Choices for Commercial Refrigeration - Finding the Right Balance. Technical report. URL http://www.emersonclimate.com/europe/Documents/Resources/TGE124_Refrigerant_Report_EN_1009.pdf.

[77] Currency converter. URL https://www.oanda.com/currency/converter/. Accessed May 2016.

[78] SWEP. SSP Calculation Software. URL http://www.swep.net/support/ssp-calculation-software/. Accessed May 2016.

[79] Geoff F. Hewitt and Simon J. Pugh. Approximate Design and Costing Methods for Heat Exchangers. *Heat Transfer Engineering*, 28(2):76–86, 2007. ISSN 0145-7632. URL http://dx.doi.org/10.1080/01457630601023229.

[80] EEX - European Energy Exchange. TTF PEGAS. URL https://www.eex.com/en/market-data/natural-gas/spot-market/ttf#!/2016/06/15. Accessed June 2016.

[81] Nicola Lonardi. *Modelling and Optimisation of Cascade and Mixed-Refrigerant Cycles for Natural Gas Liquefaction*. Master thesis - unpublished work, Technical University of Denmark, 2016.

[82] M. Adelt, M. Hoppe, M. Montero, and G. Peureux. Report on gas composition range in Europe. Technical report, 2010. URL http://www.ingas-eu.org/docs/DB0.1.pdf.

[83] Gestore Mercati Energetici. MGP-GAS. URL http://www.mercatoelettrico.org/It/esiti/MGP-GAS/EsitiGasMGP.aspx. Accessed 28/06/2016.

[84] Joachim Gross and Gabriele Sadowski. Application of the Perturbed-Chain SAFT Equation of State to Associating Systems. *Ind. Eng. Chem. Res.*, 41:5510–5515, 2002. ISSN 0888-5885. doi: 10.1021/ie010954d.

A Influence of property methods on the simulation results

The property method is a thermodynamic model which is implemented in simulation tools to predict the thermophysical properties of pure substances and mixtures. The most well-known models are the Equations of State (EOS). Different Equations of State exist and simulation results can significantly differ depending on which EOS is employed, thus leading to uncertainties in optimal design determination. The aim of this Appendix Section is to quantify the numerical deviations which are obtained when simulating the same natural gas liquefaction configuration with various property methods.

The single-expander configuration in Figure A.1 is considered and is simulated using Peng-Robinson (PR) and Soave-Redlich-Kwong (SRK) cubic EOS, Benedict-Webb-Rubin-Starling (BWRS) and Lee-Kesler-Plöcker (LKP) virial EOS, Perturbated Chain with Statistical Association Fluid Theory (PC-SAFT) molecular-based EOS[1] and GERG-2008 empirical multi-parameter EOS.

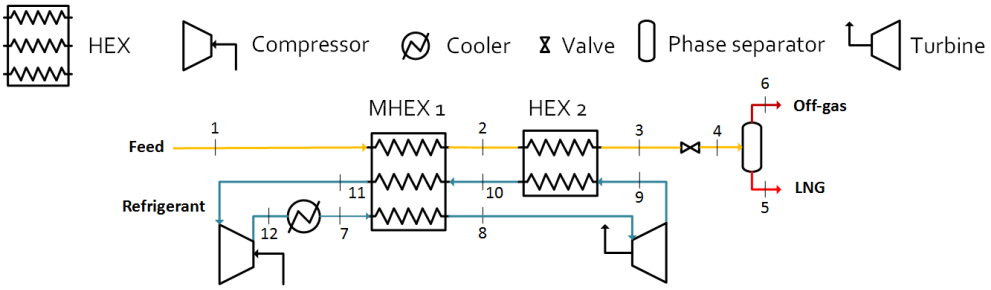

Figure A.1: Process flowsheet of the single-expander cycle

The natural gas feed enters the liquefaction cycle at 20°C and 33 bar (state point 1). It is cooled in isobaric conditions down to -150°C (state point 3).

[1] Pure component parameters of the PC-SAFT EOS are taken from the work of Gross and Sadowski [84].

Refrigerant is nitrogen and its mass flow rate is set equal to 8 kg/s. Nitrogen enters the cold box at 20°C and 120 bar (state point 7), while its temperature at the expander inlet -45°C. Expander discharge pressure is 10 bar.
The modelling assumptions are those applied in Chapter 4. In particular pressure losses are disregarded. Compressor polytropic efficiency is 0.82, while expander isentropic efficiency is set equal to 0.85.

Coherently with what exposed in Section 2.2.3, results obtained using GERG-2008 property package are regarded as the reference case. The percentage deviations from the reference value of the model variable are therefore calculated when testing the other Equations of State (Equation A.1).

$$\text{Deviation} = \frac{\text{Variable} - \text{Variable}_{\text{GERG}-2008}}{\text{Variable}_{\text{GERG}-2008}} \cdot 100 \qquad [\%] \tag{A.1}$$

The model variables which are considered in the assessment are natural gas cooling demand, $\dot{Q}_C$, compressor power consumption $\dot{W}_{comp}$, expander power production $\dot{W}_{exp}$, system Figure of Merit and UA-values and MITA's for the Multiple-Stream and the two-stream Heat Exchangers.

Table A.1 reports the reference results obtained when using GERG-2008 Equation of State.

Table A.1: Simulation results using GERG-2008 property method

Variable	**Unit**	**Value**
$\dot{Q}_C$	kW	795.3
$\dot{W}_{comp}$	kW	3327
$\dot{W}_{exp}$	kW	679
FOM	%	15.96
UA_1	kW/K	46.6
$MITA_1$	K	6.7
UA_2	kW/K	24.1
$MITA_2$	K	4.2

Figures A.2 and A.3 reports the calculated percentage deviations on the simulation results when using different property methods.
Peng-Robinson cubic EOS proves to be accurate when predicting natural gas cooling load, with a percentage variation of -0.25 % with respect to the prediction of GERG-2008 EOS. This confirms the good accuracy of the model for the evaluation of enthalpy and isobaric specific heat capacity in the two-phase region, as shown by Yuan *et al.* [44]. Conversely, deviations on the prediction of compression and expansion power are larger. Compression power requirement is underestimated by 0.8 %, while expansion power is underestimated by 2.6 %.

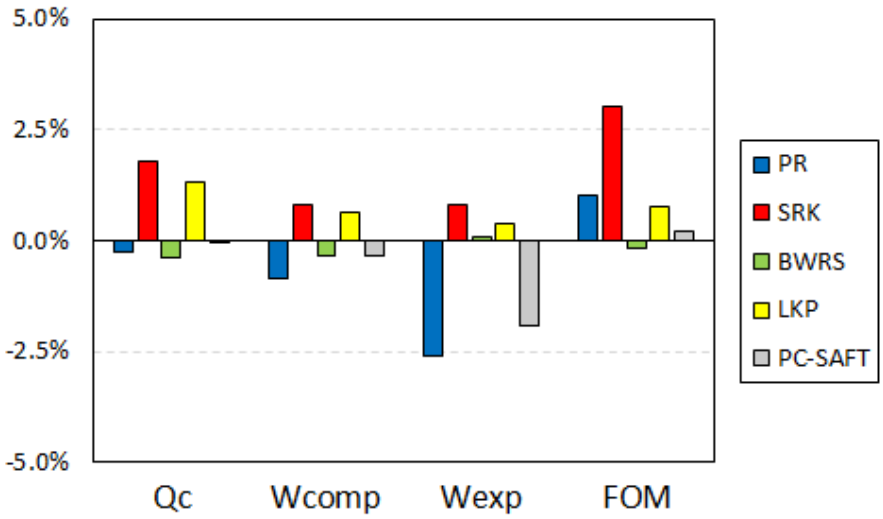

Figure A.2: Comparison of the property methods in terms of percentage deviation from the results obtained using GERG-2008 for natural gas cooling load, compressor and expander power and system Figure of Merit

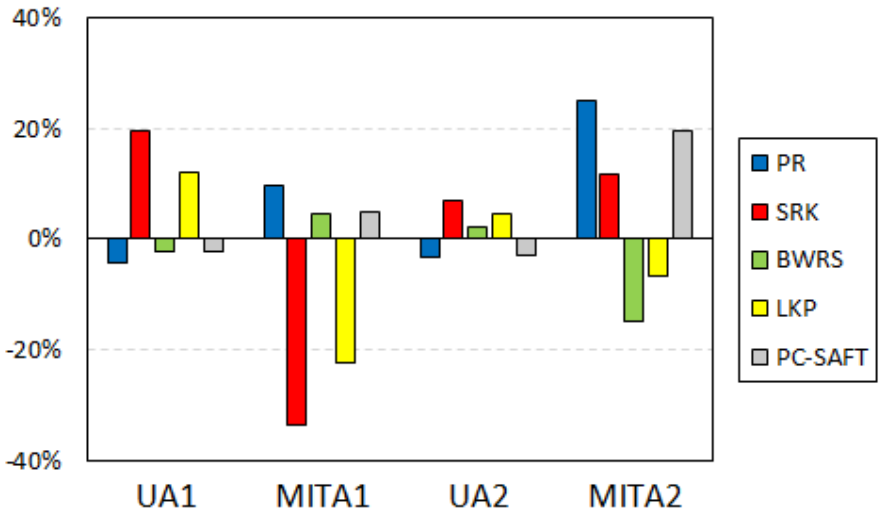

Figure A.3: Comparison of the property methods in terms of percentage deviation from the results obtained using GERG-2008 for UA-values and Minimum Internal Temperature Approaches at the first MHEX and at the second two-stream HEX

Except for Benedict-Webb-Rubin-Starling virial EOS, all the remaining Equations of State overestimate the system Figure of Merit with respect to the one calculated using GERG-2008 property method. Using Peng-Robinson EOS the deviation is +1 %. BWRS EOS proves to be the closest to the reference result, with a percentage deviation of -0.17 %, closely followed by PC-SAFT EOS (percentage variation of +0.19 %).

Appendix A. Influence of property methods on the simulation results

Considering the variables associated to the heat exchange process at the cold box, it can be observed that the percentage deviations are overall greater in magnitude, ranging from +19.4 % to -33.5 %. PR property method leads to an underestimation of the heat exchanger conductance, thus the required heat transfer area (percentage deviation of -4.4 % for the MHEX and of -3.2 % for the two-stream HEX). Benedict-Webb-Rubin-Starling virial EOS proves to be the most accurate, closely followed by PC-SAFT molecular-based EOS.
As to the MITA evaluation, the use of PR property method leads to an overestimation for both heat exchangers. Percentage deviations are +9.8 % (7.4°C against the reference case of 6.7°C) for the MHEX and +25 % at the two-stream HEX (5.2°C against 4.2°C). BWRS and PC-SAFT Equations of State prove to be the most accurate for the first Multiple-Stream Heat Exchanger (+4.7 % and +4.8 %, respectively), while Lee-Kesler-Plöcker virial EOS is the most accurate for the second two-stream Heat Exchanger (-6.8 %).

In light of this assessment it can be concluded that the use of Peng-Robinson EOS leads to a slight overestimation of the cycle performance, as this property method is not accurate in the prediction of compression and expansion power.
Furthermore the heat exchanger UA-value is underestimated, leading to an underestimation of the required heat transfer area for the liquefaction facility.
Finally the use of Peng-Robinson property method leads to large inaccuracy in the evaluation of heat exchanger temperature approaches. This has a non-negligible impact on the outcomes of the thermodynamic analysis, as in most cases the model variables are calculated by Aspen Plus in order to respect the 3 K-approach condition. This is not shown in this Appendix due to non-convergence of Aspen Plus design specifications when using GERG-2008 property method. This is also the reason why result validation is not performed.

B Sensitivity analyses on the single-expander cycle

A series of sensitivity analyses is performed on the single-expander configuration in order to understand how input parameters affect the liquefaction cycle and its performance. The configuration which is simulated is the single-expander cycle with one compression stage reported in Figure 4.2.
The investigated inputs are natural gas feed temperature, pressure and composition, and turbo-machinery efficiency.

B.1 Sensitivity on natural gas feed temperature

The influence of natural gas feed temperature is assessed following two different modelling approaches:

1. the temperature approach at the two-stream HEX is controlled by nitrogen temperature at the expander inlet. Nitrogen mass flow rate is kept constant and equal to 10 kg/s;
2. the second approach implies the definition of an additional design specification in order to obtain the 3 K-approach at the Multiple-Stream Heat Exchanger as well by varying the refrigerant mass flow rate.

Natural gas feed temperature is varied from 5°C to 40°C with a step change of 0.5°C. Nitrogen high pressure level is set equal to 120 bar, while the expander outlet pressure is 10 bar. The pressure ratio as well as the turbo-machinery efficiency is kept constant during the assessment.
The increase of feed temperature causes natural gas cooling load to increase passing from 758 kW to 841 kW (percentage variation of +11 %).

Results for the first approach show that net power consumption increases as NG feed temperature increases. Since the refrigerant mass flow is kept constant, compressor inlet experiences a higher refrigerant temperature with the increasing cooling load. This causes compression power to increase.

The increase in net power consumption is shown in Figure B.1. Relative increase is 3.9 %. Correspondingly an increase in the COP is recorded from 0.259 to 0.277 given the fact that natural gas cooling load increases relatively more than the net power consumption. On the contrary system FOM decreases, passing from 14.5 % to 13.95 %, as depicted in Figure B.1 on the secondary vertical axis.

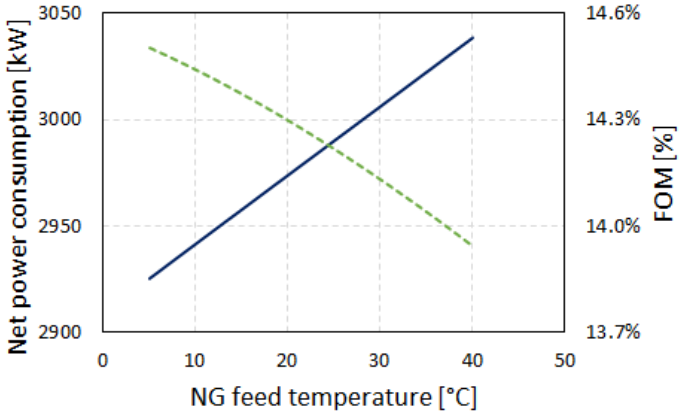

Figure B.1: Trend of net power consumption (continuous line, primary vertical axis) and of system Figure of Merit (dotted line, secondary vertical axis) when varying NG feed temperature according to the first modelling approach

When implementing the second modelling approach the pinch point at the Multiple-Stream Heat Exchanger is always activated at the warm end. For this reason the feasible range in which natural gas feed temperature can be varied goes up to 24°C. For higher feed inlet temperatures the requirement of 3 K-approach at the MHEX results in crossovers of the Hot and Cold Composite Curves.
In the feasible interval two behaviours can be identified, corresponding to two temperature intervals: 5°C - 20°C and 20°C - 24°C. This is clearly visible in Figure B.2.
As long as natural gas feed temperature stays below 20°C, nitrogen temperature at the compressor inlet is specified to be 17°C, as the approach is governed by the nitrogen inlet temperature (20°C). Therefore in this interval the refrigerant mass flow rate has to steadily increase in order to satisfy the increasing cooling load on natural gas side, causing in turn power consumption to increase (as shown in Figure B.2 on the left). Correspondingly the cycle FOM steadily decreases passing from 17.81 % to 17.04 %.
It should be noted that the values of Figure of Merit are overall higher when implementing the second approach compared to the first one. The reason for this lies on the calculated value of nitrogen mass flow rate in order to achieve the 3 K-approach at the hot end of the MHEX. This value leads to a closer match of the temperature profiles.
On the contrary when natural gas feed temperature exceeds 20°C, nitrogen temperature at the compressor inlet starts to increase from 17°C in order to respect the condition on the temperature approach at the MHEX, reaching 21°C for a natural gas feed temperature of 24°C.

This is achieved with a slight decrease of the refrigerant mass flow rate (from 7.48 kg/s to 7.28 kg/s), as the total heat duty at the Multiple-Stream Heat Exchanger decreases, which in turn results in a slight decrease of the power consumption (Figure B.2 on the left) and in a slight increase of the cycle FOM. The decrease rate of the power consumption is lower than its increase rate in the previous interval and does not follow the decrease rate of the refrigerant mass flow rate, as this beneficial drop is partly compensated by the increase of the enthalpy difference supplied by compressor, connected to the increase of compressor inlet temperature.

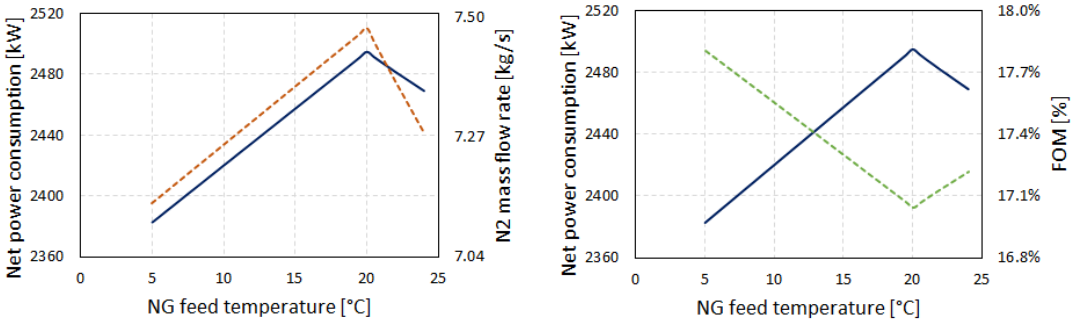

Figure B.2: On the left: trend of net power consumption (continuous line, primary vertical axis) and of refrigerant mass flow rate (dotted line, secondary vertical axis) when varying NG feed temperature according to the second modelling approach. On the right: trend of net power consumption (continuous line, primary vertical axis) and of system Figure of Merit (dotted line, secondary vertical axis) when varying NG feed temperature according to the second modelling approach

From this sensitivity analysis it can be concluded that it is beneficial for the liquefaction system that natural gas feed temperature is as low as possible. This determines a decrease in the cooling load which, depending on the modelling approach, leads to a decrease of the compressor inlet temperature once the refrigerant mass flow rate is fixed (first approach) or to a decrease of the necessary refrigerant mass flow rate once compressor inlet temperature is specified (second approach). As a consequence, a decrease in the net power consumption is obtained in both cases.
Furthermore it is shown that having the temperature approach of 3 K at both ends of the cold box is possible only for a natural gas feed temperature below 24°C. Above this limit a simultaneous change in nitrogen flow rate and cold box inlet temperature has to be applied.

B.2 Sensitivity on natural gas feed pressure

Natural gas feed pressure is varied from 15 bar to 50 bar with a step change of 0.5 bar. Again nitrogen high pressure level is set equal to 120 bar, while the expander outlet pressure is 10 bar. Pressure ratio as well as turbo-machinery efficiency are kept constant during the assessment. Natural gas feed pressure influences the shape of the Hot Composite Curve in the liquefaction part of the cold box. This is reported in Figure B.3 where the HCC is drawn for three NG feed pressures, namely 15, 33 and 50 bar. Nitrogen temperature at the expander inlet is -41.5°C to achieve the 3 K-approach at the cold end of the two-stream Heat Exchanger.

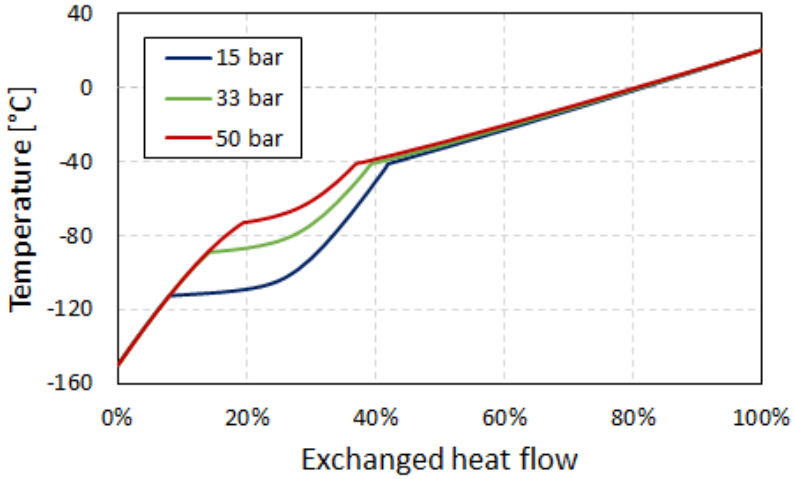

Figure B.3: Hot Composite Curves for different NG feed pressures

It can be observed that the lower the feed pressure is, the lower the liquefaction temperature range becomes. This has to be taken into account since, for instance, it is not possible to achieve a 3 K-approach at both extremities of the cold box when NG feed pressure falls below 15 bar, due to a crossover of the temperature profiles in the liquefaction part. The 15 bar-case is the one allowing to achieve the approach of 3 K at the extremities of the cold box and in the liquefaction zone and is therefore regarded as the lower bound for this sensitivity analysis.

Natural gas cooling load decreases as the feed pressure increases passing from 818.9 kW to 768.7 kW (relative variation of -6.1 %). This can be explained referring to a generic log P-h diagram. The enthalpy of vaporisation, i.e. the enthalpy difference between saturated liquid condition and saturated vapour condition at the same pressure, decreases as the pressure increases. This positively compensate the increase in sensible heat load connected to the increase of the isobaric specific heat.
The influence of natural gas feed pressure is assessed following the same methodology applied for the sensitivity on the feed temperature, that is with the same two modelling approaches.

Results from the first approach show that it is beneficial to increase the natural gas feed pressure since this allows to reduce the required compression power for the liquefaction system. The reason for this decrease is once again found in the lower nitrogen temperature at the compressor inlet, connected to the decrease of the cooling load. As depicted in Figure B.4, net power consumption decreases passing from 3009 kW to 2940 kW (relative variation of -2.3 %).

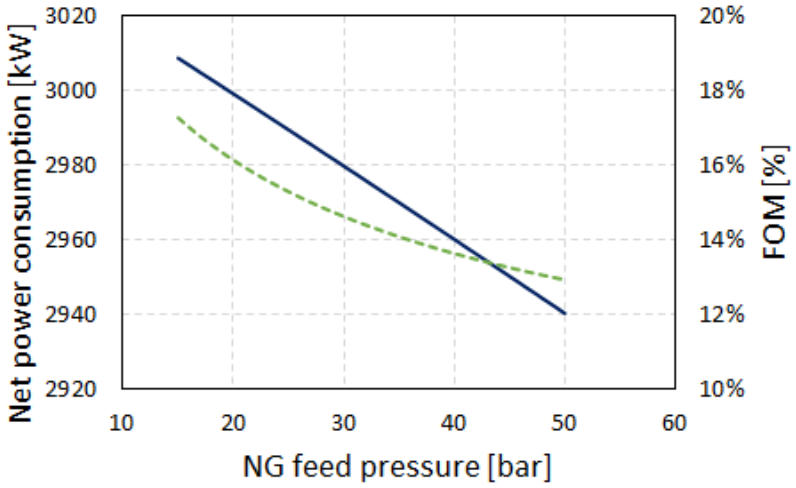

Figure B.4: Trend of net power consumption (continuous line, primary vertical axis) and of system Figure of Merit (dotted line, secondary vertical axis) when varying NG feed pressure according to the first modelling approach

Nevertheless two drawbacks can be identified. The first one deals with the liquefaction rate, that is the amount of LNG produced per unit of feed flow rate (1 kg/s). Given a flashing pressure of 1.7 bar, results show that an increasing feed pressure causes the liquefaction rate to decrease, passing from 96.8 % to 96 % (relative variation of -0.8 %). Methane is the most abundant component in the off-gas (molar fraction of 96 % for a feed pressure of 33 bar) and the amount of methane which is flashed slightly increases with increasing feed pressure. In the present case, however, unit energy consumption steadily decreases given the fact that the net power consumption diminishes relatively more than the liquefaction rate.
The second drawback regards the system Figure of Merit which is found to be decreasing as natural gas feed pressure increases. This is illustrated in Figure B.4. Figure of Merit drops from 17.26 % for the 15 bar-case to 12.95 % for the 50 bar-case (relative variation of -25 %). The reason for this trend lies on the shape of the HCC's on varying NG feed pressure (as shown in Figure B.3). A higher feed pressure determines a larger mean temperature difference between the Composite Curves, thus a less efficient heat exchange process.

Considering the second modelling approach results are analogous to the ones above presented. Given the specification of the 3 K-approach at the MHEX by varying nitrogen mass flow rate, the refrigerant temperature at the compressor inlet is fixed at 17°C. Therefore the system responds to the decrease of the cooling load by decreasing the refrigerant mass flow rate, which in turn causes the compressor power to decrease. As presented in Figure B.5, the percentage variation is -6.1 % (from 2575 kW to 2417 kW). Moreover, the system FOM is found to be decreasing as the natural gas feed pressure increases (from 20.16 % to 15.75 %, relative variation of -22 %). Once again this behaviour is caused by the larger temperature difference between the Composite Curves, as already explained. Moreover, as in the sensitivity on feed temperature, the second approach gives overall higher values for the exergetic efficiency given the closer match of the temperature profiles.

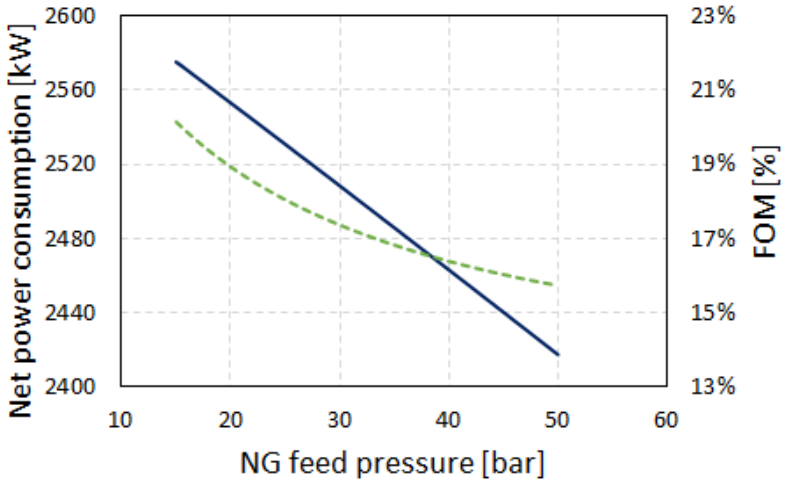

Figure B.5: Trend of net power consumption (continuous line, primary vertical axis) and of system Figure of Merit (dotted line, secondary vertical axis) when varying NG feed pressure according to the second modelling approach

In conclusion, the results of this sensitivity analysis highlight that is beneficial to increase natural gas feed pressure as this allows to decrease the cooling load and in turn the net power consumption of the liquefaction system. Nevertheless this reduction should be compared with the higher compression power required by the feed natural gas in order to fairly assess the benefits arising from a higher feed pressure.
It is also found that both liquefaction rate and system FOM are negatively affected by higher feed pressures. The decrease of liquefaction rate is found not to be enough to cause an increase of the unit energy consumption, whereas the system Figure Of Merit is significantly influenced by the mean temperature difference between the Composite Curves, which increases as the natural gas feed pressure increases.

B.3 Sensitivity on natural gas feed composition

The influence of natural gas feed composition on the liquefaction cycle and on its performance is assessed according to two different modelling approaches:

1. the first approach implies the definition of two design specifications to achieve the MITA at the cold box, one on the approach at the two-stream HEX by varying nitrogen temperature at the expander inlet, and the other one on the approach at the MHEX by varying the refrigerant mass flow rate. The cycle low-pressure level is fixed at 10 bar. Both approaches are set to 3 K;
2. the second approach is similar to the first as to the design specification on the approach at the two-stream HEX, whereas it imposes the 3 K-approach at the MHEX by varying the cycle low-pressure level, i.e. the expander discharge pressure. Refrigerant mass flow rate is kept fixed at 10 kg/s.

The reference case for the feed composition is the Danish grid natural gas composition as suggested by *Kosan Crisplant A/S*. Five different compositions are evaluated corresponding to the natural gas grid composition found in Italy, France, Germany, United Kingdom and Spain, as given in [82]. From the natural gas mixtures presented in [82] CO_2, water and heavier hydrocarbon (C8+) content is removed and redistributed equally to the remaining components. The analysed compositions are listed in Table B.1 in terms of molar fractions.
Italian grid natural gas is the one presenting the highest fraction of methane in the mixture, while the Spanish one is the one characterized by the smallest methane presence. The highest nitrogen fraction is recorded for the case of Germany, while Denmark presents the minimum value. Spanish grid natural gas is the one characterized by the highest presence of C2+ hydrocarbons, followed by the Danish one. Leanest natural gases are found in the cases of Italy and UK.

Table B.1: Natural gas grid composition for Denmark (suggestion of *Kosan Crisplant A/S*) and for five different European countries as given in [82] in terms of molar fractions

	CH_4	C_2H_6	C_3H_8	n-C_4H_{10}	i-C_4H_{10}	n-C_5H_{12}	i-C_5H_{12}	N_2
Denmark	0.903	0.060	0.024	0.006	0.004	0.000	0.000	0.003
Italy	0.980	0.007	0.002	0.001	0.000	0.000	0.000	0.009
France	0.899	0.062	0.015	0.005	0.002	0.003	0.002	0.011
Germany	0.839	0.038	0.008	0.004	0.002	0.003	0.002	0.104
UK	0.923	0.038	0.008	0.002	0.001	0.000	0.001	0.027
Spain	0.816	0.134	0.037	0.004	0.003	0.000	0.000	0.007

For the different natural gas compositions the cooling load is calculated together with the Lower Heating Value, the Higher Heating Value[1], the minimum ideal work requirement[2] and the liquefaction rate. Natural gases are cooled down from 20°C to -150°C in isobaric conditions at 33 bar. Pressure is later reduced to 1.7 bar. A natural gas feed mass flow rate of 1 kg/s is applied. Values are listed in Table B.2.

Table B.2: LHV, HHV, cooling load, minimum ideal liquefaction work and liquefaction rate for the analysed natural gas compositions

	LHV [MJ/kg]	**HHV** [MJ/kg]	Q_C [kJ/kg$_{NG}$]	w_{min} [kJ/kg$_{NG}$]	**Liquefaction rate** [%]
Denmark	49.19	54.45	793.3	425.2	96.40
Italy	49.15	54.57	804.8	470.2	94.53
France	48.56	53.75	787.0	424.1	95.12
Germany	41.77	46.27	722.9	416.5	83.53
UK	47.54	52.71	784.0	444.7	92.54
Spain	48.61	53.70	781.3	392.8	96.58

The cooling load increases as the natural gas mixture gets richer in methane. The heat of condensation is highest for methane, steadily decreases for C2+ hydrocarbons and is minimum for nitrogen. Consequently German grid natural gas has the lowest cooling load. The same trend is observed when considering the heating values of the gas mixtures.
Regarding the minimum work ideally required to liquefy the unitary mass of natural gas, it can be inferred that it increases when methane fraction in the mixture is increased at the expense of C2+ hydrocarbon content, as in the cases of Denmark and Italy. The same happens when methane fraction is increased at the expense of N_2 content (UK and Germany cases).
As to the liquefaction rate, methane and nitrogen are the components which are mostly present in the off-gas. Therefore the higher the nitrogen content is, the lower the liquefaction rate results. This is the case of Germany with a liquefaction rate of 83.53 %. Furthermore, given the same nitrogen content the liquefaction rate is higher for richer natural gases. This can be spotted when comparing Italian and Spanish grid natural gases.

Results from the first modelling approach are reported in Table B.3.
The refrigerant mass flow rate and the net power consumption follow the trend in cooling load. N_2 flow rate and net power consumption are maximum for the Italian case, being the one with the highest presence of methane, and minimum for Germany, being the German grid natural gas the one with the highest nitrogen molar fraction.

[1] LHV and HHV are given directly by Aspen Plus on a mass basis and for a reference temperature of 15°C.
[2] This is the numerator of FOM expression, see Equation 3.6.

Table B.3: Refrigerant mass flow rate, net power consumption, unit energy consumption and Figure of Merit when simulating the system according to the first modelling approach

	N_2 mass flow rate [kg/s]	$\dot{W}_{net}$ [kW]	w [kJ/kg$_{LNG}$]	FOM [%]
Denmark	7.48	2495	2588	17.04
Italy	7.59	2531	2677	18.58
France	7.42	2475	2602	17.14
Germany	6.81	2273	2722	18.32
UK	7.39	2465	2664	18.04
Spain	7.36	2457	2544	15.99

Italy and Germany are the cases for which the largest unit energy consumptions are observed. In the Italian case this is linked to the high cooling load, thus the relatively high refrigerant mass flow rate. Conversely in the German case this is due to the high nitrogen molar fraction in the natural gas mixture, which leads to a relatively small liquefaction rate.
As to the Figure of Merit, Italian and German grid compositions are also the ones giving the most efficient liquefaction cycles. One of the drivers for this outcome is spotted when looking at the temperature profiles at the cold box. Figure B.6 depicts the Hot Composite Curves for Italian, German and Spanish grid natural gas, the Spanish one brought as example of a low-FOM liquefaction cycle. The shape of the HCC's for the Italian and German cases allows a closer match of the temperature profiles, hence a better thermodynamic performance.

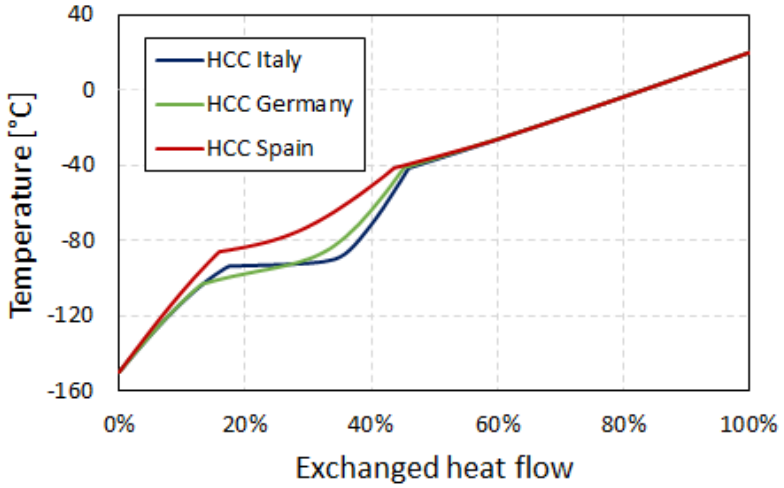

Figure B.6: Hot Composite Curves for Italian, German and Spanish grid natural gas compositions

Results from the second modelling approach are reported in Table B.4. As expected, the refrigerant low pressure level increases as natural gas cooling load decreases. This occurs when nitrogen molar fraction increases at the expense of methane molar fraction (UK and Germany cases) or when C2+ hydrocarbon content increases at the expense of methane molar fraction (Italian and Danish cases). Unit energy consumption confirms to be highest for Italian and German grid natural gases.
Similarly to what above discussed, Italian case shows the highest Figure of Merit closely followed by the German one, whereas Spanish case is the poorest liquefaction cycle from a thermodynamic viewpoint.

Table B.4: Refrigerant low pressure level, net power consumption, unit energy consumption and Figure of Merit when simulating the system according to the second modelling approach

	N_2 low pressure [bar]	$\dot{W}_{net}$ [kW]	w [kJ/kg$_{LNG}$]	FOM [%]
Denmark	16.1	2492	2585	17.06
Italy	15.8	2524	2670	18.63
France	16.3	2474	2601	17.14
Germany	18.2	2300	2753	18.11
UK	16.4	2466	2664	18.04
Spain	16.5	2458	2545	15.98

B.4 Sensitivity on turbo-machinery efficiency

The influence of compressor polytropic efficiency and expander isentropic efficiency on the thermodynamic cycle is assessed. The sensitivity analysis is performed by changing one parameter at the time.
Natural gas inlet temperature is 20°C while its inlet pressure is 33 bar. It exits the cold box at -150°C. Nitrogen hot stream enters the Multiple-Stream Heat Exchanger at 20°C and 120 bar. Expander discharge pressure is set equal to 10 bar.
Two design specifications are implemented at the heat exchangers, in order to achieve the 3 K-approach at the two-stream HEX by varying nitrogen temperature at the expander inlet, and the 3 K-approach at the MHEX by varying nitrogen mass flow rate.
Results are displayed in spider plots. A spider plot reports the percentage variation on the calculated variable Y corresponding to a percentage variation on the investigated parameter X. Moreover the average Sensitivity Ratios are calculated. The Sensitivity Ratio (SR) is defined as the ratio of the percentage variation on the calculated variable Y to the percentage variation of the investigated parameter X.

$$\mathrm{SR} = \frac{\Delta Y / Y_0}{\Delta X / X_0} = \frac{(Y - Y_0)/Y_0}{(X - X_0)/X_0} \tag{B.1}$$

The reference value for compressor polytropic efficiency is 0.82. It is varied with a step change of ±2.5 % up to ±5 %.
Given the fact that compressor inlet temperature is fixed by design specification at 17°C, compressor polytropic efficiency influences the compressor power consumption and the refrigerant outlet temperature, thus the cooler heat duty. The liquefaction part of the cycle is not altered. Results are presented in Figure B.7. In the reference case compression power is 3130 kW, compressor outlet temperature is 407.5°C and the cooler duty is 3288 kW.

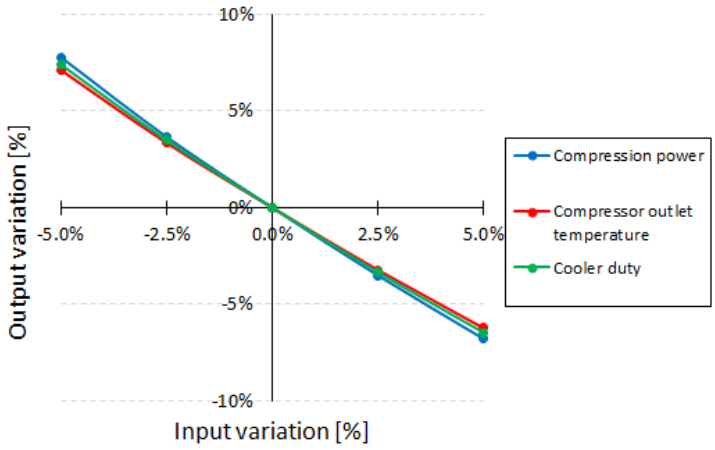

Figure B.7: Percentage variations of compression power, compressor outlet temperature and cooler heat duty when varying compressor polytropic efficiency

It can first be noticed that the three variables present the same dependency direction, that is compression power, compressor outlet temperature and cooler duty increase when compressor polytropic efficiency decreases, and vice versa. A lower polytropic efficiency determines a higher real compression work compared to the minimum ideal one. Given the higher outlet enthalpy, compressor outlet temperature is higher when polytropic efficiency is lower. Finally a higher compressor outlet temperature determines a higher heat load at the cooler.
From Figure B.7 it can also be seen that the percentage variations for the three variables are close to each other, with a value between +7.1 % and +7.8 % when polytropic efficiency is 0.779 (-5 %) and between -6.2 % and -6.8 % when polytropic efficiency is 0.861 (+5 %). The average SR's are -1.44 for the compression power, -1.32 for the compressor outlet temperature and -1.37 for the cooler duty.

Considering the expander isentropic efficiency the reference value is set equal to 0.85. It is varied with a step change of ±2.5 % up to ±5 %.
Contrary to the compressor polytropic efficiency, the expander isentropic efficiency affects the liquefaction part of the thermodynamic cycle. It has to be remarked that nitrogen temperature at the expander outlet is fixed at -153°C through a design specification and the expander pressure ratio is kept constant. Therefore a change in the expander isentropic efficiency will affect the refrigerant temperature at the expander inlet. More specifically, if the expander isentropic efficiency increases, nitrogen temperature at the expander inlet will increase, i.e. it will move towards temperatures closer to 0°C. As a consequence the total duty at the cold box will decrease, leading to a decrease in the required refrigerant mass flow rate.
These behaviours can be graphically observed in Figure B.8 together with the dependency of expansion power on expander isentropic efficiency. In the reference case the expander power production is 635 kW, nitrogen temperature at the expander inlet is -41.5°C and nitrogen mass flow rate is 7.48 kg/s.
Expander inlet temperature and refrigerant mass flow rate present the same dependency direction[3]. On the contrary expansion power increases with the increase of expander isentropic efficiency, as the real expansion work is closer to the maximum ideal one.
Expansion power increases by 1.76 % when expander isentropic efficiency is 5 % higher than the reference case, while it decreases by 1.86 % in the opposite situation. Its average SR is 0.36. The absolute value of expander inlet temperature is 12.4 % higher when expander isentropic efficiency is 5 % lower, while it is 13.7 % lower in the opposite situation. For the refrigerant mass flow rate the percentage variations are +7.6 % and -7.1 %, respectively. The average SR's are -2.61 and -1.46, respectively.

[3]A negative percentage variation on a negative quantity (as nitrogen temperature at the expander inlet) results in an increase of the negative variable.

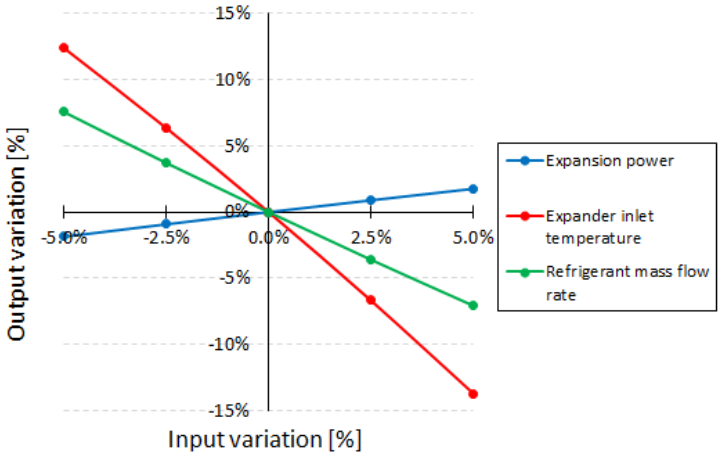

Figure B.8: Percentage variations of expander power, expander inlet temperature and refrigerant flow rate when varying expander isentropic efficiency

Both the compressor polytropic efficiency and the expander isentropic efficiency impact the cycle Figure of Merit. As above presented, compressor polytropic efficiency only influences the power requirement at the compressor, while expander isentropic efficiency influences both expansion and compression power, the latter through the impact on the refrigerant mass flow rate. In order to understand which component efficiency has the greatest impact on the thermodynamic performance, the Figure of Merit is calculated for the two different sensitivity analyses and its percentage variations are reported in the spider plot of Figure B.9. It has to be remarked that natural gas inlet and outlet conditions are kept fixed, i.e. the numerator in the FOM expression is constant.

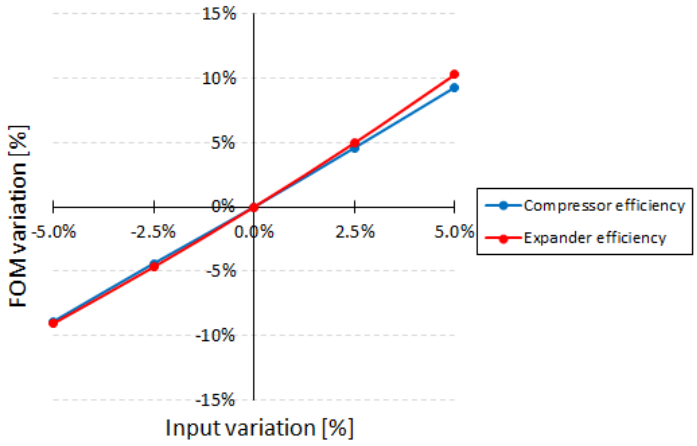

Figure B.9: Percentage variations of FOM when varying compressor polytropic efficiency and expander isentropic efficiency

As expected an increase in turbo-machinery efficiency allows the cycle Figure of Merit to increase. From Figure B.9 it can be inferred that the expander isentropic efficiency is slightly more influencing than the compressor polytropic efficiency. A 5 %-increase in compressor polytropic efficiency results in a FOM percentage increase of 9.3 %, while a 5 %-increase in expander isentropic efficiency results in a FOM percentage increase of 10.3 %. As a remark, average SR's are 1.81 and 1.93, respectively. These results reflect the fact that a change in expander isentropic efficiency affects the power consumption of both expander and compressor, as aforementioned.

C Composite Curves for the optimised expander-based configurations

This Appendix reports the cold box Composite Curves (CC's) and the temperature profiles for the optimised expander-based configurations. Correspondingly the values of heat duty, UA-value and Logarithmic Mean Temperature Difference are listed for all the heat exchangers.

C.1 Single-expander configurations

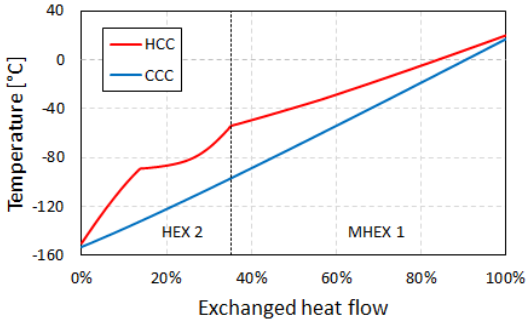

	$\dot{Q}$ [kW]	UA [kW/K]	LMTD [K]
MHEX 1	1073	76.9	14.0
HEX 2	583	23.5	24.8

Figure C.1: CC's and heat exchange characterisation for the optimal single-expander cycle with one compression stage presented in Section 5.3.1

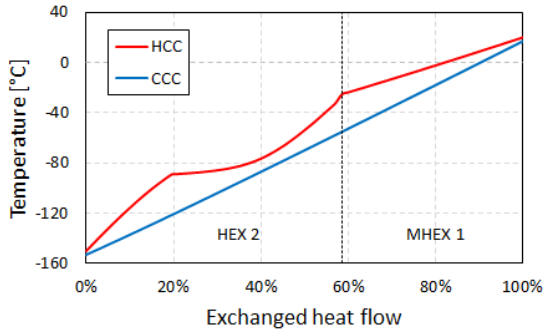

	$\dot{Q}$ [kW]	UA [kW/K]	LMTD [K]
MHEX 1	483	42.1	11.5
HEX 2	684	44.5	15.4

Figure C.2: CC's and heat exchange characterisation for the optimal single-expander cycle with two compression stages and no mechanical coupling presented in Section 5.3.2

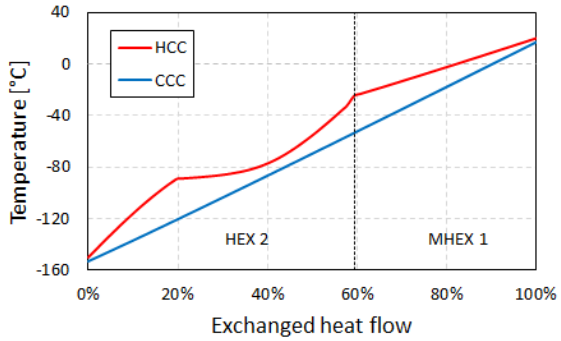

	$\dot{Q}$ [kW]	UA [kW/K]	LMTD [K]
MHEX 1	469	42.1	11.1
HEX 2	686	47.2	14.5

Figure C.3: CC's and heat exchange characterisation for the optimal single-expander cycle with two compression stages and with mechanical coupling presented in Section 5.3.2

C.2 Pre-cooling configurations

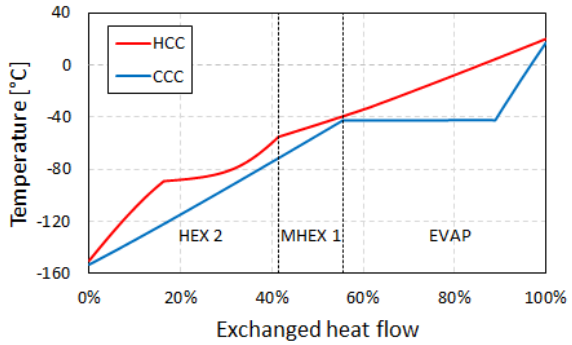

	$\dot{Q}$ [kW]	UA [kW/K]	LMTD [K]
EVAP	621	40.1	15.5
MHEX 1	197	24.9	7.9
HEX 2	579	38.1	15.2

Figure C.4: CC's and heat exchange characterisation for the optimal single-expander cycle with R410A pre-cooling presented in Section 5.4

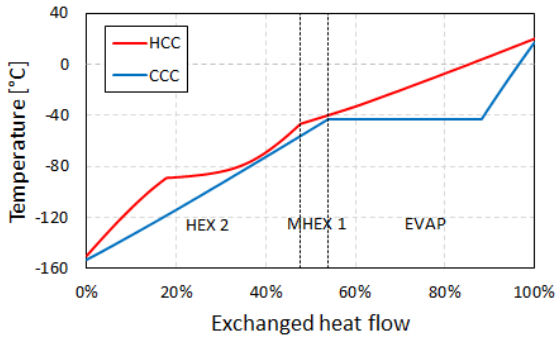

	$\dot{Q}$ [kW]	UA [kW/K]	LMTD [K]
EVAP	592	38.9	15.2
MHEX 1	79	13.9	5.7
HEX 2	613	73.2	8.4

Figure C.5: CC's and heat exchange characterisation for the optimal single-expander cycle with propane pre-cooling presented in Section 5.4

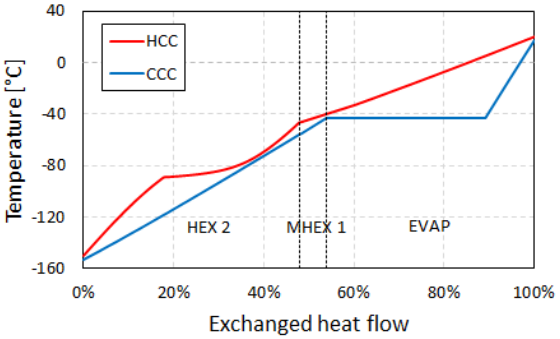

	$\dot{Q}$ [kW]	UA [kW/K]	LMTD [K]
EVAP	590	37.9	15.6
MHEX 1	77	13.7	5.6
HEX 2	613	76.3	8.0

Figure C.6: CC's and heat exchange characterisation for the optimal single-expander cycle with sub-critical CO_2 pre-cooling presented in Section 5.4

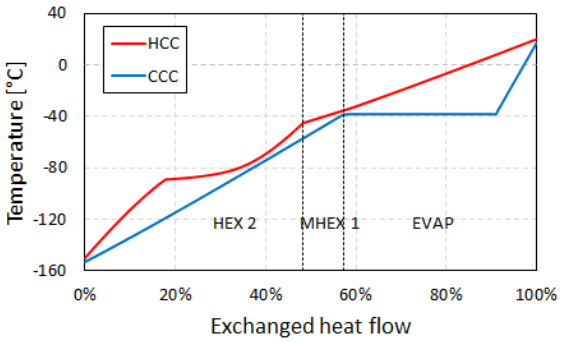

	$\dot{Q}$ [kW]	UA [kW/K]	LMTD [K]
EVAP	548	35.8	15.3
MHEX 1	115	17.4	6.6
HEX 2	619	61.4	10.1

Figure C.7: CC's and heat exchange characterisation for the optimal single-expander cycle with super-critical CO_2 pre-cooling presented in Section 5.4

C.3 Dual-expander configurations

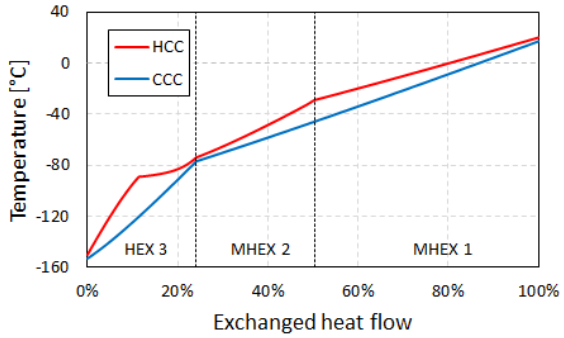

	$\dot{Q}$ [kW]	UA [kW/K]	LMTD [K]
MHEX 1	999	125.7	7.9
MHEX 2	526	76.7	6.9
HEX 3	485	44.1	11.0

Figure C.8: CC's and heat exchange characterisation for the optimal dual-turbine cycle with different pressure ratio presented in Section 5.5

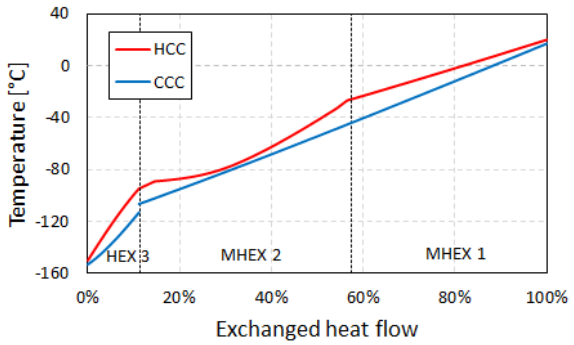

	$\dot{Q}$ [kW]	UA [kW/K]	LMTD [K]
MHEX 1	785	93.7	8.4
MHEX 2	820	133.6	6.1
HEX 3	201	17.6	11.4

Figure C.9: CC's and heat exchange characterisation for the optimal dual-turbine cycle with the same pressure ratio presented in Section 5.5

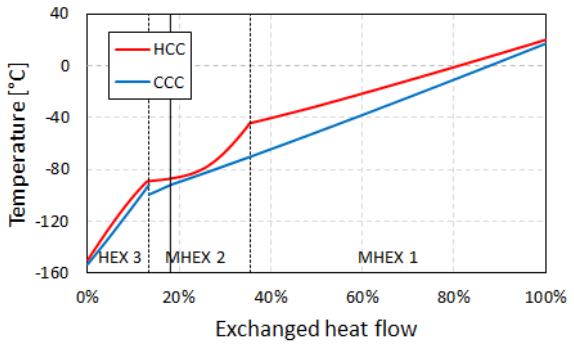

	$\dot{Q}$ [kW]	UA [kW/K]	LMTD [K]
MHEX 1	1134	110.6	10.3
MHEX 2	387	67.3	5.7
HEX 3	235	38.6	6.1

Figure C.10: CC's and heat exchange characterisation for the optimal two-stage expansion cycle presented in Section 5.5

C.4 Dual-refrigerant configurations

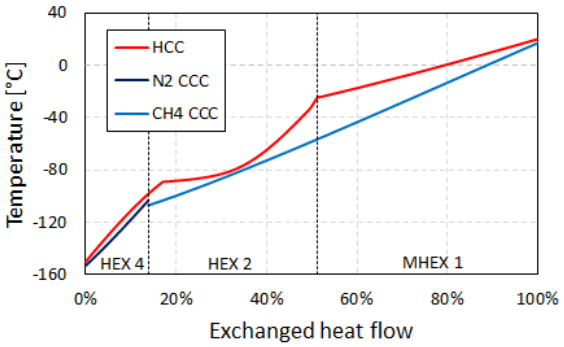

	$\dot{Q}$ [kW]	UA [kW/K]	LMTD [K]
MHEX 1	653	56.4	11.6
HEX 2	500	71.9	7.0
HEX 4	186	32.2	5.8

Figure C.11: CC's and heat exchange characterisation for the optimal N_2 sub-cooling dual-refrigerant cycle presented in Section 5.6

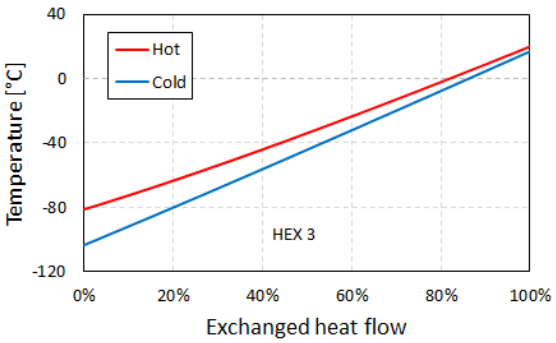

	$\dot{Q}$ [kW]	UA [kW/K]	LMTD [K]
HEX 3	400	48.7	8.2

Figure C.12: Temperature profiles and heat exchange characterisation for the optimal N_2 sub-cooling dual-refrigerant cycle presented in Section 5.6

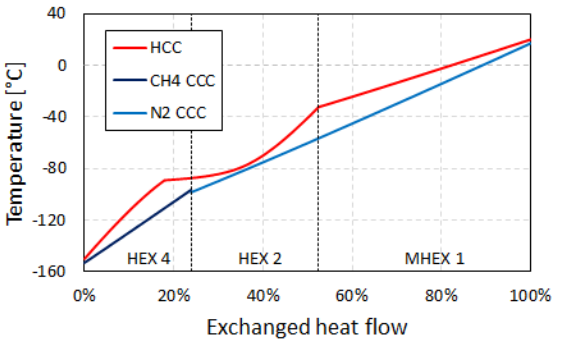

	$\dot{Q}$ [kW]	UA [kW/K]	LMTD [K]
MHEX 1	605	60.0	10.1
HEX 2	363	56.8	6.4
HEX 4	304	25.4	11.9

Figure C.13: CC's and heat exchange characterisation for the optimal CH_4 sub-cooling dual-refrigerant cycle presented in Section 5.6

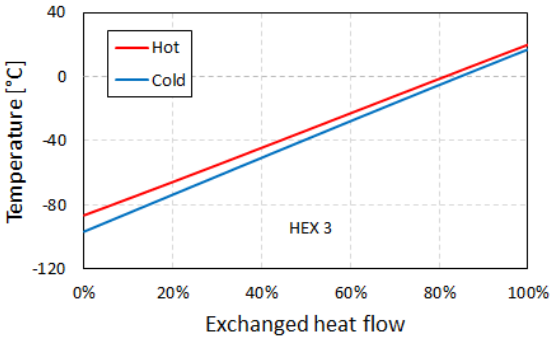

	$\dot{Q}$ [kW]	UA [kW/K]	LMTD [K]
HEX 3	614	118.7	5.2

Figure C.14: Temperature profiles and heat exchange characterisation for the optimal CH_4 sub-cooling dual-refrigerant cycle presented in Section 5.6

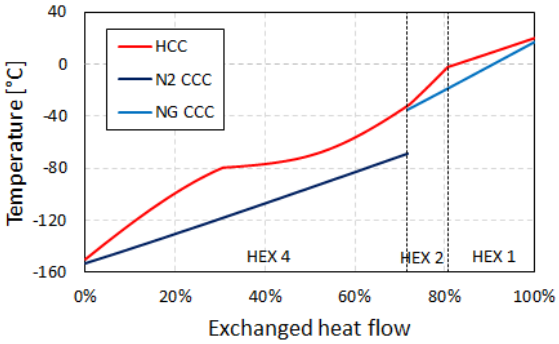

	$\dot{Q}$ [kW]	UA [kW/K]	LMTD [K]
HEX 1	173	22.0	7.9
HEX 2	80	10.8	7.4
HEX 4	643	643.4	22.0

Figure C.15: CC's and heat exchange characterisation for the optimal *Niche* cycle presented in Section 5.6

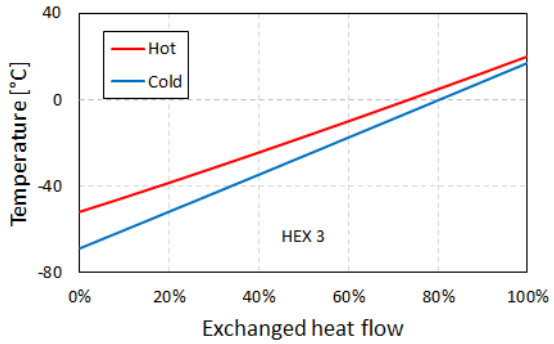

	$\dot{Q}$ [kW]	UA [kW/K]	LMTD [K]
HEX 3	624	84.6	7.4

Figure C.16: Temperature profiles and heat exchange characterisation for the optimal *Niche* cycle presented in Section 5.6

D Influence of penalty function formulations on the optimisation outcome

The optimisation problem is constrained through the introduction of penalty functions. They have to ensure that all the solutions fulfil specific conditions, i.e. the temperature approach cannot be lower than 3 K and the refrigerant has always to be in gaseous form at the suction and discharge of turbo-machinery equipment.
Penalty functions can be formulated differently. The aim of this Appendix Section is to show how the penalty formulation influences the optimisation outcome.

As presented in Chapter 5 penalty functions are addressed differently whether they concern the refrigerant vapour fraction or the temperature approaches at the heat exchangers.
An example for the penalty function regarding the vapour fraction x is the following:

if $x \leq 0.995$
$\dot{W}_{\text{net}} = 10^9$ [W]
Total UA-value = 10^9 [W/K]
end

This penalty formulation is referred to as single-value penalty. The values which are assigned to the objective functions are on purpose extremely high so that the optimiser can discard the solutions which violate the condition on the vapour fraction.
A single-value penalty function can be also implemented for the temperature approach at the heat exchangers.

if MITA ≤ 2.995
$\dot{W}_{\text{net}} = 10^9$ [W]
Total UA-value = 10^9 [W/K]
end

However this formulation does not distinguish between thermodynamic infeasibility (i.e. negative MITA) and technical infeasibility (i.e. positive MITA but lower than 3 K). To take this into account two alternative formulations can be identified, namely a two-value penalty and a "functional" formulation.
The two-value penalty formulation is handled as following:

if $0.01 \leq \text{MITA} \leq 2.995$
$\dot{W}_{\text{net}} = 5 \cdot 10^7$ [W]
Total UA-value = $5 \cdot 10^6$ [W/K]
elseif $\text{MITA} \leq 0.01$
$\dot{W}_{\text{net}} = 10^9$ [W]
Total UA-value = 10^9 [W/K]
else
end

The "functional" penalty formulation is instead managed as following:

if $0.01 \leq \text{MITA} \leq 2.995$
$\dot{W}_{\text{net}} = 2 \cdot 10^7 + (3 - \text{MITA}) \cdot 10^7$ [W]
Total UA-value = $2 \cdot 10^6 + (3 - \text{MITA}) \cdot 10^6$ [W/K]
elseif $\text{MITA} \leq 0.01$
$\dot{W}_{\text{net}} = 10^9$ [W]
Total UA-value = 10^9 [W/K]
else
end

In both cases the aim is to differentiate a thermodynamic violation from a technical violation. It is expected that addressing the constraint on temperature approaches according to a two-value or functional approach can improve the optimisation outcome.
For this reason the single-expander cycle with one compression stage and the N_2 sub-cooling dual-refrigerant cycle are optimised using the three possible penalty formulations for the Minimum Internal Temperature Approaches. Only Single-Objective Optimisations are addressed, with the aim of minimising the net power consumption. The single-expander cycle with one compression stage is the simplest configuration and has the smallest number of decision variables (4). On the contrary the dual-refrigerant cycle represents a complex design and has the highest number of decision variables (9).
The size of the initial population is 300 for the single-expander cycle with one compression stage, 700 for the dual-refrigerant cycle. The number of evaluations is set to 3000 and 5000, respectively. The analysis is performed only once, without changing the optimisation parameters.
The penalty formulations are compared by plotting the minimum value of the objective function at different numbers of iterations. Figure D.1 refers to optimisation of the single-expander cycle with one compression stage, while Figure D.2 refers to the optimisation of the N_2 sub-cooling dual-refrigerant cycle.

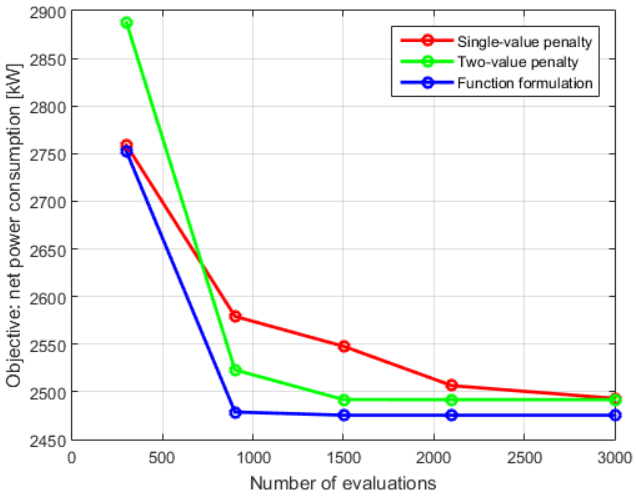

Figure D.1: Minimum values of the objective function for the three different penalty formulations in the optimisation of the single-expander cycle

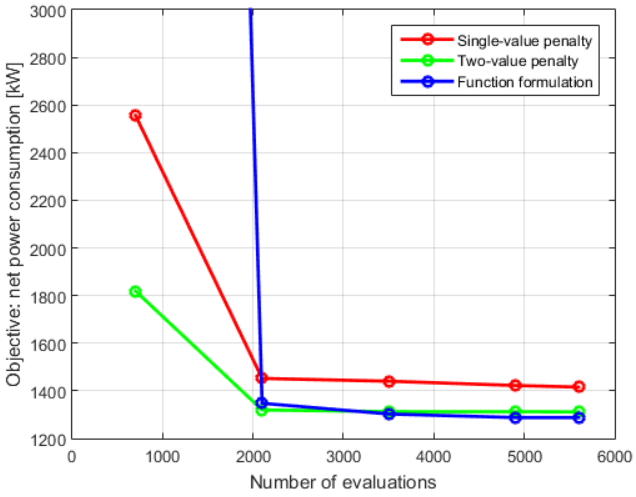

Figure D.2: Minimum values of the objective function for the three different penalty formulations in the optimisation of the dual-refrigerant cycle

The functional approach results to be the best among the penalty formulations, leading to the lowest value of the objective function in both cases. The two-value penalty formulation is found to give intermediate results, while the single-value penalty approach performs the worst in both cases.
In light of this assessment it can be concluded that the use of a functional approach is beneficial for the optimisation algorithm to converge towards the global optimum. This confirms the robustness of the optimal solutions for the investigated expander-based cycles.

E Cost correlations

This Appendix Section details the cost correlations which are applied for the economic analysis of LNG production alternatives. They report the developed Matlab scripts which are used in the post-computational phase and in which the reader can find all the relevant assumptions. For the refrigerant coolers additional explanations are given about the applied methodology for the estimation of coolers' heat transfer area.

E.1 Compressors

```
function[BareModul_cost_comp]=cost_CentrifugalCompressors(power,efficiency)

%% DESCRIPTION
% Cost of the centrifugal compressor without electric driver
%
% REFERENCE:            R. Turton, Analysis, Synthesis and Design of
%                       chemical processes, Prentice Hall, NJ, 1998
%
% INPUTS:               Mechanical power [kW]
%                       Compressor polytropic efficiency [-]
%
% CAPACITY PARAMETER:   Fluid power [kW]
%
% Currency is USD to be later converted in DKK
% 1 USD = 6.6 DKK
%
% ASSUMPTION:           Whenever the fluid power exceeds the maximum limit,
%                       an additional compressor is purchased
%
% OUTPUT: Bare Module Cost of the compressor
%=========================================================================
%% BARE MODULE COST CALCULATION
% Compressor type: centrifugal
```

```
k1 = 2.9945;
k2 = 0.9524;
k3 = 0;

% Compressor material
% f_BM = 2.5; %carbon steel
f_BM = 6.3; %stainless steel
% f_BM = 13; %nichel alloy

fluid_power = efficiency*power;

if fluid_power < 50 %[kW]
    warning('Fluid Power for Centrifugal Compressor is too low!');
end

C_P_1996 = 10^(k1 + k2*log10(fluid_power) + k3*(log10(fluid_power))^2);

if fluid_power > 8000 %[kW]
    warning('Fluid Power for Centrifugal Compressor is too high!');
    limit_ratio = fluid_power/8000;
    number_compfull = floor(limit_ratio);
    exceedance = 8000*(limit_ratio - number_compfull);
    C_P_1996 = number_compfull*(10^(k1 + k2*log10(8000) +
    + k3*(log10(8000))^2)) + 10^(k1 + k2*log10(exceedance) +
    + k3*(log10(exceedance))^2);
end

% Actualisation and currency conversion
CEPCI_1996 = 382;
CEPCI_2014 = 576.1;
f_actualisation = CEPCI_2014/CEPCI_1996;
f_conversion = 6.6;

BareModul_cost_comp = C_P_1996 * f_BM * f_actualisation * f_conversion;
end
```

E.2 Compressor drives

```
function[BareModul_cost_drive]=cost_ElectricDrives(power)
%% DESCRIPTION
% Cost of the electric drive for the compressors
% Given the application an explosion-proof expander is selected
%
% REFERENCE:            R. Turton, Analysis, Synthesis and Design of
%                       chemical processes, Prentice Hall, NJ, 1998
%
% INPUTS:               Shaft power [kW]
%
% CAPACITY PARAMETER:   Shaft power [kW]
%
```

```
% Currency is USD to be later converted in DKK
% 1 USD = 6.6 DKK
%
% ASSUMPTION:           Whenever the shaft power exceeds the maximum limit,
%                       an additional electric drive is purchased
%
% OUTPUT: Bare Module Cost of the compressor
%=========================================================================
%% COST CALCULATION
% Drive type: electric- explosion-proof
k1 = 2.3006;
k2 = 1.0947;
k3 = -0.10160;

f_BM = 1.5;

if power < 3 %[kW]
    warning('Shaft power for Electric Drive-Explosion-Proof is too low!');
end

C_P_1996 = 10^(k1 + k2*log10(power) + k3*(log10(power))^2);

if power > 6000 %[kW]
    warning('Shaft power for Electric Drive-Explosion-Proof is too high!');
    limit_ratio = power/6000;
    number_drivefull = floor(limit_ratio);
    exceedance = 8000*(limit_ratio - number_drivefull);
    C_P_1996 = number_drivefull*(10^(k1 + k2*log10(6000) +
    + k3*(log10(6000))^2)) + 10^(k1 + k2*log10(exceedance) +
    + k3*(log10(exceedance))^2);
end

% Actualisation and currency conversion
CEPCI_1996 = 382;
CEPCI_2014 = 576.1;
f_actualisation = CEPCI_2014/CEPCI_1996;
f_conversion = 6.6;

BareModul_cost_drive = C_P_1996 * f_BM * f_actualisation * f_conversion;
end
```

E.3 Expander

```
function[BareModul_cost_expander]=cost_Expander(power)
%% DESCRIPTION
% Cost of the expander
%
% REFERENCE:            R. Turton, Analysis, Synthesis and Design of
%                       chemical processes, Prentice Hall, NJ, 1998
%
```

```
% INPUTS:               Shaft power [kW]
%
% CAPACITY PARAMETER:   Shaft power [kW]
%
% Currency is USD to be later converted in DKK
% 1 USD = 6.6 DKK
%
% ASSUMPTION:           Whenever the shaft power exceeds the maximum limit,
%                       an additional expander is purchased
%
% OUTPUT: Bare Module Cost of the compressor
%=========================================================================
%% COST CALCULATION
% Expander type: radial gas expander
k1 = 3.1143;
k2 = 0.6923;
k3 = 0;

% Expander material
% f_BM = 3; %carbon steel
f_BM = 5; %stainless steel
% f_BM = 6; %nichel alloy

if power < 100 %[kW]
    warning('Shaft power for Expander is too low!');
end

C_P_1996 = 10^(k1 + k2*log10(power) + k3*(log10(power))^2);

if power > 1500 %[kW]
    warning('Shaft power for Expander is too high!');
    limit_ratio = power/1500;
    number_expfull = floor(limit_ratio);
    exceedance = 8000*(limit_ratio - number_expfull);
    C_P_1996 = number_expfull*(10^(k1 + k2*log10(1500) +
    + k3*(log10(1500))^2)) + 10^(k1 + k2*log10(exceedance) +
    + k3*(log10(exceedance))^2);
end

% Actualisation and currency conversion
CEPCI_1996 = 382;
CEPCI_2014 = 576.1;
f_actualisation = CEPCI_2014/CEPCI_1996;
f_conversion = 6.6;

BareModul_cost_expander = C_P_1996 * f_BM * f_actualisation * f_conversion;
end
```

E.4 Phase separator

```
function[BareModul_cost_FlashSep]=cost_FlashDrum(volumeflow, pressure)
%% DESCRIPTION
% Cost of the phase separator
%
% REFERENCES:           G.D.Ulrich, A Guide to Chemical Engineering Process
%                       Design and Economics, Wiley, NJ, 1984
%                       R. Turton, Analysis, Synthesis and Design of
%                       chemical processes, Prentice Hall, NJ, 1998
%
% INPUTS:               Volume flow rate [m^3/s]
%                       Inlet pressure [bar]
%
% CAPACITY PARAMETER:   Vessel height [m]
%
% Currency is USD to be later converted in DKK
% 1 USD = 6.6 DKK
%
% ASSUMPTIONS:          Vertical vessels are considered
%                       Limitations for flash diameter:
%                       diameter [m]  0.3:4
%                       height [m] 1: 20
%                       Length to diameter ratio:
%                       L/D = 3 below 19 barg;
%                       L/D = 4 for 19-34 barg;
%                       L/D = 5 above 34 barg
%
% OUTPUT: Bare Module Cost of the phase separator
%=========================================================================
%% Size calculation
d_max = 4; % maximum diameter for fixed bed

% --- Number of units -----
% residence time = 600[s]
d = (2/pi*600*volumeflow)^(1/3);
units = ceil((d/d_max)^3); % cubic relation between diameter and volume
volumeflow = volumeflow/units;

diameter = (2/pi*600*volumeflow)^(1/3);
%% COST CALCULATION
% Correlation coefficients
K = [3.3392 0.5538  0.2851
    3.4746  0.5893  0.2053
    3.6237  0.5262  0.2146
    3.7559  0.6361  0.1069
    3.9484  0.4623  0.1717
    4.0547  0.4620  0.1558
    4.1110  0.6094  0.0490
    4.3919  0.2859  0.1842];
```

```
49
50  if diameter <= 0.3
51      diameter = 0.3;
52      if (pressure-1) <= 19
53          H = 3*diameter;
54      elseif (pressure-1) <= 34
55          H = 4*diameter;
56      else
57          H = 5*diameter;
58      end
59      k1 = K(1,1);
60      k2 = K(1,2);
61      k3 = K(1,3);
62  end
63
64  if diameter > 0.3 && diameter <= 0.5
65      diameter = 0.5;
66      if (pressure-1) <= 19
67          H = 3*diameter;
68      elseif (pressure-1) <= 34
69          H = 4*diameter;
70      else
71          H = 5*diameter;
72      end
73      k1 = K(2,1);
74      k2 = K(2,2);
75      k3 = K(2,3);
76  end
77
78  if diameter > 0.5 && diameter <= 1
79      diameter = 1;
80      if (pressure-1) <= 19
81          H = 3*diameter;
82      elseif (pressure-1) <= 34
83          H = 4*diameter;
84      else
85          H = 5*diameter;
86      end
87      k1 = K(3,1);
88      k2 = K(3,2);
89      k3 = K(3,3);
90  end
91
92  if diameter > 1 && diameter <= 1.5
93      diameter = 1.5;
94      if (pressure-1) <= 19
95          H = 3*diameter;
96      elseif (pressure-1) <= 34
97          H = 4*diameter;
98      else
99          H = 5*diameter;
100     end
```

```
101     k1 = K(4,1);
102     k2 = K(4,2);
103     k3 = K(4,3);
104 end
105
106 if diameter > 1.5 && diameter <= 2
107     diameter = 2;
108     if (pressure-1) <= 19
109         H = 3*diameter;
110     elseif (pressure-1) <= 34
111         H = 4*diameter;
112     else
113         H = 5*diameter;
114     end
115     k1 = K(5,1);
116     k2 = K(5,2);
117     k3 = K(5,3);
118 end
119
120 if diameter > 2 && diameter <= 2.5
121     diameter = 2.5;
122     if (pressure-1) <= 19
123         H = 3*diameter;
124     elseif (pressure-1) <= 34
125         H = 4*diameter;
126     else
127         H = 5*diameter;
128     end
129     k1 = K(6,1);
130     k2 = K(6,2);
131     k3 = K(6,3);
132 end
133
134 if diameter > 2.5 && diameter <= 3
135     diameter = 3;
136     if (pressure-1) <= 19
137         H = 3*diameter;
138     elseif (pressure-1) <= 34
139         H = 4*diameter;
140     else
141         H = 5*diameter;
142     end
143     k1 = K(7,1);
144     k2 = K(7,2);
145     k3 = K(7,3);
146 end
147
148 if diameter > 3
149     diameter = 4;
150     if (pressure-1) <= 19
151         H = 3*diameter;
152     elseif (pressure-1) <= 34
```

```
153         H = 4*diameter;
154     else
155         H = 5*diameter;
156     end
157     k1 = K(8,1);
158     k2 = K(8,2);
159     k3 = K(8,3);
160 end
161 
162 % Pressure factor calculation
163 if (pressure-1) <= -0.5
164         FP = 1.25;
165     elseif (pressure-1) > -0.5 && (pressure-1) <= 3.7
166         FP = 1;
167     else
168         FP = 0.5146 + 0.6838*log10(pressure-1) +
169         + 0.2970*(log10(pressure-1))^2 + 0.0235*(log10(pressure-1))^6 +
170         + 0.0020*(log10(pressure-1))^8;
171 end
172 
173 % Geometry coefficients
174 b1 = 2.5;
175 b2 = 1.72;
176 
177 % Material factor
178 % FM_SS = 4; %stainless steel
179 FM_CS = 1; %carbon steel
180 
181 % Bare Module Cost Factor calculation
182 F_BM = b1 + b2*FM_CS*FP;
183 
184 C_P_1996 = 10^(k1 + k2*log10(H) + k3*(log10(H))^2);
185 
186 % Actualisation and currency conversion
187 CEPCI_1996 = 382;
188 CEPCI_2014 = 576.1;
189 f_actualisation = CEPCI_2014/CEPCI_1996;
190 f_conversion = 6.6;
191 
192 BareModul_cost_FlashSep = C_P_1996*F_BM*f_actualisation*f_conversion*units;
193 end
```

E.5 Flat-plate heat exchangers

The author is not allowed to publish the Matlab script relative to flat-plate heat exchangers because it contains confidential cost data.
The Bare Module Cost Factor given by Turton *et al.* [71] is applied. It has the following expression:

$$F_{\mathrm{BM}} = b_1 + b_2 \cdot F_{\mathrm{M}} \tag{E.1}$$

in which

b_1 = 1.53

b_2 = 1.27

F_M = 2.3 (stainless steel)

E.6 Coolers

As mentioned in Chapter 6, the heat transfer area is directly estimated using *SWEP* software for the refrigerant coolers and for the condensers (applicable only in the pre-cooling configurations).
The cooler area is estimated for two refrigerant cases, namely nitrogen and methane. Given the significant differences in terms of mass flow rate and cooler inlet temperature that the refrigerants present in the thirteen expander-based configurations, a matrix of heat transfer area is created as a function of refrigerant mass flow rate and inlet temperature. For the nitrogen case mass flow rate ranges between 0.5 and 20 kg/s with a step change of 0.5 kg/s, while inlet temperature is varied between 50°C and 500°C with a step change of 25°C. For methane the ranges are 0.5 kg/s - 10 kg/s and 50°C - 300°C, respectively and with the same step changes. The value of heat transfer area is determined using the Matlab function *interp2*. The range of the mass flow rate is extended through an interpolation function defined on the average value of the heat transfer area for each temperature level.
The maximum pressure level applicable in *SWEP* software is considered, namely 60 bar for nitrogen and 50 bar for methane. Pressure drops are 1 % of refrigerant pressure on gas side, 1 bar on water side [79]. A correction factor is applied to take into consideration the refrigerant pressure level as in the optimised models.

For the condenser the following values of heat transfer area are applied. The condenser cost is calculated applying the cost correlation provided by *SWEP* for flat-plate heat exchangers.

- **R410A**: 90 m^2;
- **Propane**: 120 m^2;
- **CO_2**: 90 m^2 both in sub- and super-critical cases.

E.6.1 Nitrogen coolers

```
function[BareModul_cost_gascooler]=cost_GasCoolers_N2(pressure,mass_flow,
temperature)
%% DESCRIPTION
% Cost of the Nitrogen coolers
%
% REFERENCE:            R. Turton, Analysis, Synthesis and Design of
%                       chemical processes, Prentice Hall, NJ, 1998
%
% INPUTS:               Nitrogen inlet pressure [bar]
```

```
%                       Nitrogen mass flow rate [kg/s]
%                       Nitrogen inlet temperature [C]
%
% CAPACITY PARAMETER:   Heat transfer area [m^2]
%
% Currency is USD to be later converted in DKK
% 1 USD = 6.6 DKK
%
% ASSUMPTION:           Heat transfer area is determined using SWEP
%                       software;
%                       Water is the fluid on the secondary side
%                       Water enters the cooler at 10 C and exits at 40 C
%                       Nitrogen pressure is set at 60 bar
%                       Pressure drops on nitrogen side is 1% of nitrogen
%                       pressure: 60 kPa
%                       1 bar on water side
%                       If nitrogen pressure is below 60 bar,
%                       a correction factor on the area is applied
% OUTPUT:               Bare Module Cost of the nitrogen gas cooler
%=========================================================================
%% AREA CALCULATION

if pressure-1 > 250 %[barg]
    warning('Pressure is too high!');
end

A = [1.43   2.6    9.4    18.2  24.4   40.2  50.3   67.9    88.8    80.3
     0.93   2.35   6.39   15.4  27.8   39    53     72.5    66.3    78
     0.93   2.24   6.77   14.5  29.6   40.6  55.8   77.6    68.6    81.1
     0.992  2.3    7.71   14.9  32.1   43.3  60.1   73.8    73.3    86.6
     1.05   2.41   8.08   15.4  32     46    64.7   83.6    77.2    92
     1.05   2.46   8.84   16.4  33.5   48.7  69.4   67.1    81.1    97.5
     1.12   2.52   9.96   18    35.1   51.1  74.5   70.2    85      102
     1.18   2.58   8.46   19.7  36.7   53.8  79.9   73.3    89.7    108
     1.24   2.63   8.65   22    38.2   56.9  74.8   76.4    93.6    114];

mass = [0.5, 1, 2.5, 5, 7.5, 10, 12.5, 15, 17.5, 20];
temp = [50; 87.5; 125; 187.5; 200; 312.5; 375; 437.5; 500];

% Mass flow correction factor
if mass_flow > 20
    f_mass = 2.3428*mass_flow^1.2329;
    mass_flow = 0.5;
else f_mass = 1;
end

if temperature >= 50 && temperature <= 500
    area =interp2(mass,temp,A,mass_flow,temperature);
elseif temperature < 50
        warning('Cooler inlet gas temperature is below 50 degrees');
        temperature = 50;
        area =interp2(mass,temp,A,mass_flow,temperature);
```

```
elseif temperature > 500
        warning('Cooler inlet gas temperature is above 500 degrees');
        temperature = 500;
        area =interp2(mass,temp,A,mass_flow,temperature);
else
end

%Pressure correction factor
if pressure >= 60
        f_pressure = 1;
    else f_pressure = 85.402*pressure^(-1.085);
end

area = area*f_pressure*f_mass;

if area < 3.5 %[m^2]
    warning('Heat exchange area is too low!');
end

if area > 20000 %[m^2]
    warning('Heat exchange area is too high!');
end

if area < 1
    area = ceil(area);
end
%% BARE MODULE COST CALCULATION
% Turton's correlation for air coolers is applied
k1 = 3.6418;
k2 = 0.4053;
k3 = 0;

c1 = -0.06154;
c2 = 0.0473;
c3 = 0;

b1 = 1.53;
b2 = 1.27;

F_M = 3; %stainless steel

C_P_1996 = 10^(k1 + k2*log10(area) + k3*(log10(area))^2);
F_P = 10^(c1 + c2*log10(pressure-1) + c3*(log10(pressure-1))^2);

F_BM = b1 + b2*F_M*F_P;

% Actualisation and currency conversion
CEPCI_1996 = 382;
CEPCI_2014 = 576.1;
f_actualisation = CEPCI_2014/CEPCI_1996;
f_conversion = 6.6;

```

```
BareModul_cost_gascooler = C_P_1996*F_BM*f_actualisation*f_conversion;
end
```

E.6.2 Methane coolers

```
function[BareModul_cost_gascooler]=cost_GasCoolers_CH4(pressure,mass_flow,
temperature)
%% DESCRIPTION
% Cost of the Methane coolers
%
% REFERENCE:            R. Turton, Analysis, Synthesis and Design of
%                       chemical processes, Prentice Hall, NJ, 1998
%
% INPUTS:               Methane inlet pressure [bar]
%                       Methane mass flow rate [kg/s]
%                       Methane inlet temperature [C]
%
% CAPACITY PARAMETER:   Heat transfer area [m^2]
%
% Currency is USD to be later converted in DKK
% 1 USD = 6.6 DKK
%
% ASSUMPTION:           Heat transfer area is determined using SWEP
%                       software;
%                       Water is the fluid on the secondary side
%                       Water enters the cooler at 10 C and exits at 40 C
%                       Methane pressure is set at 60 bar
%                       Pressure drops on nitrogen side is 1% of methane
%                       pressure: 50 kPa
%                       1 bar on water side
%                       If methane pressure is below 60 bar,
%                       a correction factor on the area is applied
% OUTPUT:               Bare Module Cost of the methane gas cooler
%=========================================================================
%% AREA CALCULATION

if pressure-1 > 250 %[barg]
    warning('Pressure is too high!');
end

A =    [2.13    5.12    16.7    26      52.6    92.4
        1.74    5.04    13.2    30.3    47.2    76.4
        1.86    5.28    13.5    29.2    48.7    81.5
        1.92    5.52    13.9    30      50.7    73.8
        1.98    5.08    14.5    30.8    52.3    78.4
        2.17    5.08    16.5    37.8    65.1    75.7];

mass = [0.5, 1, 2.5, 5, 7.5, 10];
temp = [50; 100; 150; 200; 250; 300];

```

```
% Mass flow correction factor
if mass_flow > 10
    f_mass = 2.4343*mass_flow^1.2023;
    mass_flow = 0.5;
else f_mass = 1;
end

if temperature >= 50 && temperature <= 300
    area =interp2(mass,temp,A,mass_flow,temperature);
elseif temperature < 50
        warning('Cooler inlet gas temperature is below 50 degrees');
        temperature = 50;
        area =interp2(mass,temp,A,mass_flow,temperature);
elseif temperature > 300
        warning('Cooler inlet gas temperature is above 500 degrees');
        temperature = 300;
        area =interp2(mass,temp,A,mass_flow,temperature);
else
end

% Pressure correction factor
if pressure >= 50
        f_pressure = 1;
    else f_pressure = 52.2982*pressure^(-1.036);
end

area = area*f_pressure*f_mass;

if area < 3.5 %[m^2]
    warning('Heat exchange area is too low!');
    area = 3.5;
end
if area > 20000 %[m^2]
    warning('Heat exchange area is too high!');
end

if area < 1
    area = ceil(area);
end
%% BARE MODULE COST CALCULATION
% Turton's correlation for air coolers is applied
k1 = 3.6418;
k2 = 0.4053;
k3 = 0;

c1 = -0.06154;
c2 = 0.0473;
c3 = 0;

b1 = 1.53;
b2 = 1.27;

```

```
F_M = 3; %stainless steel

C_P_1996 = 10^(k1 + k2*log10(area) + k3*(log10(area))^2);
F_P = 10^(c1 + c2*log10(pressure-1) + c3*(log10(pressure-1))^2);

F_BM = b1 + b2*F_M*F_P;

% Actualisation and currency conversion
CEPCI_1996 = 382;
CEPCI_2014 = 576.1;

f_actualisation = CEPCI_2014/CEPCI_1996;

f_conversion = 6.6;

BareModul_cost_gascooler = C_P_1996 *F_BM*f_actualisation*f_conversion;
end
```

E.7 Additional correlations

The general formulation is given in Equation E.2.

$$C_P = C_P^0 \cdot \left(\frac{X}{X^0} \right)^{\alpha} \tag{E.2}$$

X is the capacity parameter and the superscript 0 refers to the base case. α is the scaling coefficient.

E.7.1 Compressor

The correlation is provided by *FK Teknik A/S* and is relative to a propane compressor inclusive of electric motor.

$C_P^0 = 10631$ [€]
$X^0 = 178.4$ [m^3/h]
$\alpha = 0.79$

The Bare Module Factor as given by Turton *et al.* is applied.

E.7.2 Flat-plate heat exchanger

The correlation is provided by *FK Teknik A/s* and *Ahlsell Danmark ApS* and is valid for flat-plate heat exchangers working with propane, hydrocarbons and low-pressure corrosive chemicals.

$C_P^0 = 15526$ [€]
$X^0 = 42$ [m^2]
$\alpha = 0.8$

The Bare Module Factor as given by Turton *et al.* is applied.

F Process flowsheet for cascade and Mixed-Refrigerant cycles and updated optimisation results

This Appendix Section complements the economic comparison of different LNG production concepts which is the content of Chapter 7.
The process flowsheet of the included cascade and Mixed-Refrigerant cycles is sketched. These cycles are analysed in details in the work of Lonardi [81], to which the reader is referred. Furthermore the new set of optimal decision variables is presented for the three considered expander-based configurations. The need for a further thermodynamic optimisation is justified by the change in expander isentropic efficiency when considering large-scale applications.

F.1 Process flowsheet

One-stage cascade cycle

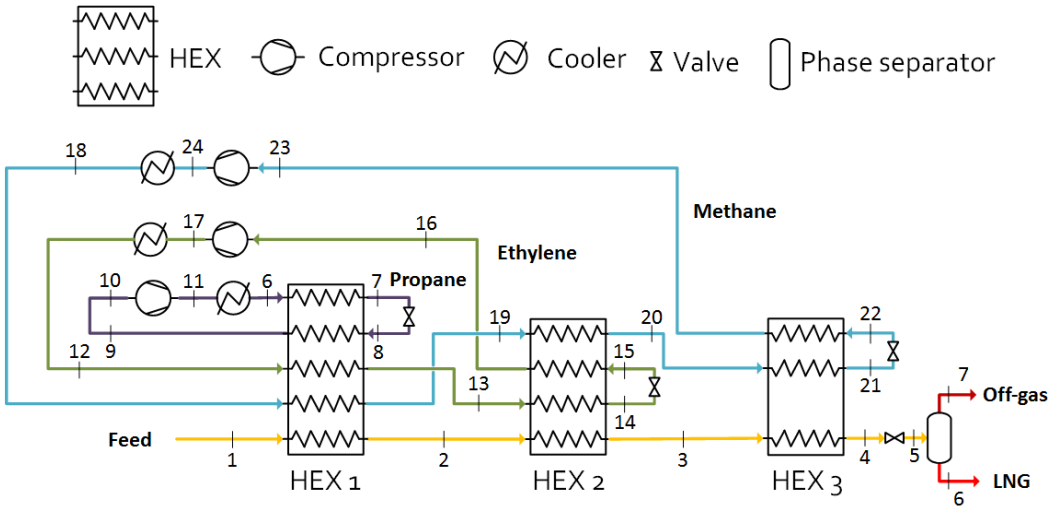

Figure F.1: Process flowsheet of the small-scale one-stage cascade cycle [81]

Appendix F. Process flowsheet for cascade and Mixed-Refrigerant cycles and updated optimisation results

Table F.1: Values of the main parameters in the optimised one-stage cascade cycle [81]

Parameter	Variable	Unit	Value
Pre-cooling temperature	T_2, T_7, T_{13}, T_{19}	°C	-35.2
Liquefaction temperature	T_3, T_{14}, T_{20}	°C	-95.0
Propane high pressure	P_6	bar	8.54
Propane low pressure	P_8	bar	1.20
Propane flow rate	$\dot{m}_6$	kg/s	2.79
Ethylene high pressure	P_{12}	bar	17.76
Ethylene low pressure	P_{15}	bar	1.42
Ethylene flow rate	$\dot{m}_{12}$	kg/s	1.83
Methane high pressure	P_{18}	bar	31.71
Methane low pressure	P_{22}	bar	1.96
Methane flow rate	$\dot{m}_{18}$	kg/s	0.57

Two-stage cascade cycle

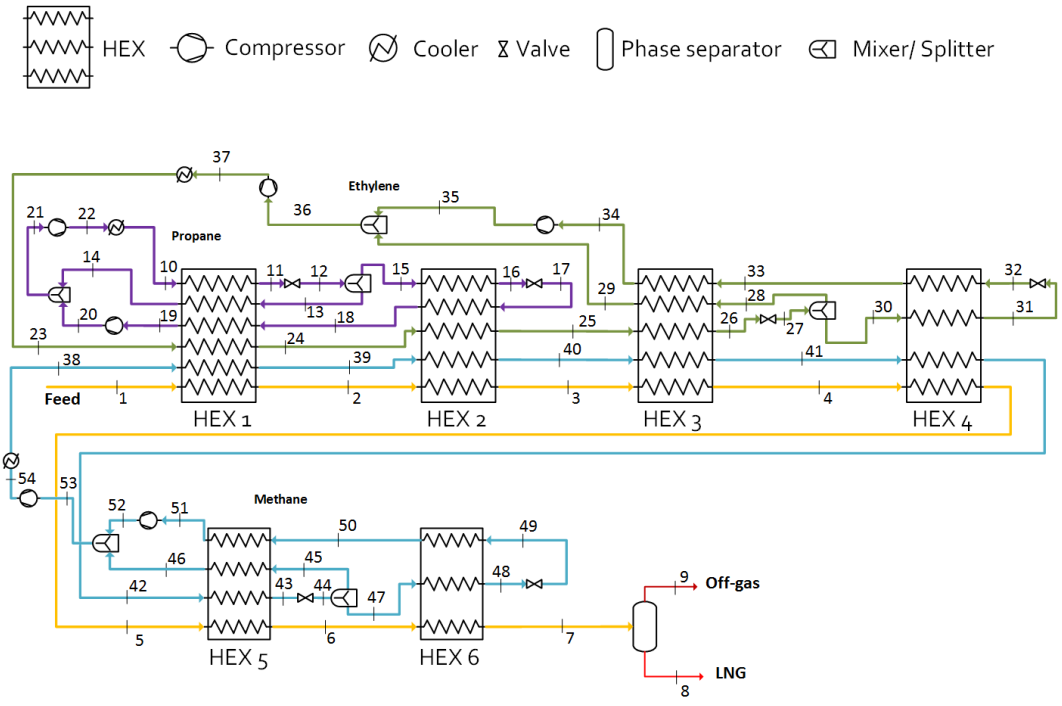

Figure F.2: Process flowsheet of the large-scale two-stage cascade cycle [81]

Table F.2: Values of the main parameters in the optimised two-stage cascade cycle [81]

Parameter	Variable	Unit	Value
Pre-cooling temperature	T_3, T_{16}, T_{25}, T_{40}	°C	-39.3
Liquefaction temperature	T_5, T_{31}, T_{42}	°C	-94.1
Propane high pressure	P_{10}	bar	8.37
Propane intermediate pressure	P_{12}, P_{20}	bar	3.12
Propane low pressure	P_{17}	bar	1.01
Propane flow rate	$\dot{m}_{10}$	kg/s	2.89
Ethylene high pressure	P_{23}	bar	14.93
Ethylene intermediate pressure	P_{27}, P_{35}	bar	4.58
Ethylene low pressure	P_{32}	bar	1.48
Ethylene flow rate	$\dot{m}_{23}$	kg/s	1.77
Methane high pressure	P_{38}	bar	32.20
Methane intermediate pressure	P_{44}, P_{52}	bar	6.53
Methane low pressure	P_{49}	bar	1.96
Methane flow rate	$\dot{m}_{38}$	kg/s	0.60

PRICO cycle

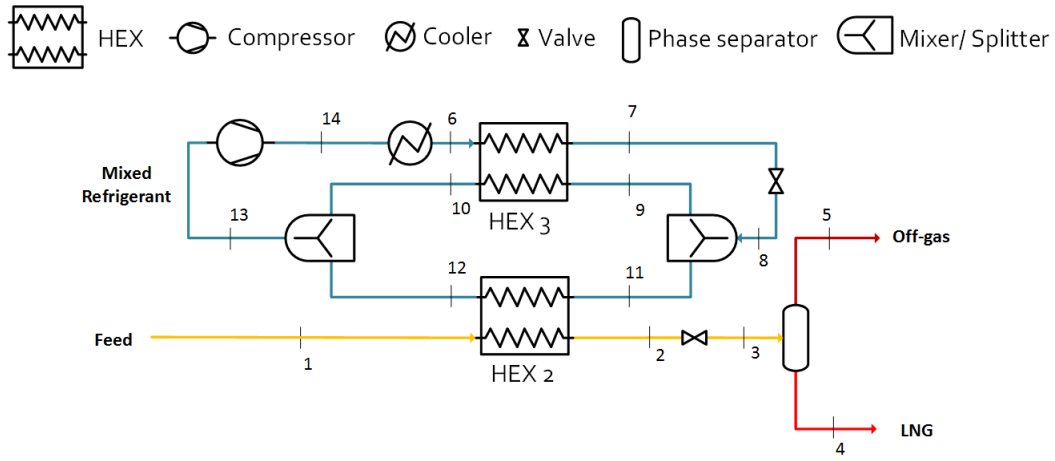

Figure F.3: Process flowsheet of the small-scale *PRICO* cycle [81]

Table F.3: Values of the main parameters in the optimised *PRICO* cycle [81]

Parameter	Variable	Unit	Value
Mixed Refrigerant flow rate	$\dot{m}_6$	kg/s	11.17
Methane flow rate	$\dot{m}_{CH_4}$	kg/s	1.32
Ethane flow rate	$\dot{m}_{C_2H_6}$	kg/s	2.52
Propane flow rate	$\dot{m}_{C_3H_8}$	kg/s	0.16
n-Butane flow rate	$\dot{m}_{\text{n-}C_4H_{10}}$	kg/s	0.14
i-Butane flow rate	$\dot{m}_{\text{i-}C_4H_{10}}$	kg/s	2.26
n-Pentane flow rate	$\dot{m}_{\text{n-}C_5H_{12}}$	kg/s	3.48
i-Pentane flow rate	$\dot{m}_{\text{i-}C_5H_{12}}$	kg/s	0.53
Nitrogen flow rate	$\dot{m}_{N_2}$	kg/s	0.75
Split flow rate	$\dot{m}_{11}$	kg/s	1.73
High pressure level	P_6	bar	5.67
Low pressure level	P_8	bar	1.07

C3-MR cycle

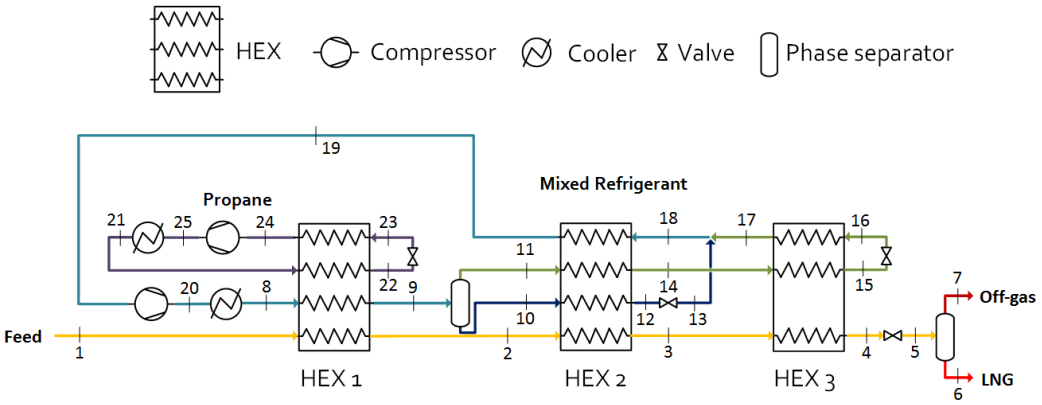

Figure F.4: Process flowsheet of the large-scale *C3-MR* cycle [81]

Table F.4: Values of the main parameters in the optimised *C3-MR* cycle [81]

Parameter	Variable	Unit	Value
Pre-cooling propane flow rate	$\dot{m}_{21}$	kg/s	2.76
Pre-cooling high-pressure level	P_{21}	bar	8.37
Pre-cooling low-pressure level	P_{23}	bar	1.74
Pre-cooling temperature	T_2, T_9, T_{22}	°C	-26.1
Mixed Refrigerant flow rate	$\dot{m}_8$	kg/s	3.06
Methane flow rate	$\dot{m}_{CH_4}$	kg/s	0.37
Ethane flow rate	$\dot{m}_{C_2H_6}$	kg/s	1.59
Propane flow rate	$\dot{m}_{C_3H_8}$	kg/s	0.28
n-Butane flow rate	$\dot{m}_{\text{n-}C_4H_{10}}$	kg/s	0.48
i-Butane flow rate	$\dot{m}_{\text{i-}C_4H_{10}}$	kg/s	0.30
n-Pentane flow rate	$\dot{m}_{\text{n-}C_5H_{12}}$	kg/s	0.00
i-Pentane flow rate	$\dot{m}_{\text{i-}C_5H_{12}}$	kg/s	0.00
Nitrogen flow rate	$\dot{m}_{N_2}$	kg/s	0.03
High pressure level	P_8	bar	12.01
Low pressure level	P_{13}, P_{16}	bar	1.36
Intermediate temperature	T_3, T_{12}, T_{14}	°C	-122.8

F.2 Optimal decision variables for large-scale expander-based configurations

Propane pre-cooling single-expander cycle

Table F.5: Decision variables, corresponding variation ranges and optimal values for the large scale single-expander cycle with propane pre-cooling

Decision variable	Unit	Range	Optimal value
$\mathbf{P_{high,N_2}}$	bar	[60 130]	120.7
$\mathbf{P_{low,N_2}}$	bar	[1 15]	13.0
$\mathbf{T^{in}_{exp}}$	°C	[-100 -45]	-48.8
$\dot{\boldsymbol{m}}_{\mathbf{N_2}}$	kg/s	[1 15]	6.0
$\mathbf{P_{high,PC}}$	bar	[8.37 42.5]	8.37
$\mathbf{P_{low,PC}}$	bar	[0.5 5]	1.36
$\mathbf{T_{PC}}$	°C	[-40 0]	-32.2

N_2 sub-cooling dual-refrigerant cycle

Table F.6: Decision variables, corresponding variation ranges and optimal values for the large scale N_2 sub-cooling dual-refrigerant cycle

Decision variable	Unit	Range	Optimal value
$\mathbf{P_{high,N_2}}$	bar	[60 90]	85.7
$\mathbf{P_{high,CH_4}}$	bar	[60 90]	76.0
$\mathbf{P_{low,N_2}}$	bar	[5 30]	14.5
$\mathbf{P_{low,CH_4}}$	bar	[5 30]	17.0
$\mathbf{T^{in}_{exp,N_2}}$	°C	[-100 -50]	-73.7
$\mathbf{T^{in}_{exp,CH_4}}$	°C	[-50 0]	-24.1
$\mathbf{T^{NG}_{int}}$	°C	[-120 -20]	-92.9
$\dot{\boldsymbol{m}}_{\mathbf{N_2}}$	kg/s	[1 5]	3.0
$\dot{\boldsymbol{m}}_{\mathbf{CH_4}}$	kg/s	[1 5]	3.6

CH_4 sub-cooling dual-refrigerant cycle

Table F.7: Decision variables, corresponding variation ranges and optimal values for the large scale CH_4 sub-cooling dual-refrigerant cycle

Decision variable	Unit	Range	Optimal value
$\mathbf{P_{high,N_2}}$	bar	[60 130]	103.0
$\mathbf{P_{high,CH_4}}$	bar	[2.5 20]	4.3
$\mathbf{P_{low,N_2}}$	bar	[1 30]	29.9
$\mathbf{P_{low,CH_4}}$	bar	[0.1 2]	0.91
$\mathbf{T^{in}_{exp,N_2}}$	°C	[-100 0]	-6.0
$\mathbf{T^{in}_{exp,CH_4}}$	°C	[-130 -80]	-101.8
$\mathbf{T^{NG}_{int}}$	°C	[-120 -20]	-76.7
$\dot{\boldsymbol{m}}_{\mathbf{N_2}}$	kg/s	[1 8]	4.0
$\dot{\boldsymbol{m}}_{\mathbf{CH_4}}$	kg/s	[1 8]	4.8

If you aren't in over your head,
how do you know how tall you are?

— T.S. Eliot